



Four Degrees of Global Warming:

Effects on the New Zealand Primary Sector

MPI Technical Information Paper No: 2013/49

Prepared for the Ministry for Primary Industries

ISBN No: 978-0-478-42081-4

ISSN No: 2253-3923

December 2013

Disclaimer

The information in this publication is not government policy. While every effort has been made to ensure the information is accurate, the Ministry for Primary Industries does not accept any responsibility or liability for error of fact, omission, interpretation or opinion that may be present, nor for the consequences of any decisions based on this information. Any view or opinion expressed does not necessarily represent the view of the Ministry for Primary Industries.

Requests for further copies should be directed to:

Publications Logistics Officer
Ministry for Primary Industries
PO Box 2526
WELLINGTON 6140

Email: brand@mpi.govt.nz
Telephone: 0800 00 83 33
Facsimile: 04-894 0300

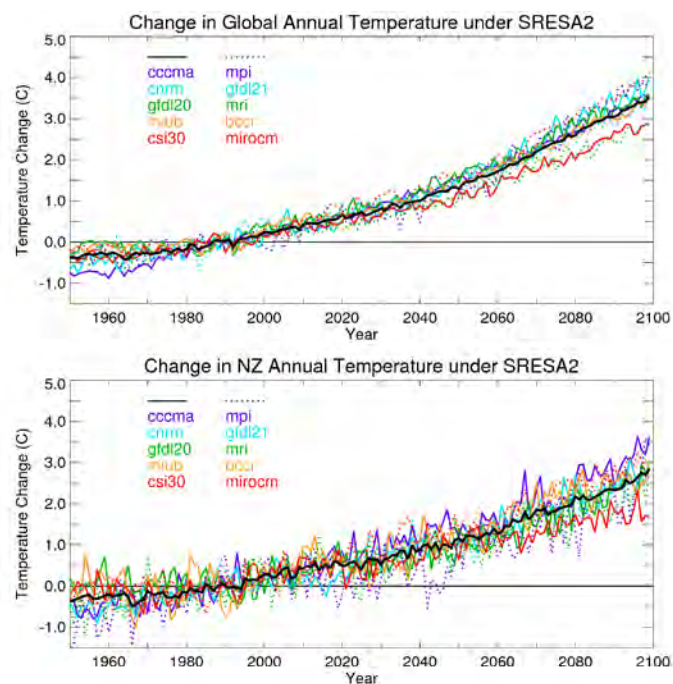
This publication is also available on the Ministry for Primary Industries website at <http://www.mpi.govt.nz/news-resources/publications.aspx>

© Crown Copyright - Ministry for Primary Industries

Four Degrees of Global Warming: Effects on the New Zealand Primary Sector

Prepared for the Ministry for Primary Industries

December 2012



Authors/Contributors:

James Renwick (NIWA)
Brett Mullan (NIWA)
Lara Wilcocks (NIWA)
Christian Zammit (NIWA)
James Sturman (NIWA)
Troy Baisden (GNS Science)
Liz Keller (GNS Science)
Miko Kirschbaum (Landcare Research)
Dean Meason (Scion)
D. Harrison (Scion)
Gwyn Verkerk (DairyNZ)
Andrew Cooke (Rezare Systems)
Paul Marshall (Rezare Systems)
Anthony Clark (DairyNZ)

For any information regarding this report please contact:

Brett Mullan
Principal Scientist, Climate
+64-4-386 0508
Brett.mullan@niwa.co.nz

National Institute of Water & Atmospheric Research Ltd
301 Evans Bay Parade, Greta Point
Wellington 6021
Private Bag 14901, Kilbirnie
Wellington 6241
New Zealand
Phone +64-4-386 0300
Fax +64-4-386 0574

NIWA Client Report No:	WLG2012-24
Report date:	December 2012
NIWA Project:	MAF12303

Cover image: Projected surface temperature increases, globally and over New Zealand, from a range of global climate model 'A2' scenario runs.

© All rights reserved. This publication may not be reproduced or copied in any form without the permission of the copyright owner(s). Such permission is only to be given in accordance with the terms of the client's contract with NIWA. This copyright extends to all forms of copying and any storage of material in any kind of information retrieval system.

Whilst NIWA has used all reasonable endeavours to ensure that the information contained in this document is accurate, NIWA does not give any express or implied warranty as to the completeness of the information contained herein, or that it will be suitable for any purpose(s) other than those specifically contemplated during the Project or agreed by NIWA and the Client.

Contents

1	Executive Summary	5
2	Overview and global setting	7
2.1	Project background	7
2.2	Global setting	9
3	Climate scenarios.....	10
3.1	Summary.....	10
3.2	Global models and 4° scaling.....	10
3.3	New Zealand.....	13
4	Frosts and Growing Degree Days	23
4.1	Introduction	23
4.2	Results: Frost frequency	23
4.3	Results: Growing Degree-days.....	27
4.4	Summary and Implications	29
5	Extreme rainfall and flood flows	30
5.1	Introduction	30
5.2	Extreme rainfall	30
5.3	River/flood flows.....	34
6	New Zealand Pasture Production (from water balance)	56
6.1	Introduction	56
6.2	Potential Pasture Growth Model.....	56
6.3	Potential Pasture Growth Results.....	59
6.4	Conclusions	77
7	New Zealand pasture production in 2100: Biome-BGC	78
7.1	Summary.....	78
7.2	Methods	78
7.3	Results.....	81
7.4	Regional and Seasonal Results by Pasture Type.....	84
7.5	Discussion.....	88
8	New Zealand Forestry	89
8.1	<i>Pinus Radiata</i> Simulation: the CenW model.....	89

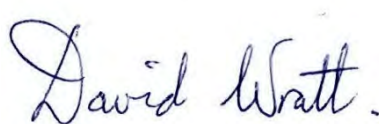
8.2	<i>Eucalyptus fastigata</i> Simulation: the 3PG model	105
9	Impact of projected climate change on thermal stress in dairy cattle.....	118
9.1	Summary.....	118
9.2	Predictive models used to generate risk maps	118
9.3	Impact on Heat Load Index	119
9.4	Impact on Cold Stress Index	124
9.5	Discussion of Results	125
10	Further information	128
11	References.....	129
12	Appendices.....	140
12.1	Appendix A1: Seasonal climate change scenarios	140
12.2	Appendix A2: Details of daily scenarios for APSIM files	154
12.3	Appendix A3: Detailed catchment-based TopNet results.....	158
12.4	Appendix A4: Heat Stress Predictive risk maps.....	159
12.5	Appendix A5: Predictive risk maps with extended differentiation for summer and summer shoulder months	172

Reviewed by



Andrew Tait

Approved for release by



David Wratt

1 Executive Summary

At the time of the Intergovernmental Panel on Climate Change (IPCC) 4th Assessment Report (AR4) in 2007, the 'mid-range' estimate of global mean warming by 2100 was around 3°C, with the 'likely range' across a suite of scenarios lying between approximately 1°C and 6°C. The average warming by 2100 for the 'high' scenario (A1FI) was close to 4°C, while for the 'low' scenario (B1) the average warming was just under 2°C. While greenhouse gas emissions in recent years have tracked close to the A1FI scenario, the level of warming this century, and its timing, will be critically dependent on global emissions over the coming several decades. The results presented here represent a 'what-if' scenario for aspects of the New Zealand primary sector, should a global average temperature rise of 4°C eventuate.

The results from two global climate models (GCMs) exhibiting four degrees of global mean surface warming (over approximately the coming century) were downscaled for New Zealand and applied to a range of models relevant to the primary sector. Of the GCMs, the 'CCC' (Canadian Climate Centre) model produced the larger warming over New Zealand, 4.4°C in the annual and national average in some regions and seasons, while the 'Planck' (Max Planck Institute – Germany) model¹ produced 3.1°C warming on average over New Zealand. Differences in the level of local warming relate to differences in hemispheric-scale patterns of change simulated by each model, and to the relative sensitivity of the downscaling scheme to changes in specific climate parameters such as westerly wind strength and atmospheric moisture content. Associated with these changes were changes in precipitation, relative humidity and other climate parameters which were generally more pronounced for the CCC model that exhibited the largest temperature rises.

Each section of the document that follows was written as a stand-alone report by the relevant authors and may be read as such. Each of the sections went through an independent review process before inclusion here. This summary provides a brief overview of the main findings in each section.

Basic climate changes: Temperature rises were projected to be largest in inland and eastern areas. Seasonally, temperature rises were projected to be largest in winter and smallest in summer. Hence, the greatest increase is seen with the CCC model, for the eastern South Island in winter, with a rise of 5.3°C. The smallest increase was with the Planck model, for the western North Island in summer, with a rise of 2.3°C. Precipitation changes followed an east-west pattern in many seasons, with increases in the west and decreases in the east, especially in winter and spring, associated with stronger westerly winds. Summer saw a marked drying everywhere with the CCC model, but little change with the Planck model.

Growing degree-days and frosts: Overall, there were large increases in growing degree days and frost-free period. Under both scenarios, frosts occurrence ceases at most lowland sites of both Islands. Growing degree-days above thresholds of 5 and 10°C increase between 50 and 100% in most locations.

Extreme rainfalls and river flows/flood flows: Extreme rainfalls (100-year average recurrence interval; 12, 24, and 48h totals) were assumed to increase by 32% everywhere, on the basis

¹ Also referred to as the 'MPI' (for Max Planck Institute) model in some Figure legends.

of an 8% rise in saturation atmospheric moisture content per degree of global warming (i.e., these were unrelated to the regional detail of downscaled temperature changes over New Zealand). This is associated with increases in extreme rain totals of between 50 and 150mm in many locations. For all rivers analysed here, average annual discharge is projected to increase, with a wider range of flows: higher flood flows and lower low flows, brought about by an increase in extreme maximum rainfall amounts and by an increased frequency and duration of dry spells. Water availability during times of highest irrigation demand is projected to decrease. Changes to snow accumulation and melt (less accumulation, more rain in winter; less melt in spring/summer) are projected to significantly change the seasonality of flows in major rivers.

Pasture growth (water balance model): Significant changes in seasonality of pasture growth are projected, generally with increases in winter (temperature rise) and decreases in summer (reduced soil moisture). Irrigation demand is projected to increase in spring and summer.

Pasture growth (Biome-BGC model): Even including the CO₂ fertilisation effect, the CCC scenario is associated with a pronounced decline in both sheep/beef and dairy pasture production. The Planck scenario produces milder changes, with a slight decrease in sheep/beef production and an increase in dairy production. The magnitude of warming appears closely tied to the level of impact on pasture production in the Biome-BGC model. Under a milder warming scenario, such as the Planck model, results suggest that pasture production would not change much, but with a more extreme pattern of climate change, New Zealand pasture could experience significant adverse effects. Note that these results are for non-irrigated pasture only.

Forestry: Underlying changes to the climate (temperature, precipitation) are associated with decreases in *Pinus radiata* productivity at most sites. However this is more than offset by the enhanced fertilisation effect of increased atmospheric CO₂. Productivity is projected to increase 30 to 40% on average, dependent on the climate change scenario chosen. For *Eucalyptus fastigata*, large increases in productivity are projected using both model scenarios, even without taking account of the enhanced fertilisation effect of increased atmospheric CO₂. With CO₂ fertilisation included, productivity is projected to approximately double in many locations. The main factors promoting productivity are reduced frost frequency and higher temperatures. Note that in this analysis, no account has been taken of future increased risk of forest fires, nor of the possible effects of changes in pest species and their mortality.

Animal heat stress: Heat load is projected to increase to an extent that dairy cows would experience significant thermal stress in many dairying areas of New Zealand. Summers with 20 or more days of conditions that induce heat stress days are projected to become widespread. Northland and northern Waikato consistently experience increased heat load index across both climate scenarios. Without measures to reduce heat load, cattle could be expected to exhibit a range of negative responses, which would have a detrimental impact on production, reproduction and welfare. Adaptive measures could include introduction of more heat-tolerant breeds, milking only during the cooler months and providing more shade and cooling.

2 Overview and global setting

2.1 Project background

This project, funded from the Sustainable Land Management and Climate Change (SLMACC) scheme, addresses the SLMACC Theme 3.1 priority: *The likely impacts of climate change on the land based sectors in New Zealand with a temperature increase of 4°C globally, including droughts, floods etc.* The goals of the project were to provide scientific information and understanding to enhance and support primary-sector adaptation to climate change in New Zealand. Given the modest size of the overall project, it was not intended to be fully comprehensive or integrated, but was designed to look at a number of 'indicator' sectors and species, based on existing capabilities. The aim was to develop practical new information from existing models and understanding.

Key tasks in the project, and the basis of the chapters in this report, were:

1. Scenario development: *Generate two new scenarios (using established downscaling methods), based on 4°C global temperature change. These will span most of the projected range in New Zealand rainfall changes from a suite of global climate models. Provide current climate and future scenarios on the Virtual Climate Station Network (VCSN; 5x5km) grid in formats suitable for impact models.*

The project used output from two different global climate models (GCMs) from the 'CMIP3' suite of models documented in the IPCC AR4, forced with the Special Report on Emissions Scenarios (SRES, Nakicenovic et al. 2000) A2 greenhouse gas emissions scenario. Both model simulations exhibit around 4°C of global warming over the coming century (the nominal period 1997-2011 to 2097-2111). The two models chosen were *cccma_cgcm3_1* (from the Canadian Climate Centre, hereafter "CCC") and *mpi_echam5* (from the Max Planck Institute in Germany, hereafter "Planck"). Models were chosen for their ability to correctly simulate the present climate of the New Zealand region and for their global temperature change by the end of the 21st century. See Mullan et al. (2008) for model details. The CCC model warming in the region of New Zealand was around 95% of the global mean, while for Planck the ratio was around 65%, with different changes in regional circulation and rainfall. Differences in the ratio of regional to global mean warming are related to regional differences in atmospheric and ocean circulation and heat transport changes.

Because of the scaling of New Zealand vs global temperature change, the CCC results are in many ways more extreme than those based on the Planck simulations. Hence, the CCC-based results are given emphasis here, though the Planck results are also provided for contrast.

2. Drought and soil water balance impact modelling: *Analyse impacts on drought severity and frequency plus seasonal soil moisture balance for all of New Zealand using scenarios from Task 1. Use existing models developed for the MAF SLMACC Climate Change and Drought study (C01X0818).*

Here, drought and soil water balance were not studied separately, since SLAMCC has recently funded a report specifically on changes in drought, related to changes in soil water balance (Clark et al. 2011). Soil water balance changes are however implicitly included in simulations of pasture growth changes.

3. Growing degree days and frost impact modelling: *Analyse impacts on growing degree days and timing of first and last frosts for all of New Zealand using scenarios from Task 1. Use methods developed for the FRST Adaptation to Climate Variability and Change programme (C01X0701, Tait 2008).*

This work was carried out using a straightforward analysis of the downscaled temperature information on the VCS grid. Minimum and mean temperature values were analysed and summed in relation to appropriate thresholds (below 0°C for frosts, above 5°C and 10°C for growing degree-days).

4. Extreme rainfall and flooding impact modelling: *Analyse impacts on extreme rainfall (e.g., 100-yr 24-hour ARI) for all of New Zealand, and on flood flow for a few key rivers, using scenarios from Task 1. Use HIRDS (Thompson 2002) to estimate the effects of temperature change on extreme rainfall. Use Topnet (Clark et al. 2008) to estimate changes to flood flow for selected catchments.*

Extreme rainfall changes were calculated assuming a standard rate of increase of atmospheric moisture content per degree of global warming, translated into rainfall amounts over a range of periods. River flow simulations with Topnet took account of rainfall changes, and changes in seasonal snow accumulation and melt in alpine regions.

5. Pasture growth (based on water balance) impact modelling: *Analyse impacts on pasture growth, including seasonality of growth, for all of New Zealand using scenarios from Task 1. Use models developed for the MAF SLMACC Climate Change and Drought study (C01X0818). Compare with results from Task 6.*

Potential pasture growth based on climatic controls was modelled for areas of New Zealand under “exotic grassland pasture”, covering both dairy and dry stock agriculture pasture. No distinction was made between management regimes.

6. Pasture growth (with CO₂ fertilisation effects) impact modelling: *Analyse impacts on pasture growth (with and without CO₂ fertilisation) for all of New Zealand using scenarios from Task 1. Use the existing Biome-BGC model (Thornton and Rosenbloom 2005). Compare results with those from Task 5.*

Dairy and sheep/beef pasture production was modelled with the Biome-BGC model, calibrated to New Zealand pasture, to estimate pasture production under a projected 4°C of global warming. Findings indicate that the level of warming determines the degree of impact on pasture production for both sheep/beef and dairy agriculture in New Zealand.

7. Tree productivity impact modelling: *Analyse impacts on tree productivity for New Zealand for Pinus radiata and Eucalyptus fastigata using scenarios from Task 1. Use the CenW model applied in the MAF SLMACC Productivity surfaces for Pinus radiata and a range of indigenous forest species under current and future climatic conditions, and the 3PG forest carbon allocation model for Eucalyptus fastigata.*

Pinus radiata was analysed as it is the dominant species commercially planted in New Zealand, while *Eucalyptus fastigata* was analysed as a likely 'adaptation species' for the future, even though it is not economically important at present. For both species, the fertilisation effect of increased CO₂ concentrations more than offsets any adverse influences of a changed climate.

8. Animal heat and cold stress impact modelling: Analyse impacts on animal heat and cold stress for all of New Zealand using the scenarios from Task 1. Use the model developed for the MAF SLMACC Climate Change Adaptation for the Agricultural Sector project (C01X0901).

This work focussed on the effects on dairy cows only.

2.2 Global setting

The suite of climate change scenarios summarised in the 4th Assessment Report (AR4) of the Intergovernmental Panel on Climate Change (IPCC) indicated a range of global mean surface air temperature rise by the end of this century of approximately 1°C to 6°C, with a mid-range value of around 3°C (Meehl et al. 2007). A global mean rise of around 3°C is likely to lead to a rise over New Zealand of closer to 2°C (Mullan et al. 2008). Century-scale temperature rises are generally simulated to be smaller over New Zealand than in the global mean, because of the buffering effect of the large expanses of ocean that surround the country.

Recent international negotiations have advocated for a limit to global mean warming of 2°C (compared to pre-industrial temperatures). Such a limit would imply a rise of less than 2°C on average over New Zealand. However, it has been noted that current changes in GHG emissions, and the kinds of emissions reductions pledged for this century by many developed countries fall well short of what is required to stay below the 2°C limit (Meinshausen et al. 2009). The current GHG emissions trajectory is towards the upper end of the SRES emissions scenarios considered for the AR4 (Manning et al. 2010). Recent analysis suggests that global mean warming by the end of this century is virtually certain to exceed 2°C, and may reach 4°C or more (Anderson and Bows 2011).

It is clear that policy-makers and business sectors in New Zealand must consider a range of possible future climates, from those exhibiting little change to those associated with relatively large changes. This report discusses the impacts on the primary sector in New Zealand of global mean warming of 4°C. It makes use of the output of two different models which simulate 4°C of global mean warming by around 2100, but with quite different regional climate changes in the vicinity of New Zealand.

3 Climate scenarios

3.1 Summary

Global mean surface temperature evolution to 2100 for all models considered is shown in Figure 3-1 below. Model fields were statistically downscaled for New Zealand using the same techniques as in the recent drought report (Clark et al. 2011). The present-day climate was defined in terms of observed climate during 1997-2011, represented in terms of daily climate surfaces on the gridded Virtual Climate Station Network (VCSN, Tait et al. 2006, Tait 2008). Four-degree scenario-based changes were calculated for a matching 15-year period, nominally dated as the years 2097-2111.

3.2 Global models and 4° scaling

This project calls for an assessment of likely climate change impacts in New Zealand, as a consequence of a 4°C global temperature increase. The phrase “4°C global temperature increase” is interpreted to mean 4°C of global warming *since pre-industrial* (confirmed by Gerald Rys, MPI); that is, since the nominal date of 1750.

In practice, there are neither observational data, nor climate model simulations, from as far back as 1750. When generating global model scenarios, one usually starts with the “current climate”, and then examines changes to some future time-point. The approach here is to use climate simulations from the IPCC Fourth Assessment global models, and downscale projected changes relative to the 1980-1999 average, hereafter abbreviated as “1990”. So the year 1990 is the IPCC ‘starting point’ for the current climate.

Thus, the global temperature increase is made up of two components:

- an observed temperature increase from 1750 up to 1990, and;
- a model-generated scenario change from 1990 to some future date.

It seems to be relatively common to assume the warming from 1750 to ‘present’ to be 0.5°C (NZCCC, 2011; Reisinger *et al.*, 2010), but obviously this is only an approximate value. In the absence of a global temperature record back to 1750, Joshi *et al* (2011) took the 1880-1909 average to represent the ‘pre-industrial’. Table 3.1 shows the changes in global mean temperature between 1880-1909 and 1980-1999 from three data sets.

Table 3-1: Estimated global temperature changes to 1990

Temperature Data Set	Temperature change, 1880-1909 to 1980-1999
HadCRUT3 ‘best estimate’ from UKMO	+0.480°C
HadCRUT3 Global Land Ocean Temp from CRU	+0.537°C
GISTEMP	+0.507°C

Thus, it would appear that assuming a value of +0.5°C from pre-industrial to present is reasonable, and this value is adopted for the purpose of this study. It is therefore necessary to have an additional +3.5°C of projected future warming, relative to the current climate (“1990”), in order to reach the target of 4°C above pre-industrial.

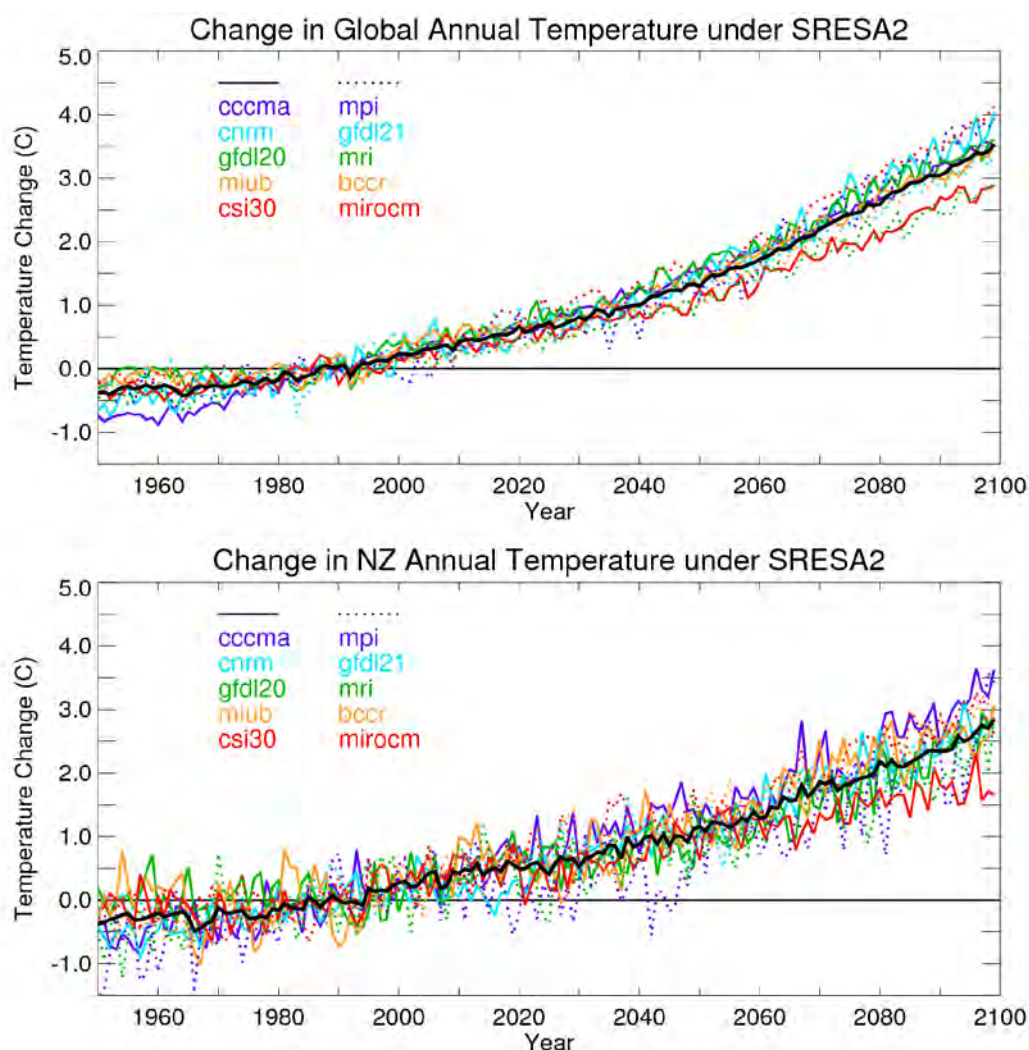


Figure 3-1: Time evolution of global mean (top) and New Zealand mean (bottom) annual average surface temperature anomalies (differences from 1980-1999 mean) for a range of global climate models using the SRES A2 emissions scenario. Model names and associated line colour/style is indicated in the upper left of each panel. The multi-model mean is shown as the heavy black line. The “New Zealand” value here is indicative only and taken directly from the global models, without statistical downscaling. It represents the average over a box covering 165°E-180 by 35°S-48°S.

Many of the IPCC global models terminated their scenario simulations at 2100, or sometimes 2099, and so 100-year changes from “1990” to “2090” (the 2080-2099 average) are calculated. The downscaled New Zealand climate changes for 1990 to 2090 will be associated with a global temperature change $\Delta T[1990-2090]$. In general, $\Delta T[1990-2090]$ will not equal the required $+3.5^{\circ}\text{C}$, so additional scaling is necessary.

Output was examined from a suite of global models that validate well in the New Zealand region and have been used in other studies (MfE, 2008; Reisinger *et al.*, 2010). Figure 3-1 shows the time evolution of global and “New Zealand” annual temperature from 10 such models since 1950, where the post-2000 temperatures are driven by the SRES A2 emission scenario. Note that in this figure, the “New Zealand” temperature increase is taken directly from the gridded global model output, without any statistical downscaling. The A2 scenario is

used, since this is the highest scenario for which many model simulations are available, and the global temperature increases exceed 3°C for most models, which means minimal additional scaling will be required.

Table 3-2 shows 1990 to 2090 annual temperature changes, comparing the global-average changes from 10 climate models with the corresponding statistically downscaled NZ-average changes. The statistical downscaling for New Zealand follows the so-called “Clark” approach (Clark et al., 2011), rather than the “Mullan” approach (Mullan et al., 2001; MfE, 2008; Reisinger et al., 2010). The “Clark” downscaling methodology results in New Zealand warming at a similar rate to the globe, although model-dependent, whereas in the “Mullan” methodology New Zealand warms at a slower rate of about 75% of the global rate. The Clark downscaled temperatures are also higher than for the New Zealand box-average of Figure 3-1, whereas the Mullan downscaled temperatures are (by design) very similar to the box average that includes large regions of ocean. Research into downscaling methods is ongoing, and no single approach is considered optimal. This report has used the “Clark” approach for consistency with the recently-completed report on drought occurrence (Clark et al. 2011).

Table 3-2: Global and NZ-downscaled annual temperature changes (°C) from 1990 to 2090, under the SRES A2 emission scenario, for 10 global climate models. See Table 8.1 in Randall et al. (2007) for a full description of the global models.

Model	Global change to 2090	NZ change to 2090
cccma_cgcm3_1_t47	3.14	3.92
mpi_echam5	3.43	3.01
bccr_bcm2_0	3.01	3.59
cnrm_cm3	3.40	3.54
csiro_mk3_0	2.55	2.60
gfdl_cm2_0	3.21	3.50
gfdl_cm2_1	2.96	3.41
miroc3_2_medres	3.56	3.71
miub_echo_g	3.07	3.10
mri_cgcm2_3_2	2.50	2.87

After considering the patterns of temperature and rainfall change from these models, the first two models in Table 3-2 were selected for scenario development. The models are subsequently identified by the acronyms “CCC” (the Canadian Climate Centre t47 model) and “Planck” (the Max Planck Institute for Meteorology *mpi_echam5* model). These two models give contrasting local temperature and rainfall changes: New Zealand temperatures from the CCC model (after applying the Clark downscaling) increase more than the global average by century end, whereas the Planck model warms less than the globe. The models have contrasting seasonal patterns of rainfall and other relevant climate elements as discussed below.

3.3 New Zealand

3.3.1 Downscaled patterns of climate change

The projections for the CCC and Planck models thus require the following scaling in order to match a 3.5°C global warming since 1990 (Table 3-2), and hence a 4°C warming since pre-industrial times:

- CCC model: multiply change fields by $3.50/3.14 = 1.11$
- Planck model: multiply change fields by $3.50/3.43 = 1.02$

As noted above, the two different models chosen simulate quite different climate changes in the region of New Zealand, for an equivalent global mean warming of 3.5°C since 1990, and an approximately equivalent global mean warming of 4°C since pre-industrial. Based on the statistical downscaling employed here (the “Clark” approach, Clark et al., 2011), the CCC model simulates an annual mean increase in mean temperature over New Zealand of 4.4°C, while the Planck model simulates an increase of 3.1°C over New Zealand, relative to “1990”; ie, not relative to pre-industrial. For the purposes of this project, it is not necessary to know the New Zealand temperature change from pre-industrial to 1990.

The present-day climate was defined in terms of observed climate during 1997-2011, represented in terms of daily climate surfaces on the gridded Virtual Climate Station Network (VCSN, Tait et al. 2006, Tait 2008). Differences between the climate model baseline of 1980-1999 and the VCSN baseline of 1997-2011 were ignored, and can be considered as part of natural variability.

Figures 3-3 and 3-4 show maps of annual mean changes, for the CCC and Planck models respectively, in the four key climate elements of rainfall, mean temperature, solar radiation and relative humidity. These are the projected changes after applying the Clark statistical downscaling for the first three climate elements, and direct global model interpolation for relative humidity, followed by rescaling to match the 3.5°C global warming since “1990”. The changes are applied to the VCSN baseline patterns shown in Figure 3-2. Seasonal mean baseline patterns, and downscaled changes, are shown in the Appendix.

3.3.2 Downscaled temperature patterns

The top right panels of the figures below show annual mean temperatures for the baseline period (Figure 3-2), and the downscaled changes for the CCC model (Figure 3-3) and the Planck model (Figure 3-4). Regional and seasonal changes are summarised in Table 3-3, and are mapped in the Appendix. The six regions in Table 3-3 are those used for NIWA’s seasonal outlook products, and have a fairly homogeneous within-region response.

Table 3-3: Regional and seasonal average changes (°C) in mean temperature for downscaled CCC and Planck scenarios, for New Zealand as a whole and broken down by the six NIWA forecast regions.

	Nth N.I.	SW N.I.	East N.I.	Nth S.I.	SW S.I.	East S.I.	N.Z.
CCC DJF	3.7	3.8	3.8	4.2	4.3	4.5	4.1
CCC MAM	4.1	4.2	4.2	4.5	4.6	4.7	4.4
CCC JJA	4.1	4.2	4.5	4.7	4.8	5.3	4.6
CCC SON	3.8	3.9	4.1	4.3	4.4	4.8	4.2
CCC Annual	3.9	4.0	4.1	4.4	4.5	4.8	4.4
Planck DJF	2.4	2.3	2.4	2.5	2.5	2.7	2.5
Planck MAM	3.1	3.1	3.2	3.4	3.4	3.6	3.3
Planck JJA	3.1	3.2	3.5	3.6	3.6	4.2	3.6
Planck SON	2.7	2.7	2.9	2.9	2.9	3.3	2.9
Planck Annual	2.8	2.8	3.0	3.1	3.1	3.5	3.1

Mean temperature changes are projected to be relatively spatially uniform, somewhat larger at high elevations than near sea-level, and larger in the south than the north, decreasing the geographical range of temperatures across the country. Temperature rises are projected to be larger in winter than in summer, decreasing the seasonal range of temperatures over the country. In winter, the projected increase in westerly winds over the country (seen in both models) is associated with enhanced warming in eastern districts of both Islands.

3.3.3 Downscaled rainfall patterns

The top left panels of Figure 3-2 to 3-4 show the corresponding annual baseline and change patterns for rainfall. The current baseline pattern of higher annual mean rainfall in the west and lower rainfall in the east is accentuated in both future scenarios. Regional and seasonal changes are summarised in Table 3-4, and are mapped in the Appendix.

Table 3-4: Regional and seasonal average changes (%) in total precipitation for downscaled CCC and Planck scenarios.

	Nth N.I.	SW N.I.	East N.I.	Nth S.I.	SW S.I.	East S.I.	N.Z.
CCC DJF	-26	-35	-16	-42	-21	-43	-29
CCC MAM	+20	-14	+55	+1	-17	-6	+3
CCC JJA	-12	-3	-25	+20	+37	-3	+8
CCC SON	-27	-13	-38	-5	+17	-31	-11
CCC Annual	-11	-15	-7	-5	+3	-22	-7
Planck DJF	-7	-2	0	-4	0	+8	-1
Planck MAM	+16	+5	+28	+14	+1	+5	+10
Planck JJA	-25	-1	-32	+17	+67	+2	+15
Planck SON	-22	-2	-28	-1	+16	-12	-5
Planck Annual	-11	0	-10	+6	+20	0	+4

For rainfall, many regions are projected to experience large seasonal changes, often in different directions in different seasons, which partially cancel out in the annual mean. For example, in the CCC scenario, the eastern North Island sees a 55% increase in rainfall in autumn but decreases in all other seasons, resulting in a 7% decrease overall in the annual mean. Similarly, the southwest South Island has large increases in winter and spring, with almost compensating decreases in summer and autumn, leading to only a 3% increase in the annual mean. The pattern of change is broadly similar across the two models, but the CCC scenario is drier overall than the Planck scenario.

The seasonal patterns of rainfall change are reasonably consistent between the CCC and Planck models for the winter, spring and autumn seasons. In winter and spring, both models accentuate the existing west-east rainfall gradient, especially in terms of a wetter southwest of the South Island and a drier north and east of the North Island. In autumn, both models project significant rainfall increases in Northland, Coromandel, Bay of Plenty, Gisborne and Hawkes Bay. In summer, however, the projected changes are quite different: the CCC model shows large decreases in seasonal rainfall over much of the country, especially the east of the South Island, whereas the Planck model shows increases in the eastern South Island.

Note that the statistical downscaling used does not take account of changes in cloud composition and the ‘spill-over’ of liquid or frozen precipitation across the Southern Alps, beyond what is simulated in the global-scale model. Such aspects of precipitation changes are currently being investigated using dynamical downscaling approaches.

3.3.4 Downscaled solar radiation patterns

The bottom left panels of Figure 3-2 to 3-4 show the corresponding annual baseline and change patterns for solar radiation. Seasonal baselines and changes are mapped in the Appendix. Like rainfall and temperature, the Clark statistical downscaling also adjusts the global climate model fields to reflect local effects on solar radiation at the 5 km VCSN scale.

The CCC model shows an increase in solar radiation in the annual mean, and in all seasons too, over virtually all of New Zealand. The annual mean increase is consistent with the large decrease in rainfall (and by inference, cloudiness) in the summer season when solar radiation levels are at their highest. The Planck model has quite a different pattern of radiation change. In the annual mean, radiation decreases in the west and south of the South Island, and increases by a small amount (0 to 5%) in the remainder of the country. Seasonally, the Planck model shows a fairly bland pattern of small increases or decreases for spring, summer and autumn, but a pattern of strong gradients in the winter season: reduced radiation in the west where rainfall increases, and increased radiation in the east where rainfall reduces.

3.3.5 Change patterns for relative humidity and wind speed

The Clark downscaling has not been developed for either relative humidity or wind speed. The approach taken for relative humidity is a simple interpolation from the global model grid-point scale to the VCSN grid. The bottom right panels of Figure 3-2 to 3-4 show the corresponding annual baseline and change patterns for relative humidity, with corresponding seasonal maps in the Appendix. The linear interpolation is evident in the regularity of the contours, especially for the lower resolution CCC model (approximately 2.8° latitude-longitude spacing) compared to the Planck model (approximately 1.9° latitude-longitude spacing).

The Planck model projects only small changes in relative humidity in a future climate; in most cases within $\pm 1\%$ of the current climate. The CCC model projects similarly small relative humidity changes for most seasons; the exception is summer where large decreases of more than 3% are projected over much of the North Island and upper South Island, coinciding with large rainfall reductions and solar radiation increases in that season.

As far as wind changes are concerned, the global model pressure pattern changes imply an increase in mean westerly winds, especially over the South Island in winter and spring, but it is not straightforward to convert this large-scale change in vector-mean wind into the VCSN-scale change in scalar wind speed. Figure 3-5 shows the annual changes in mean sea-level pressure for the CCC and Planck models, where the 1990-2090 changes have again been scaled to match a global temperature increase of 3.5°C since “1990”. The summer and winter baselines and changes are mapped in the Appendix.

NIWA has not yet developed an approach for downscaling wind speed at the national level from climate model projections because of the complexity of local interactions. A report produced for the Ministry for the Environment (Mullan et al. 2008) suggested an increase of ~10% in mean westerly wind speeds by the end of the 21st century. However, a recent study of changes in extreme winds in the New Zealand region (Mullan et al., 2011) found an increase in the extreme wind speed of only a few per cent by century end under the mid-range SRES A1B scenario. Thus, for this study, a simple assumption was made of no change in the wind speed climatology. This simplification is not expected to have serious consequences on the evaluation of impacts, since wind speed is not a major factor in most of the impacts models used in this study.

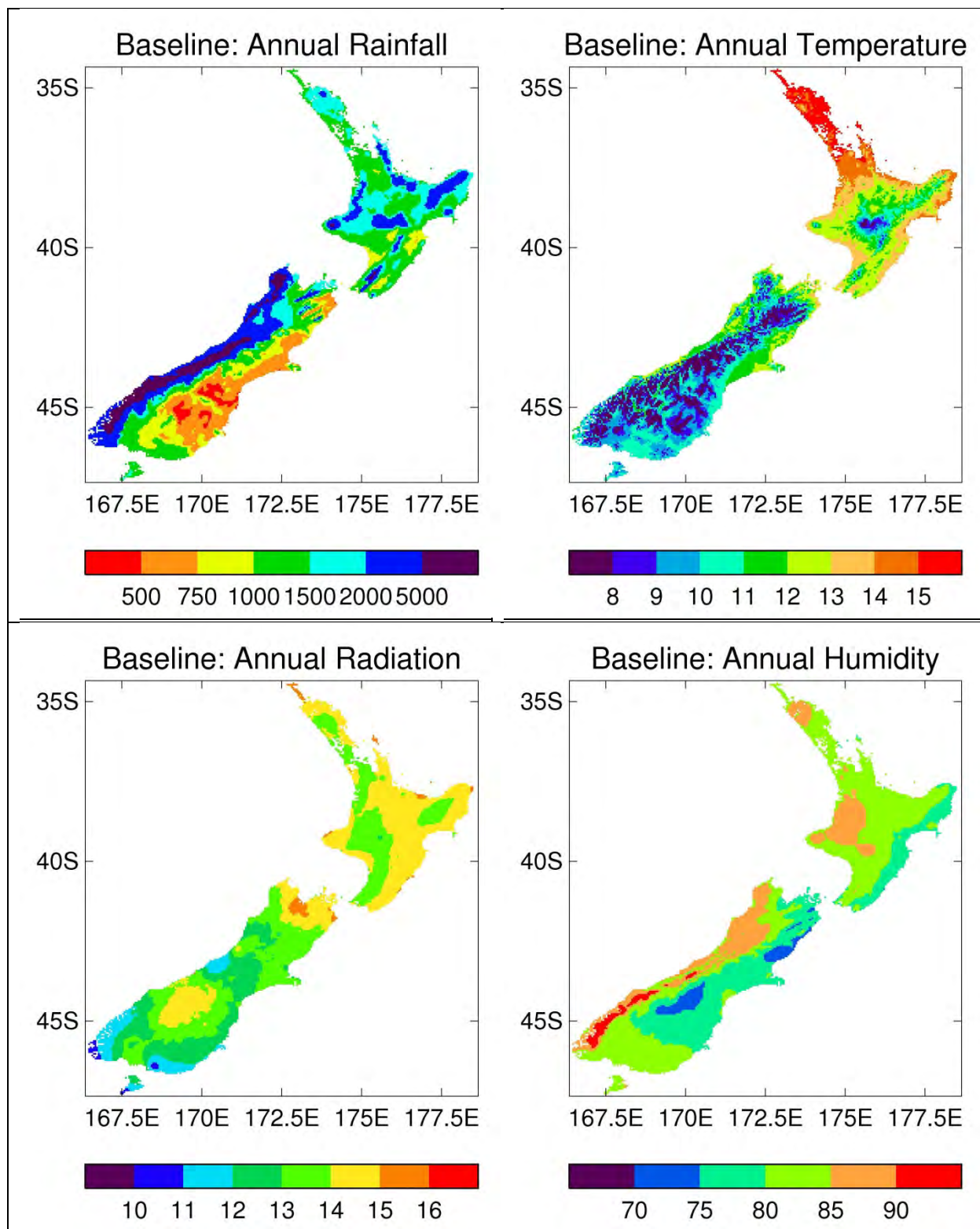


Figure 3-2: Annual maps of key climatic elements for 1997-2011 baseline period: total annual rainfall (in mm, top left); mean temperature (in °C, top right); mean-daily solar radiation (in MJ.m⁻².day⁻¹, bottom left); relative humidity (in %, bottom right).

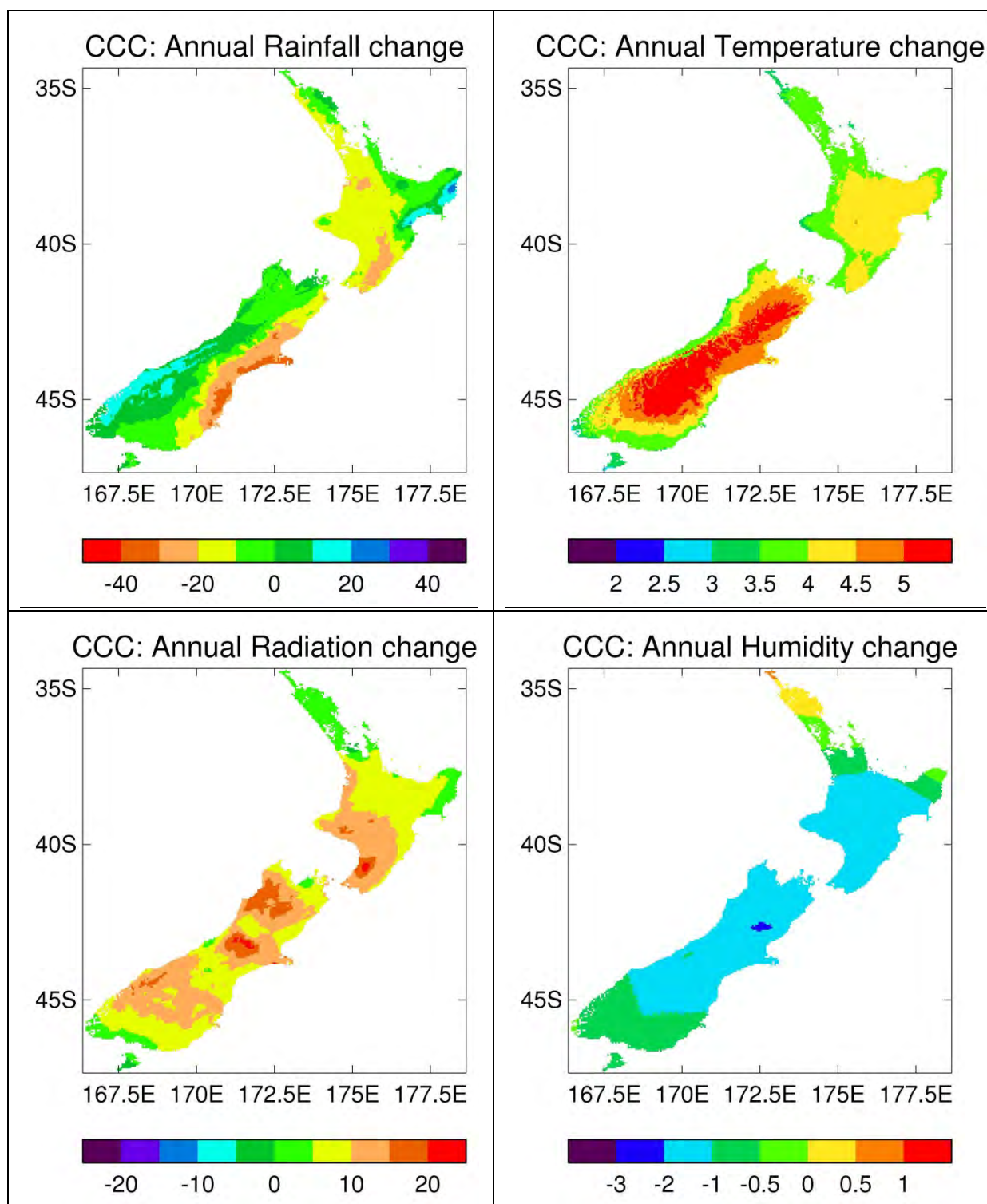


Figure 3-3: Downscaled projections of annual changes between 1990 and date of 4°C global warming, for CCC model: rainfall (as %, top left); mean temperature (in °C, top right); mean-daily solar radiation (as %, bottom left); relative humidity (in %, bottom right).

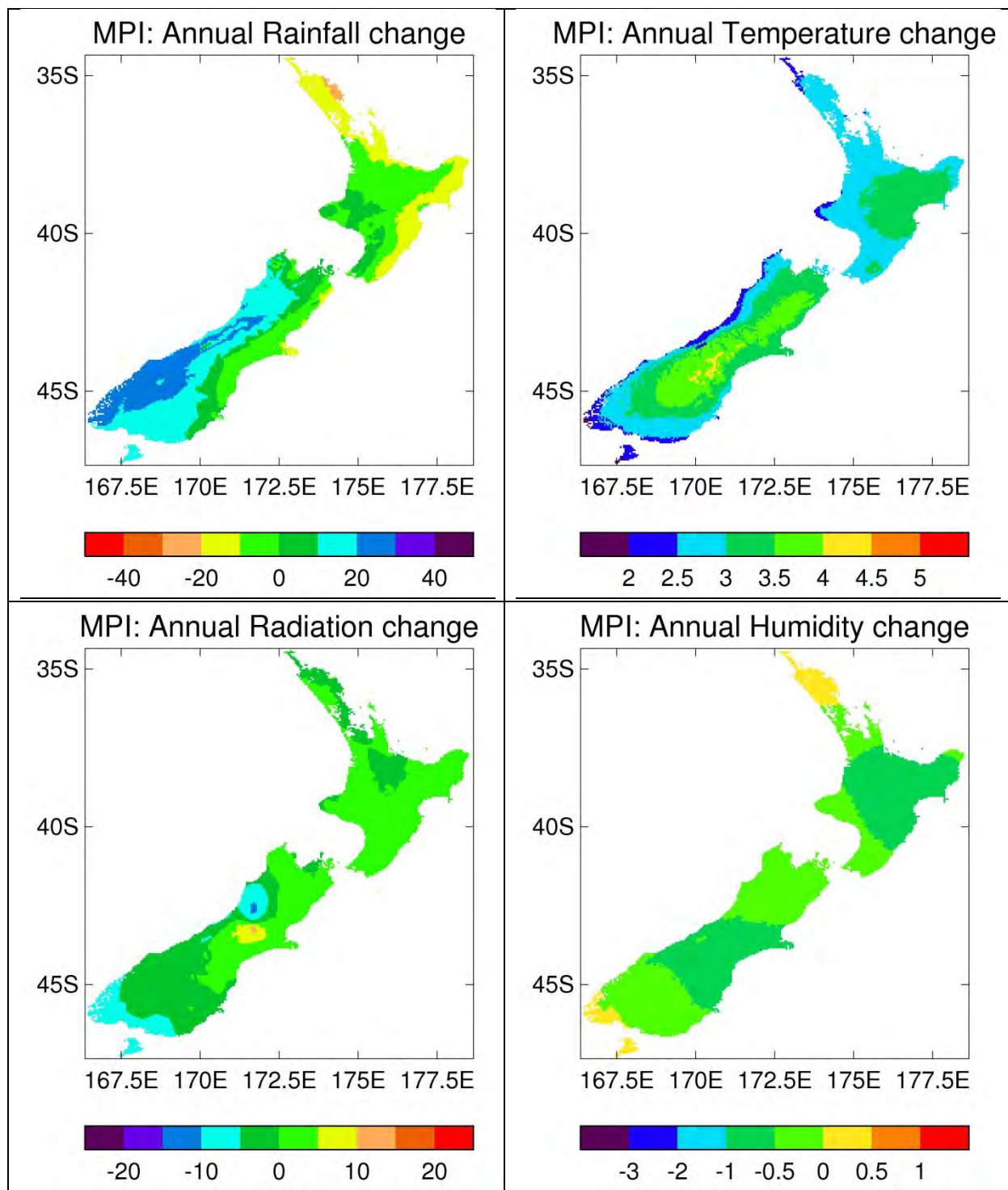


Figure 3-4: Downscaled projections of annual changes between 1990 and date of 4°C global warming, for Planck model: rainfall (as %, top left); mean temperature (in °C, top right); mean-daily solar radiation (as %, bottom left); relative humidity (in %, bottom right).

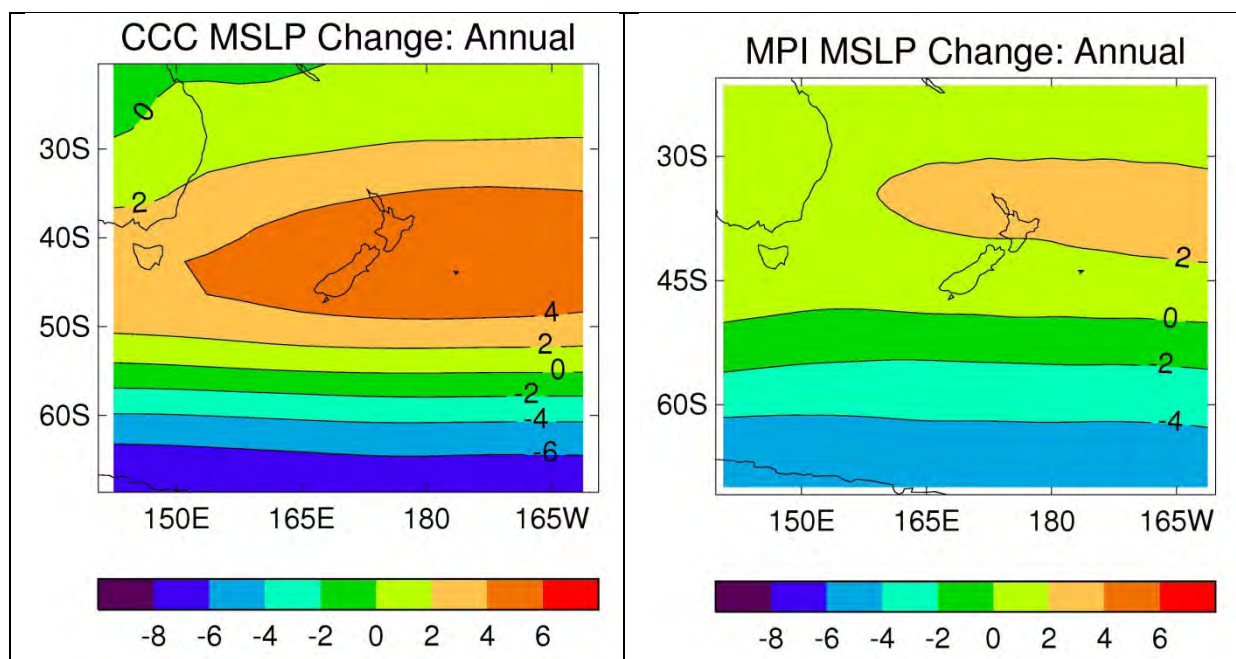


Figure 3-5: Global model changes in annual mean sea-level pressure (in hPa) between 1990 and date of 4°C global warming, for: CCC model (left) and Planck model (right).

3.3.6 Changes in carbon dioxide concentration

Some of the impact models used in this study require a value for the daily atmospheric concentration of carbon dioxide (CO_2). While CO_2 levels for the past climate are readily available, it is not straightforward to specify the future levels. The global model climate projections are taken from simulations driven by the IPCC SRES A2 scenario, where greenhouse gas concentrations are specified up to 2100, but not beyond. Because the CCC and Planck scaling is greater than 1, the effective date of 4°C warming is beyond 2100, for which no CO_2 levels are available.

The decision made here is as follows:

- For the current climate, CO_2 concentrations are taken as representative of the years 1997 to 2011, which corresponds to the 15-year period of baseline data.
- For the “4°C warming” climate, CO_2 concentrations are taken from the last 15 years of the SRES A2 scenario; that is, the years 2085 to 2099.

Table 3-5 shows the annual CO_2 concentrations used with the current and future climate data. The CO_2 data have been taken from the ISAM Reference carbon cycle model, as given in a table published by the European ENSEMBLES regional scenario project, <http://www.cnrm.meteo.fr/ensembles/public/results/results.html>. The same CO_2 concentrations are assumed in the scenario files of both models, even though the CCC and Planck models will reach the 4°C warming point at different times.

Table 3-5: Annual carbon dioxide concentrations (in ppmv) used in the study, for the two 15-year periods of the current baseline period and the future “4° warming” period.

Current Climate		“4° warming” Climate	
Year	CO2 concentration	Year	CO2 concentration
1997	362.7	2085	716.8
1998	364.1	2086	724.0
1999	365.6	2087	731.4
2000	367.0	2088	738.8
2001	368.6	2089	746.3
2002	370.2	2090	754.0
2003	371.9	2091	761.8
2004	373.6	2092	769.6
2005	375.5	2093	777.5
2006	377.4	2094	785.6
2007	379.4	2095	793.7
2008	381.4	2096	802.0
2009	383.7	2097	810.3
2010	386.0	2098	818.8
2011	388.5	2099	827.3

3.3.7 Daily time series

The Virtual Climate Station Network (VCSN) provides the daily weather input required by the impact models used in this study, such as the Biome-BGC model (Section 8). The baseline scenario covers inputs for the 15-year period 1997-2011. Future climate under the scenario of 4°C of global warming circa 2100 was statistically downscaled to the VCSN by NIWA using the two GCMs CCC and Planck. This input also covers a future 15-year period, nominally assigned the years 2097-2111.

The climate data are provided in what is known as the APSIM Met file format (APSIM=Agricultural Production Systems Simulator). Table 3-6 below shows an example of layout of the file. Each row of the table represents climate elements for a specific day. Each APSIM file has 15 years of data daily at an identified VCSN data point, of which there are 11,491 to cover all of New Zealand. Separate sets of files are provided for the current climate and for the CCC and Planck 4-degree future climates.

Note that the SRES CO₂ concentrations are not defined past the year 2100. For the purpose of the APSIM scenario files, the CO₂ concentrations from Table 3-5 are assumed to apply to the nominal scenario years of 2097-2111, instead of 2085-2099.

Table 3-6: Sample APSIM file data for the first five days in 1997, and the first 5 days in 2097 under the CCC model scenario, for the VCSN grid-point number 3027, centred at latitude 45.325°S and longitude 166.825°E (near Doubtful Sound in Fiordland).

year (¹)	day (¹)	rain (mm)	maxt (°C)	mint (°C)	mean (°C)	radn (MJ/m ² /d)	wind (m/s)	vpd (mbar)	9am_vp (mbar)	9am_RH (%)	9am_svp (mbar)	9am_vpd (mbar)	CO2 (ppm)
1997	1	0.0	14.1	11.3	12.7	27.1	4.2	2.3	12.4	77.2	16.1	3.7	362.7
1997	2	1.2	13.9	9.7	11.8	14.1	1.5	0.8	13.2	89.4	14.8	1.6	362.7
1997	3	6.1	17.1	7.9	12.5	24.6	4.4	3.8	11.3	79.5	14.2	2.9	362.7
1997	4	0.0	13.0	6.1	9.6	25.4	5.8	4.0	8.2	68.0	12.1	3.9	362.7
1997	5	0.0	14.4	3.2	8.8	25.3	4.6	4.1	7.9	67.7	11.7	3.8	362.7
2097	1	0.0	17.9	15.1	16.5	29.8	4.2	3.2	15.7	76.3	20.6	4.9	716.8
2097	2	0.0	17.7	13.5	15.6	15.5	1.5	1.1	16.8	88.5	19.0	2.2	716.8
2097	3	4.7	20.9	11.7	16.3	27.0	4.4	5.0	14.3	78.6	18.2	3.9	716.8
2097	4	0.0	16.8	9.9	13.4	27.9	5.8	5.2	10.5	67.1	15.6	5.1	716.8
2097	5	0.0	18.2	7.0	12.6	27.8	4.6	5.4	10.1	66.8	15.1	5.0	716.8

Climate elements include the daily precipitation, maximum and minimum and daily-mean temperatures, solar radiation, wind run, vapour pressure deficit, relative humidity and CO₂ concentration. The climate scenario changes are evaluated at the monthly time scale, and applied as offsets to the current climate (Appendix A2 provides details of the procedure). This means that the future data will follow essentially the same weather sequence of wet/dry, warm/cool, windy/calm, etc, days, but the actual values of the weather variables will be adjusted according to the scenario offsets.

In the sample data of Table 3-6, the following changes for the first five January days are evident:

- Temperature is increased by 3.8°C, and applied equally to maximum and minimum;
- After applying the monthly rainfall offsets for a future climate (drier in summer in the CCC model, Figure A1-2), the daily rainfall is redistributed to increase the extremes in the upper tail. This requires also introducing more dry days and reducing rainfall amounts on low rainfall days (e.g., days 2 and 3 in Table 3-6);
- Solar radiation increases by 10% in January (CCC model, Figure A1-8);
- Wind speed is unchanged;
- Relative humidity reduces by 0.9% (CCC model, Figure A1-11).

Changes in the other humidity variables are discussed in Appendix A2.

4 Frosts and Growing Degree Days

4.1 Introduction

The occurrence of frosts, and the amount of heating provided to developing plants, are important constraints on plant growth in all regions. Changes in frost frequency and growing degree-day totals were calculated directly from the VCSN temperature information provided for the current climate (1997-2011) and the two future scenarios (nominally 2097-2111) for the CCC and Planck GCMs (e.g. Tait 2008). Statistics of frost occurrence are based on the number of times the minimum temperature at each VCSN point falls below 0°C. Three basic statistics were calculated:

1. The mean frost period, calculated as the number of days from the average date of first frost for the year to the average date of last frost for the year.
2. The 1-in-5-year earliest day of frost occurrence, i.e., the 20th percentile of the distribution of day of first frost (at each VCSN point).
3. The 1-in-5-year latest day of frost occurrence, i.e., the 80th percentile of the distribution of day of last frost (at each VCSN point).

For each statistic, a baseline was calculated from the present climate data, and future changes from the downscaled scenario estimates.

Growing degree-days (GDDs) are a measure of heat accumulation used to estimate plant development and crop maturity. They are calculated above a set threshold or base temperature, for example 5°C. The mean temperature (average of maximum and minimum) for a day has the base temperature subtracted from it, and if the difference is positive (i.e., the average temperature for the day is above the base temperature), it is added to the GDD total for the season, year or whatever time period is being considered.

Here, GDD accumulations were averaged over the years in the present climate data set (1997-2011) and for the two '4-degree' scenarios.

4.2 Results: Frost frequency

As expected from the magnitude of the temperature rises over New Zealand (section 3), under both scenarios, the frequency of frosts and the mean length of the frost 'season' decreases dramatically at all locations. Maps of annual mean frost period (average number of days between average dates of first and last frost), and timing of 1-in-5-year day of first and last frost are shown in Figures 4-1 to 4-4, for the current climate and for both future scenarios.

For the CCC scenario, frosts cease to occur in the North Island lowlands, but still occur on the volcanic plateau and at higher elevations in the Urewera and Tararua ranges, where the mean frost period reduces to around two to three months during winter. In the South Island, frosts no longer occur in coastal regions of Marlborough, Canterbury, and Southland. For the Planck scenario, a similar pattern emerges, but the frost-free region is confined to lower altitudes.

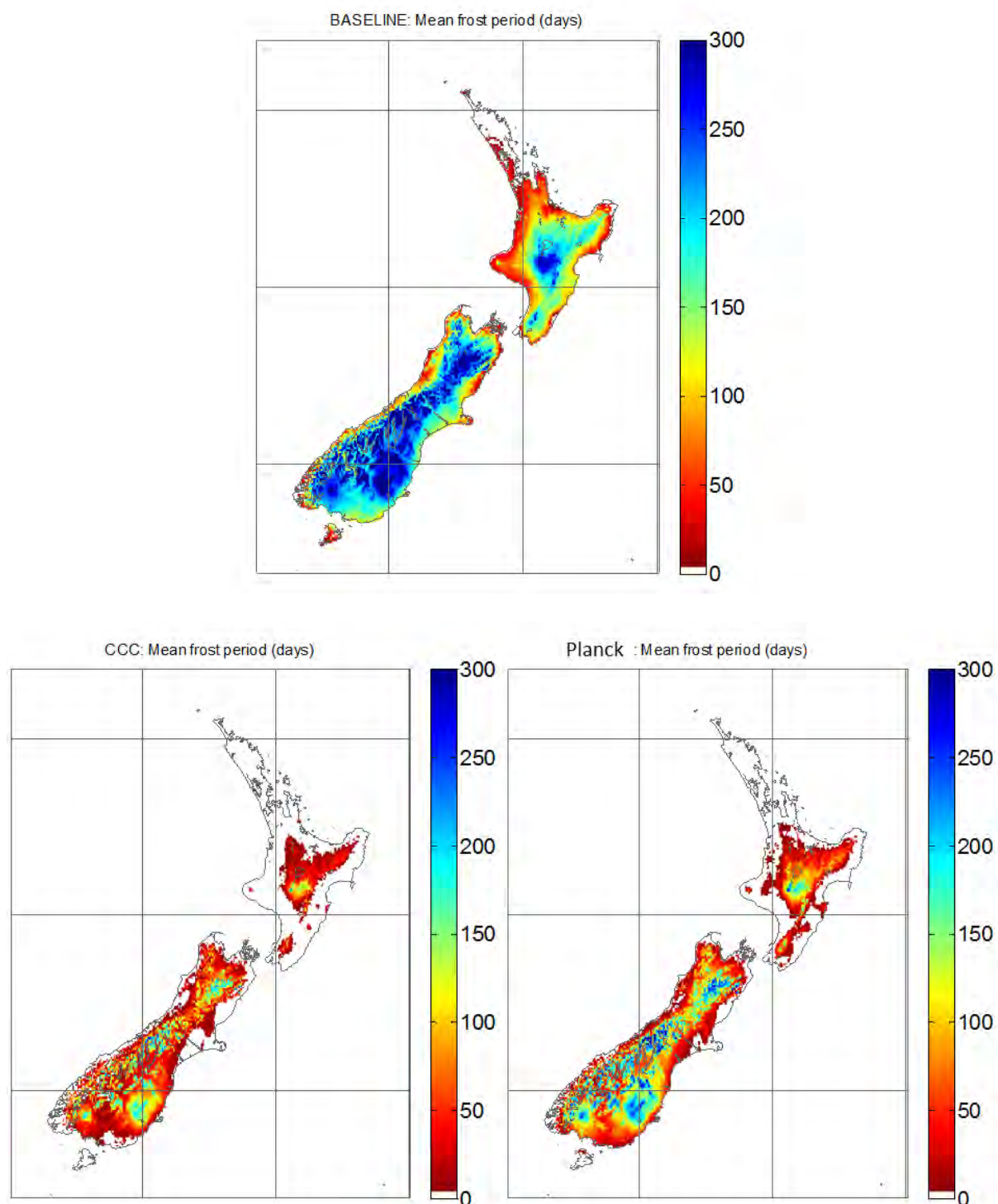


Figure 4-1: Top – mean present-day (1997-2011) length of the frost period (time in days from the average day of first frost to average day of last frost). Bottom, left – mean frost period (days) for the CCC scenario. Bottom, right – mean frost period (days) for the Planck scenario.

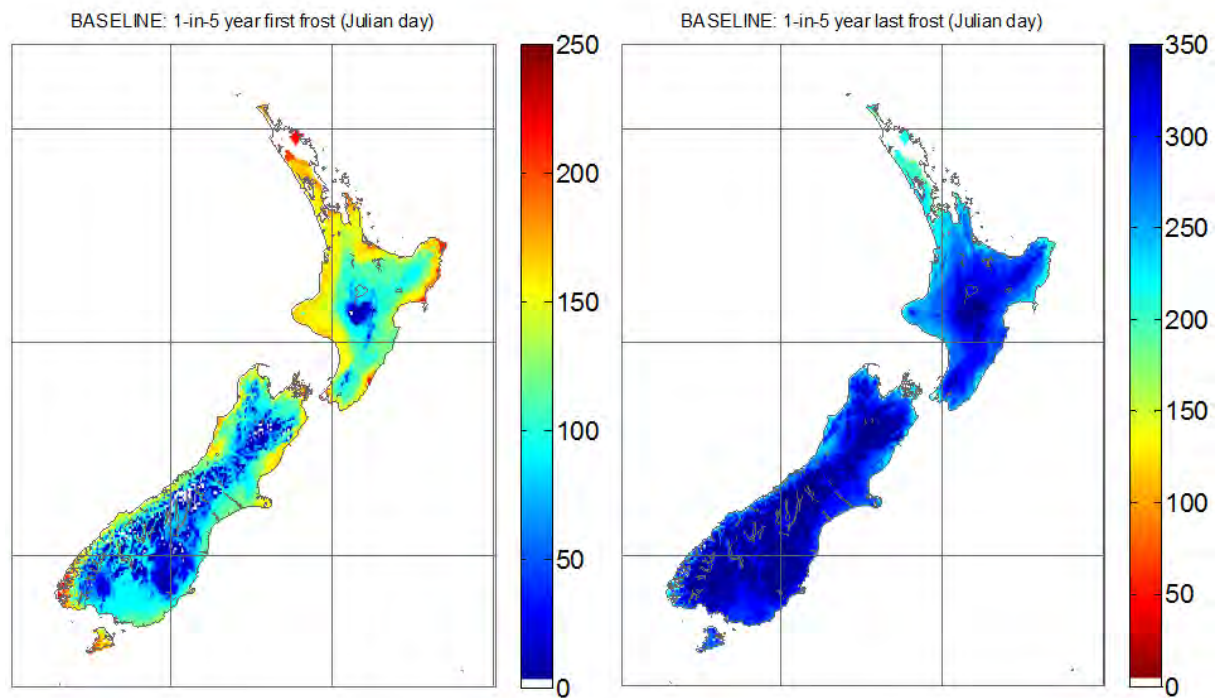


Figure 4-2: Mean present-day (1997-2011) Julian day of the (left) 1-in-5-year first frost, and (right) 1-in-5-year last frost.

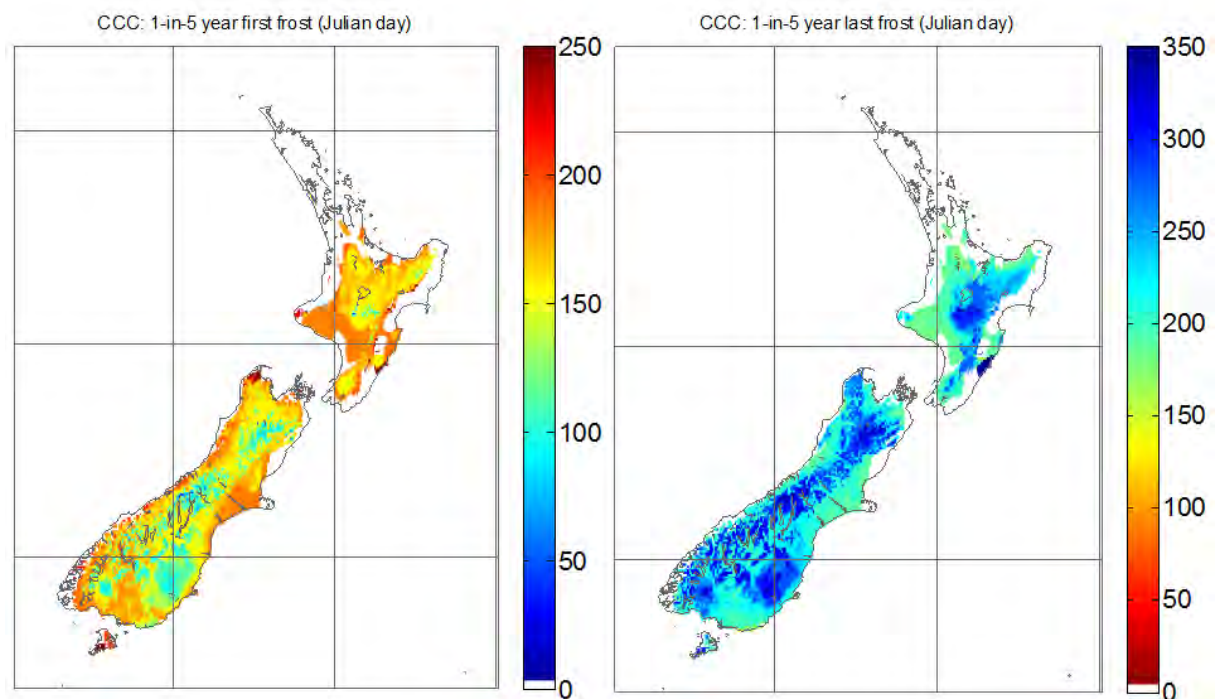


Figure 4-3: As in Figure 4-2 but for the CCC scenario (nominally 2097-2111 average).

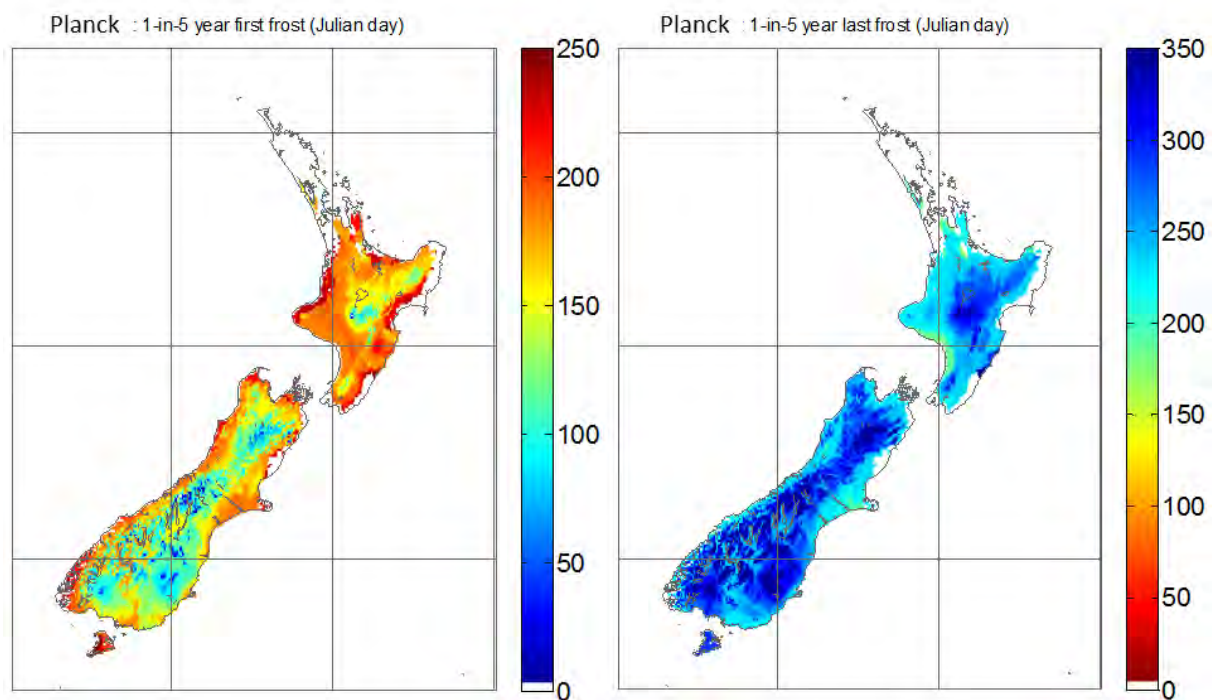


Figure 4-4: As in Figure 4-2 but for the Planck scenario (nominally 2097-2111 average).

4.3 Results: Growing Degree-days

Growing degree days above a base temperature of 5°C (GDD05) range over approximately a factor of two across New Zealand, from around 2000 in alpine regions to 4000 degree-days at lower-elevation northern locations (Figure 4-5, left). Growing degree days above a base temperature of 10°C (GDD10) also range over approximately a factor of two across New Zealand, from around 1000 in alpine regions to 2000 degree-days at lower-elevation locations (Figure 4-5, right).

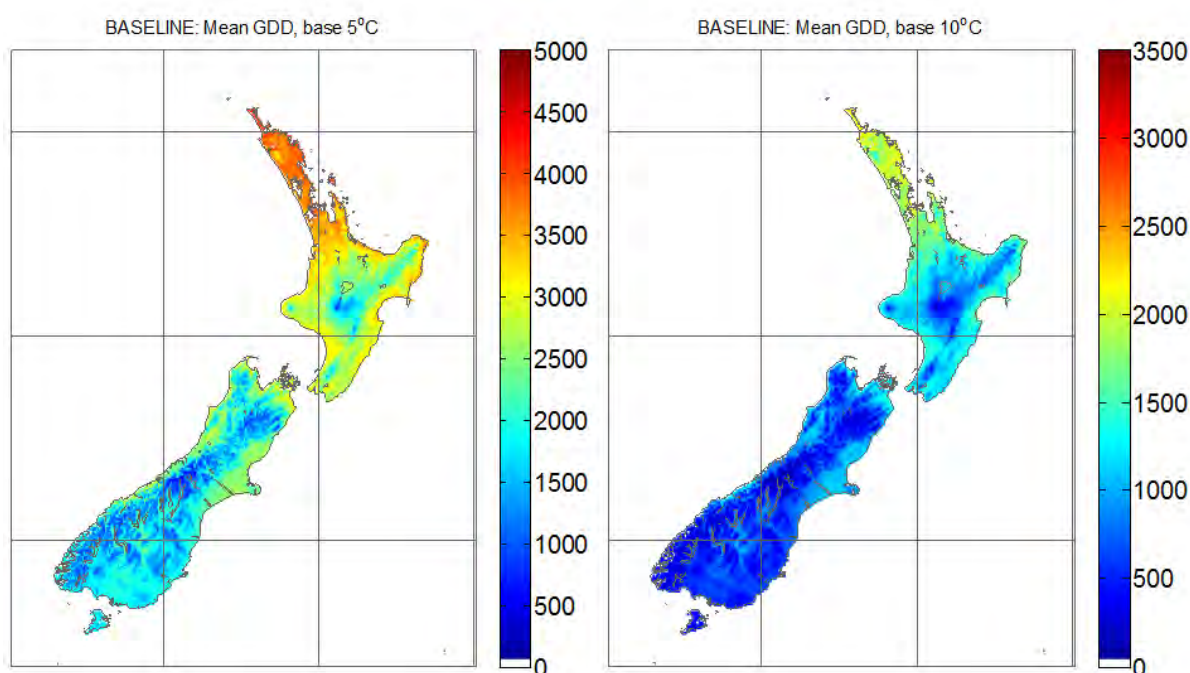


Figure 4-5: Mean present-day (1997-2011) GDD05 units (left, base temperature 5°C) and GDD10 units (right, base temperature 10°C). Note the different colour scales.

The large projected increases in temperature associated with both future scenarios are associated with significant increases in growing degree day (GDD) totals across the whole country (Figs. 4-6 and 4-7). Projections indicate an increase of 1000-1500 GDD05 units across all regions of New Zealand, and increases of 500-1500 GDD10 units across the whole country. The CCC scenario shows the largest increases, as it exhibits the largest increases in mean temperature. For both models, increases of 30-60 percent are typical for GDD05, and 70-120 percent for GDD10.

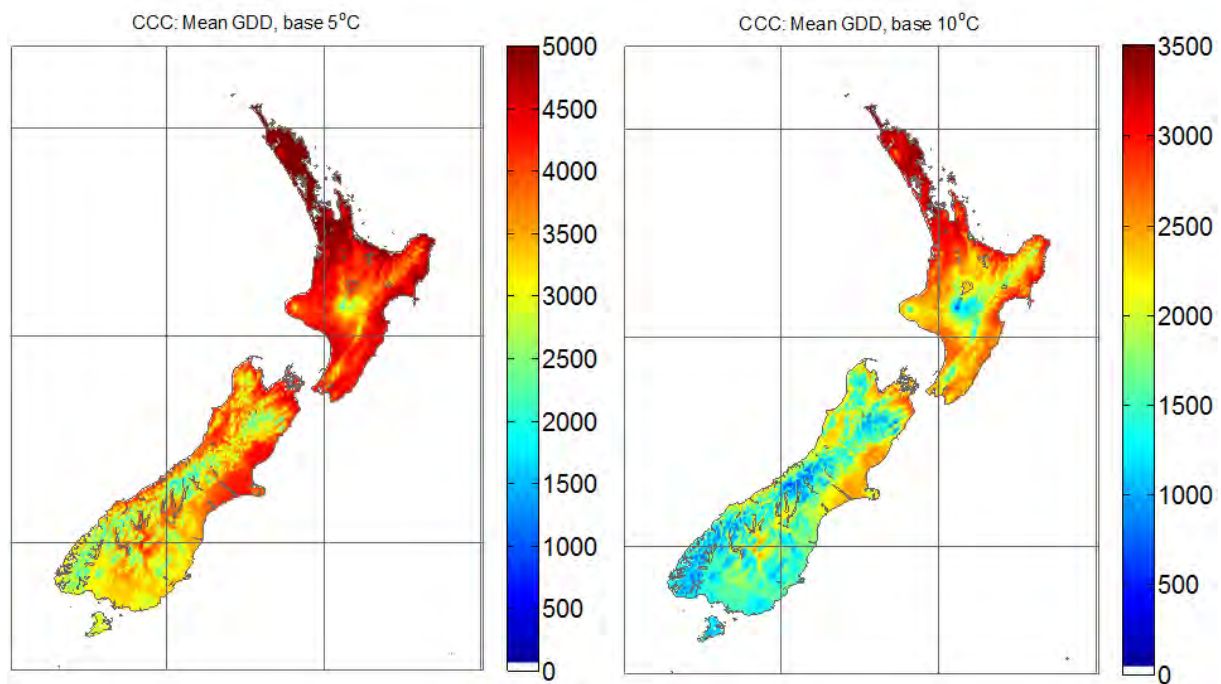


Figure 4-6: As in Fig. 4-5 but for the CCC scenario (nominally 2097-2111 average).

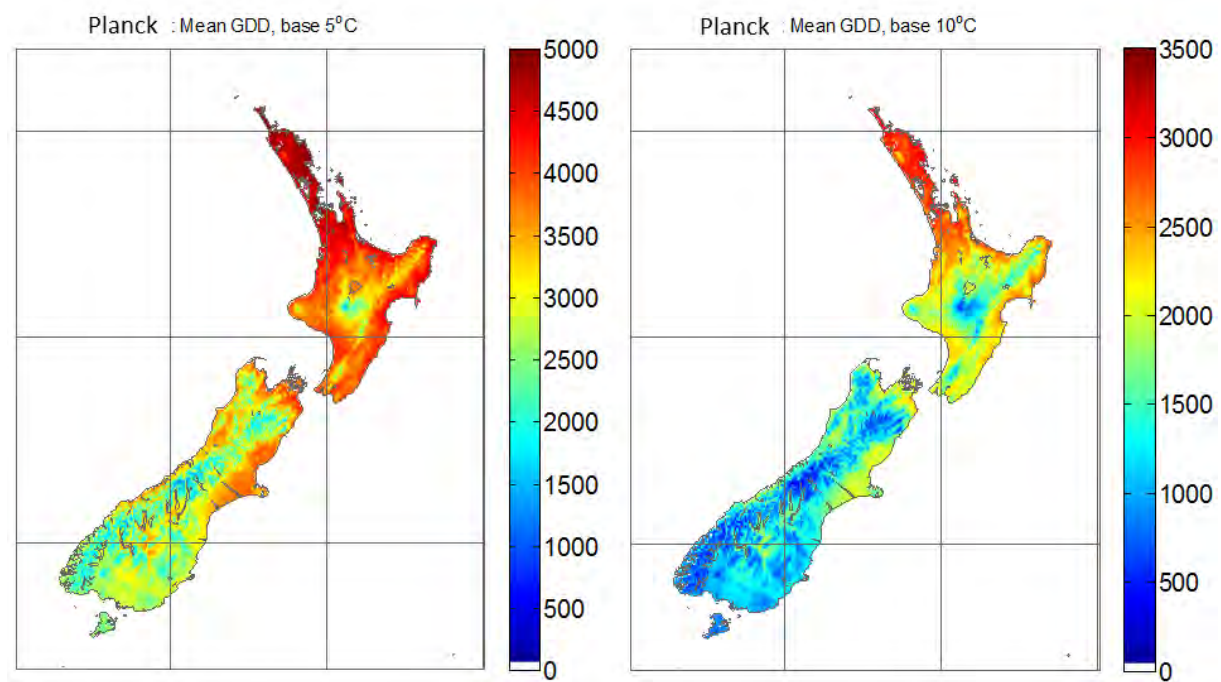


Figure 4-7: As in Fig. 4-5 but for the Planck scenario (nominally 2097-2111 average).

4.4 Summary and Implications

For all regions of the country, frost frequency is projected to decrease sharply, and GDD accumulations to increase by between (roughly) 50 and 100 percent, depending on location and scenario. Frosts become very rare or unknown at most lowland locations, implying considerably lengthened growing seasons and reduced temperature limitations for crop growth. Conversely, warmer winters imply reduced die-off of pest species and reduced winter chilling for crops that require it (e.g. pip- and stone-fruit). Broadly speaking, eastern districts of both Islands are projected to see the largest changes.

Growing degree-day increases on the order of 1000 units are very significant for New Zealand agriculture, horticulture and viticulture. A rough rule of thumb is that grape vines require at least 1000 GDD units (above a base temperature of 10°C) to mature. On that basis, grapes could be grown at all lowland locations in New Zealand under either scenario, right through to the Southland coast and in some parts of Stewart Island. Note however that conditions may become too warm in summer for some grape varieties in some parts of the country, and no account has been taken here of other factors such as changes in pest species.

As another example, kiwifruit currently grow successfully in the Bay of Plenty, where the mean frost period is 50-100 days (Figure 4-1) and the average number of GDD10 units is around 1500 (Figure 4-5). Under the CCC scenario, such climate statistics are projected to occur on the volcanic plateau and in parts of inland south Canterbury and Otago. Under the Planck scenario, again the volcanic plateau, Canterbury, Otago and Southland are projected to exhibit those kiwifruit-related climate statistics currently seen in the Bay of Plenty.

5 Extreme rainfall and flood flows

5.1 Introduction

Extreme rainfalls and flood flows are an important consideration for the primary sector in New Zealand, as they are associated with hillside slipping and erosion, and loss of topsoil and nutrients through enhanced runoff.

The maximum amount of moisture in the air (the 'saturation vapour pressure') is a very strong function of temperature. For each 1°C increase in temperature, the saturation vapour pressure increases approximately 8%. Maximum rainfall amounts could therefore increase by a similar amount as the climate warms, or even more rapidly if changes to the atmospheric circulation act in a mechanical sense to enhance precipitation processes (e.g., increased westerly wind strength increases the uplift and rainfall over the steep topography of the Southern Alps).

Here, rainfall extremes are considered purely from the point of view of increasing saturation vapour pressure, and were calculated assuming four degrees of warming at all locations on the VCSN grid. This approach was taken since moisture is transported long distances in the atmosphere, and it is difficult to ascribe an increase water vapour to an increase in temperature at any one location.

River flows are considered in much more detail (as described below), in terms of modelled changes in many aspects of the hydrological cycle, including rainfall, temperature, snow accumulation and melt, and evaporation (related to the above parameters as well as to wind speed and solar radiation).

5.2 Extreme rainfall

High intensity rainfall estimation for any location in New Zealand is provided by the NIWA software package HIRDS-Version 3, available from the NIWA web site (www.niwa.co.nz/software/hirds). HIRDS provides storm rainfall depths for durations from 10 minutes to 72 hours for storm events with average return intervals (ARIs) ranging from one year to 100 years.

Changes in extreme rainfall were calculated for the 100-year ARI, based on a temperature change of four degrees at all locations. Such a temperature change is assumed to be associated with a 32% increase in extreme rainfall at all locations: a factor of 8% increase per degree of warming, which is appropriate for the 100-year ARI shown here (Ministry for the Environment 2008). At most lowland locations, total rainfall increases are between 50 and 100mm for 24 and 48h durations, and less than 50mm for the 12h duration. The 8% factor is an average, based on the physical relationship between temperature and saturation water vapour pressure). However, changes in the atmospheric circulation (leading for example to increased near-surface moisture convergence) can lead to larger increases. Preliminary analysis of NIWA regional climate model results indicates that increases substantially higher than the upper limit of 8% given in this table are possible in limited areas.

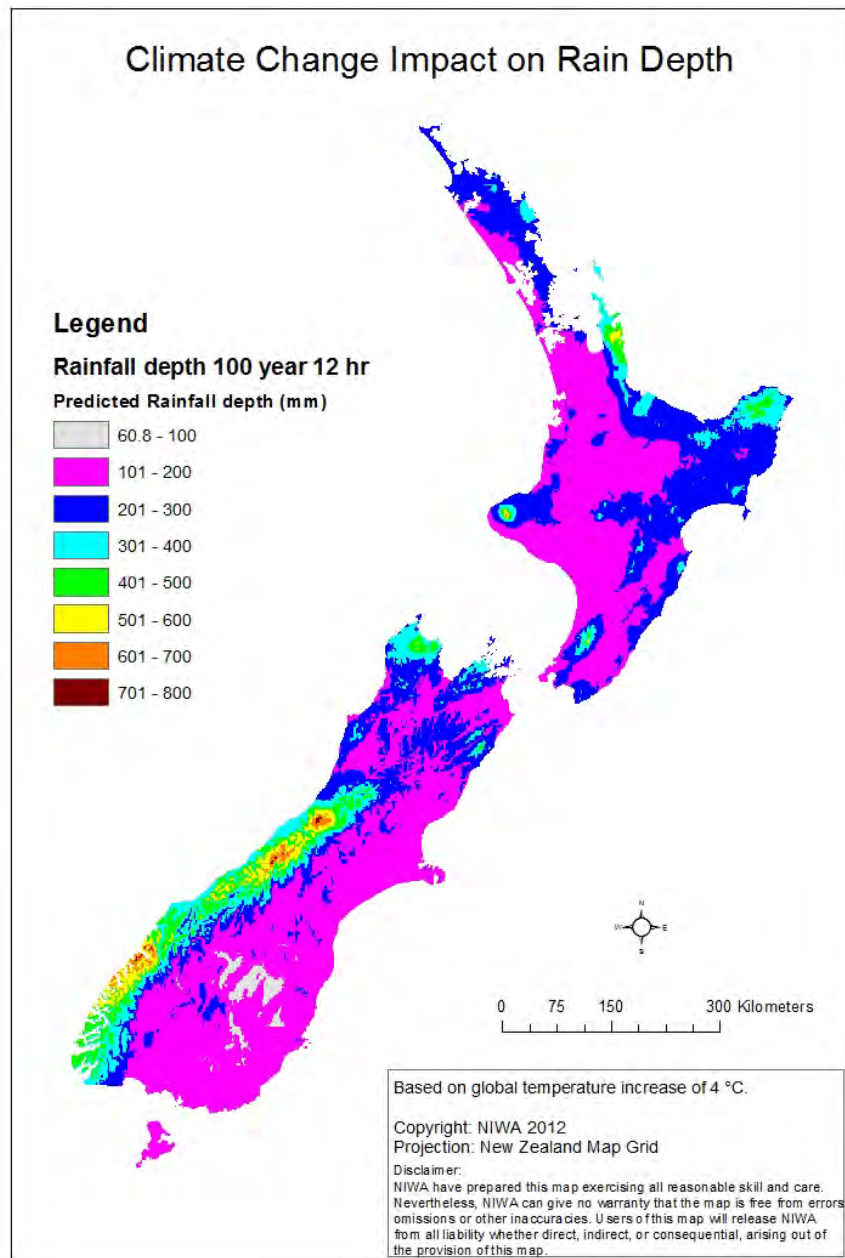


Figure 5-1: Twelve-hour duration rainfall totals for the 100-year ARI, assuming a warming of four degrees Celsius.

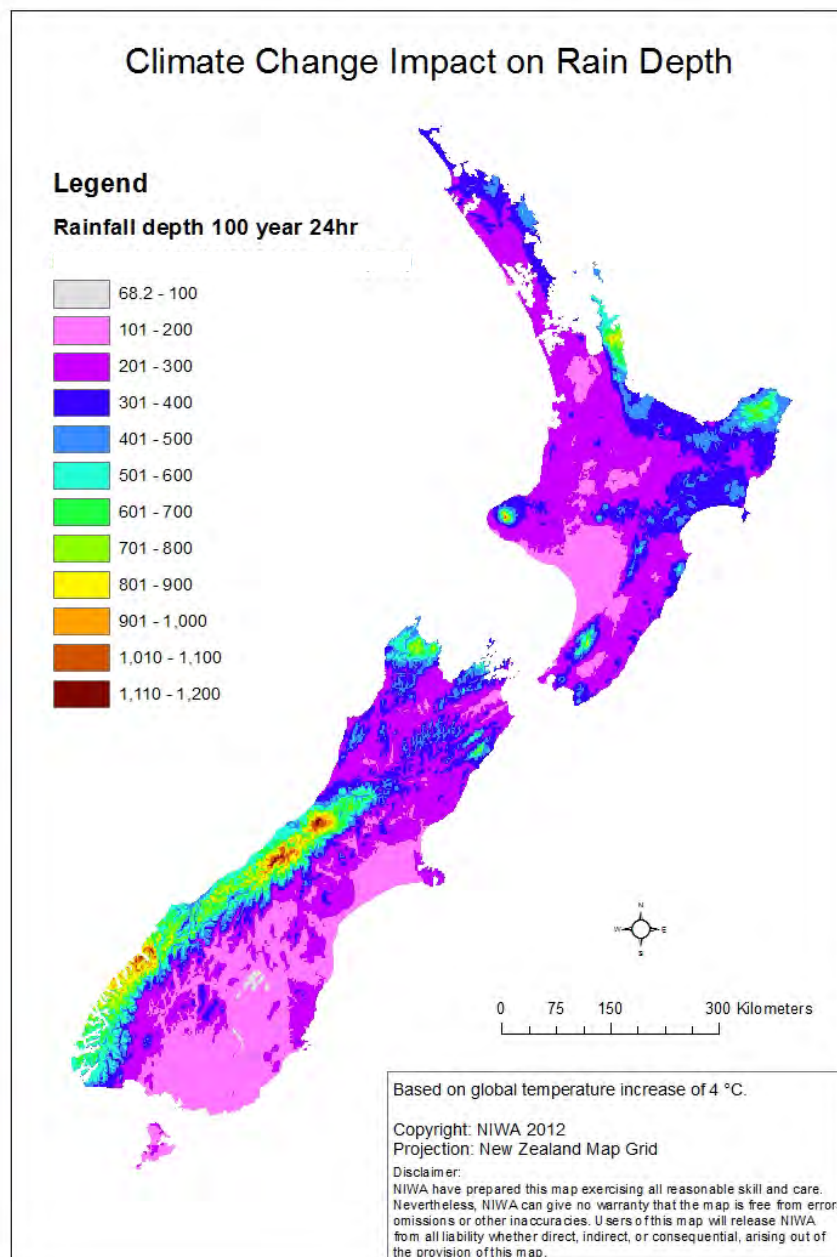


Figure 5-2: Twenty-four-hour duration rainfall totals for the 100-year ARI, assuming a warming of four degrees Celsius.

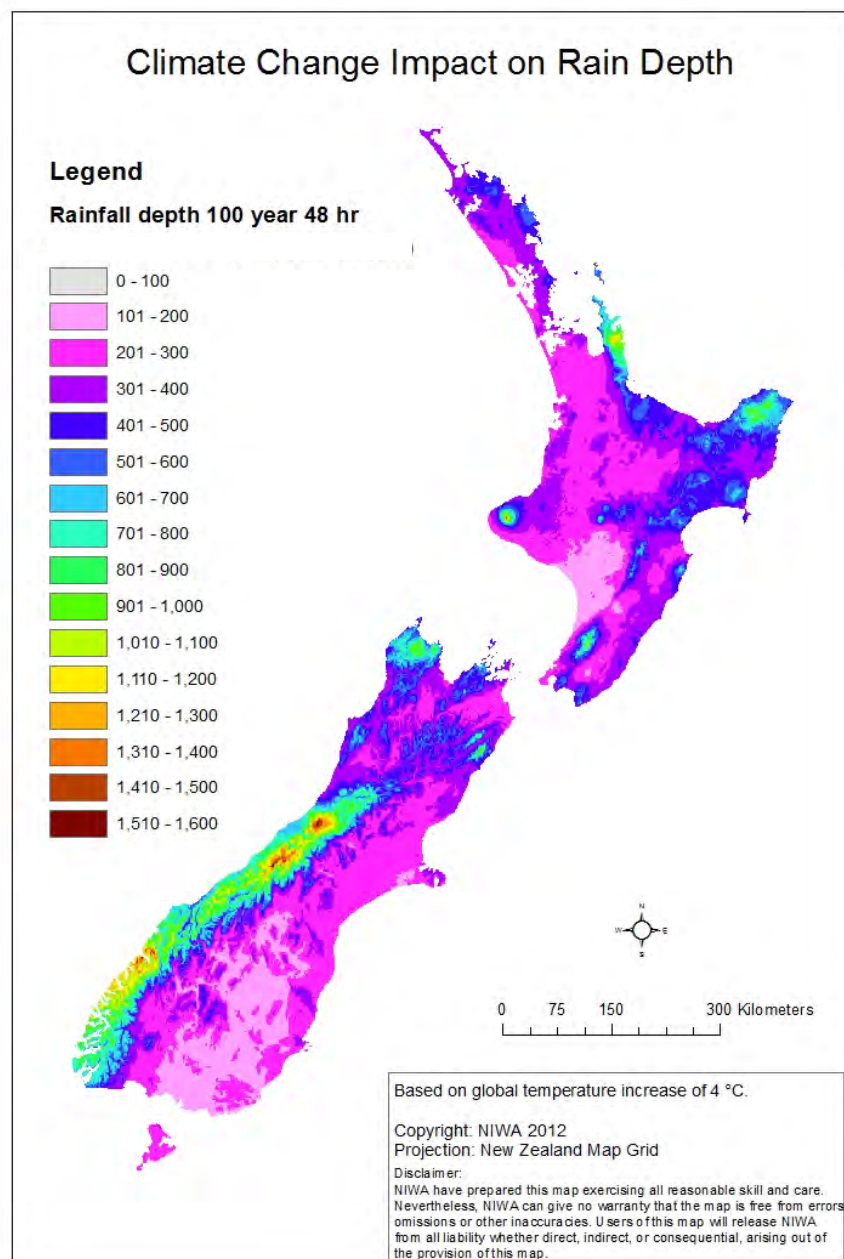


Figure 5-3: Forty-eight-hour duration rainfall totals for the 100-year ARI, assuming a warming of four degrees Celsius.

All the above changes in rainfall totals, for the 100-year ARI at different accumulation periods from 12 to 48 hours, represent a 32% change from the current totals for each period. However, the impacts of such changes vary regionally, dependent on the background mean rainfall and on details of the topography, susceptibility to land slipping or runoff/flooding.

Regions that are projected to experience the largest increases in extreme rainfall totals, and which are susceptible to erosion events, include the Coromandel Peninsula and eastern North Island regions from Bay of Plenty to Gisborne/Hawkes Bay where, for example, increases in the 24h 100y ARI totals are projected to be between 50 and 150mm. Such increases in extreme rainfalls suggest that current agricultural practices (such as stocking rates, land use, tree planting and infrastructure design, e.g., culverts, tracks and bridges on-farm) may need to be adapted to manage the change in flooding and erosion risk. For further information, refer to Chapter 5 of the Clark et al. (2012) Sustainable Land Management report on *Impacts of climate change on land-based sectors and adaptation options*.

5.3 River/flood flows

5.3.1 Methods

TopNet description

TopNet uses a spatially explicit representation of the catchment, based on subcatchment boundaries (area of around 10 km²). A schematic representation is shown in Figure 5-4. TopNet operates in three steps:

1. Input precipitation and temperature is disaggregated to the subcatchment hourly scale.
2. Water balance is solved for each subcatchment for each timestep, including snow calculations (Clark et al. 2008, 2009).
3. Streamflow is routed using a one-dimensional Lagrangian kinematic wave routing scheme, through the stream network to the basin outlet (Clark et al. 2008).

The snow module in TopNet is based on the temperature index method (Clark et al. 2008), which tracks snow quantity in the subcatchment, defined as SWE (snow water equivalent), controlled by snow accumulation and melt rates, and the sublimation rate. Snow is especially sensitive to temperature, so each subcatchment is divided into elevation bands (typically 100 m vertical distance), which have differing air temperatures calculated using a standard lapse rate. Snow accumulation and melt is calculated per elevation band, and summed to give totals for each subcatchment.

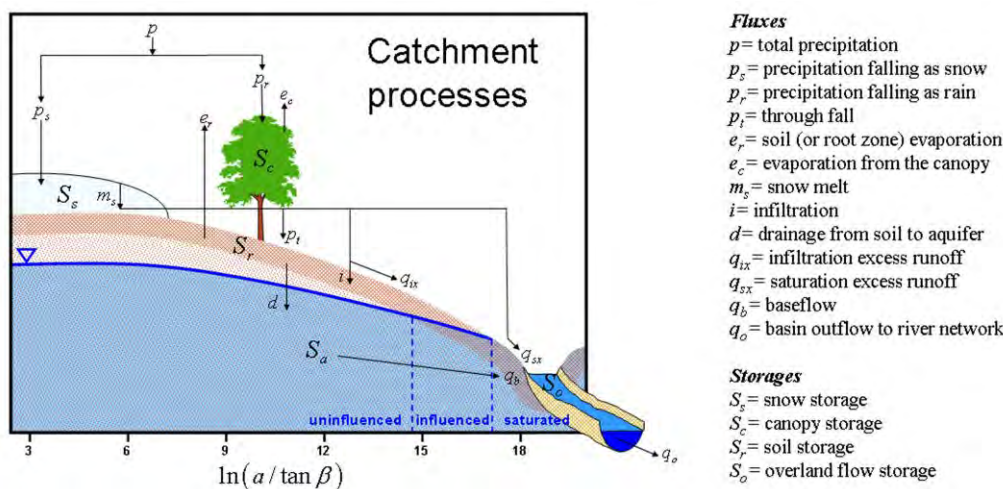


Figure 5-4: Schematic representation of TopNet; the topographic index $\ln(a/\tan\beta)$ increases towards the stream indicating areas of topographic convergence and areas where the water table intersects the soil zone.

A temperature threshold defines whether precipitation falls as rain or snow. Snow melt is largely controlled by temperature, at the expense of ignoring many important melt processes (Clark et al. 2009). Therefore a time-varying melt factor has been introduced, which takes into account seasonality (availability of energy for melt), enhanced melt during rain-on-snow events and changes in albedo (Clark et al. 2009).

Model calibration

For each subcatchment, initial values of spatial parameters (elevation distribution, wetness index, soil hydraulic conductivity, infiltration capacity, overland flow velocity) are estimated from the New Zealand River Environment Classification (Snelder and Biggs, 2002) and the New Zealand Land Resource Inventory and the New Zealand Land Cover Database (Newsome et al., 2008), and are then calibrated. For calibration, a subset of the spatial parameters (mainly around soil hydraulic properties) are modified, while retaining the initial spatial distribution of the parameters. Two catchments were calibrated using the ROPE (Robust Parameter Estimation) algorithm (Bárdossy and Singh 2008), while the remaining catchments were calibrated using a semi-objective method based on assessment of a large series of trials with different parameter settings.

The hydrological/snow model was calibrated using historical precipitation and temperature data from the Virtual Climate Station Network (VCSN) (Tait and Turner, 2005, Tait et al., 2006, Cichota et al. 2008). The VCSN precipitation was corrected for spatial bias, based on a water balance approach (Woods et al., 2006). Daily maximum and minimum temperatures were altitude-adjusted using standard atmospheric temperature lapse rates (Norton 1985, Clark et al. 2009). Uncertainty in observed data was not modelled, as the uncertainties regarding which emissions scenario and GCM will best approximate future climate were assessed as more important.

Using a hydrological model for a future climate may require the model to be used outside the range of conditions used for calibration. The TopNet model has a relatively strong physical basis, and considerable effort has been made to ensure that the dominant rainfall-runoff dynamics are adequately represented by the model. For example, the soil water dynamics of TopNet have been compared with a small-scale 3D Richards Equation model (McMillan et al., 2010b). During calibration, further care is taken to ensure that the model remains realistic: model parameters are bounded to ensure they lie between physically reasonable limits, and model behaviour is checked using multiple diagnostics including seasonal patterns and model water-balance. Accuracy is estimated in terms of the Nash–Sutcliffe efficiency coefficient calculated on the discharge (NS) and on the logarithm of the discharge (NS Log).

5.3.2 Study area

The research aims to provide a broad range of national-scale information about the vulnerability of New Zealand’s primary sector to climate change, focussing on a high end scenario. As a result, the hydrological modelling effort was focussed mainly on catchments where the main land use is for primary sector activities, as well as catchments that will be used as a reference for the effect of climate change on hydrological regime. These catchments are:

- Ahuriri: An alpine catchment within the Upper Waitaki basin in the South Island (Appendix A – note that all hydrology-related appendices are in a companion document). A small proportion of the catchment, close to the outlet of the catchment and the streamflow gauging station, is subject to primary sector use. Due to the importance of snowmelt in flow generation during the irrigation season, the catchment is used as a reference for climate change impact on river flows.
- Rangitaiki: The only North Island catchment in this study (Appendix B). It contains four gauging stations, one being affected by a large storage area located at Matahina, which affects discharge at the most downstream gauging station (Te Teko). Analysis of the land use information shows two large primary production areas. The most upstream area is downstream of the gauging stations at Galatea and Murupara, while the downstream area covers the outlet of the catchment and contains the gauging station at Te Teko (see Appendix B). Additional information regarding hydrological modelling of the Rangitaiki catchment is contained in McMillan and Clark (2009).
- Waimakariri: The Waimakariri River is an alpine river that emerges from the eastern face of the Southern Alps, flows through the Canterbury Plains and discharges to the ocean. The majority of the agricultural areas and population centre in the Waimakariri catchment are located on the Canterbury Plains (Srinivasan et al, 2011, Zammit and Woods, 2011a). All the primary sector users in the Waimakariri catchment are located on the Canterbury Plains, downstream of the Otarama gauging station (Appendix C). All results are reported for the Waimakariri at Old Highway Bridge.

- Ashley: The Ashley is a foothills river that emerges from the southern end of the Puketeraki range, and flows through the Canterbury Plains. The Ashley Irrigation Area is a subpart of the Waimakariri Irrigation Area, and covers a significant part of the Canterbury Plains. (Zammit and Woods, 2011b). Primary sector users are located upstream in the catchment (downstream of the Lees Valley gauging station, see Appendix D) and on the Canterbury Plains. The three gauging stations are located upstream of each of the primary sector users (Appendix D). The results will be presented only for the gauging station with the largest catchment area (i.e., Ashley at Gorge). All the results for the two remaining gauging stations are available in Appendix D.
- Rangitata: The Rangitata also drains the Southern Alps through the Canterbury Plains and discharges to the ocean. The catchment upstream of the gauging station has a small area covered by primary sector users. However, land further downstream has been considered as a prime importance for irrigation with the establishment of additional irrigated area (Woods et al, 2008). All the results are available in Appendix E.
- Clutha: The Clutha catchment in Otago lies on the south-east side of the Divide. With a mean flow of approximately 600 m³/s, the Clutha is New Zealand's largest-volume river, draining 21,960 km². The catchment is characterised by its large lakes (Lake Wakatipu, Lake Wanaka and Lake Hawea), as well as the hydropower dams at Clyde and Roxburgh. Lake Hawea's outflow is significantly modified for hydropower production, whereas Lake Wanaka and Lake Wakatipu have natural outflow regimes (Poyck et al, 2011). Results at four streamflow gauging stations are available for this climate change study. However, only the most downstream gauging station is of interest for primary sector users. As a result, climate change impacts will be presented only for Clutha at Balclutha, but are available for the remaining three gauging stations in Appendix F.

5.3.3 Methodology

The method used to define the changes to rainfall and temperature is described in Section 3. Two GCMs, 'CCC' and 'Planck' are used to simulate the effects of climate change. In order to allow comparison with existing time series of flow discharge, results are presented only at most downstream flow gauging station for each of the catchments. The climate change impact will be determined and presented in terms of impacts on:

- Maximum and average annual discharge, as well as flow duration curve. This provides information on the general hydrological characteristics of the discharge.
- High flow and low flow threshold. This provides information on important flow characteristics for primary sector users.
- Distribution of the flow during each month of the year, providing information on changes to the seasonality of the discharge.
- Distribution of the minimum, average, maximum flow estimated for each month.
- Distribution of the total monthly flow.

5.3.4 Results and discussion

For sake of simplicity, this section will present only the results of the simulations at the most downstream gauging station. However all the results are presented for all gauging stations in Appendices A to F.

Base line catchment: Ahuriri

The Ahuriri catchment has been used as a reference catchment in regard to the effect of climate change. The Ahuriri is an alpine catchment in which flows are significantly affected by snow melt processes. Based on the analysis carried out in Section 3 it is expected that climate change impacts on discharge will be the most extreme in snow-affected areas.

Figure 5-5 presents the climate change impacts on the annual flow. In order to represent the interannual variability, the results are presented in a box plot format showing the inter-quartile range. Further results are presented in Appendix A. The results indicate that average annual flows are expected to increase in the Ahuriri catchment, more so using Planck than using CCC. The Planck GCM estimates an increase of the mean annual flow of nearly 30%, while CCC estimates an increase of 5% of the mean annual flow.

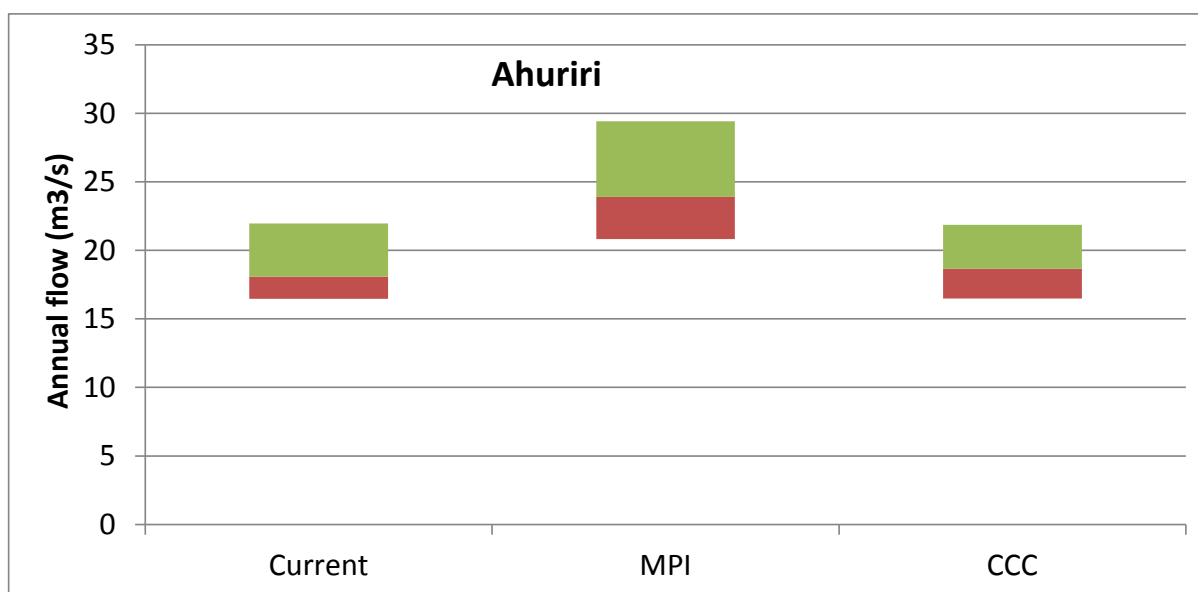


Figure 5-5: Box plot of climate change impact for the annual flow for the Ahuriri catchment for the current time period 1997-2011 (Current), for the future climate using Planck (labelled as MPI); and using CCC. The median annual flow is at the green/brown boundary, the 75th percentile of annual flow is at the top of the green box, and the 25th percentile is at the bottom of the brown box.

The main source of the projected increase in flow is the projected increase in precipitation during June to October. The predicted increase in temperature means that there is a reduction in modelled snowmelt in summer, in spite of increased spring precipitation. This is because the hydrology model calculates that much of the extra precipitation is expected to either fall as rain and be discharged as river flow in spring, or to melt relatively quickly. This results in a reduction of the snow accumulation in the catchment headwaters, which leads to a reduction of the snow available for melting.

Figure 5-6 presents the impact of climate change on different flow thresholds for the two models. The following two thresholds were estimated in order to represent the potential impact of climate change on the primary sector:

- Flood threshold, which is defined as the flow that is exceeded 0.1 percent of the time during the period of interest. This quantifies the impact on peak flows (i.e., protection of arable or agricultural land from river floods). For the Ahuriri, this flow rate is approximately equal to the average annual flood.
- Low Flow threshold, defined as the flow that is exceeded 90 percent of the time during the period of interest. This quantifies the impact on irrigation capability, defined as a flow threshold at which restrictions might be placed on the operation of consented water abstractions.

Analysis of the effects on flow thresholds indicates a reduction in the flow volume in low flows (i.e., lower low flows, up to 80% for CCC, Fig. 5-6) and an increase in the flow volume of the high flows (148 to 160%). This is consistent with the analysis of the estimated flow duration curves presented in Appendix A, and is linked to the combined effect of increased temperature, increased liquid precipitation (for high flows), and reduced snow melt discharge for low flows resulting from climate change. Table 5-1 summarises the findings in term of impacts on low and high flows at the outlet of the catchment.

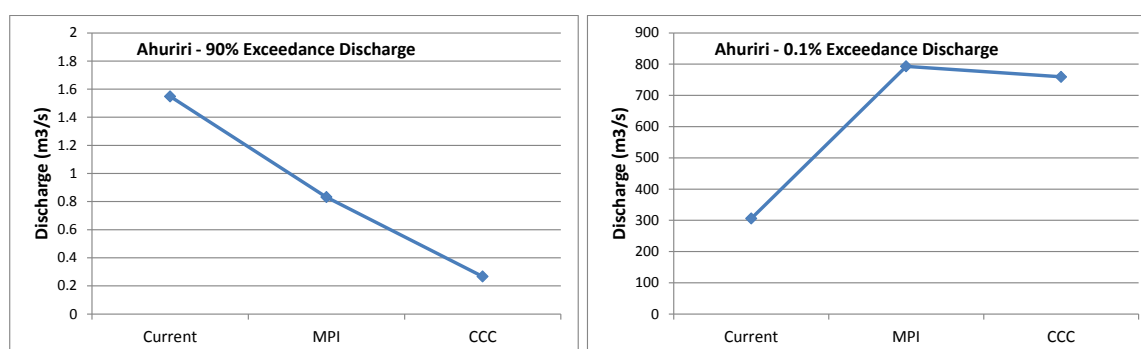


Figure 5-6: Climate change impact on low flow (left) and high flows (right) for the Ahuriri catchment for the current time period (Current), for the future using the Planck (MPI) model; and using the CCC model.

Table 5-1: Summary of climate change impact on flow characteristics for the Ahuriri catchment.

	Planck	CCC
Low Flow Threshold (Q_{90})	-46%	-82%
High Flow Threshold ($Q_{0.1}$)	159%	149%
% of time that flow will be lower than current scenario	62%	89%

Primary sector stakeholders rely heavily on irrigation to deliver the right amount of water at the right time. Hence the seasonality of climate change impacts on flow is of prime importance. For the sake of simplicity in the remainder of this section, the median of the annual minimum flows is referred to as the minimum flow, the median of the annual maximum flows is referred to as the maximum flow, while the median of the average flows is referred to as the average flow. The climate change impact on the seasonality of monthly flow is presented in Appendix A. Analysis of the results indicate that:

- Minimum flow is expected to decrease (according to both models) for most months.
- Minimum flows are generally expected to increase in autumn (March to May) for the Planck model. The minimum flows expected from CCC are lower than the current minimum flows, however the range of minimum flows is larger than the current observed range.
- Average flows are expected to increase in autumn and winter, slightly decrease in spring (up to 20%), and generally decrease in summer.
- Maximum flows are expected to increase (according to both models) in most months.
- Maximum flows during the months of November to January are expected to decrease. Note that the decrease is not only in the median maximum flow, but also in the range.

Climate change impacts not only the average flow, but also the distribution of the flow generated by the catchment. This is translated into change across the whole period of simulation (i.e., change in the hourly flow duration curve) as well seasonal change (i.e., change in the distribution of the flow within each month). Here we characterise the change in distribution through the percentage of time that the simulated future flow is lower than the current flow distribution (Table 5-1). Appendix A presents the distribution of the flow within each month for the current and each of the climate change scenarios and can be summarised as:

- The shape of the flow distribution in autumn remains unchanged. Climate change impacts seem to be characterised by a scaling-up of the discharge. This is expected as this catchment is projected to have a large increase in precipitation during autumn.
- The shape of the flow distribution in winter is expected to change, especially for the lowest monthly discharge expected. The change of distribution is significant in July, and reflects the large increase in liquid (rather than frozen) precipitation expected for headwater catchments.
- The shape of the flow distribution in spring is expected to undergo important changes; larger using the CCC model than the Planck model, as CCC-based flows are lower than those simulated for the baseline scenario (especially in October).

- The shape of the flow distribution in summer is expected to be heavily modified and characterised by a general reduction of discharge during summer. This is consistent with the expected decrease of total precipitation experienced during these months in conjunction with higher temperatures, resulting in increased evaporative demand from vegetation, as well as a large reduction of snow melt discharge. Note that the reduction of flow is mainly from the CCC model while the Planck model produces flow similar to that produced from the baseline climate data.

Summary of climate change impact for Ahuriri catchment

- Average annual discharge is expected to increase
- Extreme flows are expected to change. Maximum flows are expected to increase, while minimum flows are expected to decrease.
- The shape and the scale of the predicted flow distribution within the irrigation period is expected to change, and would be characterised by a reduction of flow. As a result, availability of surface water during the irrigation season is expected to decrease.

North Island

Analysis of climate change impacts on North Island flows is presented in this section only for the Rangitaiki at Te Teko. Results are available in Appendix B for the remaining three gauging stations.

Figure 5-7 presents climate change impacts on the annual flow. Results indicate that the average annual flows are expected to slightly decrease (7-9%) in the Rangitaiki catchment (according to both GCMs). The main source of the projected decrease in flow using Planck is the projected decrease in precipitation in March to February, resulting in a 15% decrease in annual average rainfall.

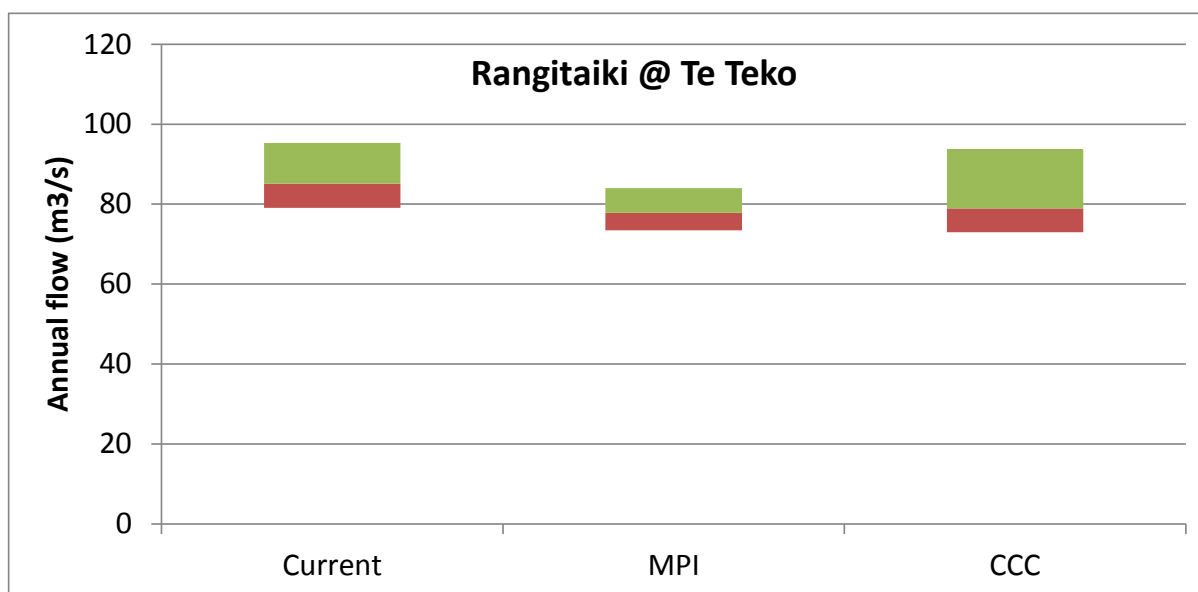


Figure 5-7: Box plot of climate change impact for the annual flow for the Rangitaiki catchment at Te Teko for the current time period (Current), for the future using Planck model; using CCC model. The median annual flow is at the green/brown boundary, the 75th percentile of annual flow is at the top of the green box, and the 25th percentile is at the bottom of the brown box.

Figure 5-8 presents the impact of climate change on different flow thresholds over the future period 2097-2111. Note that impacts on the flow thresholds are affected by the operation of the storage area, which is used for electricity production. A reduction in the low flow (up to 20% for CCC model) is seen, but little impact on the high flow threshold. This result is confirmed by the analysis of the estimated flow duration curves presented in Appendix B and is linked to the combined effect of increased temperature and reduced liquid precipitation (summer rainfall is reduced by 30% for the CCC model). Table 5-3 summarises the findings in term of climate change impacts on low and high flow at Te Teko.

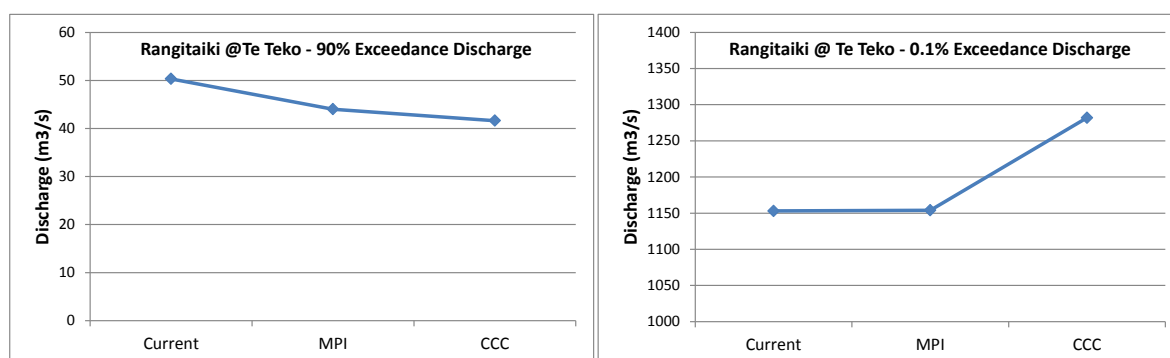


Figure 5-8: Climate change impact on low and high flows for the Rangitaiki catchment at Te Teko for the current time period (Current), for the future using Planck and CCC models.

A summary of impacts on the distribution of flow for the Rangitaiki catchment at Te Teko is presented in Table 5-2. The impact on the seasonality of monthly flow is presented in Appendix B.

Table 5-2: Statistical summary of climate change impact on flow characteristics for the Rangitaiki catchment at Te Teko.

	Planck	CCC
Low Flow Threshold (Q_{90})	-12%	-17%
High Flow Threshold ($Q_{0.1}$)	~1%	11%
% of time that flow will be lower than current scenario	85%	83%

Results indicate that:

- Minimum flow is expected to slightly decrease (according to both models) in most months.
- Minimum flows are generally expected to slightly decrease or remain stable in autumn and winter using Planck. The median minimum flows expected from CCC are usually lower than the current minimum flows, except in May.
- Minimum flows are expected to remain stable during summer, and to decrease in spring according to both models.
- Average flows are expected to increase in summer, remain stable in autumn and decrease in winter and spring.
- Maximum flows are expected to increase only during summer. This behaviour is different from that seen for the South Island headwaters, where maximum flows are expected to increase in all seasons.

Impacts on the distribution of flow within each month are:

- Planck results show lower-than-present flows for most seasons, while the CCC scenario results in little change.
- The shape of the distribution of flow in winter is expected to change, similarly for both models. This result is linked to the reduction of average monthly rainfall during winter.
- The shape of the distribution of flow in spring is expected to remain unchanged, but is characterised by a reduction of flows, as average monthly rainfall is reduced by an average of 15% across the models and the season.
- The shape of the distribution of flow is expected to remain unchanged during January and February. The flow distribution in December is representative of transient climatic conditions between spring and summer.

Summary of climate change impact for Rangitaiki catchment

- Average annual discharge is expected to decrease.
- Extreme flows are expected to change. Maximum flows are expected to increase, while minimum flows are expected to decrease.
- The shape and the scale of the predicted flow distribution within the irrigation period is expected to change, and is characterised by a reduction of flow discharge. As a result, availability of surface water during irrigation season is expected to decrease.

South Island

Waimakariri

Results presented here are only for the Old State Highway Bridge. All the results are available in Appendix C for the remaining gauging station (Waimakariri at Otarama).

Figure 5-9 presents the climate change impact on annual flow. Results indicate that the average annual flows are expected to increase in the Waimakariri catchment, according to the Planck GCM, while they are expected to decrease according to the CCC GCM. This reflects the different change in atmospheric circulation between models. Planck estimates a decrease of annual rainfall over the Canterbury Plains (up to 10%) and an increase of annual rainfall on the foothills and headwaters of the catchment (up to 20%). CCC estimates a decrease of annual rainfall over the Canterbury Plains and foothills (up to 20%) and a slight increase of the annual rainfall in the headwater area (up to 6%). This results in an increase of the mean annual flow of nearly 17% according to Planck, while the use of the CCC model results in a decrease of 10% of the mean annual flow.

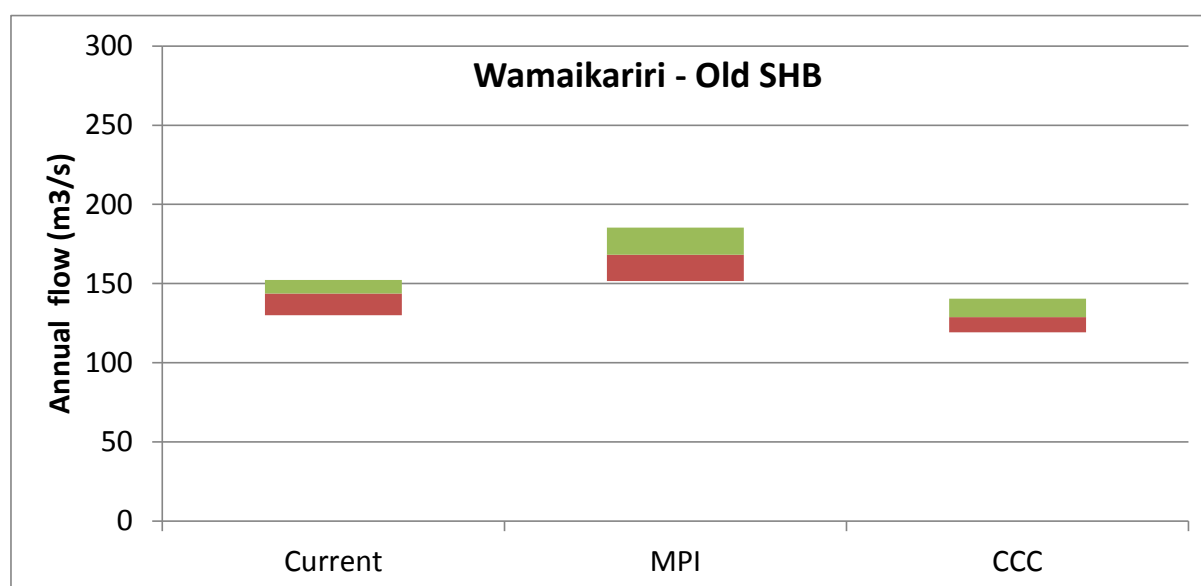


Figure 5-9: Box plot of climate change impact for the annual flow for the Waimakariri catchment at Old State Highway Bridge for the current time period (Current), for the future using Planck model; and using CCC model. The median annual flow is at the green/brown boundary, the 75th percentile of annual flow is at the top of the green box, and the 25th percentile is at the bottom of the brown box.

The main source of the projected increase in flow is the projected increase in precipitation in winter in the headwaters. The projected increase in temperature means that there is a reduction in the modelled snowmelt in summer from the increased spring precipitation. This is because the hydrology model calculates that much of the extra precipitation is expected to either fall as rain, and thus be discharged as river flow in spring, or to melt relatively quickly. This results in a reduction of the snow accumulation in the catchment headwaters, which leads to a reduction of the snow available for melting.

Figure 5-10 presents the impact of climate change on different flow thresholds over the nominal period 2097-2111. A reduction is seen in the low flow (up to 50% according to CCC), as well as an increase of the high flow (50 to 70% according to both GCMs). This is confirmed by analysis of the estimated flow duration curves presented in Appendix C, and is linked to the combined effect of increased temperature and increased liquid precipitation (for high flows). Table 5-3 summarises the findings.

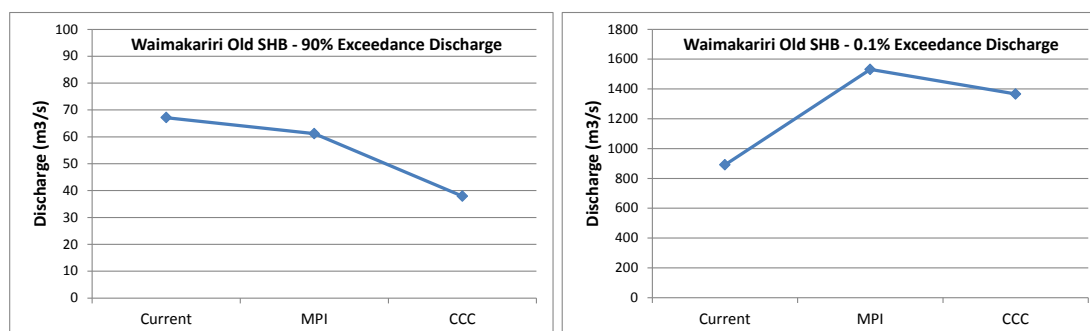


Figure 5-10: Climate change impact on low flow and high flows for the Waimakariri catchment at old State Highway Bridge for the current time period (Current), and for the future using Planck and CCC models.

Table 5-3: Statistical summary of climate change impact on flow characteristics for the Waimakariri catchment at Old State Highway Bridge.

	Planck	CCC
Low Flow Threshold (Q ₉₀)	-8%	-43%
High Flow Threshold (Q _{0.1})	71%	53%
% of time that flow will be lower than current scenario	44%	85%

Results indicate that:

- Minimum flow is expected to decrease in future, in most months.
- Minimum flows are generally expected to increase in autumn, using Planck. Median minimum flows expected from CCC are lower than current minimum flows, but the range of minimum flow is larger than the current observed range.
- Average flows are expected to increase in autumn, slightly decrease in winter, and to decrease in summer. However, spring flows are expected to remain stable using Planck, while a sharp decrease is expected with the CCC scenario.
- Maximum flows are expected to increase across both models, for most months.
- Maximum flows during November to January are expected to decrease. The decrease is not only expressed in term of median maximum flow, but also in terms of the range.

- Maximum flows are expected to increase strongly during autumn and winter. Spring discharges are expected to increase using the Planck model, but decrease using the CCC model, associated with different modelled changes in precipitation and atmospheric circulation.
- The distribution of flow in autumn seems to remain unchanged across the models, but with a scaling up of the discharge. Catchment headwaters are projected to experience increased precipitation during autumn.
- The shape of the flow distribution in winter is expected to change, especially around the lowest discharge during the season, and especially using the CCC scenario.
- The shape of the flow distribution in spring and summer is expected to change significantly using the CCC model, while little change is seen with the Planck model.

Summary of climate change impact for Waimakariri catchment

- Average annual discharge is expected to increase if atmospheric circulation is driven by Planck GCM model. It is expected to decrease if the atmospheric circulation is driven by CCC GCM model.
- Extreme flows are expected to change. Maximum flows are expected to increase, while minimum flows are expected to decrease.
- The shape and the scale of the predicted flow distribution within the irrigation period are expected to change, and would be characterised by a reduction of flow discharge. As a result, availability of surface water during irrigation season is expected to decrease.

Ashley

Results are presented here only for the Ashley catchment at Gorge. All results are available in Appendix D for the remaining two gauging stations in the catchment.

Figure 5-11 presents the climate change impact on the annual flow. Results indicates that the average annual flows are expected to decrease in the Ashley catchment. The Planck scenario estimates a decrease of the annual rainfall over the Canterbury Plains (up to 10%) and an increase of annual rainfall on the foothills of the catchment (up to 10%). The CCC scenario estimates a decrease of the annual rainfall over the Canterbury Plains and foothills (up to 30%). The Planck model results in a slight decrease of the mean annual flow of nearly 3%, while the CCC model results in a decrease of 30% of the mean annual flow.

The main source of the projected decrease in flow is the projected decrease in precipitation in winter and spring.

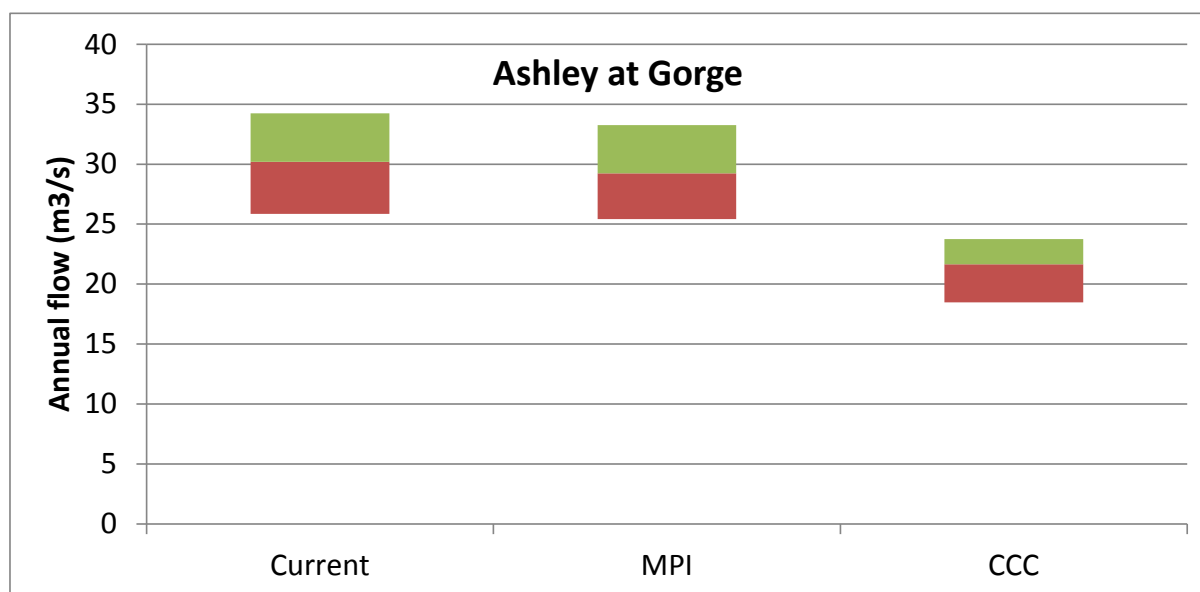


Figure 5-11: Box plot of climate change impact for the annual flow for the Ashley catchment at Gorge for the current time period (Current), for the future using Planck model and using CCC. The median annual flow is at the green/brown boundary, the 75th percentile of annual flow is at the top of the green box, and the 25th percentile is at the bottom of the brown box.

Figure 5-12 presents the impact of climate change on different flow thresholds. There is a reduction in the low flow (up to 50% according to CCC) as well as an increase of the high flow (0 to 24% according to both models). This is confirmed by analysis of the estimated flow duration curves presented in Appendix D, and is linked to the combined effect of increased temperature and increased liquid precipitation (for high flows). Table 5-4 summarises the findings in term of impacts on low and high flow at the gauging station at the outlet of the catchment.

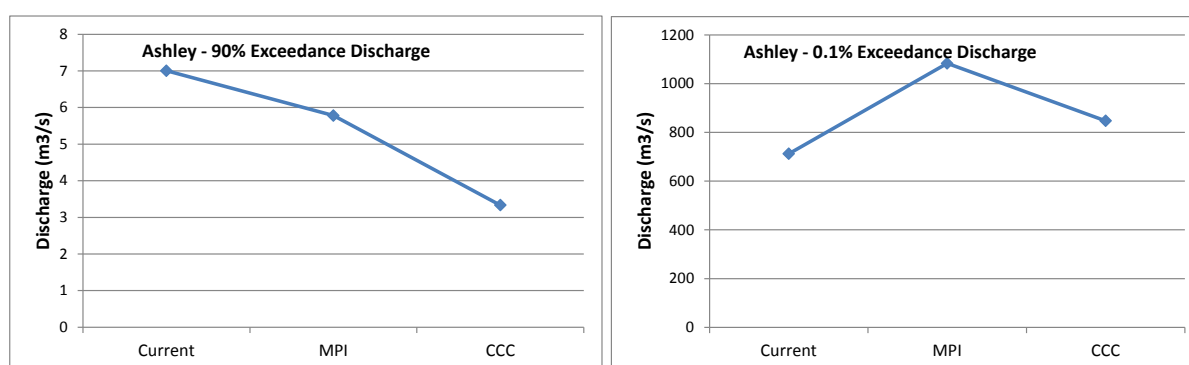


Figure 5-12: Climate change impact on low flow and high flows for the Ashley catchment at Gorge for the current time period (Current), for the future using Planck and using CCC.

Table 5-4: Statistical summary of climate change impact on flow characteristics for the Ashley catchment at Gorge.

	Planck	CCC
Low Flow Threshold (Q_{90})	-17%	-52%
High Flow Threshold ($Q_{0.1}$)	52%	19%
% of time that flow is lower than current scenario	92%	100%

Results indicate that:

- Minimum flow is expected to decrease across both models, in most months. Reduction of the minimum flows is larger using CCC.
- No strong seasonal signal can be detected for the changes in average flows across the models. Winter average flows have a tendency to decrease due to an expected reduction of winter precipitation.
- Maximum flows are expected to increase across both models, in most months.
- Maximum flows during autumn are expected to increase using the CCC scenario.
- Winter maximum median flows are expected to decrease using Planck, but increase using CCC.
- Summer maximum median flows are expected to increase across both models, reflecting the increased snow melt due to projected large increases in temperature.
- The shape of the distribution of flow remains unchanged in early autumn, but changes in April, May and in the winter, most notably using the CCC scenario.
- The shape of the flow distribution in spring is expected to see large changes, especially using the CCC scenario.
- The shape of the flow distribution is largely unchanged in summer, but is characterised by a scaling-up of the discharge.

Summary of climate change impact for Ashley catchment

- Average annual discharge is expected to decrease using both climate change scenarios.
- Maximum flows are expected to increase, while minimum flows are expected to decrease for both of the GCM scenarios.
- The shape and the scale of the predicted flow distribution within the irrigation period are expected to change, and would be characterised by a reduction of flow discharge. As a result, availability of surface water during irrigation season for the irrigation area is expected to decrease.

Rangitata

All the climate change impacts on the different flow signatures results are available in Appendix E.

Figure 5-13 presents the climate change impact on the annual flow. Results indicate that average annual flows are expected to increase in the Rangitata catchment. This increase is not uniform across the models: Planck estimates a decrease of the annual rainfall over the Canterbury Plains (up to 7%), and an increase of annual rainfall on the foothills (up to 15%) and headwater of the catchment (up to 25%), while CCC estimates a decrease of annual rainfall over the Canterbury Plains and foothills (up to 30%), a slight decrease of the annual rainfall in the foothills (up to 15%) and an increase of the annual rainfall in the headwaters area (up to 8%). Hence, mean annual flow is estimated to increase nearly 20% according to Planck, while the use of CCC results in little change to the mean annual flow.

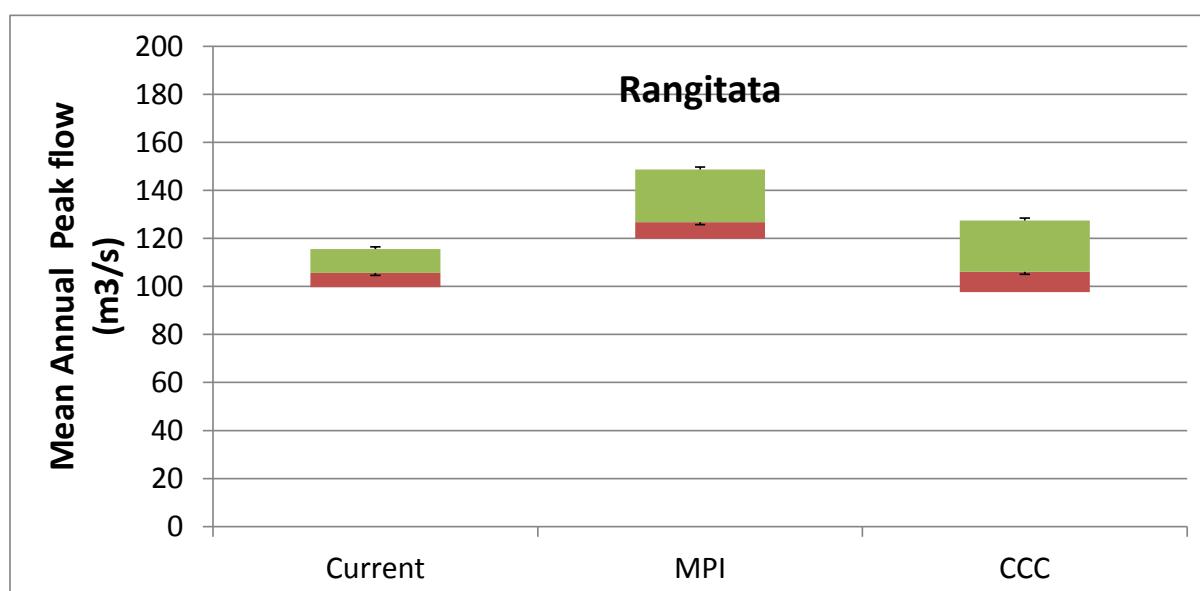


Figure 5-13: Box plot of climate change impact for the annual flow for the Rangitata catchment for the current time period (Current), for the future using Planck; and using CCC. The median annual flow is at the green/brown boundary, the 75th percentile of annual flow is at the top of the green box, and the 25th percentile is at the bottom of the brown box.

The main source of the projected increase in flow is the projected increase in precipitation in winter. The predicted increase in temperature means that there is a reduction in the modelled snowmelt in summer from the increased spring precipitation in the headwaters. The hydrology model calculates that much of the extra precipitation falls as rain, and thus is discharged as river flow in spring, or that any snow fall melts relatively quickly. This results in a reduction of the snow accumulation in the catchment headwaters, hence a reduction of the snow available for melting.

Figure 5-14 presents the impact of climate change on different flow thresholds. Results indicate a reduction in the low flow (up to 60% according to CCC) and an increase of the high flow (80% according to both GCMs). This is confirmed by the analysis of the estimated flow duration curves presented in Appendix E, and is linked to the combined effect of increased temperature and increased liquid precipitation (for high flows) resulting from climate change. Table 5-5 summarises the findings in term of climate change impacts on flows at the gauging station at the outlet of the catchment.

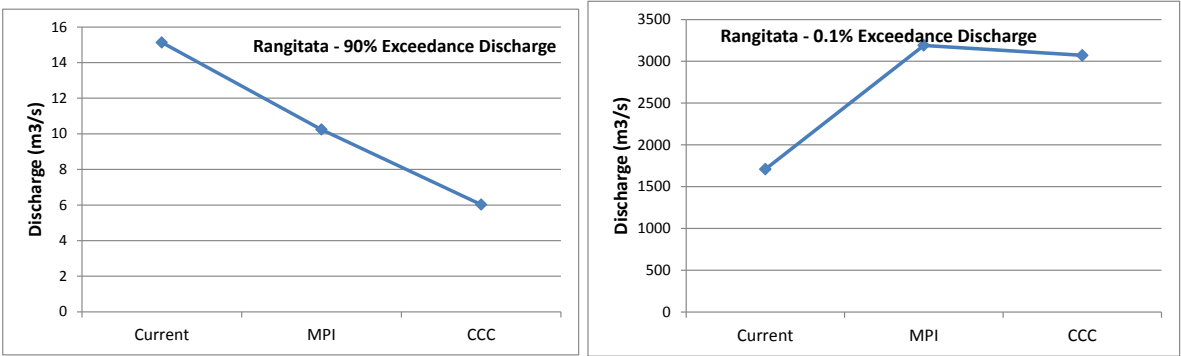


Figure 5-14: Climate change impact on low flow and high flows for the Rangitata catchment for the current time period (Current), for the future using Planck; and using CCC.

Table 5-5: Statistical summary of climate change impact on flow characteristics for the Rangitata catchment.

	Planck	CCC
Low Flow Threshold (Q_{90})	-32%	-60%
High Flow Threshold ($Q_{0.1}$)	86%	79%
% of time that flow is lower than current scenario	71%	86%

Analysis of results indicates that:

- Minimum flow is expected to decrease, according to both GCM models for most months.
- Minimum flows are generally less affected in autumn (March to May), according to the Planck GCM. The median minimum flows expected from the CCC GCM are lower than the current minimum flows. However, the range of minimum flow is larger than the current observed range.
- Average flows are expected to increase in autumn and winter, slightly decrease in spring (up to 20%), and generally decrease in summer.
- Maximum flows are expected to increase across the models in most months.
- Maximum flows during November to January are expected to decrease, not only in term of median maximum flow, but in term of range too.
- Maximum flows during autumn and winter are expected to increase.

- The shape of the flow distribution in autumn remains largely unchanged, according to both GCMs. Climate change impacts seem to be characterised by a scaling-up of the low discharge during the different seasons. This result is unexpected, as catchment headwaters are expected to be subject to a projected decrease in precipitation during autumn.
- The shape of the flow distribution in winter is projected to change, using either GCM scenario, especially for the low discharge during winter. The change of distribution is related to the large increase in liquid precipitation combined to an increase of evaporation demand due to increased temperature.
- The shape of the flow distribution in spring is expected to be subject to important changes. These changes are more important for CCC than for Planck, as flows predicted using the CCC scenario are lower than those simulated for the baseline scenario (especially for the month of October).
- The shape of the flow distribution in summer is expected to be heavily modified, and characterised by a general reduction of the discharge. This is consistent with the expected decrease of the total amount of precipitation experienced during these months, in conjunction with higher temperatures resulting in increased evaporative demand from vegetation and reduction of snow melt in the headwaters. Note that the reduction of flows is seen mostly using the CCC scenario.

Summary of climate change impact for Rangitata catchment

- Average annual discharge is expected to increase using the Planck model, and remain stable using the CCC model.
- Extreme flows are expected to change to become more extreme. Maximum flows are expected to increase, while minimum flows are expected to decrease.
- The shape and the scale of the predicted flow distribution within the irrigation period is expected to change, and would be characterised by a reduction of flow discharge. As a result, availability of surface water during irrigation season to the irrigation area (located downstream of the gauging station) is expected to decrease.

Clutha

Analysis of the climate change impact on flows is presented in this section only for the Clutha at Balclutha. All the results are available in Appendix F for the remaining three gauging stations.

Figure 5-15 presents the climate change impact on the annual flow at Balclutha. Results indicate that the average annual flows are expected to increase in the Clutha catchment. This increase (up to 30% according to the Planck GCM) is not uniform across models. The Planck GCM estimates an increase of the annual rainfall over the whole catchment (up to 30%), while the CCC GCM estimates a decrease of the annual rainfall over the Plains and foothills (up to 15%) and a slight increase of the annual rainfall in the headwater/high elevation area (up to 10%).

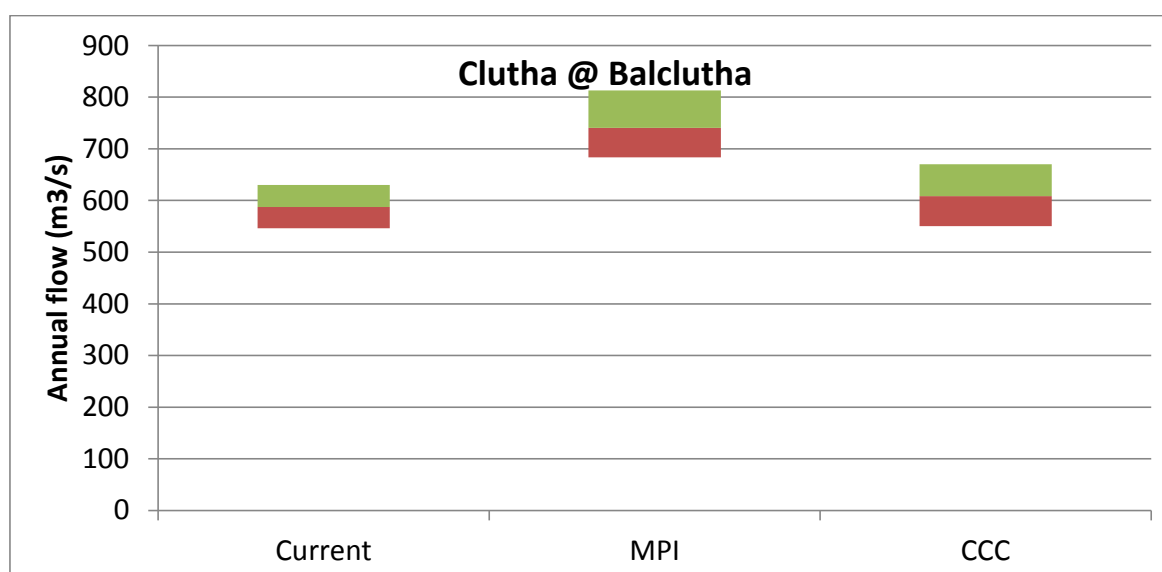


Figure 5-15: Box plot of climate change impact for the annual flow for the Clutha at Balclutha catchment for the current time period (Current), for the future using Planck; and using CCC. The median annual flow is at the green/brown boundary, the 75th percentile of annual flow is at the top of the green box, and the 25th percentile is at the bottom of the brown box.

The main source of the projected increase in flow using the Planck GCM is the projected increase in precipitation in winter, with precipitation projected to remain stable for the remainder of the year. The predicted increase in temperature means a reduction in modelled snowmelt in summer, resulting in lower discharge in summer. The hydrology model calculates that much of the extra precipitation is expected to either fall as rain, and thus be discharged as river flow in spring, or to melt relatively quickly. This results in a reduction of the snow accumulation in the catchment headwaters, which leads to a reduction of the snow available for melting. However using the CCC model, annual seasonal precipitation is expected to increase in winter and spring, while large decreases are projected for autumn precipitation (up to 45% in the headwaters). This large reduction in spring precipitation, combined with increased temperature in winter, results in lower snow pack, contributing to lower snow melt runoff over summer.

Figure 5-16 presents the impact of climate change on different flow thresholds. Results indicate a reduction in low flow (up to 40% according to CCC), as well as an increase of high flow (30% according to both models). This is confirmed by the estimated flow duration curves presented in Appendix F, and is linked to the combined effect of increased temperature and increased liquid precipitation (for high flows). Table 5-6 summarises the findings in terms for the gauging station at the outlet of the catchment.

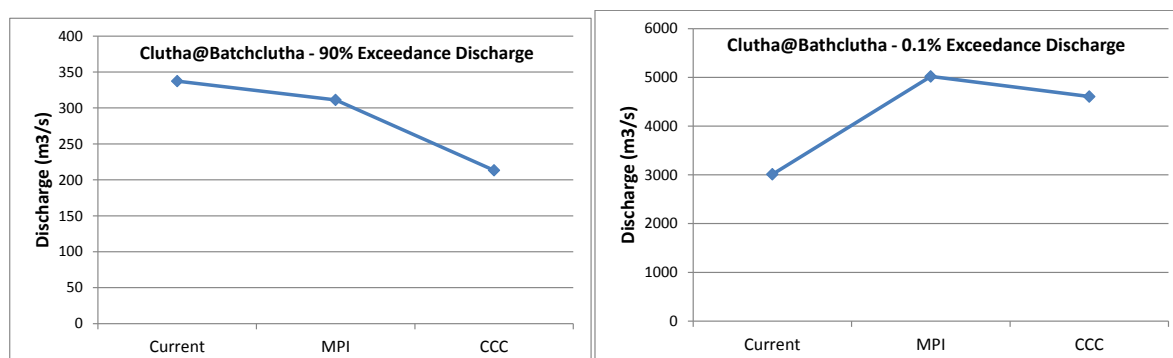


Figure 5-16: Climate change impact on low flow and high flows for the Clutha catchment at Balclutha for the current time period (Current), for the future using Planck; and using CCC.

Table 5-6: Statistical summary of climate change impact on flow characteristics for the Clutha catchment at Balclutha.

	Planck	CCC
Low Flow Threshold (Q_{90})	-8%	-36%
High Flow Threshold ($Q_{0.1}$)	66%	53%
% of time that flow is lower than current scenario	21%	64%

Results indicate that:

- Minimum flow is expected to increase in autumn, to remain stable for winter and to decrease in spring and summer, according to both GCMs.
- Average flows are expected to increase in autumn, slightly increase during winter, remain stable in spring, and generally decrease over summer.
- Maximum flows are expected to increase according to both GCMs, for most months.
- Maximum flows follow the same seasonal pattern as average flows.
- The shape of the flow distribution in autumn remains largely unchanged according to both models, but with a scaling up of the discharge. This was not expected, as catchment headwaters are subject to projected large decreases in precipitation during autumn. The result is thought to be linked with delayed discharge from the upstream lakes.
- The shape of the flow distribution in winter is expected to change, especially for the low discharge expected during a month.
- The shape of the flow distribution in spring is expected to be subject to important changes, especially using the CCC scenario, as flows predicted using CCC are lower than those simulated for the baseline scenario (especially for October).

- The shape of the flow distribution in summer is expected to be heavily modified, and characterised by a general reduction in discharge during December and January (according to both GCMs). This is consistent with the expected decrease of the total precipitation during these months, in conjunction with higher temperatures, resulting in increased evaporative demand from vegetation and reduced snow melt discharge. Note that the reduction of flow is most prominent using the CCC scenario.

Summary of climate change impact for Clutha catchment

- Average annual discharge is expected to increase/remain stable for both scenarios.
- Extreme flows are expected to change. Maximum flows are expected to increase, while minimum flows are expected to decrease. However, impacts at Balclutha are heavily reduced due to the management of hydropower lakes upstream of Balclutha.
- The shape and the scale of the predicted flow distribution within the irrigation period is expected to change, and would be characterised by a reduction of flow discharge. As a result, availability of surface water during irrigation season is expected to decrease.

5.3.5 Limitations

Climate change impacts on flow have been estimated under the assumption that the calibrated hydrological model is correct. As a result, any error in the calibration on the timing and quantity of the stream discharge will be implicit in the results presented here. The reliability of the flow projections is most strongly dependent on the reliability of the projected changes in precipitation.

The second most important factor in determining the reliability of the flow projections is the modelling of the seasonal snowpack. Because of the absence of long term systematic measurements of snow in the catchment (and in other seasonal snowfields of New Zealand), the TopNet snow sub-model has not been tested directly (but see Clark et al., 2009). The modelling of snow had to be inferred from the delays between precipitation and measured streamflow. Results are not inconsistent with the general understanding of seasonal snow in New Zealand. A more direct evaluation of the snow model is needed in future studies. A national snow and ice monitoring network has recently been set up, but information collected cannot yet be used for long-term simulations. Remote sensing of snow-covered areas is another research area under development.

In the scenario modelling, we have assumed that no hydrologically significant changes take place in (i) catchment vegetation (ii) diversion or abstraction of river water (iii) sub-daily distribution of precipitation. The first two assumptions could be addressed if they were relevant to the problem and scenario information was available.

The third point above is more problematic, since detailed scenarios for changes in sub-daily precipitation are not yet available. It is expected that extreme precipitation will increase with projected future temperature increases (see Section 5.1). This is independent of changes in seasonal or long-term mean precipitation, and is expected because a warmer atmosphere can hold (and therefore produce as precipitation) more moisture: e.g., for every 1 °C increase in temperature there is an approximate 8% increase in the 24-hour 100-year average recurrence interval precipitation amount (Ministry for the Environment, 2010).

5.3.6 Conclusion

In order to estimate the expected climate change impact on flow resulting from four degrees of global warming, the hydrological TopNet model was run for six catchments located across the North and South Islands. The expected climate change impact on discharge can be summarised as follows:

- Average annual discharge is generally expected to increase.
- Extreme flows are expected to change. Maximum flows are generally expected to increase, while minimum flows are expected to decrease.
- The shape and the scale of the predicted flow distribution within the irrigation season is expected to change. This is expected to be characterised by a reduction of the surface flow discharge available for irrigation. As a result, availability of surface water during the irrigation season is expected to decrease.

6 New Zealand Pasture Production (from water balance)

6.1 Introduction

Potential pasture production based on climatic controls was modelled for areas of New Zealand under “exotic grassland pasture”, covering both dairy and dry stock agriculture pasture. No distinction was made between different management regimes.

Modelled potential pasture production under two future climate projections, the Canadian Centre for Climate Modelling and Analysis’ model ‘CCC’ and the Max Planck Institute of Meteorology’s model ‘Planck’, were compared to modelled potential pasture production under the present climate (1997-2011). Both future scenarios correspond to an increase in global mean temperature of four degrees Celsius by the end of this century (2097-2111) relative to pre-industrial climate. The two future scenarios differ in the associated temperature increase in New Zealand and the frequency of particular atmospheric regimes in the New Zealand region.

Significant seasonal shifts in potential pasture production are seen with increases in winter growth due to reduction of temperature restriction and decreases in summer growth, the latter predominantly due to increased drought conditions in eastern areas of both islands as well as higher than optimal temperatures in Northland. These changes are more pronounced under the ‘CCC’ model than the ‘Planck’ model.

Both models show a significant strengthening of westerlies in winter and spring, amplifying the precipitation shadow in eastern areas particularly Canterbury, Northern Otago and Hawkes Bay, significantly affecting their soil moisture levels, and hence water limitation of potential pasture growth.

Under the ‘CCC’ scenario, to avoid water limitation of growth, seasonal irrigation requirements would increase by 150-200 mm in summer and 100 mm in spring for Canterbury and Marlborough. For Hawkes Bay, increases of 100mm would be required in both summer and spring under the ‘CCC’ scenario. Smaller increases in irrigation demand are seen in other regions. Increases of around 50 mm would be required in Canterbury, Marlborough Hawkes Bay and Northland under the ‘Planck’ scenario.

6.2 Potential Pasture Growth Model

Maximal pasture growth as a function of received daily short wave radiation was calculated and then multiplicatively scaled by functions for temperature and water shortage growth limitation. The pasture growth rate as a function of radiation is given as:

$$GRad = \frac{\alpha I P_m}{\alpha I + P_m}$$

where I is incoming short wave irradiance in megajoules per square metre per day. Alpha is the photosynthetic efficiency/quantum yield and gives the slope of the growth vs irradiance curve at low light levels. Here, alpha was set to 0.08 mol CO₂ assimilated per mol PAR photons (Johnson 2012). P_m is the maximum photosynthetic rate at optimal temperature and ambient CO₂. Temperature dependence is separated out as a multiplicative scaling function described below. The effects of varying atmospheric carbon dioxide concentration are not included in this study.

P_m was set to 7.72 micromol CO₂ assimilated per m² ground per second, which was derived from a maximal crop growth rate on NZ perennial ryegrass pasture of 19 g DM m⁻² day⁻¹ given in McCall & Bishop-Hurley (2003).

The model here does not model nutrient flows, and assumes that the grass growth is not nutrient-limited (or if it is, that such nutrient limitation is constant and incorporated into the P_m value used.) The model assumes a constant photosynthetically active/transpirationally active leaf area index (LAI) of 1.44 (taken as half of total LAI). The constant parameters used here for calculations of photosynthetic production and potential evapotranspiration correspond to assuming the pasture is grazed/managed to maintain it in a “steady-state” optimal condition.

The actual pasture production figures in tonnes of dry matter per hectare are sensitive to the value used for P_m . P_m will vary with grass species and variety, and in this model we have also lumped the effects of nutrient limitation, self-shading and leaf-angle into this parameter, so it will vary with these as well. In this light, and because this section is looking at potential pasture growth as determined by climatic controls, the focus here is on the changes of the future scenarios from the baseline values rather than the absolute biomass production figures.

The temperature dependence of growth was based on C3 mesotherm grasses such as perennial ryegrass. Mean daily temperature was used as the controlling temperature parameter. The parameters used here are a lower threshold for growth of 5 degrees Celsius, an upper threshold for growth of 35 degrees Celsius, and an optimal growth temperature of 19 degrees Celsius (Clark 2010). The temperature limitation on potential pasture growth is shown in Figure 6-1.

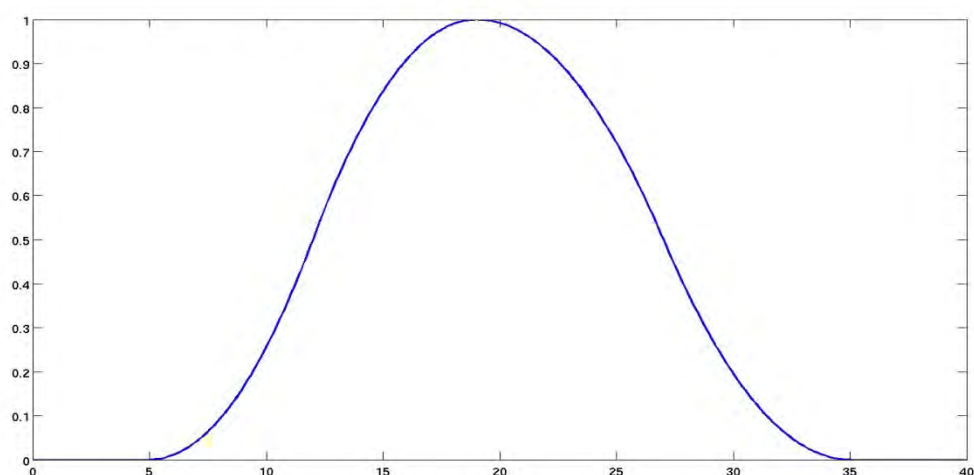


Figure 6-1: Modelled temperature dependence (°C) of C3 Mesotherm grasses.

Model predictions of pasture growth change are dependent on the shape of the temperature dependence curve, which varies between grass varieties. For some regions of New Zealand and some pasture types, a temperature dependence somewhere between C3 Mesotherm and C3 Microtherm grasses may be more appropriate: in these cases, the parameterisation

used will overestimate increases in winter pasture production. C4 grasses which are not limited by high temperatures are not included here.

A constant loss of production to respiration of 2 micromol CO₂ per m² per second is used (Johnson 2012).

Potential evapotranspiration was calculated from meteorological variables on a daily time step using the biophysically based Penman-Monteith equation (Allen et al 1998). In using the Penman-Monteith approach, the 9 am actual water vapour pressure was taken as a proxy for the average daily actual water vapour pressure. Average daily saturated water vapour pressure was taken as the average of the saturated water vapour pressure at T_{min} and the saturated water vapour pressure at T_{max}. Grass height was set to 12 cm, and grass albedo to 0.23. Actively transpiring leaf area index (LAI) was taken as constant at 1.44 (taken as half a total leaf area index of 2.88), and a constant stomatal resistance of 100 sm⁻¹ was used.

Soil moisture was calculated on a daily time step using a single layer which at field capacity (below which the model approximates drainage to zero) holds an amount of water given by PAW (profile available water). Actual evapotranspiration was determined from potential evapotranspiration by the soil water budget. If the soil water is greater than half PAW, actual evapotranspiration was set equal to potential evapotranspiration. If the soil water is less than (PAW-PRAW (profile readily available water), taken to be wilting point), then actual evapotranspiration was set to zero. In between these points, actual evapotranspiration varied linearly from zero to potential evapotranspiration.

All soil parameters (PAW, PRAW, macroporosity and permeability) were extracted from Landcare's fundamental soil layer (Webb and Wilson (1995)). Daily rainfall and drainage of water above field capacity are treated on a half-daily basis with actual evapotranspiration being calculated at the midpoint.

In each daily time step:

- (1) Half daily rainfall is added.
- (2) Soil water above field capacity (determined from fundamental soil layer PAW (profile available water)) is allowed to drain from soil, with a maximum rate determined by the soil permeability.
- (3) Soil water level is set to the minimum of the above and saturation (where the amount of water held at saturation is determined from the soil layer's macroporosity and profile available water).
- (4) Actual evapotranspiration is calculated and extracted.
- (5) Second half of daily rainfall is added
- (6) Water above field capacity is allowed to drain up to a maximum determined by the soil permeability.
- (7) Soil water level is set to the minimum of the above and saturation.

(8) In the irrigated case, irrigated water is added to bring the water in the soil up to half field capacity.

Pasture growth was calculated only for areas shown in the Land cover database (LCDB2 2001/2002) to be covered in exotic grassland (note that tussock farmland has not been included in this study). Areas not in exotic grassland appear white in all maps in this section.

6.3 Potential Pasture Growth Results

For both annual and seasonal time periods, percentage changes from baseline in the 15-year mean of cumulative pasture production were calculated for the two models of future climate. In many regions, significant interannual variability in the current climate range, and hence in current pasture production, mean that we need to consider the interannual variation to determine whether predicted changes in mean production are statistically significant or not. To test for statistical significance a two-tailed, two-sample, unequal variance t-test, with $\alpha = 0.05$ is used. The null hypothesis is that “mean seasonal (or annual) potential pasture production does not change”, and the alternate hypothesis that “mean seasonal (or annual) potential pasture production does change”. This means that where predicted changes are presented as statistically significant, there is a less than 5% chance that in the absence of a real change in the mean, the projected mean change could occur by chance as a result of observed levels of interannual variability.

Figure 6-2 shows mean modelled annual potential pasture production for the baseline climate (1997-2011) in tonnes of dry matter per hectare per year, and Figure 6-3 shows the potential pasture production broken down by season. For the C3 mesotherm temperature dependence used here, this shows the majority of pasture growth occurring in summer and spring, with little winter growth and with autumn growth mainly confined to the upper North Island.

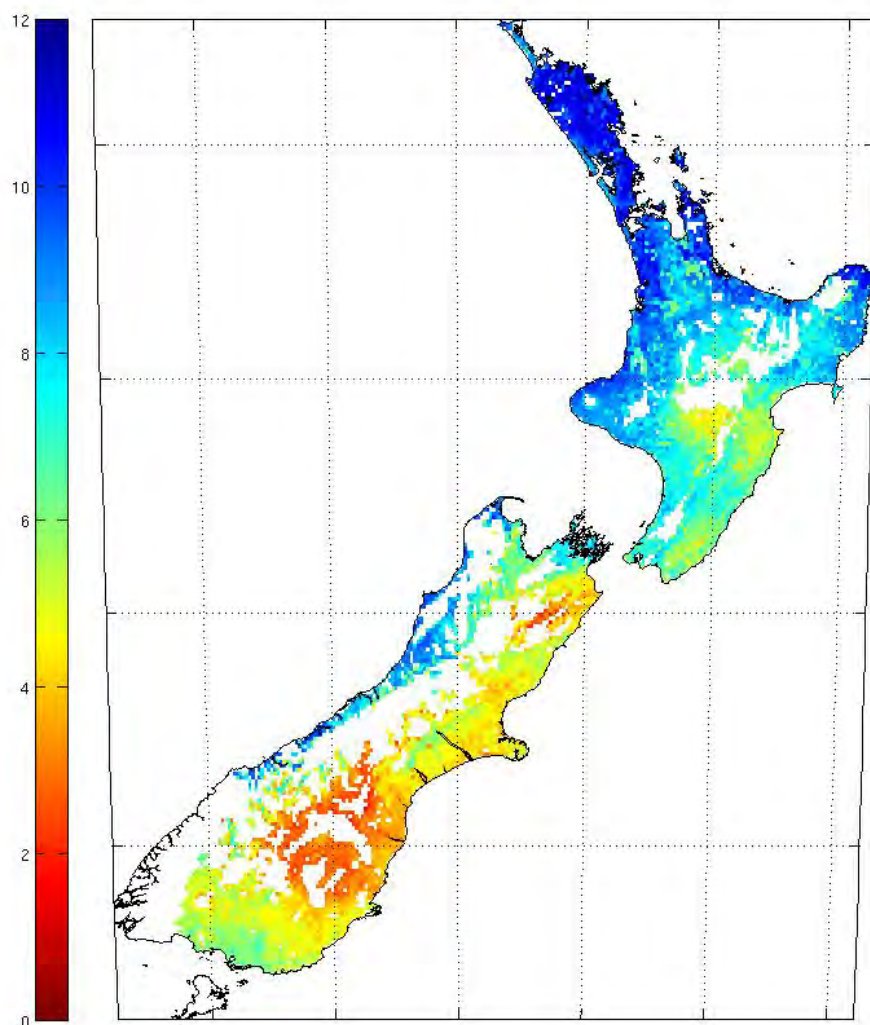


Figure 6-2: Mean annual modelled potential pasture production in tonnes dry matter per hectare per year for the baseline climate 1997-2011.

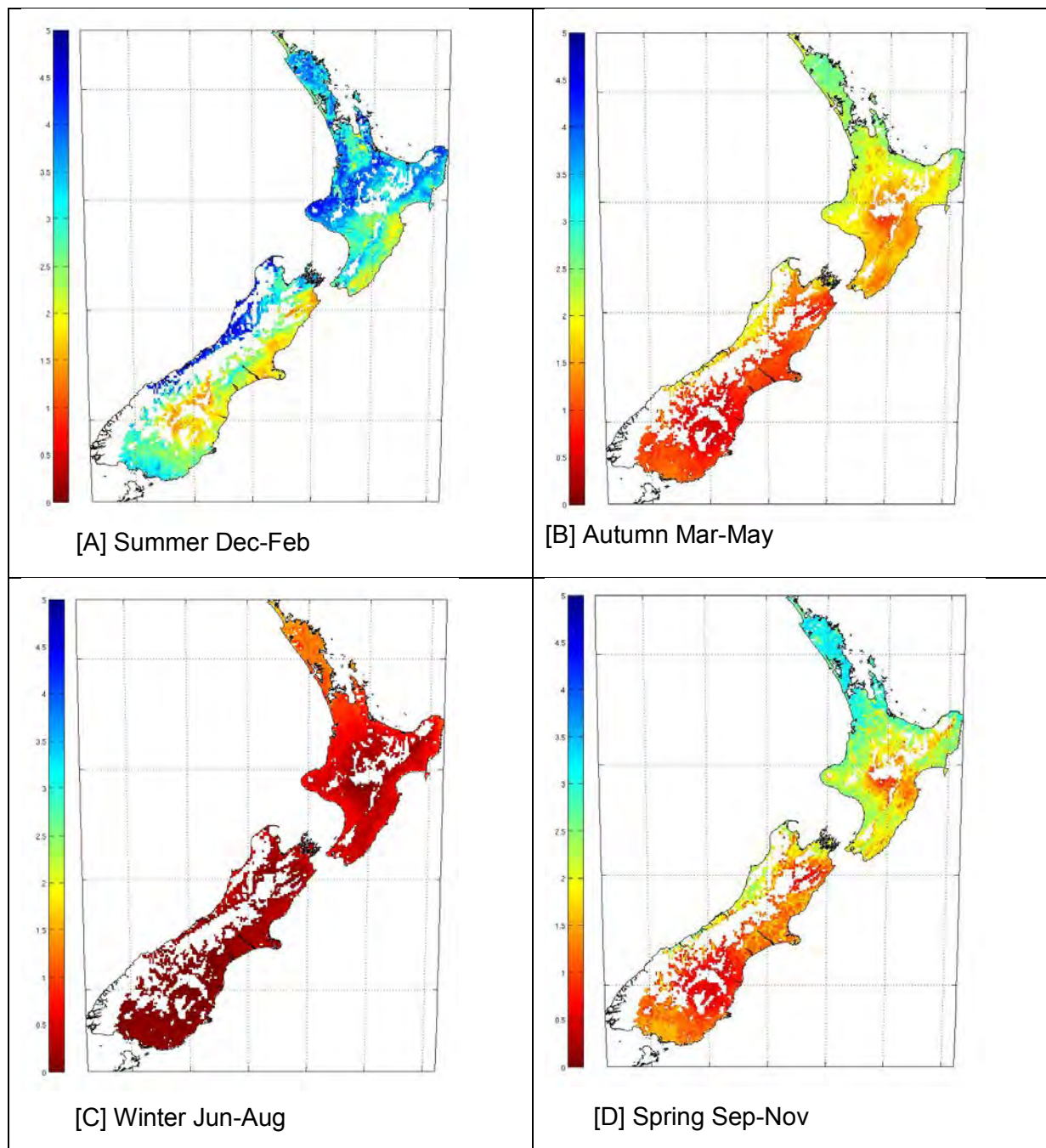


Figure 6-3: Mean seasonal potential pasture production in tonnes dry weight per hectare for the baseline climate 1997-2011.

Figure 6-4 shows percentage changes in mean annual potential pasture production for the two models. The results of a two-tailed, two-sample, unequal variance, statistical t-test for a difference in mean annual potential pasture production with 5% level of significance are shown in Figure 6-5.

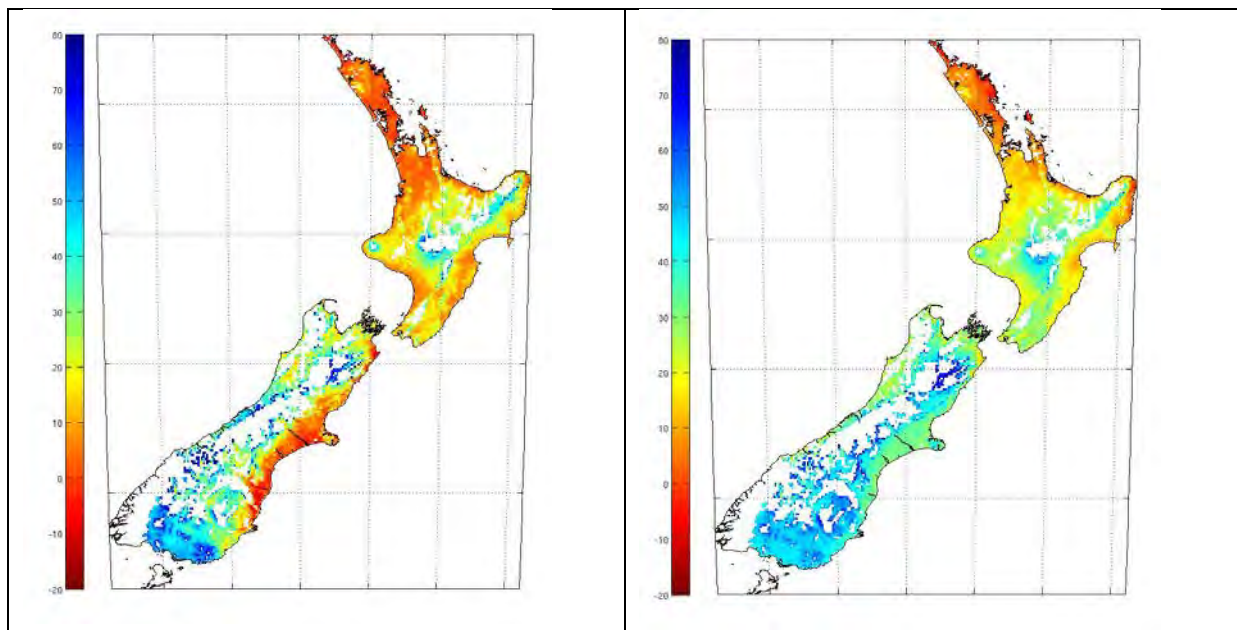


Figure 6-4: Percentage change in mean annual modelled potential pasture production, under [A] 'CCC' model and [B] 'Planck' model

It is seen from Figure 6-5 that under the 'CCC' scenario, there is a significant increase in annual potential pasture production in the majority of the South Island (with the exception of the eastern coastal plains) and in the higher elevation areas of the central North Island. There is seen to be no significant change in annual pasture production in the eastern South Island coastal plains and in Northland. It is seen later that in these areas, increased winter pasture growth counterbalances decreased summer pasture growth, giving no net change in annual pasture production. The 'Planck' model shows a significant increase in potential pasture production throughout the South Island and majority of the North Island, with no significant change in Northland and coastal regions of Hawkes Bay and East Cape.

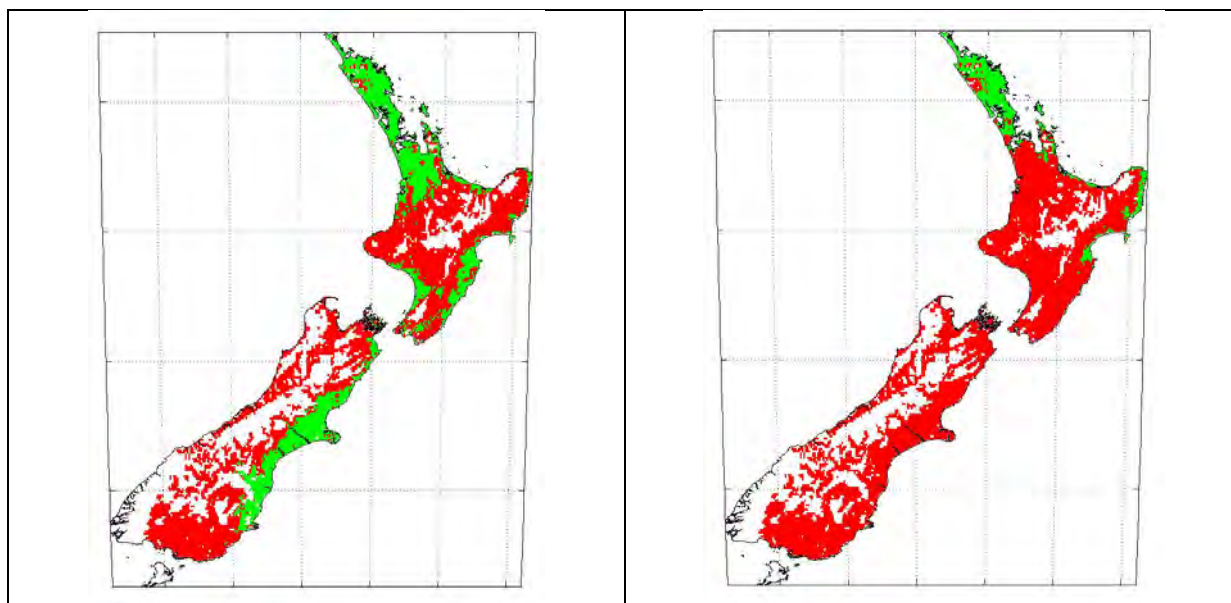


Figure 6-5: Statistically significant (Red) and not statistically significant (green) changes in modelled mean annual pasture production for [A] 'CCC' model and [B] 'Planck' model. Two sample, two tail, unequal variance t-test with $\alpha = 0.05$, H_0 No change in mean annual production, H_1 change in mean annual production.

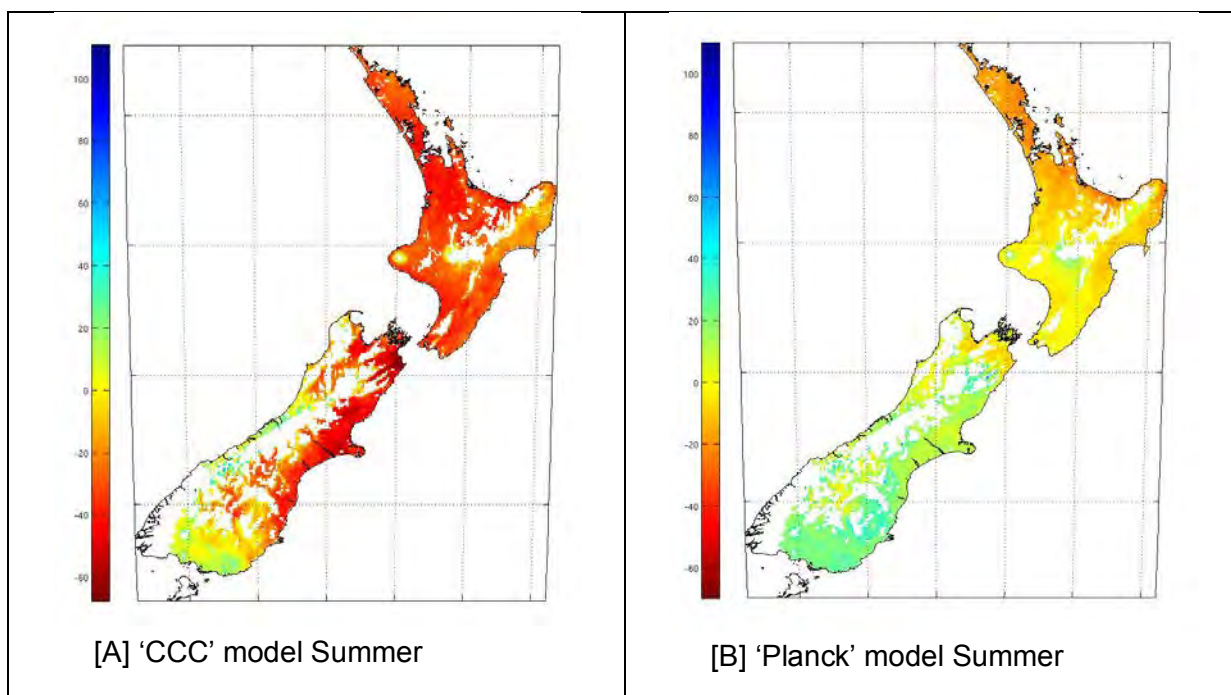


Figure 6-6: Percentage change in mean summer (Dec-Feb) potential pasture production from baseline climate. [A] Projected 'CCC' model, [B] Projected 'Planck' model for 2097-2111.

Percentage changes in summer (December to February) potential pasture production are shown in Figure 6-6. Figure 6-7 shows the results for two-tailed, two sample, unequal variance t-tests for a change in mean summer potential pasture production at the 5% level of significance.

Figure 6-6 and 6-7 show that under the 'CCC' model, mean summer potential pasture production in 2097-2111 is seen to decrease significantly by between 20 and 60 % for most North Island areas (exception of Northern Hawkes' Bay) , and in Canterbury, Marlborough, Nelson and Northern Otago. No significant change in summer potential pasture production is seen in Southland, or Northern Hawkes Bay.

The pattern under the 'Planck' model is of much milder change. Significant decreases of 10 to 20% are seen in Northland, Coromandel and coastal Bay of Plenty. Significant increases of 20 to 40 % are seen in Southland. Elsewhere there is no significant change in summer potential pasture production.

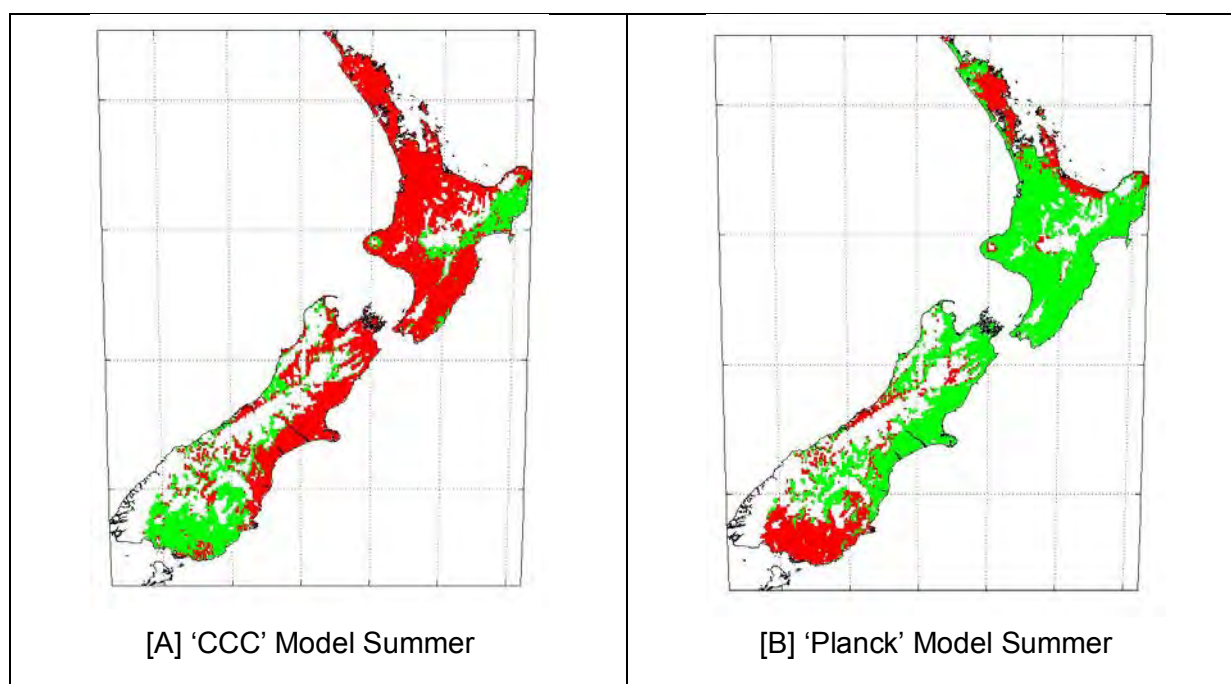


Figure 6-7: Statistically significant (Red) and not statistically significant (green) changes in summer pasture production for [A] 'CCC' model and [B] 'Planck' model in 2097-2111 relative to 1997-2011.

Percentage changes in autumn (March to May) potential pasture production are shown in Figure 6-8. Figure 6-9 shows the results for two-tailed, two sample, unequal variance t-tests for a change in mean autumn potential pasture production at the 5% level of significance.

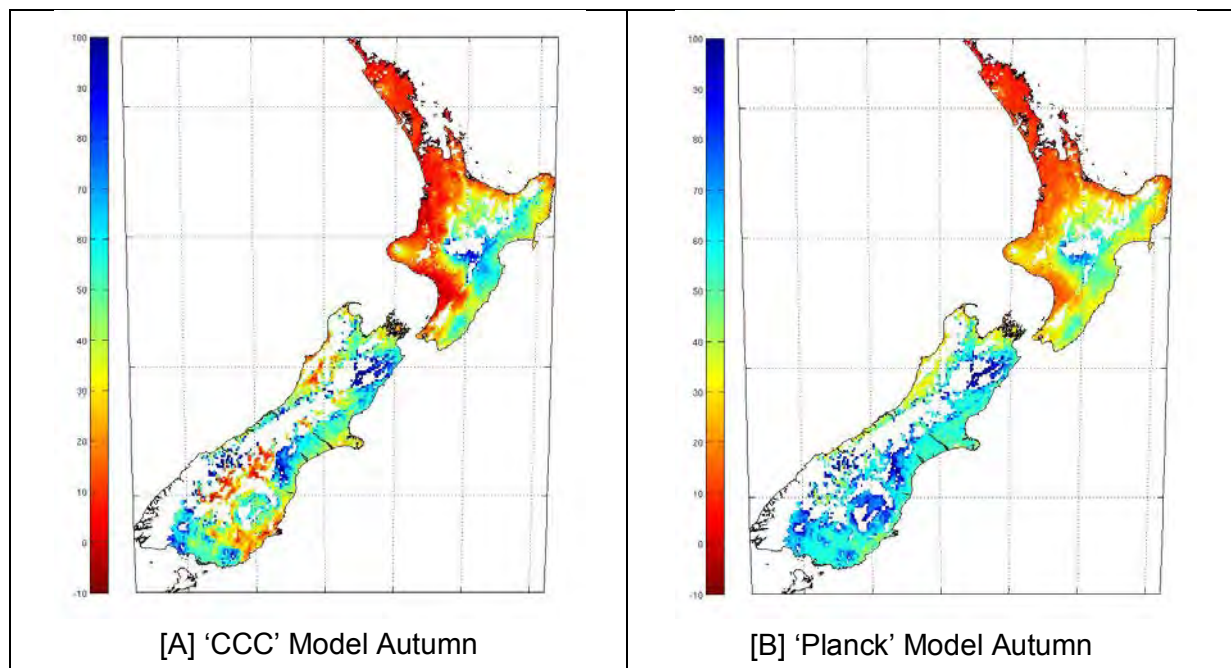


Figure 6-8: Percentage change in mean Autumn (Mar-May) potential pasture production from baseline climate. [A] Projected 'CCC' model, [B] Projected 'Planck' model.

Figures 6-8 and 6-9 show that under the 'CCC' model, mean autumn potential pasture production in 2097-2111 shows significant increases in the majority of New Zealand, with the exception of central and southern coastal Otago, and western North Island (Manawatu, King Country, Waikato, Auckland and Northland).

Figures 6-8 and 6-9 show that under the 'Planck' model, there are significant increases in autumn potential pasture production in almost all areas of New Zealand, except for Northland, Auckland, Waikato and coastal Manawatu.

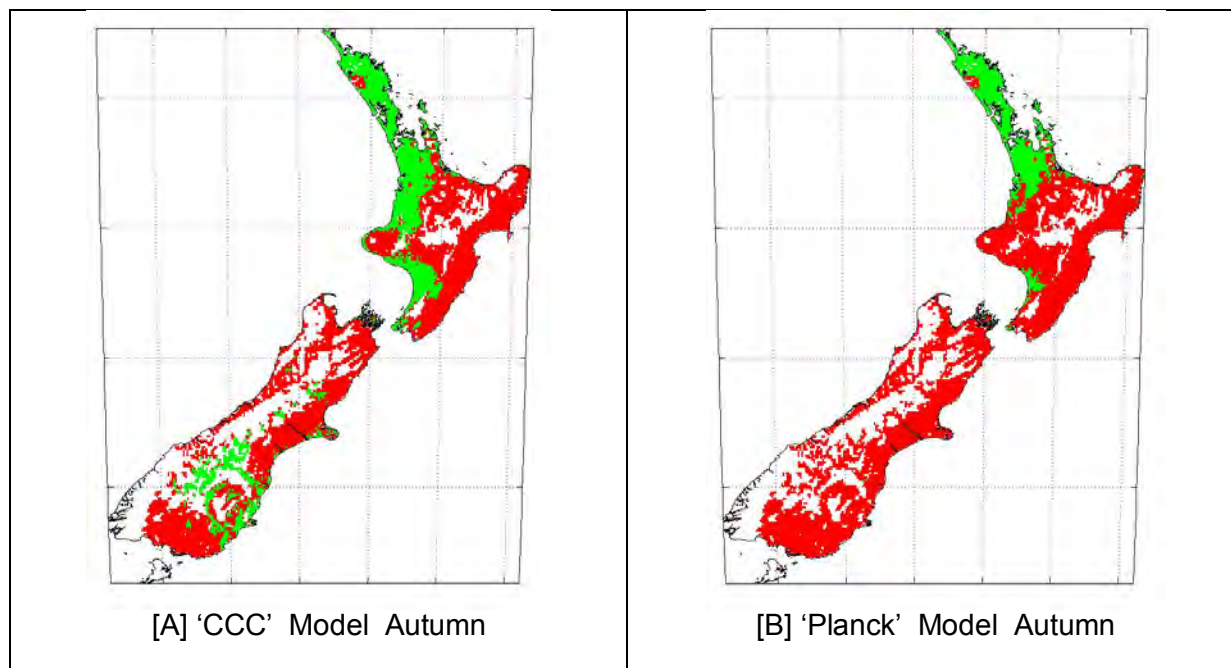


Figure 6-9: Statistically significant (Red) and not statistically significant (green) changes in autumn potential pasture production for [A] 'CCC' model and [B] 'Planck' model in 2097-2111 relative to 1997-2011.

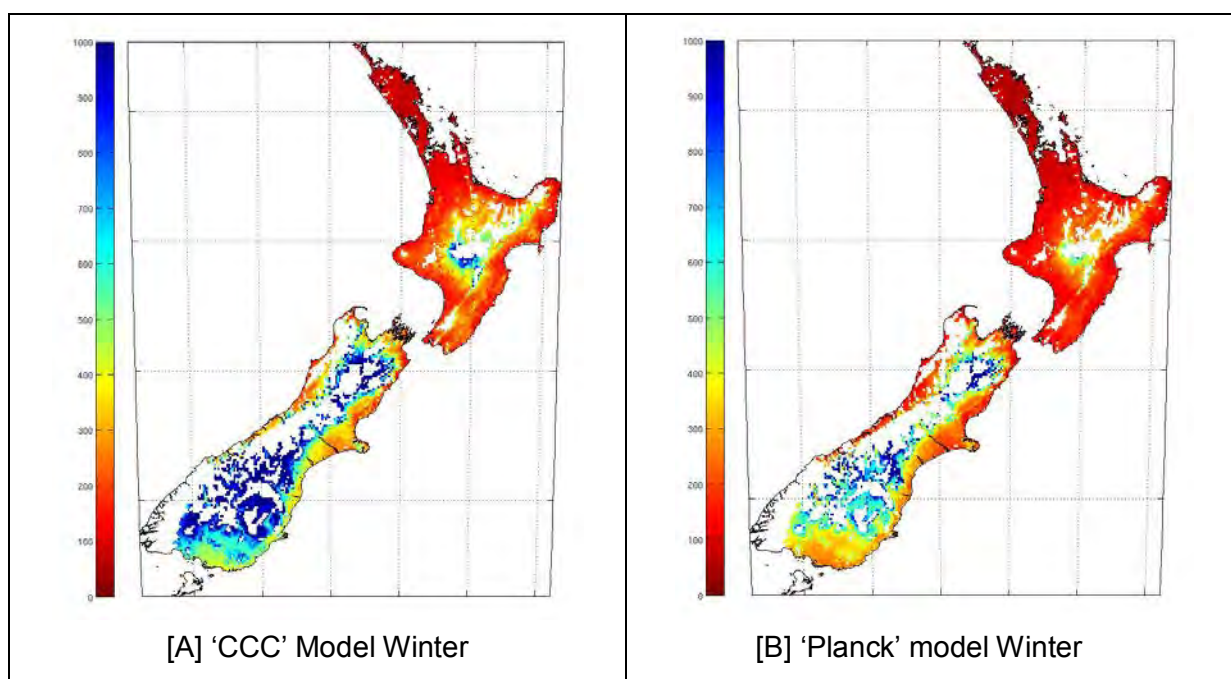


Figure 6-10: Percentage change in mean winter (Jun-Aug) potential pasture production from baseline climate. [A] Projected 'CCC' model, [B] Projected 'Planck' model.

Both models show similar changes in winter potential pasture production, showing large increases of winter pasture production in all regions. This is related to the removal of the current winter temperature limitation on pasture growth.

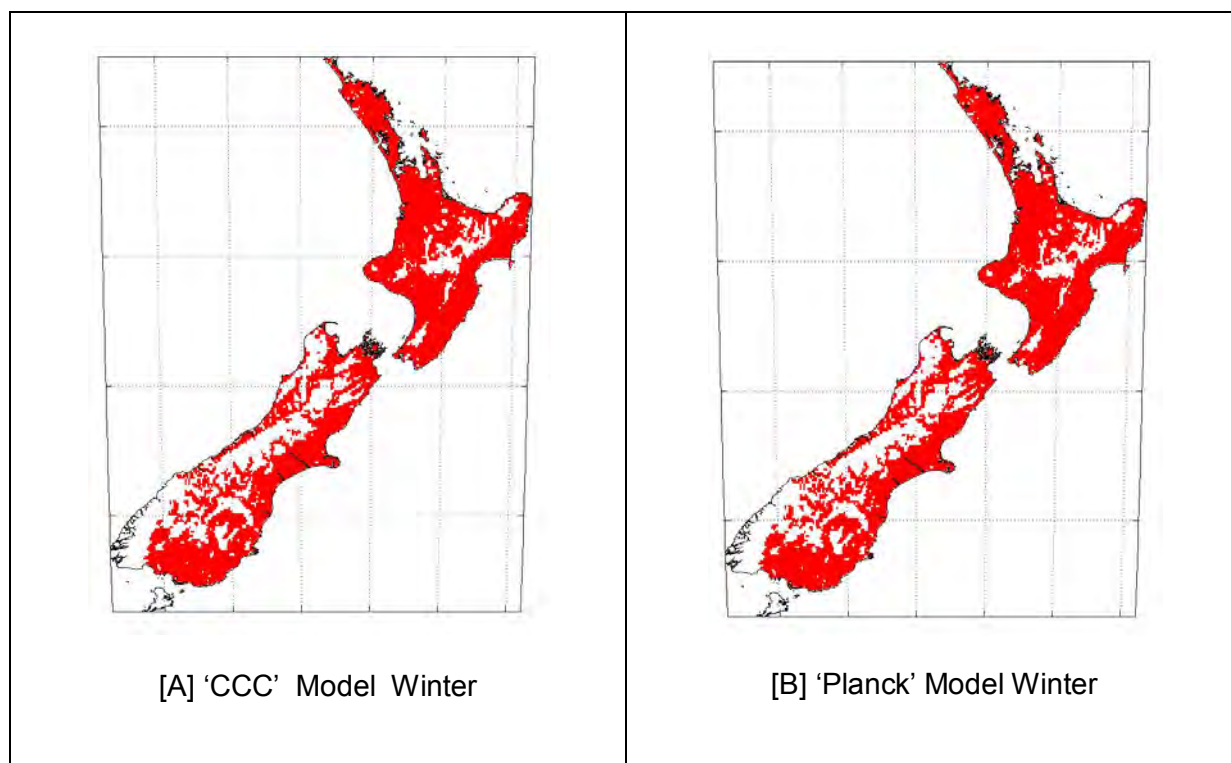


Figure 6-11: Statistically significant (Red) and not statistically significant changes in winter potential pasture production for [A] 'CCC' model and [B] 'Planck' model in 2097-2111 relative to 1997-2011.

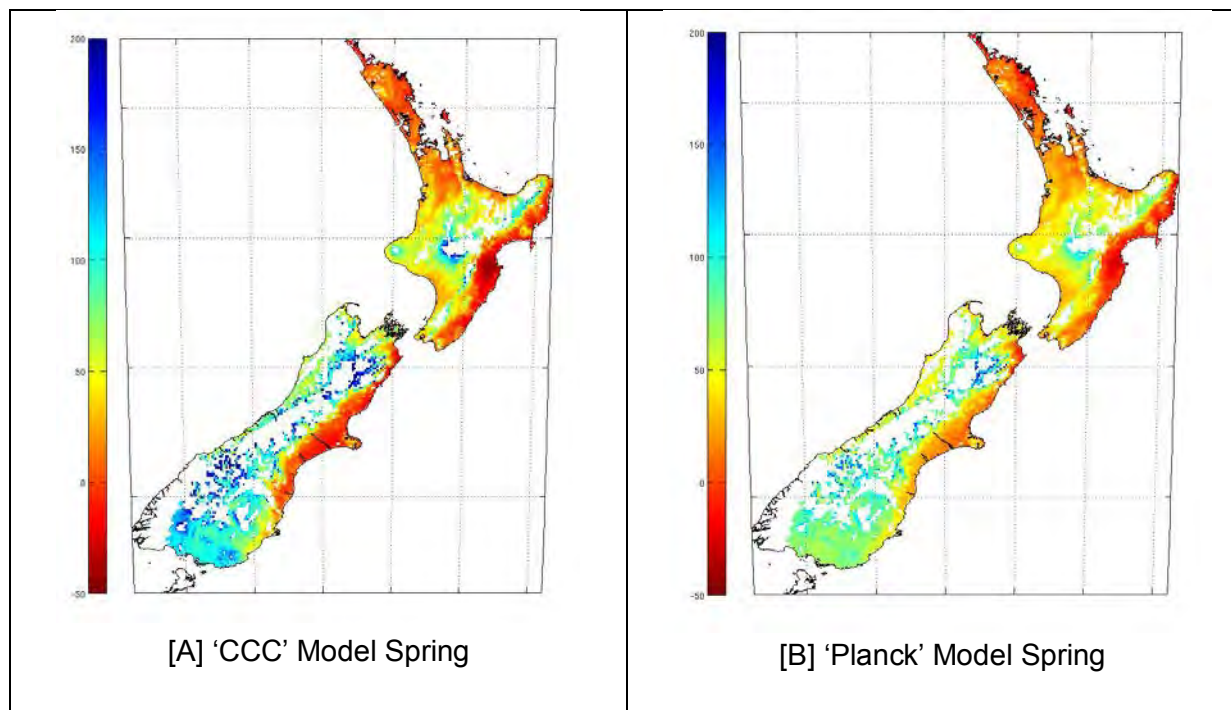


Figure 6-12: Percentage change in mean spring (Sep-Nov) potential pasture production from baseline climate. [A] Projected 'CCC' model, [B] Projected 'Planck' model.

Figures 6-12 and 6-13 show that both models predict a significant increase in spring (September to November) potential pasture production for all areas except Northland and eastern regions of both islands. In the 'Planck' model, increases of between 50 and 100% are seen. The 'CCC' model shows larger increases, with higher elevation areas and Southland showing increases of between 100 and 200%. Both models show no significant change in spring potential pasture production in Northland or in the eastern regions of both islands. They show a significant increase in spring potential pasture growth in all other areas.

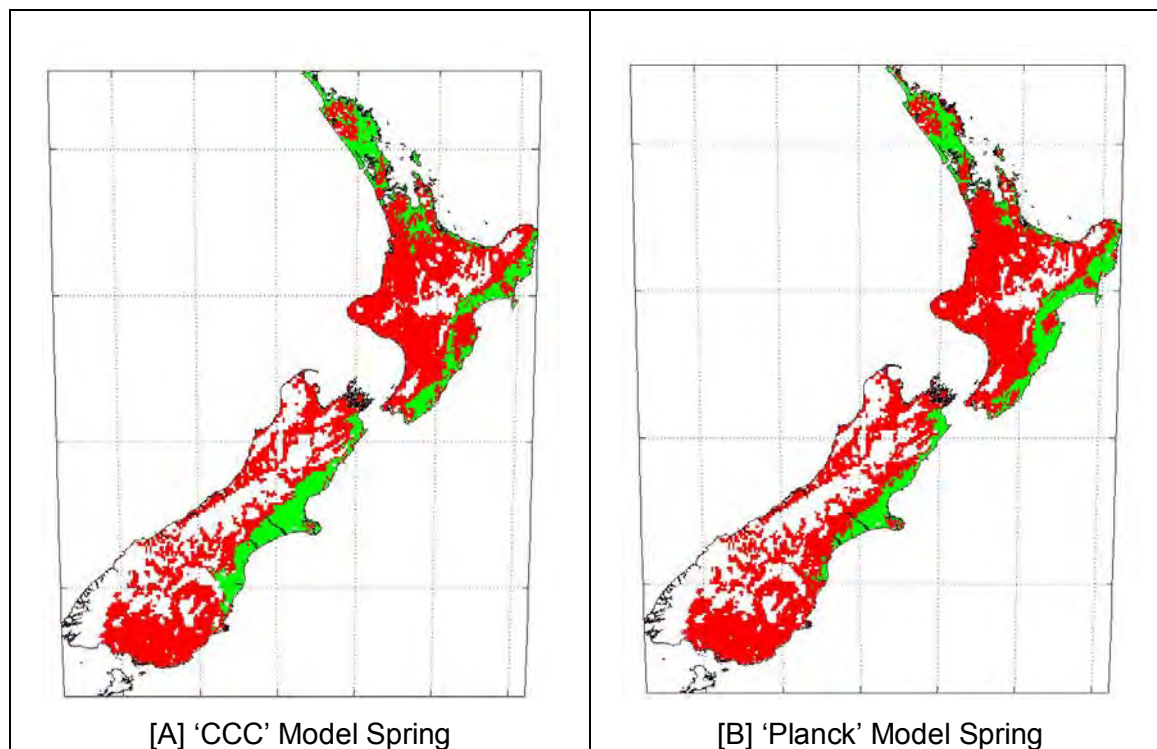
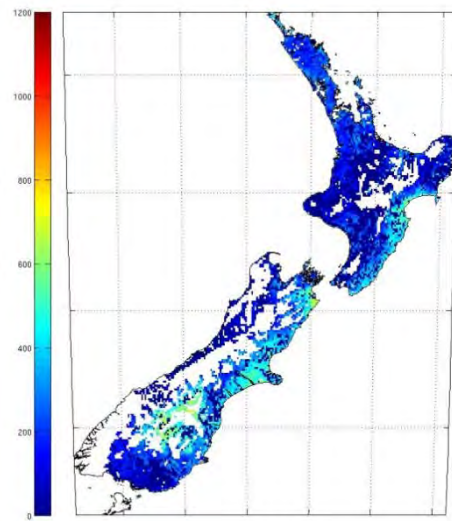
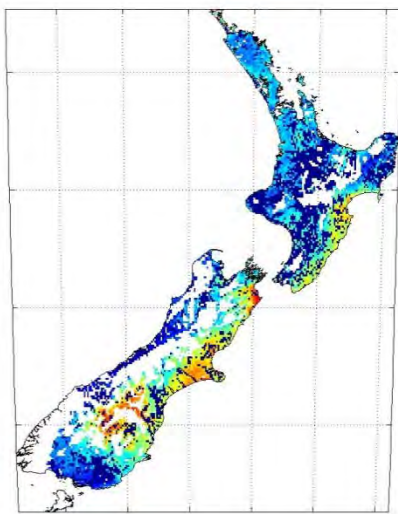


Figure 6-13: Statistically significant (Red) and not statistically significant (green) changes in spring potential pasture production for [A] 'CCC' model and [B] 'Planck' model in 2097-2111 relative to 1997-2011.

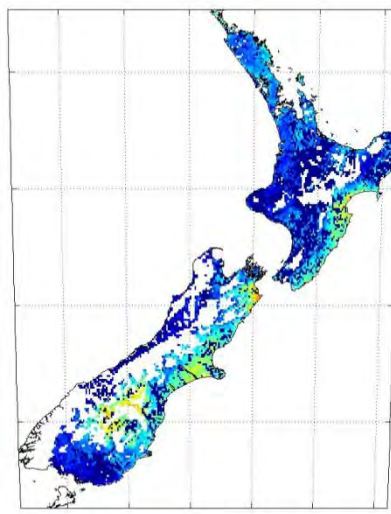
All of the results presented so far have assumed that no irrigation is used. Current pasture management in many areas of New Zealand under current climate conditions relies on irrigation. As some predicted changes in pasture production are related to predicted changes in average seasonal soil moisture, comparing potential pasture growth now and in the future in the absence of irrigation doesn't fully represent the situation faced by farmers. In the next section we consider the amount of irrigation required to avoid water shortage limitation of pasture growth and look at how these amounts are predicted to change. For annual and seasonal time periods, the 15-year means of additional required irrigation in mm per season (or annum) are calculated. One tailed, two-sample, unequal variance, t-tests at 5% significance level are performed to test whether these changes in required irrigation are significant or not. Figure 6-14, shows the mean annual irrigation demand for the baseline period and the two future projections. It shows a doubling in annual irrigation demand under the 'CCC' model in Canterbury, Marlborough and Hawkes Bay. Smaller increases in demand are seen in the same regions under the 'Planck' model.



[A] Baseline period 1997-2011



[B] 'CCC' model 2097-2111



[C] 'Planck' model 2097-2111

Figure 6-14: [A] Mean irrigation in mm per annum for baseline climate (1997-2011) to avoid water limitation. [B,C] Mean irrigation in mm per annum (same colour scale as [A]) in future climate (2097-2111) required to maintain soil moisture at half field capacity so that pasture growth is not water-limited, for the [B] 'CCC' model and [C] 'Planck' model.

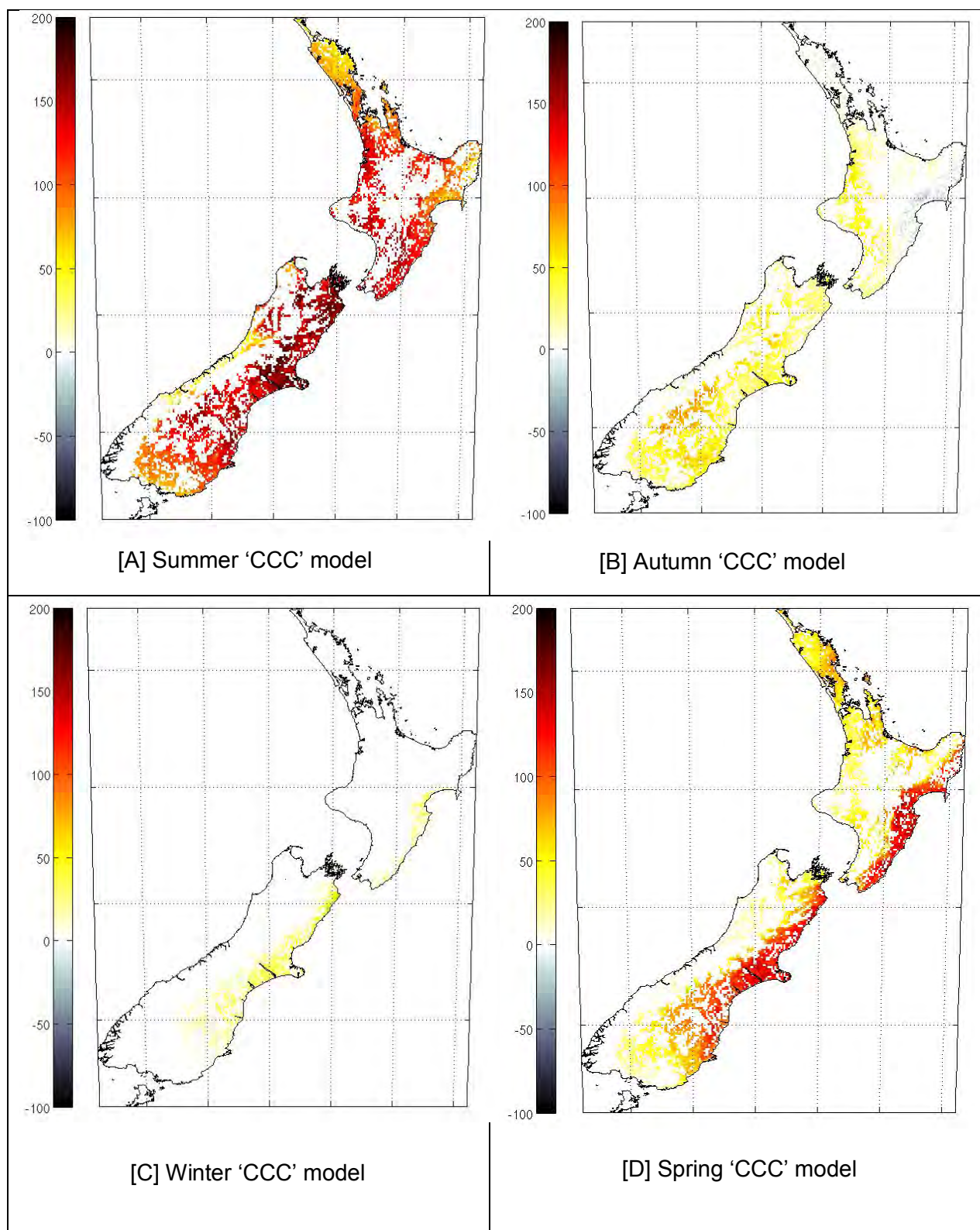


Figure 6-15: Mean additional irrigation in mm per season (2097-2111 relative to 1997-2011) required to maintain soil moisture at or above half field capacity so that pasture growth is not water-limited for the 'CCC' model.

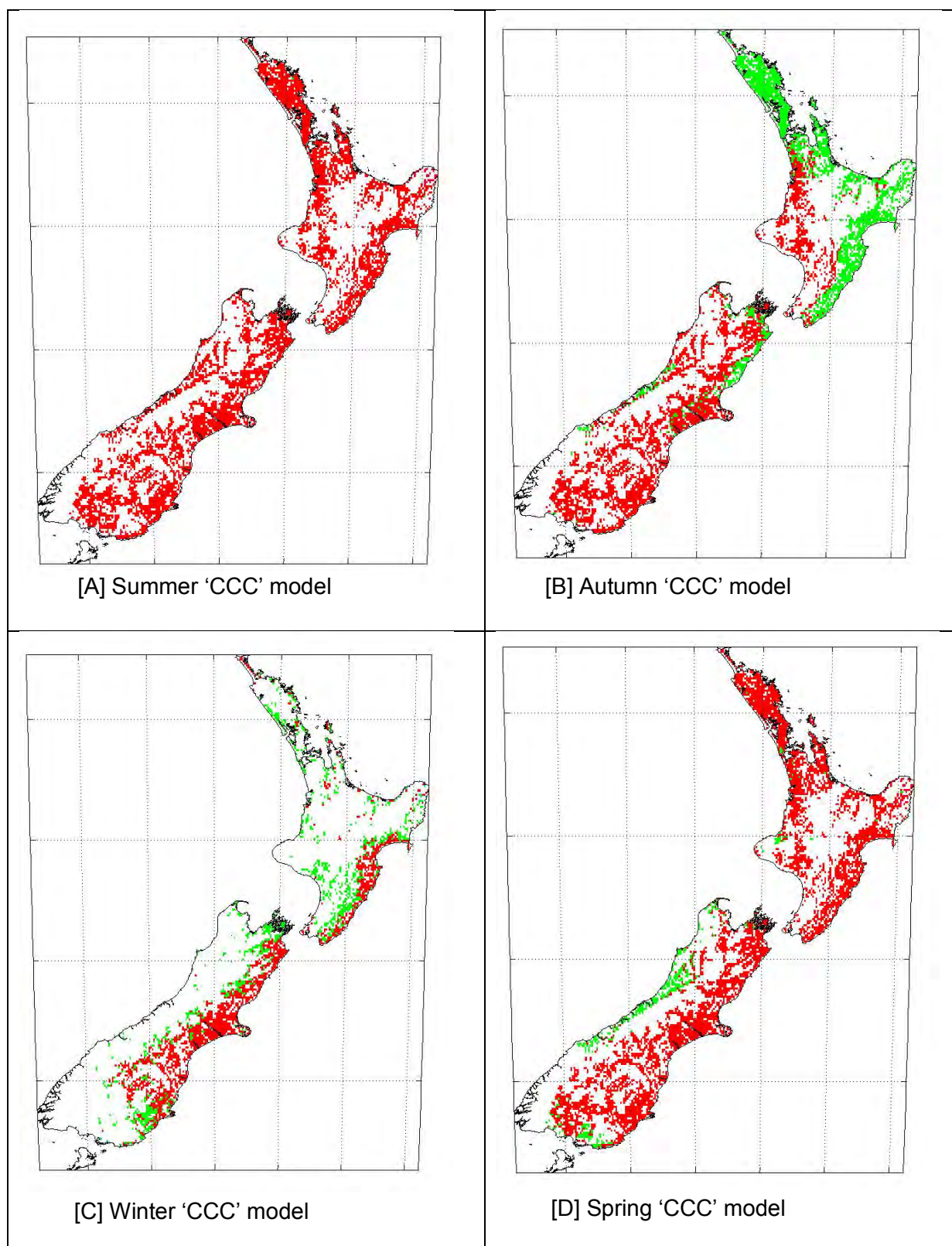


Figure 6-16: Mean irrigation required for no water limitation shows a statistically significant increase (red) or doesn't show a statistically significant increase (green). Single tail, two sample unequal variance t-test with $\alpha = 0.05$, H_0 Mean required irrigation in 2097-2111 under 'CCC' model is not greater than in 1997-2011, H_1 Mean required irrigation in 2097-2111 under 'CCC' model is greater than in 1997-2011.

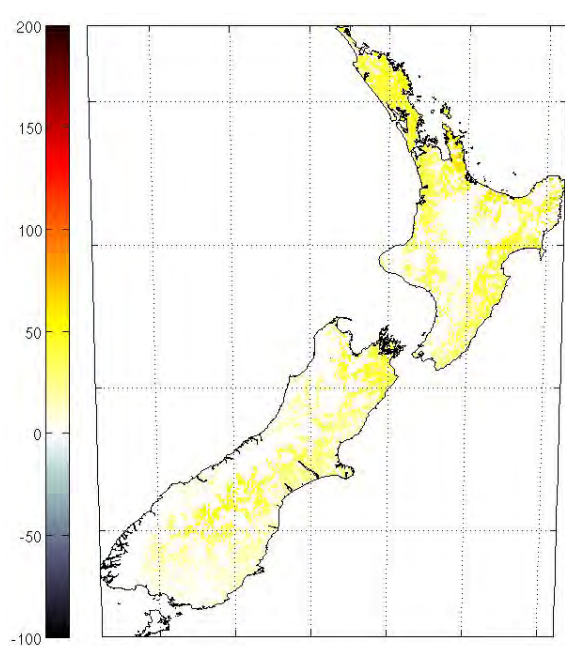
The seasonal breakdown of the change in irrigation demand is shown in Figures 6-15 and 6-16 for the 'CCC' model, and in Figures 6-17 and 6-18 for the 'Planck' model.

Figures 6-15A and 6-16A show that under the 'CCC' model, all NZ pasture regions show a statistically significant increase in required summer irrigation to avoid water limitation of pasture growth. The most affected areas are Marlborough and Canterbury, which Figure 6-15A shows to have an increase of between 150 and 200 mm in irrigation demand over the summer period. Northern Otago, Nelson, Wairarapa, Taranaki, King-Country, and Waikato show increases in irrigation demand of between 100 and 150 mm over the summer period. Northland, Southland and Northern Hawkes Bay show increases in irrigation demand of between 50 and 100 mm over the summer season.

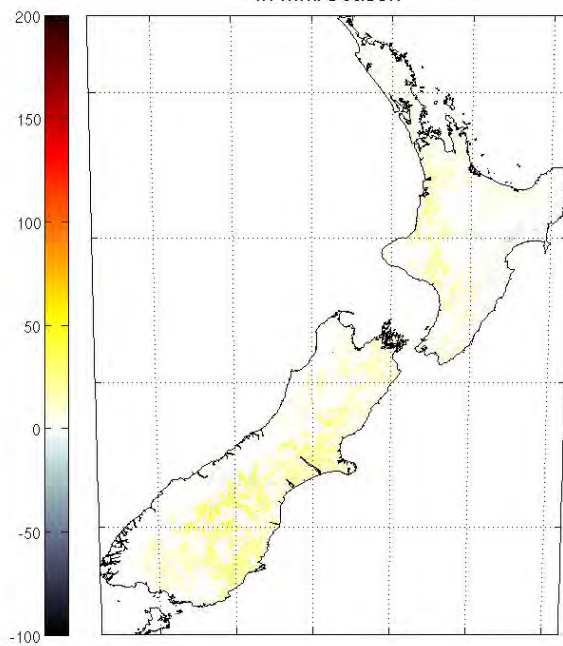
In autumn, increased irrigation demand is seen throughout most of the South Island (except the Marlborough to Kaikoura coastal areas), although amounts are in the order of 50 mm or less per season. Statistically significant increased irrigation demand is seen in coastal Waikato, King Country, Taranaki and the Manawatu; with increases in demand of 50 mm or less per season. Elsewhere in the North Island, there is no change in irrigation demand. In particular, note that the decrease in required autumn irrigation in Hawkes Bay seen in Figure 6-15B is not statistically significant (one-tail, two-sample, unequal variance t-test at $\alpha = 0.05$, with H_0 irrigation demand does not decrease).

Winter shows a statistically significant increase in irrigation demand on the east coast of both islands, though amounts are 25 mm or less per season.

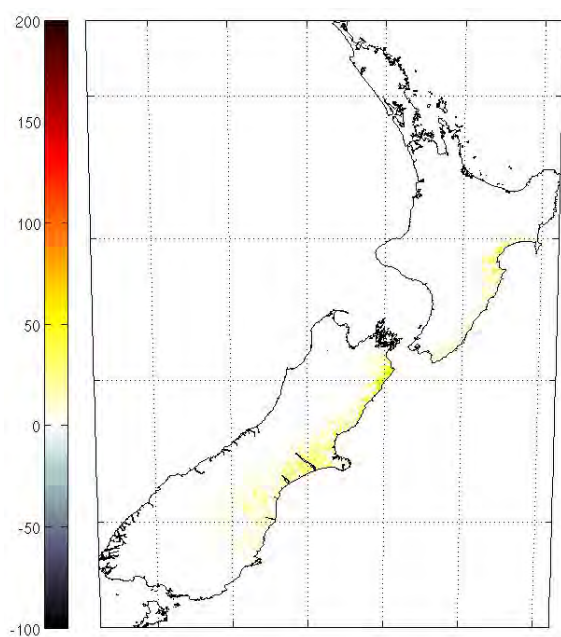
Spring shows statistically significant increased irrigation demand in all NZ pasture regions except the South Island west coast and parts of coastal Southland. Increased irrigation demand is strongest on the east coast of both islands where it exceeded 100 mm per season.



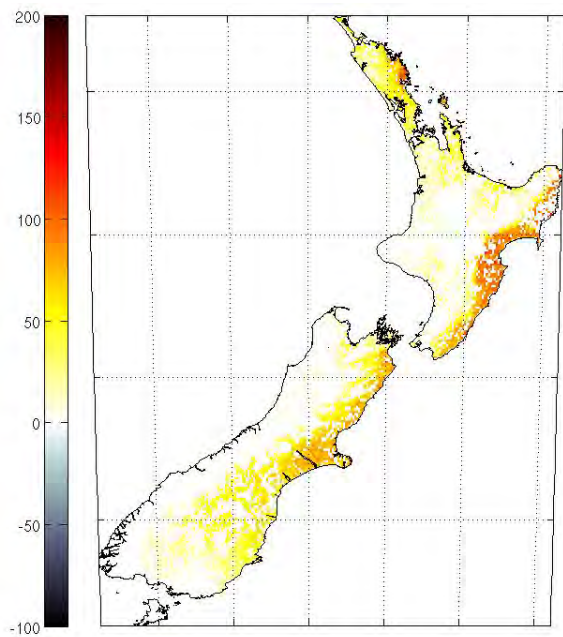
[A] Summer 'Planck' model



[B] Autumn 'Planck' model



[C] Winter 'Planck' model



[D] Spring 'Planck' model

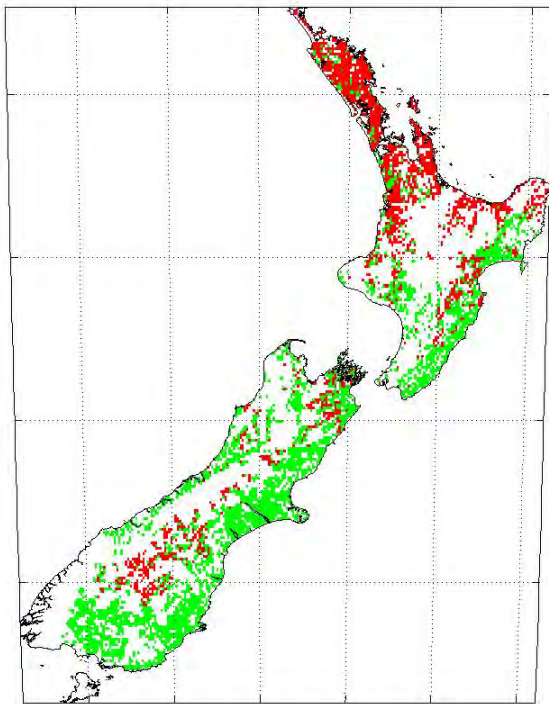
Figure 6-17: Mean additional irrigation in mm per season (2097-2111 relative to 1997-2011) required to maintain soil moisture at or above half field capacity so that pasture growth is not water-limited for the 'Planck' model.

Figures 6-17A and 6-18A show that, under the 'Planck' model, statistically significant increases in summer irrigation demand are seen in the Northern North Island (Northland, Auckland, Waikato, Coromandel, and Bay of Plenty). The irrigation demand increases are lower than seen in the 'CCC' model, with mean increased irrigation demand in these areas being 50 mm or less per summer. Elsewhere in the North Island there is no significant increase in irrigation demand. In the majority of the South Island under the 'Planck' model, there is no significant increase in summer irrigation demand; the exceptions being central Otago and inland Marlborough. As with the North Island, the increases in irrigation demand in central Otago and inland Marlborough are 50 mm or less per season.

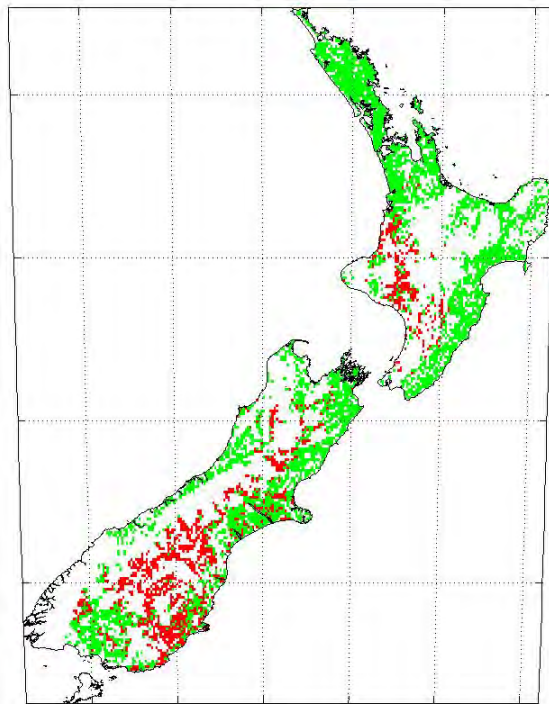
In autumn, under the 'Planck' model (Figures 6-17B and 6-18B), no significant change in irrigation demand is seen for the majority of New Zealand. Small (25 mm per season or less) statistically significant increases in irrigation demand are seen in Central Otago and the King Country/Whanganui region.

In winter, under the 'Planck' model (Figures 6-17C and 6-18C), no significant change in irrigation demand is seen for the majority of New Zealand. Small (25 mm per season or less) statistically significant increases in irrigation demand are seen in eastern coastal areas of Canterbury, Marlborough, Wairarapa and Hawkes Bay.

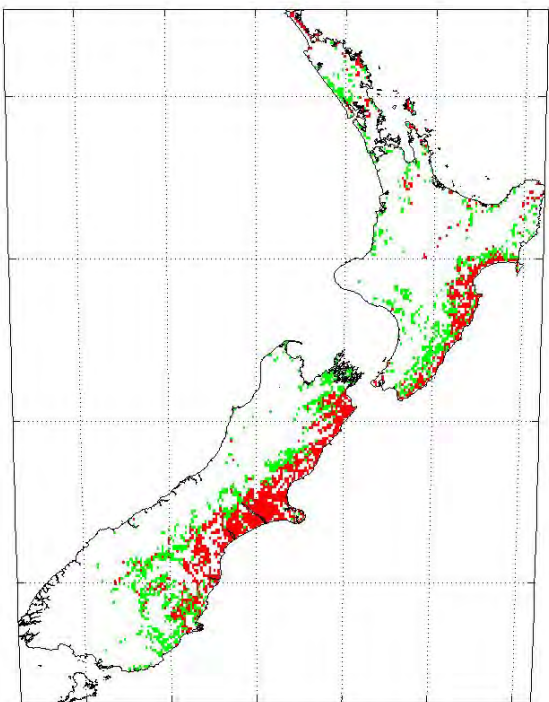
In spring, under the 'Planck' model (Figures 6-17D and 6-18D), significant increases in irrigation demand are seen in Canterbury, Wairarapa, Hawkes Bay, Bay of Plenty, Coromandel and Northland. Increases of around 75 mm a season are seen in Hawkes Bay and parts of Canterbury. Increases in other areas are smaller.



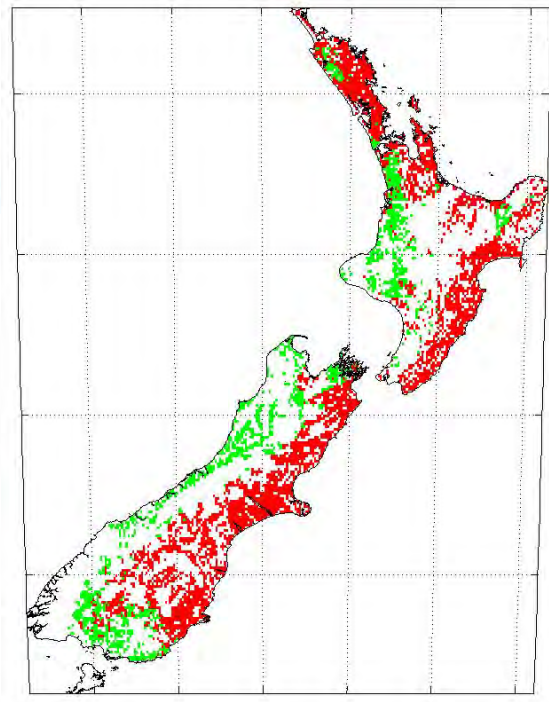
[A] Summer 'Planck' model



[B] Autumn 'Planck' model



[C] Winter 'Planck' model



[D] Spring 'Planck' model

Figure 6-18: Mean irrigation required for no water limitation shows a statistically significant increase (red) or doesn't show a statistically significant increase (green). Single tail, two sample unequal variance t-test with $\alpha = 0.05$, H_0 Mean required irrigation in 2097-2111 under 'Planck' model is not greater than in 1997-2011, H_1 Mean required irrigation in 2097-2111 under 'Planck' model is greater than in 1997-2011.

6.4 Conclusions

In this study, we have investigated the impact of changing climate on pasture growth under two models of projected future climate, both corresponding to a global mean increase of four degrees relative to pre-industrial climate. The models were chosen as ones that well represented New Zealand's current climate, but differed substantially in their future projections so as to give an idea of the range of possible change.

The observed changes are qualitatively the same for the two model scenarios but milder under the 'Planck' model compared to the 'CCC' model. This results because of two differences between the models in their projections for climate in the NZ region:

- (1) Local warming in the New Zealand region is about a degree warmer under the 'CCC' model compared to the 'Planck' model.
- (2) The two models have differing frequencies of westerly events which tend to lead to drier conditions in the east.

The most significant changes seen in pasture growth are seasonal shifts. Winter pasture growth increases significantly as a result of a reduction in the low temperature limitation of growth. Summer pasture growth in eastern areas (Canterbury and Hawkes Bay) decreases, due to lower soil moisture. Summer pasture growth in Northland also decreases as result of temperatures above the optimal growing temperature range. The same changes are seen with both models, but the changes are markedly larger under the 'CCC' model.

We also considered irrigation demand based on keeping soil moisture levels above half field capacity, to avoid water limitation of pasture growth. Under the 'CCC' model, most pasture areas of New Zealand show increases in irrigation demand, particularly in summer and spring. The most affected areas, Canterbury, Marlborough and Hawkes Bay show increases in irrigation demand of between 150-200 mm in summer and 100-150 mm in spring. The 'Planck' model shows qualitatively similar, but milder increases of around 50mm in irrigation demand.

7 New Zealand pasture production in 2100: Biome-BGC

7.1 Summary

Dairy and sheep/beef pasture production was modelled with the Biome-BGC model, calibrated to New Zealand pasture, to estimate pasture production in 2100 under a projected 4°C of global warming. This was compared to a present-day baseline scenario, which was constructed from historical climate records over the period 1997-2011. We give results for the percentage change in pasture production under our projected climate scenarios in 2100, using interpolated climate change patterns from two GCMs, CCC and Planck. We find significant differences in the impact on pasture production with the two models, with the model from the Canadian Climate Centre resulting in a pronounced decline in both sheep/beef and dairy pasture production. The Planck model results in a milder change, with only a slight decrease in sheep/beef, and an increase in dairy production. The severity of warming will determine the degree of impact on pasture production for both sheep/beef and dairy agriculture in New Zealand.

7.2 Methods

7.2.1 Biome-BGC model

The Biome-BGC (Bio-Geochemical Cycles) model² is an ecosystem process model that simulates the biological and physical processes controlling cycles of carbon, nitrogen and water of vegetation and soil in terrestrial ecosystems. The model is capable of simulating evergreen, deciduous and broadleaf forests, C3 and C4 grasslands, and shrub ecosystems. Its primary input consists of weather data at a daily time step, and it also requires site-specific elevation, soil composition and rooting depth. Weather conditions are the most important variables affecting the model processes and outputs. In addition, there is a set of 43 adjustable ecological parameters that can be customised for a particular ecosystem. The model is described in detail in references (Thornton et al. 2002; White et al. 2000; Thornton 1998; Thornton and Running 1999; White et al. 1997; Hunt et al. 1996; Kimball et al. 1997a; Kimball et al. 1997b; Running and Hunt 1993; White et al. 1999).

The Biome-BGC model's C3 grasslands mode is the primary tool we used to simulate two managed pasture systems: sheep/beef and dairy. While the model is not specifically designed for farm systems, or the presence of grazing animals, we identified some modifications of the model's ecological parameters that could be used to adequately represent grazing and harvest. Specifically, the "annual whole-plant mortality fraction" parameter can be related via a simple algebraic formula to pasture utilisation (the proportion of aboveground biomass eaten by grazing animals). We have assumed a fixed level of pasture utilisation of 0.55 and 0.90 in sheep/beef and dairy pasture systems, respectively. This results in a mortality proportion that is much higher than natural grassland. Similarly, the removal of meat and milk products from the system is factored into the "annual fire mortality fraction" parameter. Since fire is not normally a significant mechanism of nutrient removal in

² Biome-BGC Version 4.2 is developed and maintained by the Numerical Terradynamic Simulation Group, School of Forestry, The University of Montana, Missoula, Montana, USA. Available for download at <http://www.nts.g.umt.edu/project/biome-bgc#data-product>

managed pasture, this fraction represents the approximate proportion of nutrients removed from the ecosystem via milk and meat production. In our scenarios, dairy systems have a higher proportion removed (0.2) than do sheep/beef systems (0.1).

We have also included the combined effects of managed fertiliser application and fertility-driven nitrogen fixation through the model's site-specific nitrogen input parameter. The symbiotic and asymbiotic nitrogen fixation rate is typically in the order of 10^{-4} kg N/m²/year for most naturally occurring ecosystems. To mimic the application of fertiliser and animal waste deposits, we have set this rate much higher, in the order of $\sim 10^{-2}$. Dairy systems have nearly twice the rate N input via fixation and fertilisation (320 kg ha⁻¹ y⁻¹) than do sheep/beef (180 kg ha⁻¹ y⁻¹) in our scenarios.

7.2.2 Climate and input datasets

The Virtual Climate Station Network (VCSN) provides the daily weather input required by the Biome-BGC model. Our baseline scenario covers inputs from 1997-2011. Future climate under the scenario of 4°C of global warming circa 2100 was statistically downscaled to the VCSN by NIWA, using the two GCMs Planck and CCC (see Section 3.3). This input covers the nominal 15-year period 2097-2111. Direct and indirect inputs to the model from the network include maximum and minimum temperature, precipitation, solar radiation, vapour pressure deficit and wind run.

Although the Biome-BGC model does not have an explicit input mechanism for daily wind run, wind does have a significant evaporative effect on pasture growth in some New Zealand regions. We account for the role of wind in enhancing water loss from pastures by correcting the daily water vapour pressure deficit (VPD) input with the FAO Penman-Monteith effect of wind on evapotranspiration for grasslands. This effect is particularly important where hot, dry north-westerly winds enhance seasonal drought in the hill country and plains of New Zealand's east coast regions.

The required soil texture and effective rooting depth for each site was obtained from the Fundamental Soil Layers (FSL)³ dataset, which contains soil texture classes. The soil texture classes were matched to the %sand, %silt and %clay required by the model by visually identifying modal soil textures present in the National Soils Database. The FSL does not contain texture for the Gisborne region: a typical soil texture, intermediate between clay and silt, was used to represent this region.

Atmospheric CO₂ concentrations in the model are calculated by the ISAM Reference carbon cycle model for the 2097-2111 period, under the SRESA2 emission scenario (e.g., 2102 concentration is 771 ppm). CO₂ concentrations are held fixed for one year, and then updated on the first day of the year by linear interpolation.

³ maintained by Landcare Research; available at http://soils.landcareresearch.co.nz/contents/SoilData_FSL_About.aspx?currentPage=SoilData_FSL&menuitem=SoilData

7.2.3 Model Parameterisation

To optimise the Biome-BGC model for New Zealand conditions, we adjusted some key ecological parameters to best fit model output to measured pasture growth data in selected New Zealand locations. Treating New Zealand sheep/beef and dairy pasture systems as two different 'biomes' with unique parameterisations, we used an automated parameter estimation software package, PEST⁴, which uses the Gauss-Marquardt-Levenberg inversion method. We fitted the model's net primary production (NPP) output to historical pasture clipping data from six sites dispersed across New Zealand (three dairy and three sheep/beef). Data from these sites consists of monthly, bi-weekly, or weekly measurements of pasture clippings over a period of at least two continuous years. Our calibration method and model validation for New Zealand pasture was previously reported in references [Baisden et al 2010 and Keller, Baisden, and Timar 2011].

⁴ Latest version and documentation available free at <http://www.pesthomepage.org/Home.php>

7.3 Results

Figure 7-1 shows the potential pasture production for the baseline climate (1997-2011), as if all the available land was being used for either sheep/beef or dairy production. Figures 7-2 and 7-3 show how the pasture production changes under a future climate (nominally 2097-2111), for the Planck and CCC scenarios.

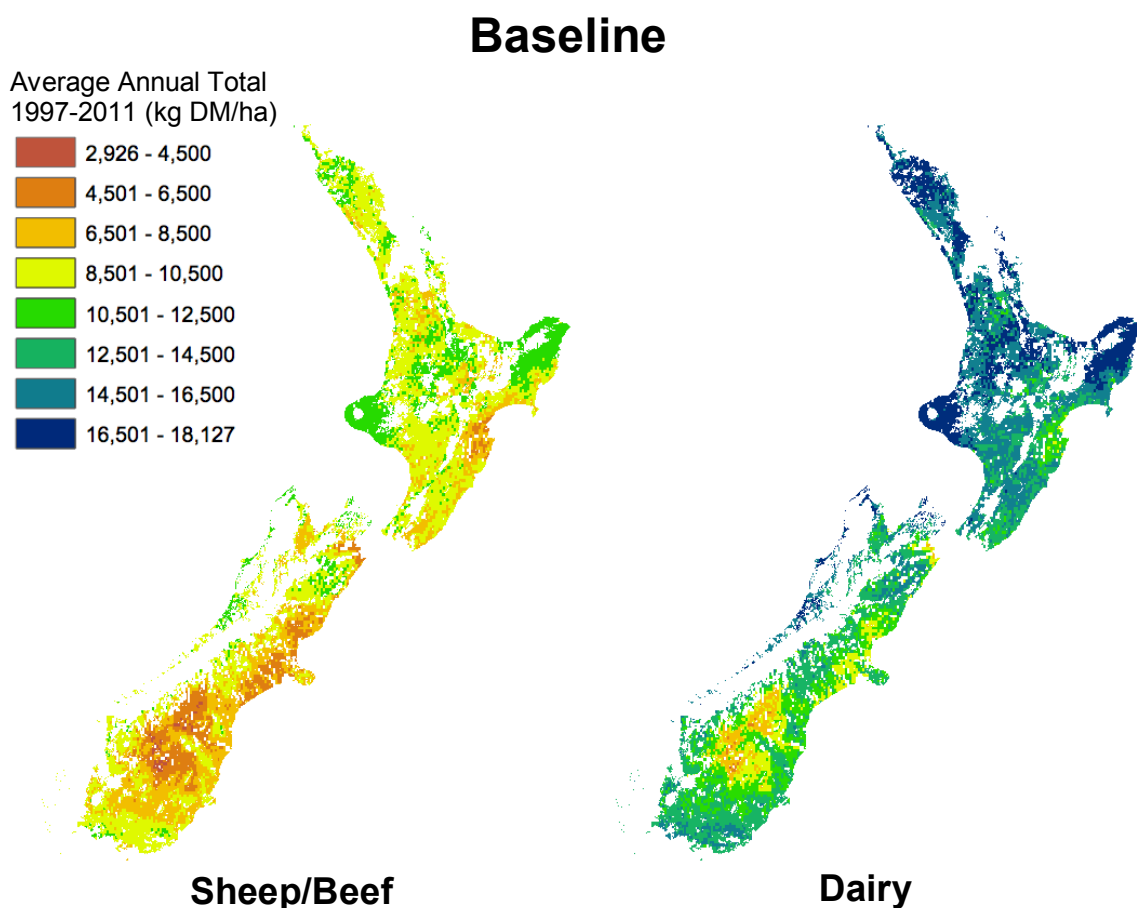


Figure 7-1: Baseline Pasture Production, average annual total over the 15 years 1997-2011 in kilograms of dry matter (DM) per hectare. Each map shows national pasture production as if all of the available land (excluding urban and conservation land) were sheep/beef (left) or dairy (right) agriculture systems, and is not an actual representation of current land use.

2100: Planck model

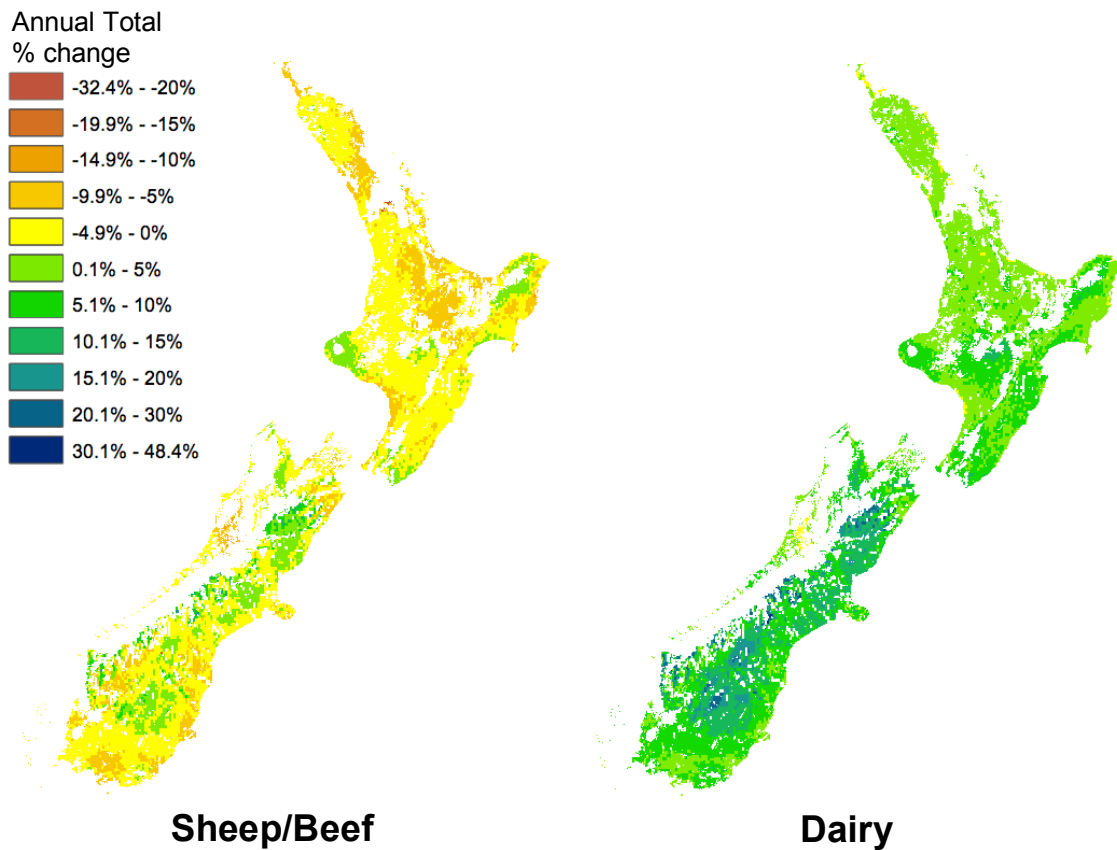


Figure 7-2: 2100 Planck model, percentage change in average annual total pasture production from the baseline model. As above, each map shows national pasture production as if all of the available land were sheep/beef (left) or dairy (right).

2100: CCC model

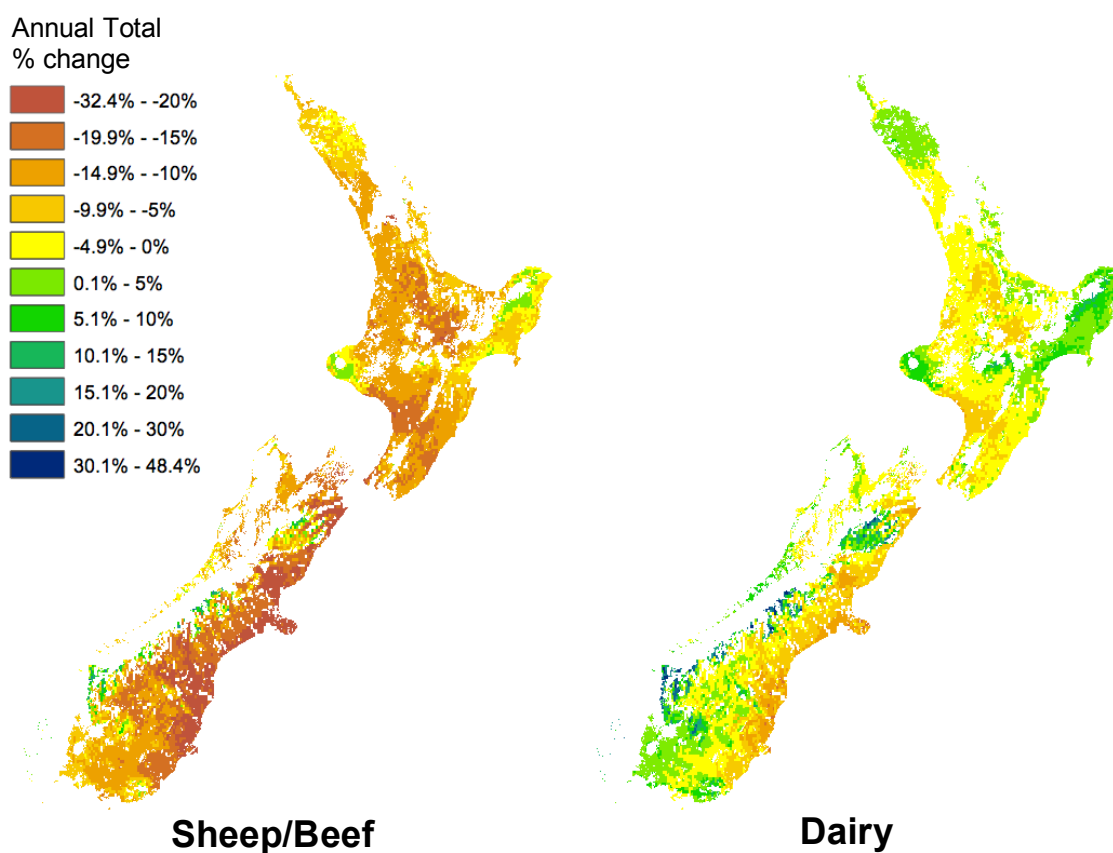


Figure 7-3: 2100 CCC model, percentage change in average annual total pasture production from the baseline model. As above, each map shows national pasture production as if all of the available land were sheep/beef (left) or dairy (right).

7.4 Regional and Seasonal Results by Pasture Type

The following tables show our modelled pasture production broken down by season, region and pasture type. All amounts shown are given in terms of metabolisable energy (ME). The amount of land under dairy and sheep/beef agriculture comes from Motu's Land Use in Rural New Zealand (LURNZ) model (data from 2008) and represents approximate present-day land-use. The sheep/beef and dairy breakdown given for future scenarios is the same as the present-day baseline case; thus land area under sheep/beef and dairy agriculture is identical in all scenarios. While we have only considered climatic factors in our analysis of national pasture production change, we note that there might be other factors (e.g., economic) that could significantly affect pasture production in the future.

Table 7-1: Baseline average production by region and season over the period 1997-2011 in units of metabolisable energy.

Region	Area kha	Winter MJ ha-1 d-1	Spring	Summer	Autumn	Average	Total ME TJ
Sheep & Beef							
Northland	239	131	435	247	151	241	20999
Auckland	85	123	452	266	134	244	7601
Waikato	473	105	446	298	143	248	42743
Bay of Plenty	66	102	416	298	174	248	5951
Gisborne	327	103	422	341	196	266	31745
Manawatu-Wanganui	936	87	438	288	137	237	81024
Hawkes Bay	586	88	387	188	153	204	43661
Taranaki	125	101	421	402	177	275	12535
Tasman	57	83	403	231	152	217	4524
Marlborough	310	58	305	253	134	187	21235
Westland	32	79	369	308	170	231	2677
Wellington	281	89	437	216	129	218	22317
Nelson City	2	83	408	258	117	217	196
Canterbury	1824	51	291	176	122	160	106386
Otago	1738	43	272	194	119	157	99507
Southland	698	57	369	268	146	210	53466
National	7778	69	350	230	135	196	556567
Dairy							
Northland	172	213	617	426	325	395	24815
Auckland	53	199	637	477	293	402	7733
Waikato	487	170	627	470	308	394	69953
Bay of Plenty	80	169	607	468	354	399	11617
Gisborne	3	173	577	539	380	418	381
Manawatu-Wanganui	127	137	604	470	261	368	17063
Hawkes Bay	16	126	561	409	303	350	2007
Taranaki	215	168	598	620	393	445	34946
Tasman	27	133	578	510	325	386	3843
Marlborough	9	118	529	422	276	337	1136
Westland	52	123	537	547	348	389	7434
Wellington	30	131	599	369	264	341	3690
Nelson City	0.4	114	497	333	266	302	47
Canterbury	119	89	462	289	246	272	11835
Otago	62	78	485	399	251	304	6833
Southland	106	85	525	497	282	347	13384
National	1557	153	588	472	311	381	216717
Combined	10983						909746

Table 7-2: 2100 CCC model average production by region and season in units of metabolisable energy. The percentage change from the baseline is shown in the last column.

Region	Area (kha)	Winter Average Production (MJ ha-1 d-1)	Spring	Summer	Autumn	Average	Total ME (TJ)	Change (%)
Sheep & Beef								
Northland	239	172	390	127	211	225	19603	-6.6%
Auckland	85	156	408	88	179	207	6470	-14.9%
Waikato	473	152	443	113	158	216	37346	-12.6%
Bay of Plenty	66	151	403	112	213	220	5289	-11.1%
Gisborne	327	157	411	216	235	255	30427	-4.2%
Manawatu-Wanganui	936	134	433	102	147	204	69621	-14.1%
Hawkes Bay	586	138	299	93	221	188	40090	-8.2%
Taranaki	125	144	471	257	133	251	11439	-8.7%
Tasman	57	132	390	90	157	192	3999	-11.6%
Marlborough	310	94	310	116	130	162	18406	-13.3%
Westland	32	107	384	205	135	208	2404	-10.2%
Wellington	281	138	388	59	163	187	19165	-14.1%
Nelson City	2	119	384	82	148	183	165	-15.5%
Canterbury	1824	80	243	80	116	130	86316	-18.9%
Otago	1738	68	259	109	98	134	84713	-14.9%
Southland	698	84	375	168	126	188	47947	-10.3%
National	7778	105	326	112	139	170	483402	-13.1%
Dairy								
Northland	172	327	577	275	419	400	25077	1.1%
Auckland	53	311	644	249	367	393	7560	-2.2%
Waikato	487	289	635	249	347	380	67506	-3.5%
Bay of Plenty	80	294	606	259	427	396	11524	-0.8%
Gisborne	3	294	588	435	437	439	400	5.0%
Manawatu-Wanganui	127	242	645	238	266	348	16136	-5.4%
Hawkes Bay	16	248	510	249	409	354	2032	1.3%
Taranaki	215	268	697	580	318	466	36594	4.7%
Tasman	27	241	638	346	318	386	3837	-0.2%
Marlborough	9	219	550	228	294	323	1090	-4.1%
Westland	52	208	617	435	305	391	7470	0.5%
Wellington	30	244	602	173	302	330	3574	-3.1%
Nelson City	0	211	484	160	321	294	46	-2.7%
Canterbury	119	176	387	158	276	249	10859	-8.2%
Otago	62	146	488	261	239	283	6381	-6.6%
Southland	106	153	613	380	257	351	13507	0.9%
National	1557	258	608	306	331	376	213593	-1.4%
Combined	10983						819994	-9.9%

Table 7-3: 2100 Planck model average production by region and season in units of metabolisable energy. The percentage change from the baseline is shown in the last column.

Region	Area (kha)	Winter Average Production	Spring Production (MJ ha-1 d-1)	Summer	Autumn	Average	Total ME (TJ)	Change (%)
Sheep & Beef								
Northland	239	168	399	183	180	233	20258	-3.5%
Auckland	85	153	422	172	157	226	7047	-7.3%
Waikato	473	142	446	218	149	239	41195	-3.6%
Bay of Plenty	66	140	410	199	189	234	5636	-5.3%
Gisborne	327	148	406	262	219	259	30890	-2.7%
Manawatu-Wanganui	936	123	440	209	146	229	78330	-3.3%
Hawkes Bay	586	131	320	147	196	199	42439	-2.8%
Taranaki	125	127	439	359	160	271	12350	-1.5%
Tasman	57	120	399	185	159	216	4490	-0.7%
Marlborough	310	87	306	209	142	186	21081	-0.7%
Westland	32	75	363	279	158	219	2532	-5.4%
Wellington	281	132	407	153	158	212	21775	-2.4%
Nelson City	2	112	393	186	134	206	186	-4.7%
Canterbury	1824	78	269	153	131	158	105037	-1.3%
Otago	1738	60	273	165	113	153	97026	-2.5%
Southland	698	68	375	228	137	202	51436	-3.8%
National	7778	97	338	185	143	191	541710	-2.7%
Dairy								
Northland	172	309	582	346	383	405	25409	2.4%
Auckland	53	292	646	363	337	410	7886	2.0%
Waikato	487	262	642	381	334	405	71941	2.8%
Bay of Plenty	80	264	613	359	396	408	11864	2.1%
Gisborne	3	270	581	470	421	435	397	4.3%
Manawatu-Wanganui	127	218	653	378	278	382	17720	3.8%
Hawkes Bay	16	224	534	335	378	368	2111	5.2%
Taranaki	215	242	651	611	382	471	37034	6.0%
Tasman	27	212	629	458	342	410	4080	6.1%
Marlborough	9	204	552	360	307	356	1202	5.8%
Westland	52	161	581	516	346	401	7665	3.1%
Wellington	30	225	621	298	309	363	3932	6.6%
Nelson City	0.4	195	502	286	310	323	50	6.9%
Canterbury	119	174	434	287	302	299	13031	10.1%
Otago	62	132	526	366	267	323	7266	6.3%
Southland	106	126	597	456	279	365	14044	4.9%
National	1557	235	608	408	336	397	225631	4.1%
Combined	10983						902754	-0.8%

7.5 Discussion

Our baseline scenario gives a total average annual national pasture production of around 910 TJ, which is consistent with the previous estimates used to compile New Zealand's UNFCCC emissions inventory. Using this baseline for comparison, we calculate the percentage change in production under the warming scenario for each of the two GCMs circa 2100 (2097-2111).

Under the two future scenarios, Planck seems to be the milder one. Sheep/Beef pasture production declines slightly, at around -3%, and dairy production increases by 4%, resulting in virtually no change nationally. With the CCC model, however, production for both sheep/beef and dairy systems declined, with sheep/beef decreasing by as much as -13%, while dairy decreases by about -3%. The decline is especially pronounced in the South Island regions of Canterbury and Otago, where sheep/beef production decreases by -19% and -15% and dairy decreases by -8% and -7%, respectively. These results are consistent with the patterns of climate change predicted for New Zealand by each climate model, with CCC predicting a larger increase in temperatures and more drastic changes in rainfall, especially in the spring and summer months. The eastern regions of the South Island in particular are drier and warmer during these crucial growing seasons.

Overall, the outlook for pasture growth appears mixed. Under a milder warming scenario, such as the Planck model, our results shows that pasture production will not change much, but with a more extreme pattern of climate change, New Zealand pasture could experience significant adverse effects. The severity of warming will determine the degree of impact on pasture production for both sheep/beef and dairy agriculture in New Zealand.

8 New Zealand Forestry

8.1 *Pinus Radiata* Simulation: the CenW model

8.1.1 Abstract

The physiologically-based growth model CenW was used to simulate the response of wood productivity of *Pinus radiata* forests to climate change in New Zealand. Climate change simulations were based on monthly climate change fields of two GCMs (CCC and Planck) that displayed more extreme climatic changes (4° global temperature increase) than used in previous studies (Kirschbaum *et al.*, 2012). These simulations essentially corresponded to runs for 2005 and 2105. For the later simulation time period, these simulations also used higher CO₂ concentrations than used in previous work.

For runs with CO₂ concentrations held constant at values corresponding to the 1990-2020 period, there were significant growth responses to climatic changes across the country, especially under the CCC scenarios. Even though mean productivity changed by only -16% and -3% under the CCC and Planck scenarios respectively, there were large changes for individual sites, with a diversity of responses most pronounced for sites currently having moderate productivity. More specifically, there were growth reductions in the warmer north and drier east coast, but gains in the cooler south, and at higher altitudes.

When increasing CO₂ concentration corresponding to the 2090-2120 period was also included, responses of wood productivity were generally positive, with average increases of 30% and 40% under the CCC and Planck scenarios, respectively. These responses varied regionally, ranging from relatively minor changes in the north of the country to very significant increases in the south, where the beneficial effect of increasing CO₂ combined with the beneficial effect of increasing temperatures.

Changes recorded for the sites of the current pine growing estate were about 10% more negative than for the average across New Zealand. Hence, for simulations with constant CO₂, productivity was modelled to change by about -17%, with 4% of sites having lowered productivity by more than 50% and 3% having productivity gains by more than 20%. For simulations with increasing CO₂, productivity changed by about +25%, with only 5% modelled to suffer slight losses, and 5% having productivity gains greater than 60%. There is still incomplete understanding of the long-term plant response to elevated CO₂, so that it is not certain that the beneficial effect of elevated CO₂ will be as large as modelled here.

8.1.2 Introduction

Pinus radiata D. Don is the most widely planted species in New Zealand, where it constitutes 90% of the 1.8 Mha plantation resource. Previous research funded by MAF allowed the physiological growth model CenW to be parameterised and run to describe wood productivity under current climatic conditions. This was based on an extensive set of plot data covering a wide environmental range within New Zealand (Kirschbaum *et al.*, 2010; Kirschbaum & Watt, 2011). Because CenW is a physiologically-based growth model, it could be used to explore the effect of changes in any of the key driving variables on resultant wood productivity (Kirschbaum *et al.*, 2010; Kirschbaum *et al.*, 2012).

Climate change is emerging as one of the key factors influencing the productivity of biological systems in future. Forest productivity is strongly controlled by environmental drivers (e.g., Kirschbaum & Watt, 2011). It is therefore likely that future wood productivity will be impacted by changes in air temperature, water availability and CO₂ concentration. Productivity responses to temperature and water availability can be modelled fairly confidently, because model performance can be compared against differences in wood productivity under current climatic conditions (e.g. Fig. 8-1).

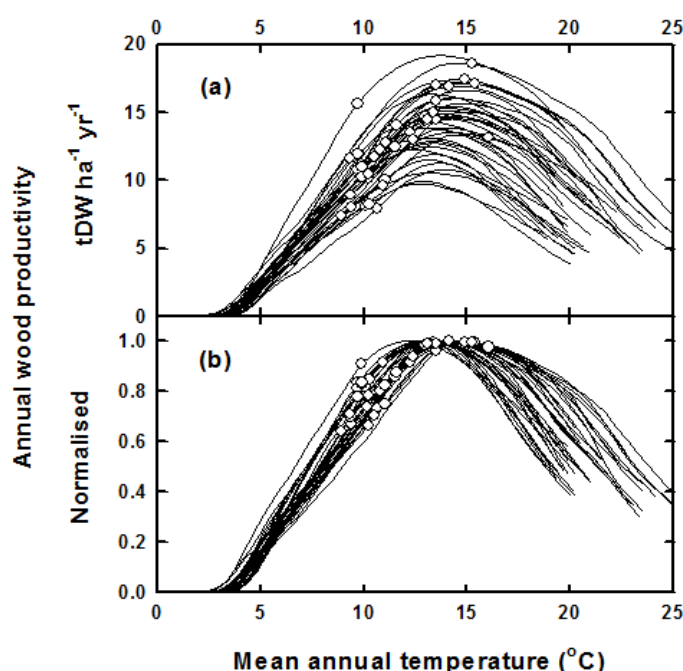


Figure 8-1: Wood weight production as a function of temperature shown as absolute values in (a) and normalised to the highest productivity at each site in (b). Symbols represent 38 distinct locations from which growth data had been available to parameterise the model. Predicted responses to variations in temperature for each site are shown as solid curves. For the simulations at each site, factors other than temperature and humidity were kept at the values observed at those sites. Data redrawn from Kirschbaum & Watt (2011).

It is more difficult to assess productivity responses to CO₂ concentration, as historic variability in CO₂ concentration is too small to make empirical testing of models practical. Model performance must therefore be judged against theoretical considerations and an analysis of plant responses from sites with experimentally enhanced CO₂ concentration. The extent of growth response to increasing CO₂ concentration still remains uncertain. Growth responses of *Pinus radiata* to doubling CO₂ concentration have been reported to be in the order of 20-30% under fertile and well-watered conditions (e.g. Norby *et al.*, 1999, 2005), but are likely to be less under nutrient-limited conditions (e.g. Kirschbaum, 1999b; Norby *et al.*, 2010). There are strong theoretical reasons for expecting greater growth responses under water-limited conditions (e.g. Kirschbaum, 1999b), but experimental support for that notion is ambiguous (e.g. Nowak *et al.* 2004). In any case, model runs need

to account for the complex, but potentially important, feedbacks between CO₂ concentration, soil nutrition and water cycling (Kirschbaum, 1999b; Simioni *et al.*, 2009; Medlyn *et al.*, 2011).

Previous work modelled wood productivity of *Pinus radiata* for 2040 and 2090 in New Zealand under a comprehensive set of three climate change emissions scenarios, with weather patterns generated under 12 different GCMs run with both constant and increasing CO₂ concentration (Kirschbaum *et al.*, 2012).

In those runs and under constant CO₂, there were only slight growth responses to climate change across the country as a whole. More specifically, there were slight growth reductions in the warmer north, but gains in the cooler south, especially at higher altitudes. For sites where *P. radiata* is currently grown, and across the full suite of GCMs and emission scenarios, changes in wood productivity averaged +3% for both 2040 and 2090.

When increasing CO₂ concentration was also included, responses of wood productivity were generally positive, with average increases of 19% by 2040 and 37% by 2090. These responses varied regionally, ranging from relatively minor changes in the north of the country to very significant increases in the south, where the beneficial effect of increasing CO₂ combined with the beneficial effect of increasing temperatures. These relatively large responses to CO₂ depend on maintenance of the current adequate fertility levels in most commercial plantations.

These responses can be understood by reference to Figure 8-1. Most plantations in New Zealand are situated at locations of slightly sub-optimal to optimal temperatures. Stands at these locations could therefore benefit from some slight increase in temperature. Most plantations also currently receive close to optimal rainfall (data not shown), so that slight deviations in rainfall would not be expected to have major effects on productivity. At the same time, climatic changes for New Zealand are likely to be fairly mild because of the buffering effect of the large ocean surrounding New Zealand: the mean temperature increase obtained from 12 GCMs under even the high-emission A2 scenario being just 2.5°C, and mean precipitation change being +3% (Kirschbaum *et al.*, 2012).

This leads to the question as to whether these mild responses would be sustained over a wider range of climatic changes as might occur either further out into the future, or if the buffering effect of the surrounding ocean might not ultimately manifest itself as strongly as currently expected in the existing GCMs. This previous work is therefore extended here by running simulations specifically under more extreme (4°C global temperature rise) climate change scenarios.

8.1.3 Models & Methods

The present work used the physiologically based CenW model vers. 4.0, which incorporates the key environmental drivers likely to change in future (Kirschbaum, 1999a). CenW has been developed primarily for climate-change investigations, and incorporates the key processes and feedbacks between plants, soils and the environment. It is therefore ideal for modelling forest growth in response to multiple changes and interactions. It was also successfully used for modelling wood productivity of *P. radiata* under current climatic conditions in New Zealand (Kirschbaum & Watt, 2011), which required a confident

parameterisation of the processes that govern the growth response to temperature and water availability.

The model runs on a daily time step and simulates stand characteristics, such as leaf-area development, stand height, basal area development, litter fall and the exchanges of water, nitrogen and carbon. The model includes explicit linkages between the carbon and nitrogen cycles in plants and the soil which allows multiple factors to constrain growth at daily and longer time scales.

Photosynthetic calculations were based on combining the photosynthesis model of Farquhar & von Caemmerer (1982) with the simple stomatal model of Ball et al. (1987). These instantaneous leaf-level equations of photosynthesis were scaled up to the canopy and to a daily time scale, using the equations of Sands (1995). Daily evapotranspiration was calculated with the Penman-Monteith equation, with canopy conductance explicitly linked to photosynthetic carbon gain through the Ball-Berry model. Maximum photosynthetic capacity depended on foliar nitrogen status temperature modifiers, water stress and constraints by water logging and excess rainfall.

Carbon allocation to different plant organs, such as foliage, wood and roots, was determined by plant nutrient status, tree height and species-specific allocation factors. The allometric relationship between height and diameter has been refined in a related study, so that the slope in this relationship is now expressed explicitly as a function of tree age, stand density, nutrient status and temperature as described by Watt & Kirschbaum (2011).

Organic matter dynamics were calculated with a version of the CENTURY model (Parton et al., 1987) that was slightly modified to better model the dynamics of forest soils and litter that have C:N ratios which are often wider than those of agricultural and grassland soils (Kirschbaum & Paul, 2002). As such, the model contains a complete and coupled nitrogen cycle, with nitrogen taken up by stands following decomposition and nitrogen mineralisation. Nitrogen was eventually returned to the soil in senescing plant organs, especially foliage and fine roots.

As external drivers, the model requires soil water holding capacity, soil texture and initial site fertility, and daily inputs of minimum and maximum temperature, precipitation, solar radiation and absolute humidity. Soil water holding capacity and soil texture were obtained as a spatial layer from the national soils data base (<http://gisportal.landcareresearch.co.nz/webforms/>), while a national surface for soil nitrogen concentration (W.T. Baisden, pers. comm.) was used to set initial site fertility.

The short-term dependence of photosynthesis on CO₂ concentration is well-constrained by short-term photosynthetic measurements. In longer term CO₂ enrichment experiments, photosynthetic rates often decline (downward acclimation) if plants have excess carbohydrate or limited access to required nutrients. Nutrient feedback limitations are included in the model through coupled carbon and nitrogen cycles in the model. However, downward acclimation sometimes occurs, even when nutrition is not limiting (Lewis et al., 2002; Ainsworth et al., 2004). This process has not yet been well quantified through prior research, and our CO₂ simulations were run without inclusion of this possible feedback effect that would have reduced the magnitude of the beneficial CO₂ fertilisation effect. In order to bracket the likely true response, simulations were run either with CO₂ concentrations

representative of the year 2005 (designated “constant CO₂”), or with that assumed for the year 2105 in the climate scenarios used here (designated “increasing CO₂”). True plant responses are likely to lie between these two extremes, but probably closer to those given by increasing CO₂.

8.1.4 Meteorological surfaces used to describe current and future climate

Simulations for the current climate were based on NIWA’s Virtual Climate Station Network of daily weather data at a regular grid across New Zealand. Daily data are estimated for the whole of New Zealand on a 0.05° latitude/longitude grid, using a thin-plate smoothing spline to spatially interpolate daily observational data (Tait *et al.*, 2006; Tait, 2008; Tait & Liley, 2009). The spline methodology incorporates topographic and other spatial information (depending upon the weather variable) to aid the interpolation.

For the purposes of this study, the 15-year period 1997–2011 was used to define the current (designated 2005) climate. As pine simulations ran for 30 years to simulate a full rotation, we used the available weather sequence twice. Future weather sequences were generated through modifying the daily temperature, rainfall and absolute humidity observations for 1997–2011 by mean changes described by the climate change surfaces (see Section 3). Two different GCM outputs were available, designated as CCC and Planck. Temperature was modified by a given offset, and precipitation and solar radiation were modified by a proportional change.

8.1.5 CO₂ concentrations

The sequence also contained CO₂ concentrations for those years. They were then extrapolated forwards and backwards, using a second-degree polynomial to estimate CO₂ concentrations from 1990–2019 and 2090–2119. The simulations thus compare the periods 1990–2019 (centred on 2005) and 2090–2119 (centred on 2105). CO₂ concentrations were 356 ppm (1990), 375 ppm (2005), 410 ppm (2019), 669 ppm (2090), 776 ppm (2105) and 899 ppm (2119).

8.1.6 Model fitting to current climate

As previously described (Kirschbaum & Watt, 2011), CenW was parameterised under the current climate against growth data from permanent sample plots covering almost the complete environmental range across which *P. radiata* is grown within New Zealand. This data consisted of 101 sites situated at 38 distinct locations with 1,297 individual observations of height and/or basal area, from which diameters and volumes could also be calculated. Using parameter values described in Kirschbaum & Watt (2011), there was excellent correspondence between model predictions and measurements over a wide range of sites and stand ages. Nash-Sutcliffe model efficiencies (Nash & Sutcliffe, 1970) for modelling forest growth ranged from 0.828–0.892 for height, basal area, diameter and volume.

8.1.7 Simulations

Using the parameters determined from the model fitting, future wood productivity was simulated at 0.05 degree resolution for all of New Zealand over a rotation length of 30 years for periods centred around 2005 and 2105, with weather data obtained as described determined for the 2005 or 2105 periods. The available data were based on observations for the 1997–2011, with little systematic trend apparent within the weather sequence. For the

forest simulations, 30 years of weather were needed, and the available weather sequence was used twice.

Soil fertility in CenW is determined by the amount of carbon and nitrogen in different organic matter pools, and by the rate at which organic matter turns over and mineralises organic nitrogen. The model was therefore initialised by setting relative soil organic matter pool sizes proportional to soil nitrogen concentrations obtained from a national surface (W.T. Baisden, pers. comm.). The same initial values were used for current-day and future simulations. No extra fertiliser was applied during the simulations. Simulations used a standard silvicultural scenario that included planting at 1,000 stems ha⁻¹, followed by two thinnings at age 5 and 8 to respective stand densities of 500 and 300 stems ha⁻¹. Simulations continued until age 30 which is a typical rotation length over which *P. radiata* is grown in New Zealand.

8.1.8 Statistics

Results are shown either for New Zealand as a whole, or only for the current forestry estate based on the current location of forestry plantations in New Zealand. Our available data base recorded the plantation area within each 0.05 degree grid used for analysis. For calculating mean productivity of stands in the forestry estate, productivity modelled for each 0.05 degree location was weighted by the area of forest within that 0.05 degree location. For the histograms in Figure 8-7, 0.05 degree locations were categorised as either containing plantation forests or not containing any: probability of productivity changes were then calculated based on the sites containing forests.

For Figure 8-5, data were combined based on current productivity in steps of 1 m³ ha⁻¹ yr⁻¹. Future productivity for those bins was then expressed as means and standard deviations.

8.1.9 Results

Growth patterns modelled for 2005 were similar to previous simulations based on the 1990 climate (Fig. 8-2), with mean productivity for all of New Zealand increased slightly from 23.7 to 24.0 m³ ha⁻¹ yr⁻¹ (Table 8-1). At the same time, there were also differences apparent in the detailed regional patterns, with increased productivity (by 2005) in eastern coastal regions and the Tasman district, while there were reductions over most of the western and central parts of the North Islands and the mountain regions of the South Island.

These differences reflect slight climatic inter-annual variations and the slightly higher CO₂ concentrations over the 2005 period. This comparison basically confirms that base line simulations were similar in the current and previous work, so that the comparison of future productivity can be done against similar base-line productivity; but they also sound a note of caution, in that productivity differences by 10% or more can be found simply as a result of on-going inter-annual or inter-decadal climatic variability, and do not necessarily reflect the consequence of on-going directional climate change. At the same time, the simulations shown in the following used climate change fields superimposed onto the existing observed weather, so that the peculiarities of a particular weather sequence were replicated in both the current and future-climate runs.

Mean responses modelled with constant CO₂ showed a general decrease in productivity between the 2005 and 2105 climates for both scenarios (Table 8-1), but with more adverse changes (-16.4%) under the CCC than the Planck (-2.8%) scenario. When increasing CO₂

was also factored in, responses became positive for both scenarios, but retained the difference between CCC (+29.9%) and Planck (+40.0%) scenarios.

Currently, existing plantations are mainly situated in regions with higher productivity, with mean productivity of $30.0 \text{ m}^3 \text{ ha}^{-1} \text{ yr}^{-1}$ for sites in the actual estate, compared to $24.0 \text{ m}^3 \text{ ha}^{-1} \text{ yr}^{-1}$ as the average for the country as a whole. Forestry is mainly situated in regions with moderate, but not very-high, growth potential, with the more profitable dairying taking precedence in the most productive regions. In response to climate change, the current forest estate is likely to be somewhat more adversely affected than the country as a whole – by about 10% more adverse changes across the combination of scenarios and constant/increasing CO_2 .

Table 8-1: Mean wood volume productivity under different scenarios. Shown are productivity in $\text{m}^3 \text{ ha}^{-1} \text{ yr}^{-1}$. Numbers in bracket gives the percentage change relative to 2005 simulations. Numbers in the top three rows refer to all locations in New Zealand, and numbers in the bottom rows refer only to those locations where *P. radiata* is currently grown.

	1990	2005	2105	
			const CO_2	incr. CO_2
Average for NZ	23.7	24.0		
CCC			20.1 (-16.4%)	31.2 (+29.9%)
Planck			23.4 (-2.8%)	33.7 (+40.0%)
Forest estate	29.8	30.0		
CCC (forest estate)			22.5 (-25.0%)	35.3 (+17.8%)
Planck (forest estate)			27.2 (-9.3%)	39.4 (+31.6%)

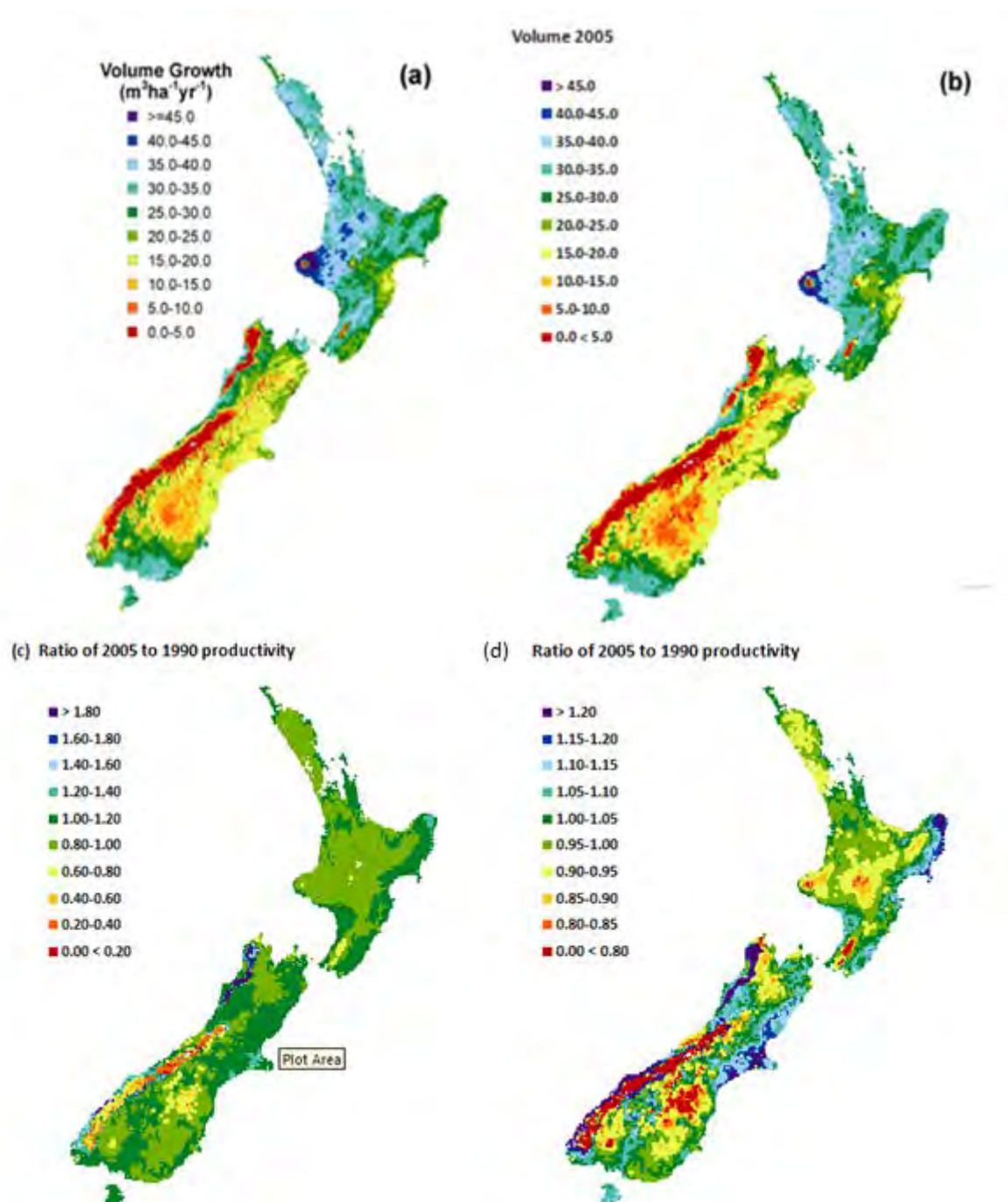


Figure 8-2: Wood volume production for 1990 (a) and 2005 (b) and the ratio of 2005 over 1990 production (c, d) at two different resolutions. Data for 1990 have been redrawn from Kirschbaum & Watt (2011).

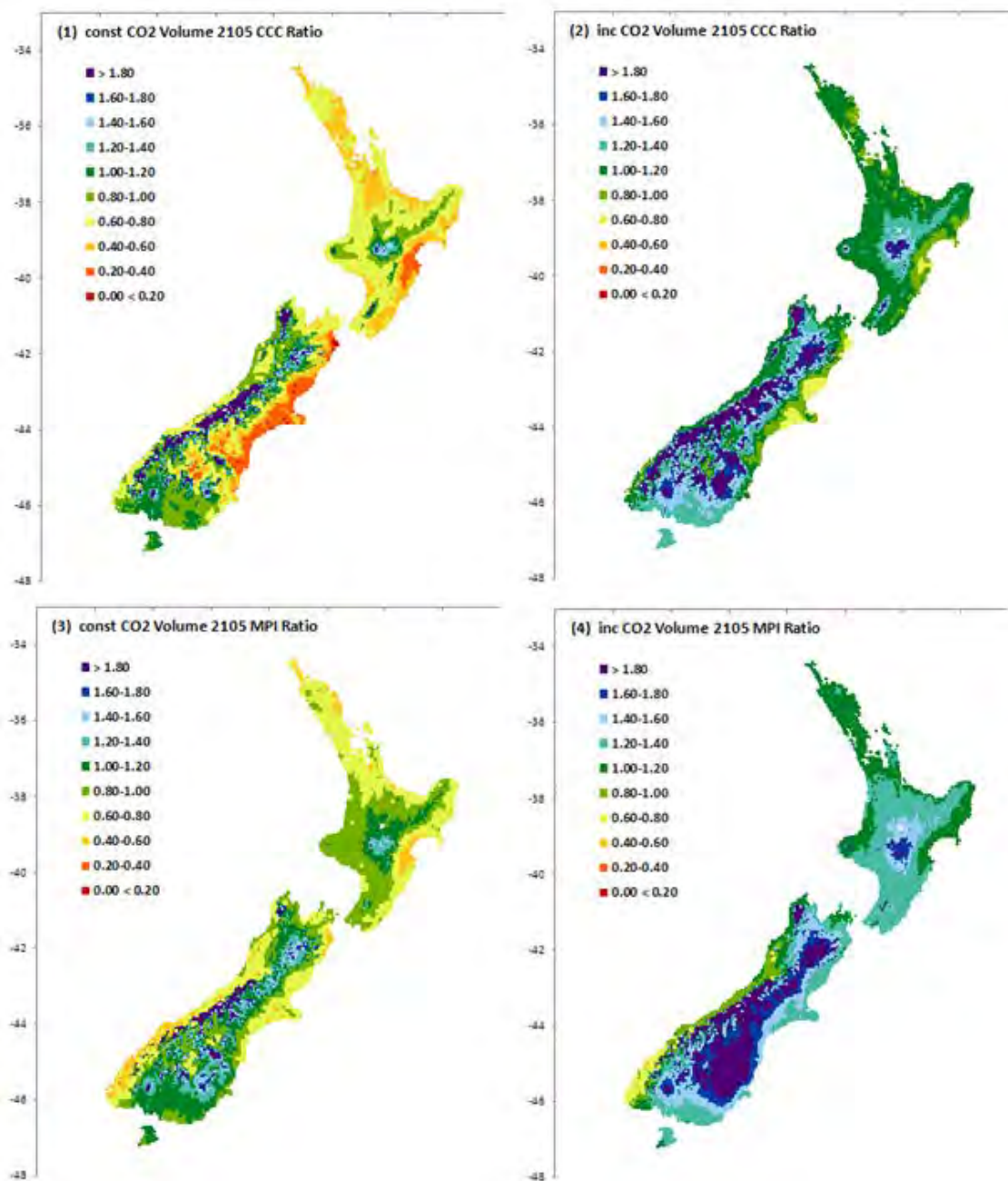


Figure 8-3: Ratio of wood volume production for 2105 (compared to the 2005 base climate) for the CCC (top panels) and Planck scenarios (bottom panels). Simulations are shown without (left panels) and with (right panels) increasing CO₂ concentration.

The regional patterns of productivity changes under climate change are shown in Figure 8-3. With constant CO₂, modelled productivity was reduced for most of the North Island, especially the far north, and the drier east coast and parts of central Otago. This pattern was much stronger under the CCC (Fig. 8-3(1)) than the Planck scenario (Fig. 8-3(3)). These large reductions in productivity probably reflect worsening water relations, with increasing temperature increasing evaporative water demand, while rainfall decreased in regions experiencing the steepest decreases.

At the same time, there were positive growth trends for the mountain regions of both islands, and the far south of the South Island. Some of these proportionately large increases started from a very low base, however. These trends were a direct consequence of increasing temperature alleviating the most important growth constraint in these cool regions. These trends, too, were stronger under the CCC than Planck scenario.

When increasing CO₂ was included, growth reductions were generally prevented and turned towards gains in almost all regions, except the east coastal regions of both islands under the CCC scenario (Fig. 8-3(2)) and the west coast of the South Island under the Planck scenario (Fig. 8-3(4)). Largest gains were generally observed in mountain regions of both islands, where the beneficial effects of increasing temperature combined with the benefits of increasing temperature.

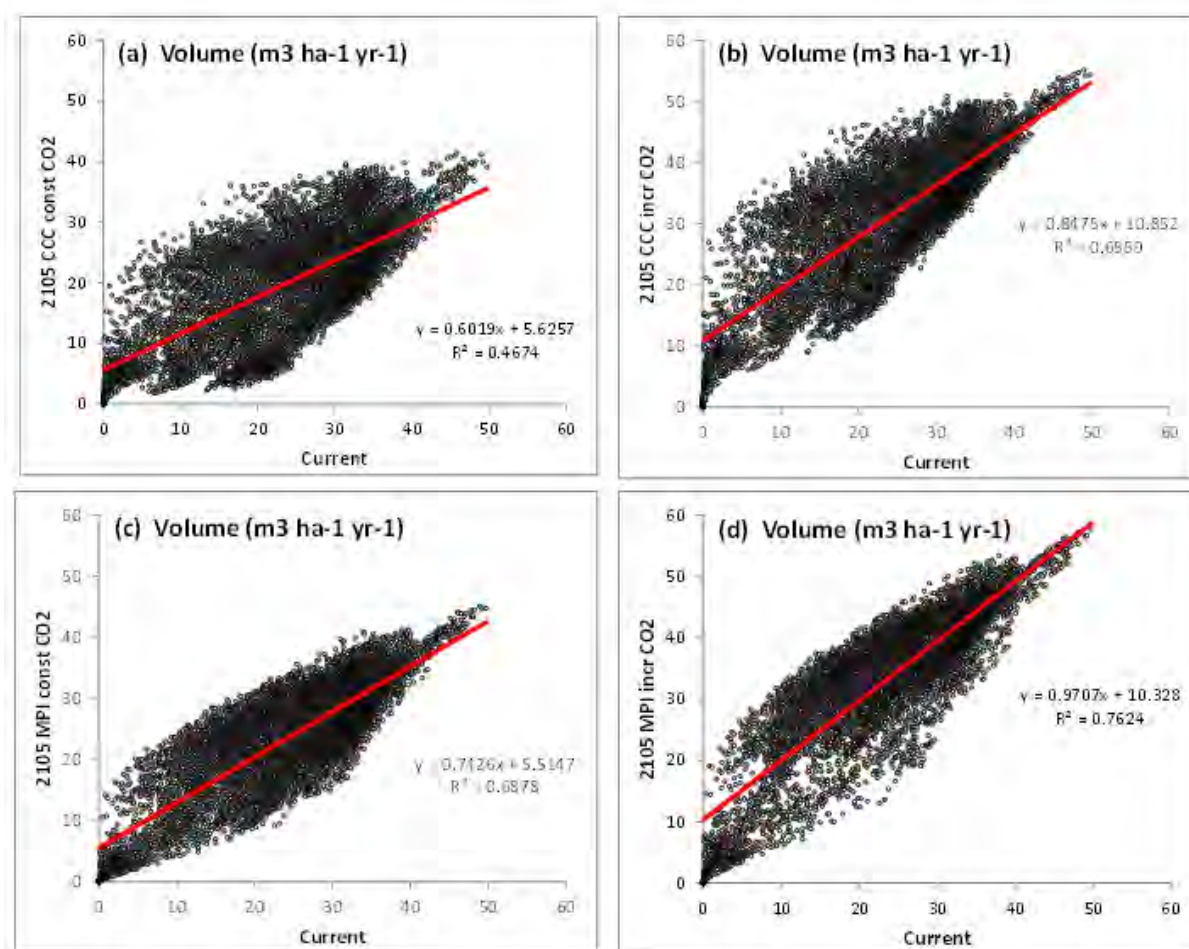


Figure 8-4: Comparison of wood volume production from the CCC (a, b) and Planck (c, d) 2105 scenarios for runs with constant (a, c) and increasing (b, d) CO₂ concentrations. All runs are compared against modelled productivity for the same sites under the observed 2005 climate. Straight lines are fitted to the data to give some indication whether responses are different across the range of productivities.

Figures 8-4 and 8-5 show modelled future productivity against current-day productivity. Figure 8-4 plots future vs current modelled productivity for each individual site, while Figure 8-5 expresses these changes statistically by pooling data in intervals of modelled current-day productivity, and expressing results as means \pm standard deviation for groups with similar current-day productivity.

It shows large changes for many individual sites. Even though modelled mean productivity with constant CO₂ changed by only -16.4% and -2.8% under the CCC and Planck scenarios, respectively (Table 8-1), there was a large degree of variability for individual sites, most pronounced for sites with moderate current productivity. So some sites could expect significantly increases in productivity, while other sites with similar current productivity would be adversely affected.

Broadly, the patterns under constant CO₂ showed increasing productivity for the currently least productive sites, potentially large increases or decreases for moderately productive sites, and relatively small decreases for the most productive sites. These patterns were much more pronounced under the CCC than the Planck scenario. Adding increasing CO₂ into the simulations made productivity changes more positive across the range of current-day productivities. That means a relatively large additional increase for the currently least productive sites, and a proportionately more moderate enhancement for the more productive sites.

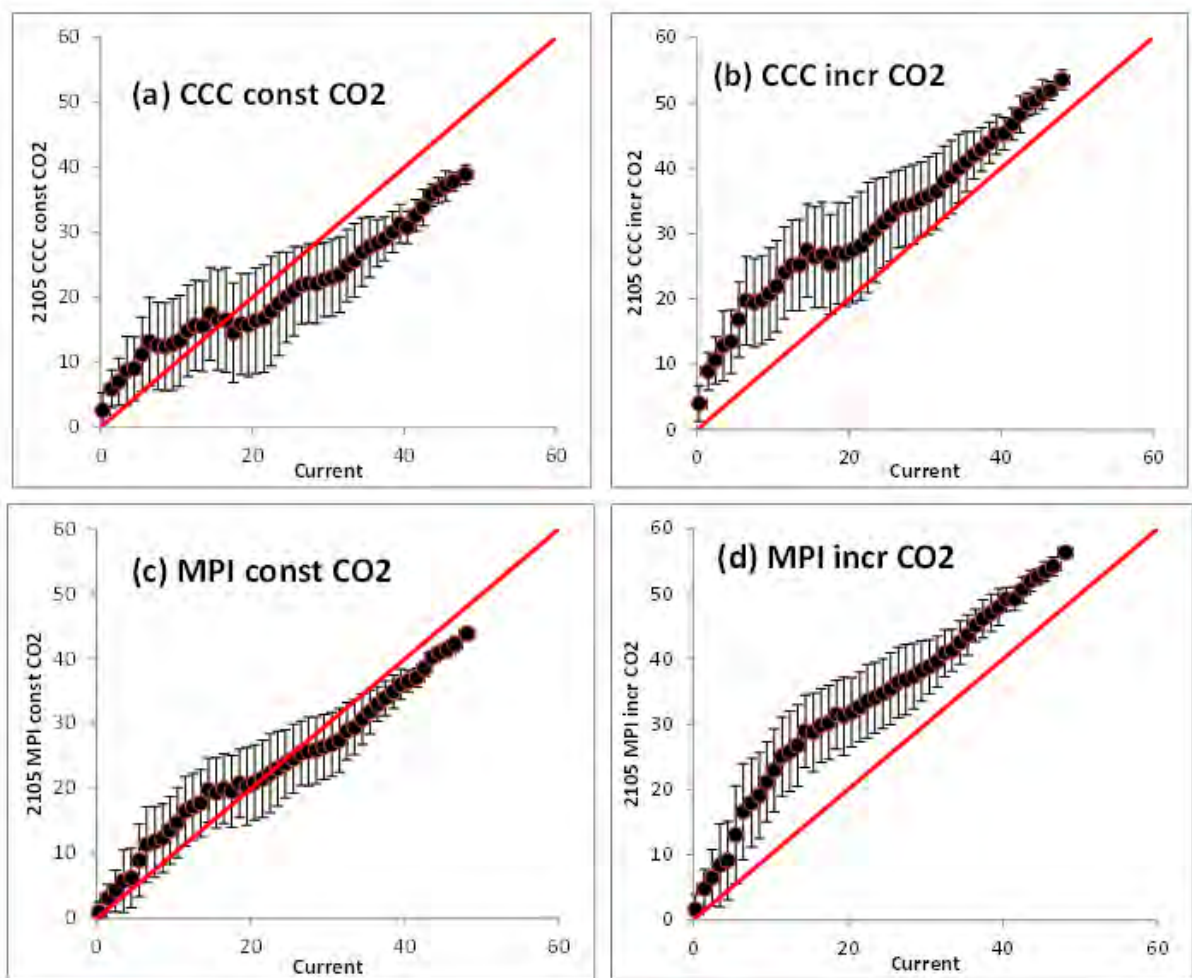


Figure 8-5: Comparison of wood volume production from different 2105 scenarios – all compared against 2005 climate observations. The data are the same as in Figure 8-4, but shown here as means with standard deviations and including 1:1 lines for comparison. Note that the Planck model is labelled as ‘MPI’ (Max Planck Institute for Meteorology).

Figure 8-5 provides a good illustration of current productivity and its response to climate change. Under the CCC scenario (Fig. 8-5a), the currently least productive sites responded most positively to climatic changes, probably reflecting sites in mountainous regions where climate change overcomes their current key temperature limitation. This is less evident under the Planck scenario (Fig. 8-5c), and probably reflects increasing precipitation in these already very wet environments where *P. radiata* responds adversely to excess precipitation (Kirschbaum & Watt, 2011).

At sites with intermediate current productivity, responses under the CCC scenario show a very large degree of variability in their response to climate change (Fig 8-5a). This is much less evident under the Planck scenario (Fig. 8-5c). Intermediate current productivity can reflect limitations due to low – or to a lesser extent, high – temperature, or precipitation being too low or too high. Depending on the nature of the current limitation, changes can potentially be positive or negative, reflected in the largest uncertainty in mean responses.

Sites currently experiencing the highest productivity generally shows fairly consistent slight reductions in productivity. With current conditions near optimal, it is understandable that any change would have to be detrimental. At the same time, temperature and precipitation response surfaces have fairly broad optima (Fig. 8-1; Kirschbaum & Watt, 2011), so that moderate climatic changes lead to only moderate reductions in productivity.

When increasing CO₂ was also included in the simulations (Fig. 8-5b, d), it broadly shifted future productivity upwards across the range of current-day productivities (see also the lines of best fit in Fig. 4), so that there was a somewhat proportionately greater response to CO₂ concentration for sites with low current productivity. With increasing CO₂ and the complete response to climate change, nearly all sites gained overall productivity benefits, especially under the Planck scenario (Figs. 8-4d, 8-5d).

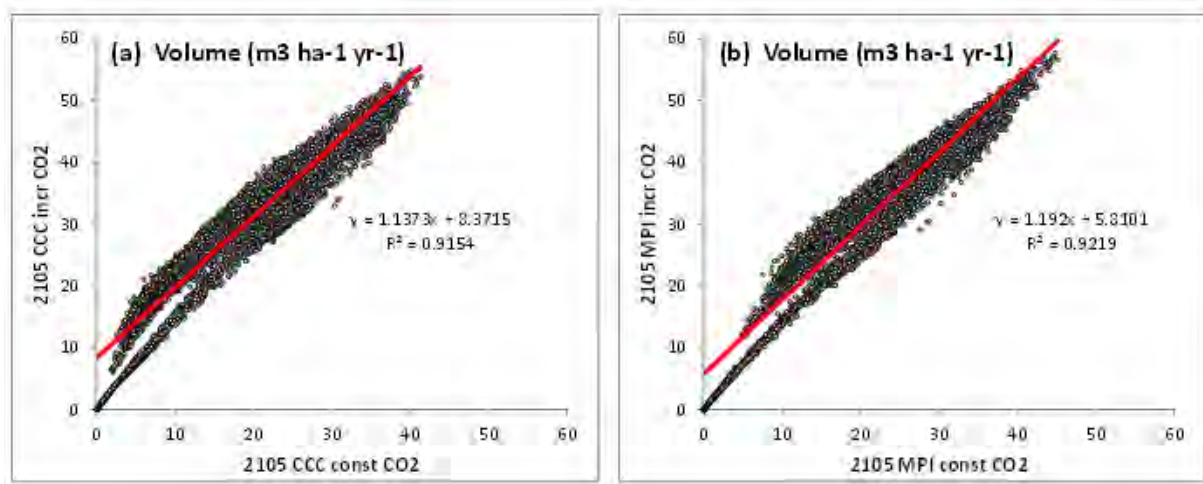


Figure 8-6. Wood volume production (m³ ha⁻¹ yr⁻¹) for the CCC (a) and Planck (b) scenarios, comparing simulations with constant and increasing CO₂.

The effect of including CO₂ concentration is further explored in Figure 8-6, comparing site by site comparisons for simulations with constant and increasing CO₂. The beneficial effect of elevated CO₂ had the proportionately largest effect at low productivities, separated out into two distinctly different response patterns that are particularly evident under the CCC scenario (Fig. 8-6a), with one group of points extrapolating to points reaching down to 0/0 and having a moderate slope. The second group had much more enhanced productivity in elevated CO₂ compared to the first, especially in the very-low productivity range. The group that showed the weaker response was indicative of sites where productivity was limited by low temperature, and the group showing the stronger response was indicative of sites with productivity limited by water availability.

Figure 8-7 shows modelled productivity changes for the current plantation estate in New Zealand. Overall productivity changes are about 10% more negatively affected for the current estate than for New Zealand as a whole (Table 8-1). This probably reflects the fact that plantations are currently located at sites with current good growth potential that could be lost with adverse climatic changes, while sites with current poor growth potential harbour no plantations currently, and are therefore unable to take advantage of any possibly improving future conditions. The overall situation is therefore somewhat better for the country as a whole than for the forest sector itself. In principle, plantations could be relocated onto sites with better developing growth potential, but such shifts will be constrained by infrastructural and institutional constraints.

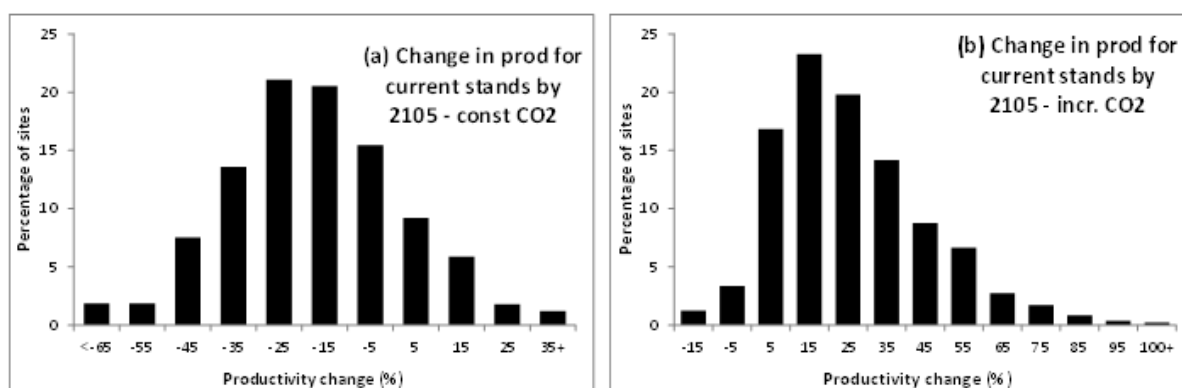


Figure 8-7: Proportion of the current plantation estate expected to undergo the indicated percentage change in productivity by 2105 under the combined CCC and Planck scenarios. This is shown for simulations with constant (a) and increasing (b) CO₂ concentration.

For simulations with constant CO₂ (Fig. 8-7a), productivity was modelled to decrease by about 15-20%, with the majority of sites within that range of moderate productivity changes. There was a only a small number of sites with more extreme responses, ranging from about 4% of sites expected to suffer productivity losses by more than 50%, while about 3% could expect productivity gains by more than 20%.

When increasing CO₂ was also included, mean responses shifted to gains of about 20-25%, with the majority of sites again in the range of moderate, but positive responses. However, even with increasing CO₂, about 5% of sites were still modelled to suffer slight productivity losses, while about 5% of sites had productivity gains by more than 60%.

8.1.10 Discussion

The simulations shown here present a somewhat more negative picture for future wood productivity than that shown by Kirschbaum et al. (2012) based on somewhat milder climate change scenarios than the ones used here. For the current forestry estate and simulations centred on 1990, Kirschbaum et al. (2012) found mean productivity increases by +3% for simulations with constant CO₂, and increases by +37% when increasing CO₂ was also included. This compares with simulated changes of -25% and -9% for simulations with constant CO₂ and under the CCC and Planck scenarios respectively, and +18% and +32% for simulations with increasing CO₂ under the two scenarios (Table 8-1).

These patterns are not unexpected. Plantations in New Zealand are currently situated at somewhat sub-optimal temperatures (Fig. 8-1) but with close to optimal precipitation (Kirschbaum & Watt, 2011). Mild climatic changes, as in the scenarios used by Kirschbaum et al. (2012), would thus be beneficial for many plantations, but if temperature increases become more extreme, it shifts plantations into the supra-optimal range with decreasing productivity as observed in the present study.

Consequently, growth enhancements were observed in most of the regions that are currently too cool, such as mountainous regions and the south of the South Island (Fig. 8-2). Negative effects of increasing temperature were most pronounced for the warmest regions in Northland and, especially under the CCC scenario, for water-limited locations on the east coast of both islands. Evaporative water loss from forests is likely to increase with warming by about 5-6% °C⁻¹ (Kirschbaum, 2000) and drive increases in evapotranspiration. Without increases in rainfall, that will lead to intensifying water limitations.

The temperature response of *P. radiata* is fairly easily and confidently described, based on observations of plantation growth under current climatic conditions, and is consistent with a large amount of empirical research that has found air temperature to be an important determinant of *P. radiata* growth in New Zealand (Jackson and Gifford, 1974; Hunter and Gibson, 1984; Watt et al., 2010; Kirschbaum & Watt, 2011). With water availability mostly not limiting in New Zealand, beneficial effects of moderate warming follow.

Soil water balance is also a major determinant of *P. radiata* productivity, with productivity in New Zealand being sub-optimal on a small number of dryland sites, where trees experience seasonal water deficits (McMurtrie et al., 1990; Richardson et al., 2002; Watt et al., 2003, 2010). Precipitation is fairly optimal for productivity for precipitation up to ~2,000 mm, with productivity reductions at supra-optimal precipitation (Kirschbaum & Watt, 2011). Future productivity could thus be affected by shifts in precipitation towards either drier or wetter conditions, and the range of patterns under the CCC scenarios probably reflect shifts in the distribution of precipitation across New Zealand.

While the present simulations showed negative impacts of climate change when simulations used constant CO₂, productivity generally increased when increasing CO₂ was also included. This was particularly pronounced in the present work, because the simulations for 2105 assumed quite high CO₂ concentrations of 776 ppm. While the relative responsiveness to increasing CO₂ diminishes with CO₂ concentration, this high concentration nonetheless conveys a significant productivity benefit in the simulations.

These simulations again highlight plant responses to increases in CO₂ concentration as a key determinant of future productivity of *P. radiata* within New Zealand. Hence, the critical question is whether the actual CO₂ response will be as strong as predicted in the model runs. The well-characterised effects of CO₂ concentration on photosynthesis (Farquhar & von Caemmerer, 1982; Long et al., 2006) suggest the potential for substantial growth responses to increasing CO₂ concentration. Such responses have been observed in both small-scale experimental studies (e.g., Luxmoore et al., 1993; Curtis & Wang 1998; Poorter & Navas, 2003) and larger-scale field studies using 'free air CO₂ enrichment' (Nowak et al., 2004; Ainsworth & Long, 2005; Norby et al., 2005; McCarthy et al., 2010).

Nonetheless, despite this large amount of experimental work, there is still considerable controversy around the magnitude of growth responses to increasing CO₂ concentration (Nowak et al., 2004; Körner et al., 2007), which makes it difficult to forecast productivity changes with a high level of confidence. Complicating factors include downward regulation of photosynthesis that has been observed in many small-scale trials (e.g., Gunderson & Wullschleger, 1994; Long et al., 1996), but has been shown to be largely attributable to low sink strength, especially with plants being grown in very small pots (e.g. Arp, 1991). Conversely, apparent growth responses can be accentuated through positive feedback during the early exponential growth phase of plants (Kirschbaum, 2011), so that enhancements of relative growth rate (Poorter & Navas, 2003) provide a better measure of plant responses to CO₂ concentration than the more typically reported biomass enhancement ratios.

In the field, responses to CO₂ concentration will be limited if increased photosynthetic carbon gain cannot be matched by similarly increased nutrient supply. Under these circumstances, lower foliar nutrient concentrations are likely to reduce inherent photosynthetic rates (e.g., Rastetter et al., 1992; Comins & McMurtrie, 1993; Nowak et al., 2004). This feedback is included in the CenW simulations but was found to be of little consequence in New Zealand's *P. radiata* forests, where fertility levels are kept high.

Commercial pine forests in New Zealand are regularly analysed for their foliar nutrient levels (Payn et al., 2000) which often indicate some degree of nutrient deficiencies (Smith et al., 2000; Davis et al., 2007). When stands are identified with deficient or marginal nutrient levels, supplemental fertilisers are usually supplied to rectify any deficiencies (Will, 1985). The predicted growth enhancements shown in the present simulations can only be achieved if the current favourable nutritional levels can be maintained into the future. Growth enhancements through climatic changes could not be sustained if they would lead to uncorrected nutritional limitations.

The magnitude of growth gains under increased CO₂ concentration clearly interacts with other environmental conditions. Greatest growth gains are likely to be found on warm sites with adequate nutrition, but where water is limiting, so that the growth response to CO₂ can

shift from a direct photosynthetic response to a dependence on the numerically more substantial increase in water-use efficiency (Kirschbaum, 1999b; Körner et al., 2007) related to stomatal closure under elevated CO₂ concentration (Medlyn et al., 2001). As most of New Zealand has relatively fertile soils and moderate to good water availability, the effects of increasing CO₂ concentration are ubiquitous, but generally only moderate. Greatest gains from CO₂ fertilisation are therefore likely to be found on dryland sites, located in eastern regions of both islands (Figs. 9-3, 9-6).

Future wood productivity will also depend on the effect of climate change on abiotic and biotic factors, and their consequent impacts on tree growth. They may be mediated through changes in the distribution and abundance of weeds, pathogens and insects, and through the severity of abiotic factors such as wind throw and fire.

Potential gains in productivity are of little benefit if stands are killed by fire or novel pest species. Fire severity is linked to temperature and fuel load, both of which may increase with climate change: either directly with warmer conditions, or indirectly as a consequence of greater biological productivity. Changes in wind speed and relative humidity are even more important in determining fire severity and any adverse changes in these variables could greatly increase fire risks (Dowdy et al., 2010). Similarly, changed distributions of pest or disease species can potentially cause significant future problems (Sutherst et al., 2007; Watt et al. 2011). Such factors can potentially negate any potential productivity gains.

The improvements in biological productivity reported here constitutes one reassuring aspect of climate change, but does not allay other concerns related to climate change. An optimal response to the prospect of climate change, including both adaptation and mitigation, needs to be based on the best overall understanding of the combined impacts of all relevant aspects, and some of those can include changes for the better. It is imperative to know of all changes so that society can take advantage of any positive changes as well as minimise the adverse consequences of negative impacts.

8.2 *Eucalyptus fastigata* Simulation: the 3PG model

Eucalyptus fastigata is a fast-growing tree species of high commercial potential for New Zealand planted forestry. It is resistant to diseases that inflict other eucalypts in New Zealand, it has good wood quality characteristics, and can tolerate a wide range of New Zealand environments. However, it is not known how the species will be affected by climate change.

This project used the process-based model 3PG (Physiological Processes for Predicting Growth), which was previously parameterised for *E. fastigata* under current climate conditions. The climate change scenario was based on a 4°C rise in global-average temperature near the end of the 21st century. Two global circulation models were used: the Canadian Centre for Climate Modelling third generation model (CCC), and the German Max Planck Institute for Meteorology ECHAM fifth generation model (Planck). The scenarios generated from these models were downscaled for New Zealand and applied to the 3PG model to determine the impact of climate change on *E. fastigata* productivity. Using the 3PG model, four scenarios were tested: CCC and Planck, with and without a CO₂ fertiliser effect.

Key results and implications

Both the CCC and Planck scenarios result in a large net increase in *E. fastigata* growth. Productivity, as measured by mean annual stem volume increment ($\text{m}^3 \text{ha}^{-1} \text{yr}^{-1}$) at age 30, increased from a New Zealand average of $20 \text{ m}^3 \text{ha}^{-1} \text{yr}^{-1}$ to 57 and $90 \text{ m}^3 \text{ha}^{-1} \text{yr}^{-1}$ for the CCC model, and to 53 and $83 \text{ m}^3 \text{ha}^{-1} \text{yr}^{-1}$ for the Planck model, without and with the CO_2 fertiliser effect, respectively. The increase in productivity varied regionally, with the largest increases occurring in regions that are currently frost prone.

Increasing temperature and fewer frost days were the climatic factors that had the greatest impact on growth with climate change. The decrease in precipitation in some regions reduced the size of productivity gains. However, the reduction in precipitation was not large enough to adversely affect productivity. A global 4°C rise in temperature is unlikely to adversely impact *E. fastigata* productivity in New Zealand. In fact, climate change is likely to be quite beneficial in terms of productivity and the expansion of favourable sites for growing the species.

This section is one of the first attempts to simulate the potential climate change impacts on an exotic forestry species other than *Pinus radiata*. Although the results provided reasonable predictions, there are a number of areas where it could be improved. Two areas that would lead to large improvements in the model are a more accurate spatial representation of soil depth, and the development of a soil fertility index for *E. fastigata*. Incorporating variation in rainfall frequency and intensity in the climate change scenarios would lead to better simulations. Future studies comparing the impact of climate change between different land uses need to consider the variation of assumptions and time scales between models that simulate forestry, dairy production, grazing, etc. Understanding these differences will allow the development of dynamic land use analysis under climate change.

8.2.1 Introduction

In the last 10 years, *Eucalyptus fastigata* (Deane and Maiden) has been identified as a promising species of high commercial potential, thus providing an alternative to *Pinus radiata* (D. Don) plantations. *E. fastigata* is a fast-growing disease resistant eucalypt that can tolerate a number of New Zealand environments. It can be grown as a timber crop, or for pulp and paper (Meason et al., 2011). It is highly suitable for carbon forestry. Research on *E. fastigata* was neglected until the establishment of Future Forests Research programme in 2008. Under the Diverse Forests Theme, knowledge on genetics, site productivity, growth dynamics, and management has been dramatically improved (e.g. Meason et al., 2011).

Global warming and its impact on the climate (climate change) will likely impact many natural and human induced ecosystems. Climate change can impact on forest ecosystems directly or indirectly in many different ways. It may impact tree growth and mortality from gradual changes in temperature, rainfall patterns, and solar radiation (Coops and Waring, 2011). More abrupt impacts may occur from increased frequency in a number of abiotic and biotic factors including wildfires, droughts, out-of-season frosts, and outbreaks of insects and diseases (Chapin et al., 2010). The complexity of climate change, and its direct and indirect impacts on forest ecosystems, means that forest models must be dynamic enough to simulate these effects.

Mathematical models typically used in forestry are statistically-derived empirical-based models (Clutter et al., 1992; Campion et al., 2005). Data for these models are collected from permanent sample plots (PSPs) located over a range of sites and stand ages for a species. The accuracy of empirical-based models is limited to the species and site conditions for which they were originally developed (Landsberg et al., 2003). Such models cannot simulate the growth and yield in changing environmental or management conditions (Battaglia and Sands, 1997 and 1998). This is a particular issue for simulating the impact of climate change on forests, as climate change may modify ecosystem processes in a number of direct and indirect ways. An alternative modelling approach is process-based modelling, which is based on a species' physiological limitation to growth. Process-based modelling is dynamic, and is able to incorporate climate changes multitude of direct, indirect, gradual and abrupt effects to the forest ecosystem to predict future growth under a range of scenarios.

The 3PG model is a process-based model for allocating forest carbon, developed by Landsberg and Waring (1997). It was designed to be more practical than other process-based models by using a combination of physiological principles and empirical data to simplify model parameterisation. Although 3PG is most commonly used for eucalypts, it is neither species- nor site-specific, and been successfully parameterised for a number of ecosystems throughout the world (Sands, 2004). Several researchers have successfully used 3PG to assess the potential impacts of climate change and vulnerability of a number of forest species (including *Pseudotsuga menziesii*) in Pacific North-West Region of North America (Waring et al., 2005; Coops and Waring, 2010; Coops and Waring, 2011) and *Eucalyptus* in Brazil (Almeida et al., 2009).

The objectives of this study are: 1) Modify 3PG to simulate the effects of climate change on *E. fastigata* productivity; 2) Develop potential productivity surfaces for *E. fastigata* under the 4°C global warming scenario.

8.2.2 Materials and Methods

The 3PG2S model

The spatial version of the 3PG growth model, 3PG2S, was used for this study. The process-based model uses subroutines to predict net primary productivity (NPP), transpiration, respiration, and growth. It also computes a water and carbon balance at monthly intervals. Absorbed photosynthetically active radiation (APAR) is calculated as a function of photosynthetic active radiation (PAR) and leaf area index (LAI). The utilised portion of APAR (APAR_u) is established by a series of modifiers with values varying from zero (total constraint) to 1 (no constraint) (Landsberg and Waring, 1997; Coops et al., 2009). 3PG2S simulates the forest's water balance; that is water entering, leaving and being stored in the system. Water movement in soil discriminates between water in the 'root zone' and 'non-root zone' of the soil profile.

Suboptimal temperatures, high vapour pressure deficits, infertile soils, and soil available water combine to limit photosynthesis and affect growth and allocation of dry mass (Landsberg and Waring, 1997). Because leaves are shed at predicted rates, the mass of leaves and their area vary seasonally, increasing when conditions are favourable, and decreasing when they are not (Landsberg and Waring, 1997). Undulations in LAI affect the amount NPP and transpiration. 3PG2S predicts the variables of interest to foresters, like

stem numbers, mean diameters, standing volume, carbon sequestered and growth over short or very long rotations.

3PG2S includes an option to simulate a potential CO₂ fertilisation effect with climate change. The 'fertilisation effect' is a term that describes the increase in a species NPP that may occur with the increase in atmospheric CO₂ concentration. The increase in NPP can be caused by the enhancement of photosynthesis factors including increased water use efficiency and photosynthesis up-regulation (Ainsworth and Long, 2005). The potential CO₂ fertilisation effect was simulated in 3PG2S by methods described by Almeida et al. (2009). Briefly, the canopy quantum efficiency and canopy conductance are normally fixed in the 3PG2S model. These parameters were given modifiers to simulate higher leaf intercellular CO₂ concentration, higher water use efficiency with higher atmospheric CO₂ concentration, and lower stomatal conductance (Almeida et al., 2009). The values of the modifications were based on simulations performed in the detailed process-based model CABALA (Battaglia et al., 2004).

3PG2S model input data

Three types of spatial datasets were required to run 3PG2S. The first dataset contained the latitude of each spatial location. The second data set was the soil textural classification and plant available soil water produced by Landcare Research and modified for this study. The third dataset contained the future climate data provided by the National Institute of Water and Atmospheric Research (NIWA). All datasets were in a grid format, at a 5000 m resolution. The soil and climatic datasets are discussed in more detail below.

Climatic data layers

The monthly climate data required by 3PG2S were mean maximum and minimum temperature (°C), total rainfall (mm), the number of rain days (days month⁻¹), mean daily solar radiation (MJ m⁻² day⁻¹), and number of frost days (days month⁻¹). Current (1997-2011) and future (nominally 2097-2111) climate data were supplied by NIWA. The climate change scenario used in this study was derived from the Intergovernmental Panel on Climate Change (IPCC) Fourth Assessment Report (AR4) special report on emission scenarios (SRES) A2 high emission scenario (IPCC, 2000 and 2007). Future climate data of the SRES A2 emission scenario were downscaled for New Zealand from two global circulation models (as discussed in Section 3):

1. The Canadian Centre for Climate Modelling and Analysis third generation global circulation model (CCC).
2. The German Max Planck Institute for Meteorology ECHAM fifth generation five global circulation model (Planck).

A subsequent small scaling was applied to set the rise in global temperature at 4°C. The CCC and Planck models were chosen, as they validated well against observed climate and circulation over the New Zealand/South Pacific Region. Future climatology from each global circulation models was generated for a 15-year period. A typical length of a *E. fastigata* rotation is 30 years. Thus, to have future climate data for the entire rotation, the 15-year climatic period was repeated for years 16 to 30. It was assumed that the same climatology would occur over the second half of the rotation.

Soil layers

Soil textural data was from Landcare Research's fundamental soil layer textural classification map, with a 100 m resolution (Newsome et al., 2008). The classification is based on the interpretation of soil surveys from the 1:63,360/1:50,000 scale New Zealand Land Resource Inventory, with reference to analytical results stored in the national soils database, or as professional estimates by pedologists acknowledged as authorities in the soils of the region in question (Newsome et al., 2008). Soil textural classes and plant available soil water for each soil unit were developed by Landcare, based on earlier research (Webb and Wilson, 1995).

Soils were classified into 27 soil units and seven non-soil units. This was used to reclassify the soils for this study into 33 different categories that represent the soil water characteristics of water drainage, storage, and availability to plants. This information was required for 3-PG2S soil water subroutine. The plant-available soil water classification is based profile total available water in the month of July to a depth of 0.9 m or to the potential rooting depth based on research by Gradwell and Birrell (1979), Wilson and Giltrap (1982), and Griffiths (1985). Soil depth information currently available was too coarse for modelling with 3PG2S, so the depth value was set to 1 m throughout the country. Soil fertility index has not been developed for *E. fastigata*, so 3-PG2S soil fertility modifier was set to 0.6 for *E. fastigata* for all soil types.

3PG2S model simulations

Following parameterisation, we simulated for the CCC and Planck climatology with 3PG2S, using a management regime that can be used for growing *E. fastigata* for pulp or carbon. Outputs included accumulated stand volume ($\text{m}^3 \text{ha}^{-1}$), mean tree diameter at 1.4 m height (cm), total stand basal area (BA, $\text{m}^2 \text{ha}^{-1}$), and mean annual volume increment (MAI, $\text{m}^3 \text{ha}^{-1} \text{yr}^{-1}$). The CO_2 fertiliser effect with increasing atmospheric CO_2 concentration may increase net primary productivity. However, the experimental evidence that the CO_2 fertiliser effect increases NPP long term is uncertain due to a number of physiological and environmental factors (Karnosky, 2003).

Thus, two values were produced for each scenario, with and without the CO_2 fertiliser effect. This provided a range of predicted productivity with the CO_2 fertiliser effect representing the high end of future productivity using projected concentrations under SRES A2 scenario (IPCC, 2000). The low end of future productivity was provided by simulations without a CO_2 fertilisation effect (using current ambient atmospheric CO_2). The results from the model scenarios were compared to simulated productivity using current climate data.

8.2.3 Results

Productivity of *E. fastigata* increased for both scenarios, from a country-wide average of $20 \text{ m}^3 \text{ha}^{-1} \text{yr}^{-1}$ under the baseline climate to a range $57\text{--}90 \text{ m}^3 \text{ha}^{-1} \text{yr}^{-1}$ for the CCC model, and a range $53\text{--}83 \text{ m}^3 \text{ha}^{-1} \text{yr}^{-1}$ for the Planck model, without and with the CO_2 fertiliser effect respectively (Table 8-2). Figure 8-8 shows the spatial pattern of *E. fastigata* productivity under the current climate, and Figures 8-9 to 8-12 the projected future productivity under the four climate change scenarios modelled.

Table 8-2: Summary statistical table of *Eucalyptus fastigata* mean annual volume increment ($\text{m}^3 \text{ha}^{-1} \text{yr}^{-1}$) in New Zealand under current and future climates - with and without the CO_2 fertiliser effect.

Climate Scenario	CO_2 fertilisation effect	Minimum ($\text{m}^3 \text{ha}^{-1} \text{yr}^{-1}$)	Maximum ($\text{m}^3 \text{ha}^{-1} \text{yr}^{-1}$)	Mean ($\text{m}^3 \text{ha}^{-1} \text{yr}^{-1}$)
Current	n/a	0.09	59.4	20.1
Future - CCC	No	25.2	79.1	57.1
	Yes	50.1	122.3	89.6
Future – Planck	No	18.8	70.0	52.6
	Yes	31.7	108.9	82.6

The increase in productivity differed by region and scenario. The Hauraki Plains, Auckland, Northland and West Coast regions had the lowest productivity (Figs. 8-9 to 8-12). This was most evident when CO_2 fertilisation was assumed as productivity in those regions lagged behind (Figs. 8-10 and 8-12). However, the lowest productivity with climate change was still higher for the same region than productivity under the current climate conditions (Fig. 8-8). Productivity was higher for the CCC model (Table 8-2). This suggests that climatic conditions in the CCC model were more beneficial for *E. fastigata* than those projected by the Planck model. This was most evident when the simulations with CO_2 fertilisation were compared (Figs. 8-10 and 8-12). Upland areas of the lower North Island, Marlborough and Tasman regions had the highest productivity ($>100 \text{ m}^3 \text{ha}^{-1} \text{yr}^{-1}$) for the CCC model with fertilisation (Fig. 8-10). Conversely, only the upland areas for the Tasman region had the highest productivity (with the productivity colour bands as plotted) for the Planck model with fertilisation (Fig. 8-12).

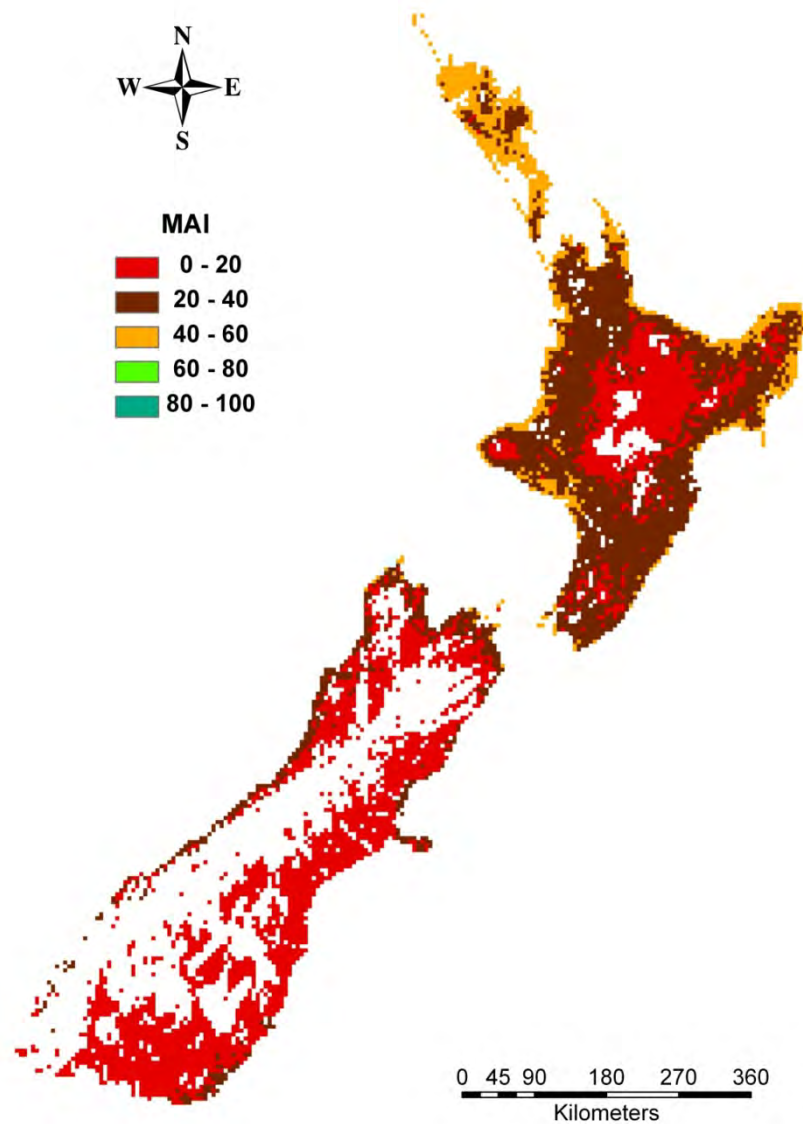


Figure 8-8: *Eucalyptus fastigata* productivity, as measured with mean annual volume increment (MAI $\text{m}^3 \text{ha}^{-1} \text{yr}^{-1}$), over a 30-year rotation under current climate conditions. White areas represent no data.

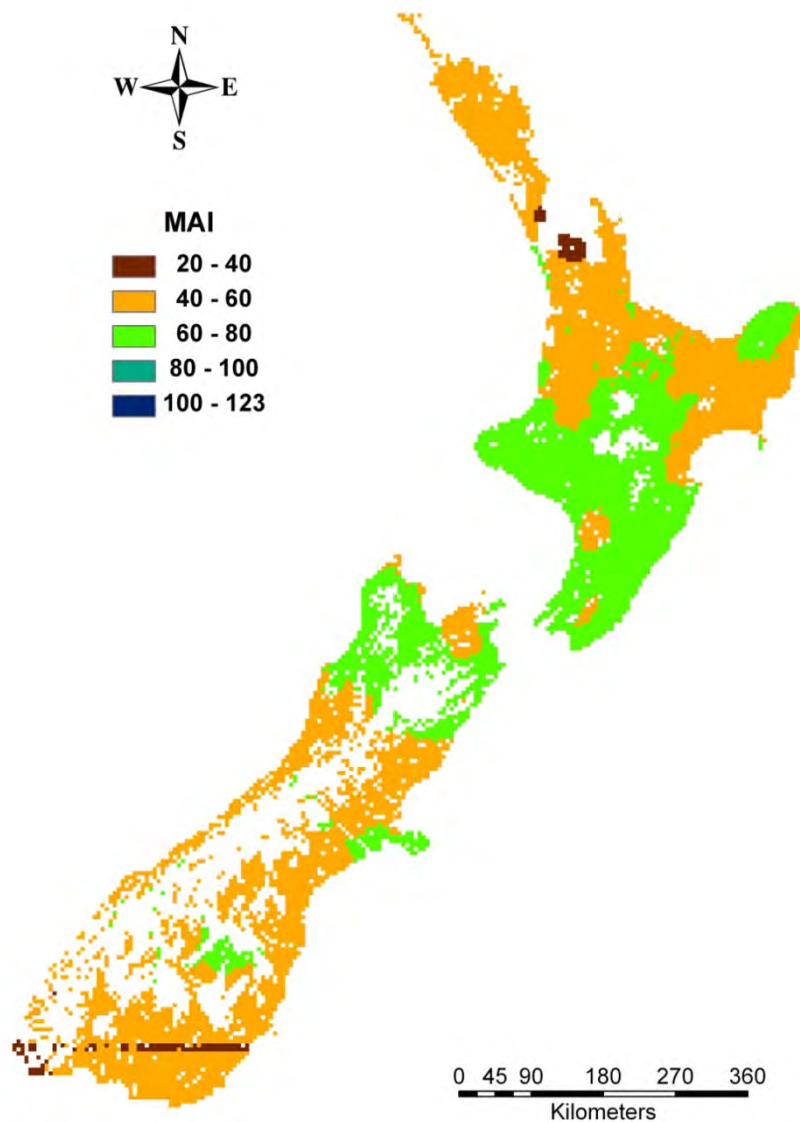


Figure 8-9: *Eucalyptus fastigata* productivity, as measured with mean annual volume increment (MAI $\text{m}^3 \text{ha}^{-1} \text{yr}^{-1}$), over a 30-year rotation (from 2080 to 2109), for the CCC 4°C climate change scenario with no CO₂ fertilisation effect. White areas represent no data.

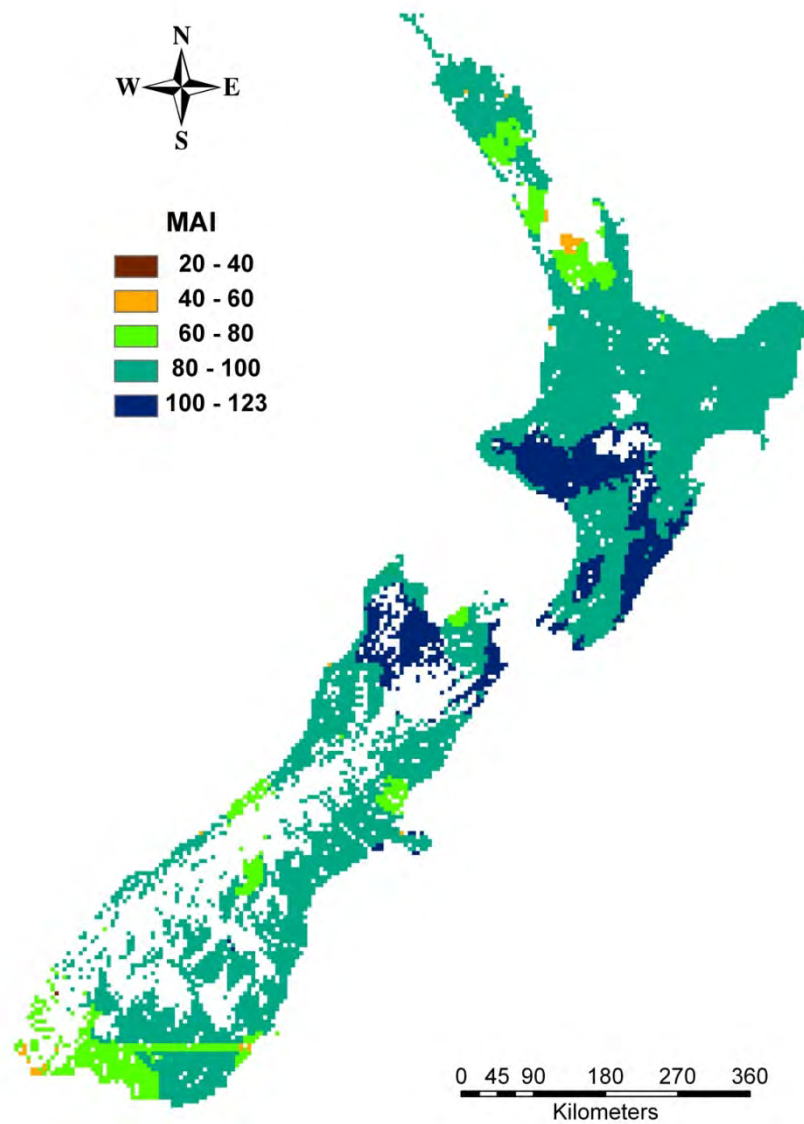


Figure 8-10: *Eucalyptus fastigata* productivity, as measured with mean annual volume increment (MAI $\text{m}^3 \text{ha}^{-1} \text{yr}^{-1}$), over a 30-year rotation (from 2080 to 2109), for the CCC 4°C climate change scenario with a CO_2 fertilisation effect. White areas represent no data.

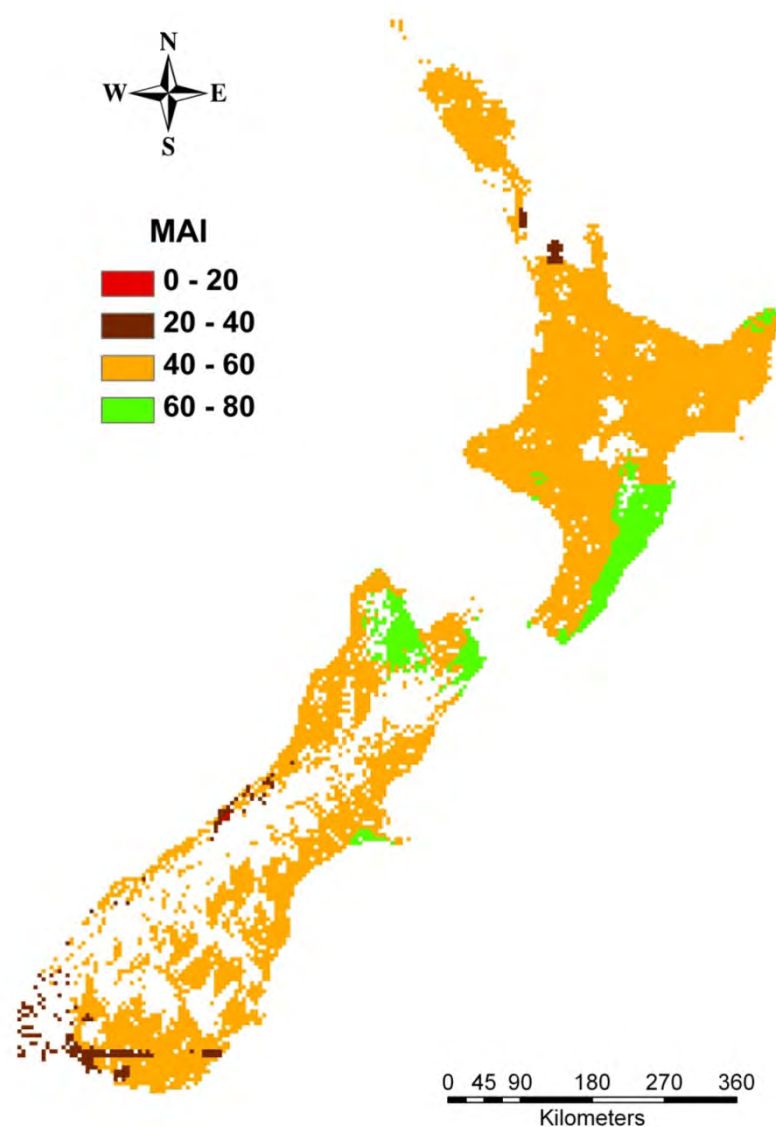


Figure 8-11: *Eucalyptus fastigata* productivity, as measured with mean annual volume increment (MAI $\text{m}^3 \text{ha}^{-1} \text{yr}^{-1}$), over a 30-year rotation (from 2080 to 2109), for the Planck 4°C climate change scenario with no CO₂ fertilisation effect. White areas represent no data.

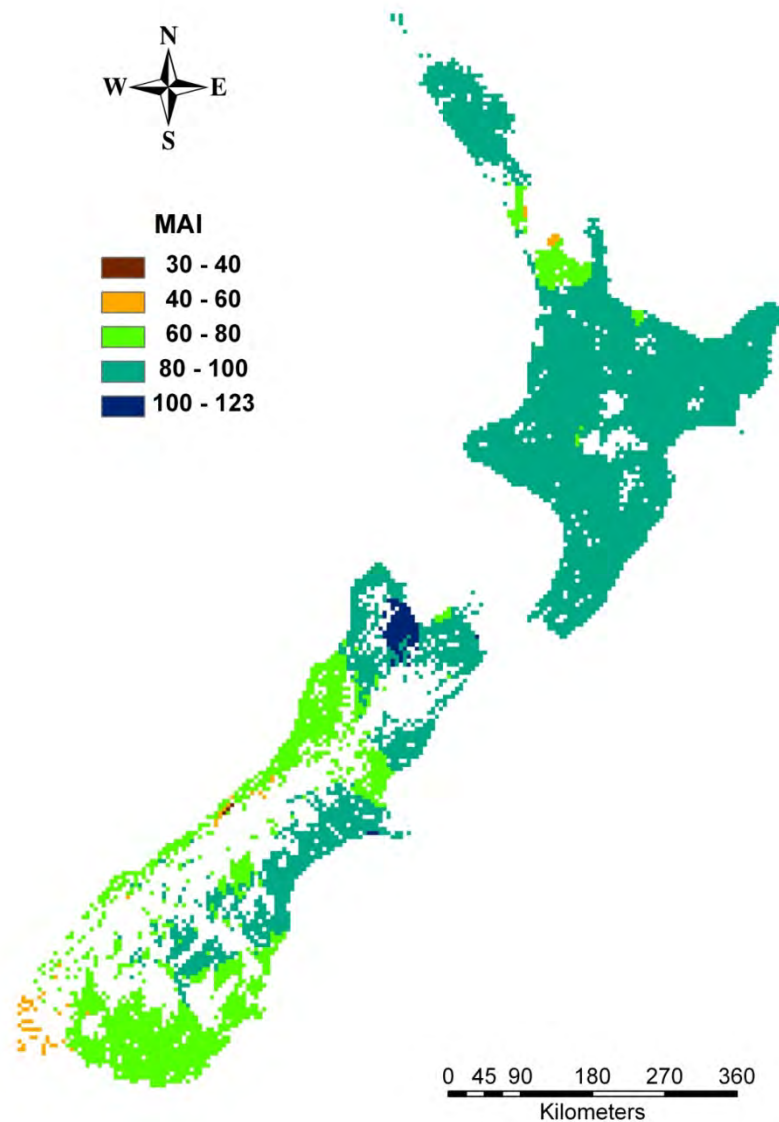


Figure 8-12: *Eucalyptus fastigata* productivity, as measured with mean annual volume increment (MAI $\text{m}^3 \text{ha}^{-1} \text{yr}^{-1}$), over a 30-year rotation (from 2080 to 2109), for the Planck 4°C climate change scenario with a CO₂ fertilisation effect. White areas represent no data.

8.2.4 Discussion

Under the current climate, inland areas that are frost prone are not suitable for growing *E. fastigata* as a commercial species. This is represented in Figure 8-8 as areas that have a MAI less than $20 \text{ m}^3 \text{ ha}^{-1} \text{ yr}^{-1}$. The climate change simulations showed that *E. fastigata* benefited from the increase in global temperature, while changes in precipitation did not have any adverse effect on productivity. The climatic factor that had the biggest impact on productivity with climate change was the reduction in frost days. As *E. fastigata* is a frost sensitive species, a reduction of frost days (see Section 4) increased current productivity in frost prone areas. It also increased the potential range of the species, especially in the inland areas of the South Island and the Central North Island.

Productivity was at its highest for upland areas in the North and South Islands for the Planck model with CO_2 fertilisation, and for the CCC model with and without CO_2 fertilisation. This was primarily due to the warmer temperatures and fewer frost days at higher elevations with the future projected climatologies. However, if precipitation decreased in these areas, then the potential increase in productivity with warmer temperatures and fewer frost days was reduced. This was most evident with the difference in productivity for the lower North Island upland areas between the two scenarios.

Two global circulation models were used in this study, as it is uncertain how a global rise in temperature will impact New Zealand's climate. By simulating future *E. fastigata* productivity with two contrasting circulation models, the potential range of climate change impacts can be explored. The impact on *E. fastigata* productivity varied between the two global circulation models, CCC and Planck, and this difference was most obvious when the scenario included the CO_2 fertiliser effect. *Eucalyptus fastigata* productivity was at its highest for CCC with CO_2 fertilisation (Fig. 8-10). Productivity was less for the same upland areas for Planck with CO_2 fertilisation (Fig. 8-12). This was due to the upland winter temperatures for Planck being colder than CCC. For the CCC with CO_2 fertilisation scenario, there was a large contrast in productivity between the upland and lowland areas for the lower North Island. This was likely due to a large decrease in precipitation in the lowland areas. This reduced productivity in lowland areas, while the upland areas remained more productive. Although productivity did vary between scenarios, no scenario had an adverse impact. Even decreases in precipitation in some areas (not shown) were not large enough to decrease productivity from current climate conditions.

The 3PG2S model has some limitations, due to the limited knowledge of the spatial variability of soil depth and soil fertility. The knowledge of depth of soil in forests and ex-pasture land is at best crude; thus, a uniform depth of 1 m was used for the model. Areas with shallow soils and decreasing precipitation are most likely to have longer periods of soil water deficit, which is likely to decrease productivity. However, more information and research is required on these areas before changes in soil water with climate change can be more accurately simulated. Current methods to measure soil fertility for *P. radiata* includes the C:N ratio and 300 index. Non-*radiata* species can be more sensitive to soil nutrients other than the C:N ratio (Ledgard et al., 2005). In a 2010 study of the eight environmental site factors influencing *E. fastigata* productivity, soil extractable phosphorus was the only significant measure of soil fertility (Meason et al., 2010). Maps of plant available phosphorus and other nutrients throughout New Zealand have been developed by researchers. However, these maps are too coarse to predict soil fertility for *E. fastigata* for existing stands, or to be used in process-

based modelling. The development of a new index of soil fertility for eucalypts and other non-radiata tree species is under development at Scion. Until it is developed, a constant soil fertility factor was used for 3PG2S.

There is no known destructive pest for *E. fastigata* in New Zealand or Australia. Indeed, this eucalypt is the focus of current research and management, as it is resistant to pathogens that afflict other eucalypts in New Zealand. Thus, it was assumed for this study that no new pathogen will adversely impact its growth under climate change. It is unlikely that climate change would have a negative impact on soil fertility for most regions in New Zealand. However, more research is needed in this area.

8.2.5 Recommendations and Conclusions

Increasing temperature and fewer frost days are the most important climatic factors impacting *E. fastigata* growth under climate change. The decrease in precipitation in some regions reduces the size of productivity gains. However, the reduction in precipitation was not large enough to adversely affect productivity in most areas in New Zealand. In conclusion, a global 4°C rise in temperature is unlikely to adversely impact *E. fastigata* productivity in New Zealand. In fact, climate change is likely to be quite beneficial in terms of productivity and the expansion of favourable sites for the species.

This study is one of the first attempts to simulate the potential climate change impacts on an exotic forestry species other than *Pinus radiata*. Although the results provided reasonable predictions, there are a number of areas where it could be improved. Two areas that would lead to large improvement in the model are a more accurate spatial representation of soil depth, and the development of a soil fertility index for *E. fastigata*.

The ability to more accurately project climate change scenarios through global circulation models for New Zealand including the variation that occurs in temperature and rainfall, and also extreme events such as droughts and rainstorms, would lead to better simulations for *E. fastigata* growth. Future studies comparing the impact of climate change between different land uses needs to consider the variation of assumptions and time scales between models that simulate for example forestry, dairy production, grazing and land use. Understanding these differences will allow the development of dynamic land use analyses under a changing climate.

9 Impact of projected climate change on thermal stress in dairy cattle

9.1 Summary

Modelling of predicted climate conditions for 2097-2111 indicates that heat load will increase compared to current conditions, to an extent that dairy cows will experience significant thermal stress in many dairying areas of New Zealand. Summers with 20 or more days of conditions that induce heat stress days will become widespread under the 2097-2111 scenarios. The full geographic extent of change varies between climate models, with the worst case scenario being widespread change across much of the North and South Islands. Northland and Northern Waikato consistently experience increased heat load index across climate models. Without measures to reduce heat load, cattle could be expected to exhibit a range of negative responses which would have a detrimental impact on production, reproduction and welfare.

Under the future climate scenario there are dramatic reductions in cold stress events for dairy cattle which will become isolated to a few events along the Southland coast and coastal and inland areas of Otago by about the end of the century.

9.2 Predictive models used to generate risk maps

DairyNZ has two predictive models – Heat-Load Index (HLI) and Cold Stress Index (CSI) – developed as tools to assess the likely welfare impacts of thermal stress on New Zealand dairy cattle.

The HLI model predictions are based on the physiological impacts of heat stress on dairy cows. The development of the HLI model, and its validation using animal behavioural preference testing, has been described by Matthews and Arnold (in press).

The CSI model is based on known additional energetic requirements of dairy cattle when exposed to cold stress (Fox and Tylutki, 1998).

For the purposes of this project, three weather datasets were investigated with each of the two thermal stress models. One dataset (Current) was derived from 1997-2011 data, and two datasets were derived from predictive climate models for the period 2097-2111 (CCC: Canadian Centre for Climate [for Modelling and Analysis]; Planck: Max Planck Institute [for Meteorology]), see Section 3 for details.

The HLI model was run using data from the relevant summer months. Two periods were examined separately for each scenario. These were:

- 1) The months of December, January and February, as a single block.
- 2) The shoulder months of November and March, also as a single block.

The CSI model was run using data from the relevant winter months. Again, two periods were examined separately for each scenario:

- 1) The months of June, July and August, as a single block.

2) The shoulder months of May and September, also as a single block.

9.2.1 Interpretation of maps

Model outputs were mapped using a colour-banding system (refer to Appendices A4 and A5 for detail of respective colour gradients used) that differentiated the number of days during the total period in which conditions were sufficient to cause thermal stress. For all maps, dark green represents minimal days in the period in which thermal stress would be experienced, either heat stress for the summer and summer shoulder maps or cold stress for the winter and winter shoulder maps.

In the first series (Appendix A4), full seasons (summer and winter period) used a bandwidth of two days to define the colour gradient, with the maximum (depicted in burgundy) being ≥ 20 days in the period. For the shoulder months, maps used a bandwidth of 1.33 days with the maximum (depicted in burgundy) representing ≥ 13.3 days. This adjustment was necessary because the shoulder period covers two months while the summer and winter maps each cover a three month period.

The level of differentiation provided in the summer and summer shoulder period maps in the first series gave insufficient differentiation of the more extreme predictions for summer and summer shoulder months using CCC and Planck data. Accordingly these predictions were re-mapped (Appendix A5) using adjusted bandwidths of 5 and 3.3 days for colour gradients in the summer and summer shoulder periods, respectively. Maximum (depicted in burgundy) in the second series of maps represents ≥ 50 days for the summer period, and ≥ 33 days in the summer shoulder months.

9.3 Impact on Heat Load Index

9.3.1 Main summer months (December, January, February)

Current situation

Maps (Appendix A4) indicate that the HLI threshold is currently rarely exceeded on ≥ 20 days during summer, apart from areas of Waikato (in particular the Hauraki Plains). At the 75th percentile (the 1-in-4-year extreme), the area affected extends to the eastern areas of Northland, a larger area of Waikato and Central Otago. The 90th percentile (1-in-10-year extreme) extends the affected areas to include most of Northland and Waikato, as well as Bay of Plenty and North Canterbury. The rest of Canterbury, as well as Wairarapa and Hawkes Bay, are affected on 10-15 days during summer.

CCC model

The initial maps (two-day-step colour scale, Appendix A4; Figure A4-2) indicate that the HLI threshold would be exceeded on ≥ 20 days during summer throughout the North Island, apart from the southern Taranaki coastal areas and the East Cape. North and South Canterbury would be similarly affected, while inland Southland and Otago would be affected on 10-15 days during summer. The 75th and 90th percentiles mainly extend and consolidate the areas that would be affected in the South Island, and the Southland coastal strip is the only area in which the HLI threshold would rarely be exceeded.

Re-mapping using bandwidth based on five days (Appendix A5; Figure A5-2) indicated that the HLI threshold would be exceeded on ≥ 50 days in Waikato, Northland and western Bay of Plenty during summer. Areas of Hawkes Bay, Wairarapa and North Canterbury would be affected for 40-45 days, and mid-Canterbury for 30 days during the summer period.

Figure 9-1 shows the average HLI exceedance during summer for the CCC 4°C scenario, using the two different colour band scales. Refer to Appendix Figures A4-2 and A5-2 for the 75th and 90th percentile maps that complement the average (50th percentile) show here.

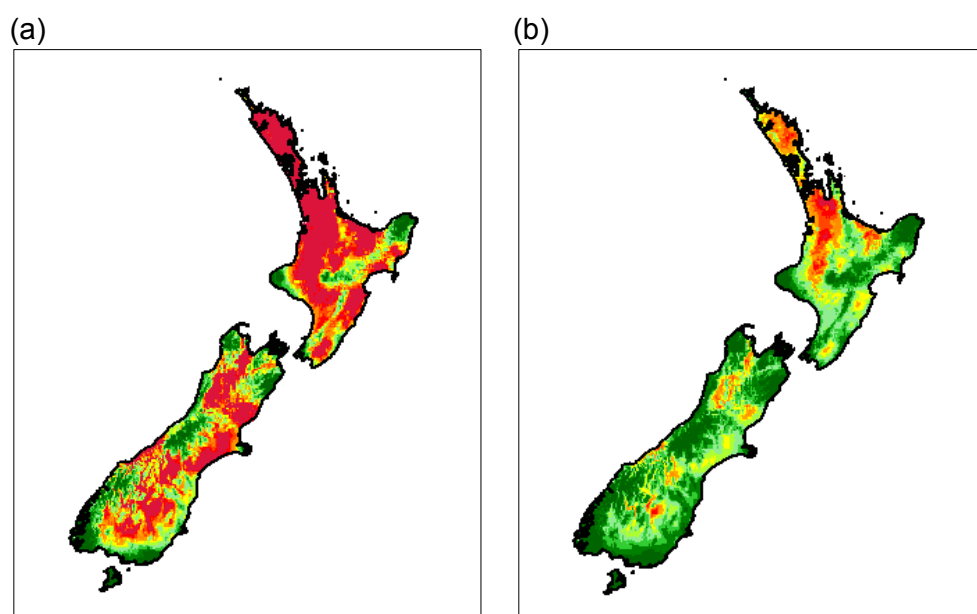


Figure 9-1: Maps for areas where the HLI threshold will be exceeded during summer (December – February) based on CCC model data for 2097-2111 (average). Map (a) is based on colour banding as in Appendix A4 (red represents ≥ 20 days and bandwidth represents two-day intervals). Map (b) is based on colour banding as in Appendix A5 (red represents ≥ 50 days and bandwidth represents five-day intervals).

Planck model

In the initial mapping (two-day-step colour scale, Appendix A4; Figure A4-3), the HLI threshold would be exceeded on ≥ 20 days during summer throughout Northland and the Waikato, as well as the western Bay of Plenty, Hawkes Bay and Wairarapa. The HLI threshold would be exceeded on 12-15 days in inland areas of Taranaki and Manawatu. The Buller region and North and Central Canterbury likewise would have ≥ 20 summer days when HLI threshold is exceeded. The 75th and 90th percentiles also consolidate the areas of both islands, where the HLI threshold would be exceeded ≥ 20 days in summer.

After re-mapping the data using a bandwidth representing five days (Appendix A5; Figure A5-3) it was confirmed that the Waikato and especially the Hauraki Plains would be affected ≥ 50 days during summer, with similar impact in limited areas in Northland and Bay of Plenty. Areas of Hawkes Bay and Wairarapa, as well as Canterbury, would be affected for around 20 days.

Figure 9-2 shows the average HLI exceedance during summer for the Planck 4°C scenario, using the two different colour band scales. Refer to Appendix Figures A4-3 and A5-3 for the 75th and 90th percentile maps that complement the average (50th percentile) show here.

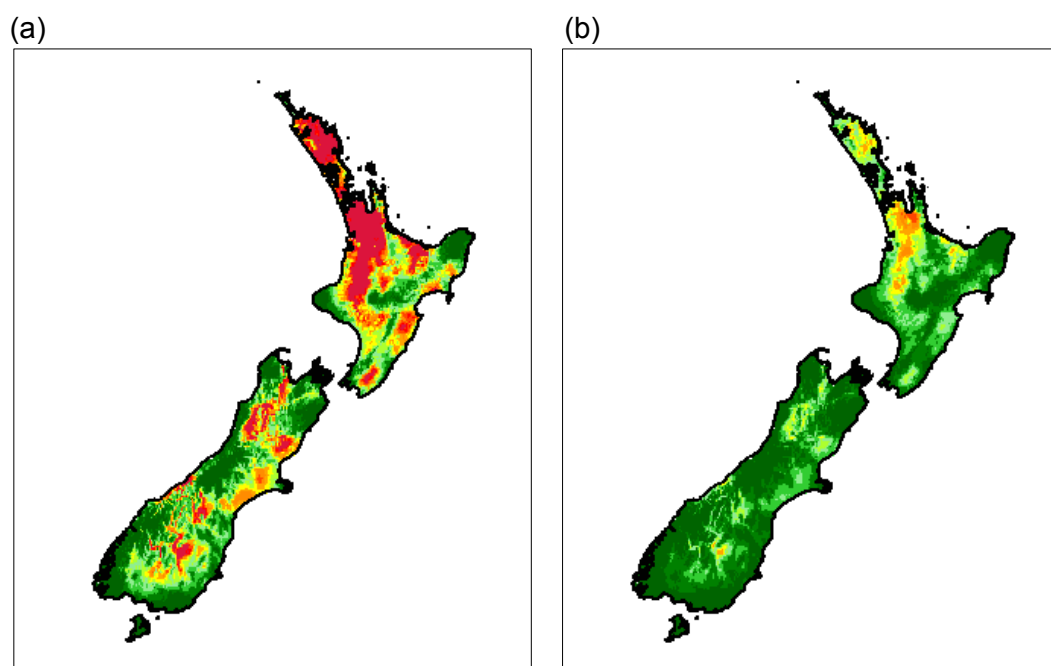


Figure 9-2: Maps for areas where the HLI threshold would be exceeded during summer (December – February) based on Planck model data for 2097-2111 (average). Map (a) is based on colour banding as in Appendix A4 (red represents ≥ 20 days and bandwidth represents two-day intervals). Map (b) is based on colour banding as in Appendix A5 (red represents ≥ 50 days and bandwidth represents five-day intervals).

The results using the Planck model data are less extreme than those using the CCC model data. In particular, the predictions for Southland, Otago and South Canterbury are that the HLI threshold would not be exceeded on more than 15 days in summer. This is largely because the CCC model projects at least 1°C greater warming for New Zealand than the Planck model, for the same 4°C global warming.

Air movement is an important factor in the experience of heat stress for dairy cows. Their most effective physiological mechanism to dissipate excessive heat is by increasing their respiration rate, where thermal energy is dispersed as water is vaporised in the lungs. High humidity and lack of air flow will impair this mechanism. In the future scenarios modelled, wind speeds were assumed to be unchanged (Section 3). Over the summer season (of highest temperatures, and therefore greatest heat stress), relative humidity was projected to decrease almost everywhere in the CCC model, but to increase in almost all regions in the Planck model (Appendix Figures A1-11 and A1-12). Thus, the Heat-Load Index model responded more strongly and adversely to the higher temperatures of the CCC model than to the higher humidities of the Planck model.

9.3.2 Summer shoulder months (November and March)

The greatest deviations from the current situation occur during the summer shoulder months.

Current situation

There are currently very few days in the summer shoulder period that the HLI threshold is exceeded (Appendix A4, Figure A4-4). Even at the 90th percentile, it is only areas of Waikato, and in particular the Hauraki plains, for which the threshold is exceeded, and then for only 5-10 days in the shoulder months.

CCC model

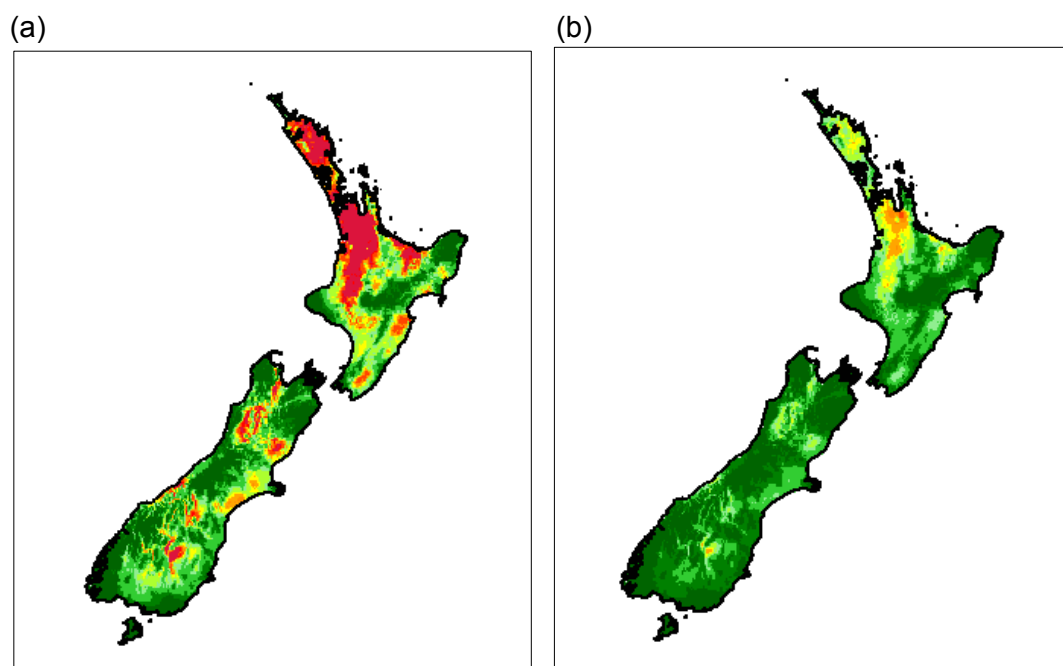


Figure 9-3: Maps for areas where the HLI threshold would be exceeded during summer shoulder months (November and March) based on CCC model data for 2097-2111 (average). Map (a) is based on colour banding as in Appendix A4 (red represents ≥ 20 days and bandwidth represents two-day intervals). Map (b) is based on colour banding as in Appendix A5 (red represents ≥ 50 days and bandwidth represents five-day intervals).

In the initial mapping (1.33-day-step colour scale, Appendix A4; Figure A4-5), the predictions for summer shoulder months were that the HLI threshold would be exceeded throughout Northland, Waikato and Bay of Plenty on ≥ 20 days. Inland areas of Hawkes Bay, Wairarapa, and North Canterbury likewise would have ≥ 20 days when the HLI threshold is exceeded. The HLI threshold would be exceeded for around 15 days in Mid-Canterbury and Central Otago. The 75th percentile result extends the area in the North Island, where the HLI threshold would be exceeded on more than 20 days, with South Taranaki and Manawatu being most affected. Likewise these areas would be extended in Canterbury and Central Otago. These trends are also evident on the 90th percentile which predicts that many southern areas would have the HLI threshold exceeded on around 15 days, apart from the coastal areas.

When data were re-mapped using a bandwidth representing 3.3 days (Appendix A5; Figure A5-5), the view that the Waikato – and especially the Hauraki Plains – would be affected for 25-30 days during the summer shoulder months was confirmed. Areas of Northland and Bay of Plenty would also have the HLI threshold exceeded for 20-25 days, while Hawkes Bay, Wairarapa and Canterbury would be affected for 10 days.

These results for the CCC model are mapped in Figure 9-3, with additional results in Appendices 4 and 5.

Planck model

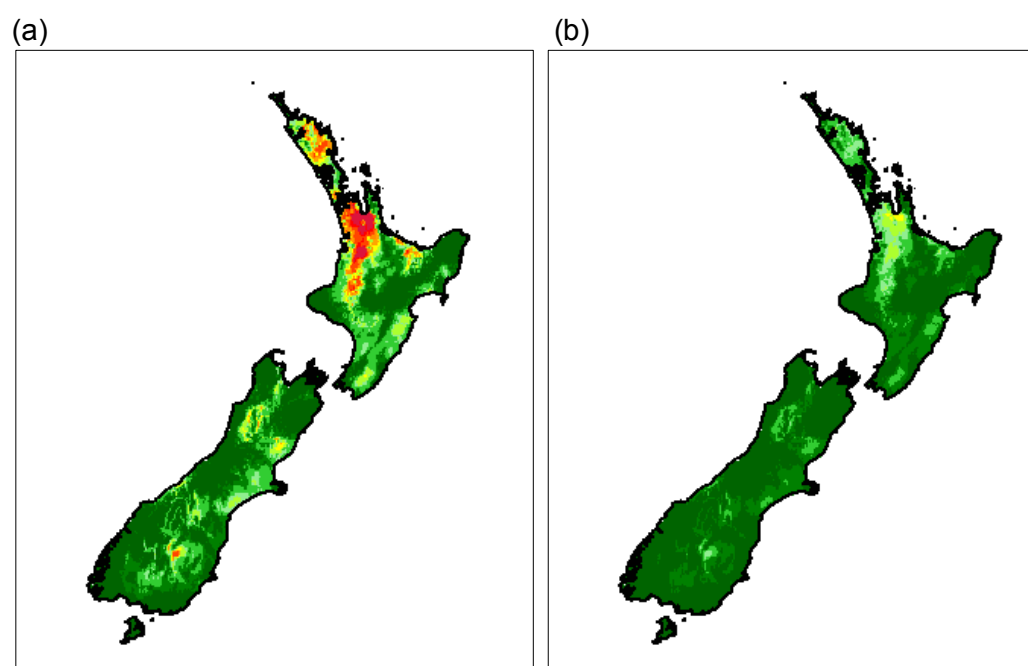


Figure 9-4: Maps for areas where the HLI threshold would be exceeded during summer shoulder months (November and March) based on Planck model data for 2097-2111 (average). Map (a) is based on colour banding as in Appendix A4 (red represents ≥ 20 days and bandwidth represents two-day intervals). Map (b) is based on colour banding as in Appendix A5 (red represents ≥ 50 days and bandwidth represents five-day intervals).

The initial mapping (1.33-day colour scale) using the Planck model data again suggest that conditions would be similar, but less extreme than with the CCC model data (Appendix A4; Figure A4-6). Much of the Waikato, as well as parts of Northland and the Bay of Plenty are predicted to have conditions that would exceed the HLI threshold on ≥ 20 days during the summer shoulder months. Hawkes Bay, Wairarapa and North Canterbury are predicted to exceed the HLI threshold on 10 days. The 75% percentile result indicates that the threshold would be exceeded in these latter areas on ≥ 20 days, with other dairying regions (except Waikato and Northland) having 5-10 of days when the HLI threshold would be exceeded. The 90th percentile presents a very similar picture, with the main difference being consolidation of the areas affected on ≥ 20 in Hawkes Bay, Wairarapa and Canterbury.

When data were re-mapped using a bandwidth representing 3.3 day intervals (Appendix A5; Figure A5-6), the prediction was that a limited area of the Hauraki Plains would be affected for 25-30 days during the summer shoulder months, while the rest of Waikato, as well as Northland and Bay of Plenty would be affected for around 10 days of the summer shoulder months. The HLI threshold would be exceeded in Hawkes Bay, Wairarapa and Canterbury on 5-10 days in the summer shoulder months.

These results for the Planck model are mapped in Figure 9-4, with additional results in Appendices 4 and 5.

9.4 Impact on Cold Stress Index

9.4.1 Main winter months (June, July, August)

Current situation

Based on the initial mapping (Appendix A4, Figure A4-7), currently the CSI threshold is never exceeded in the majority of North Island dairying areas, except for coastal Taranaki and Wairarapa, and in Horowhenua. In the South Island, the CSI threshold is never exceeded except in areas south of Oamaru. The CSI threshold is exceeded on ≥ 20 days along the south coast, particularly in South Otago, while it is exceeded on 10 days in inland areas of Southland and Otago. The 75th percentile extends the areas affected for 10 days in both North and South Taranaki and the Wairarapa. Likewise, those areas of Southland and Otago where the CSI is exceeded on 10-20 days in winter are consolidated. The 90th percentile further extends this pattern, but for most of the dairying areas of the North Island and the Canterbury region the CSI threshold is rarely exceeded.

CCC model

The first series of maps (Appendix A4, Figure A4-8) indicate that the CSI threshold would be exceeded on 5 days along the Taranaki, Wairarapa and Southland coastal strips, and on 15 days on the South Otago coast. The 75th percentile differs little, except for a consolidation of the area in Otago where the CSI threshold would be exceeded on 10 days. The map for the 90th percentile suggests the CSI threshold would be exceeded on 10 days in winter months along the North Taranaki coast, and extends the area affected on the Wairarapa coast and in Otago.

Planck model

The CSI predictions using the Planck model data are similar to those using the CCC model data (Appendix A4, Figure A4-9). The CSI threshold would be exceeded on very few days. The Taranaki coast, Wairarapa, and the Otago and Southland coastal areas would be the main areas affected, but the CSI threshold would only be exceeded on around 10 days in the winter months in these areas. The 75th percentile is little different to the average, with only some extension of the affected area into Otago and along the Southland coast where the CSI threshold would be exceeded on around 10 days. The 90th percentile further extends the area that would be affected in the south.

9.4.2 Winter shoulder months (May and September)

Current situation

Based on the maps in Appendix A4 (Figure A4-10), the pattern within which the CSI threshold is currently exceeded during the winter shoulder months is very similar to that of the main winter months. The CSI threshold is exceeded on around 5 days in the shoulder months along the Taranaki, Wairarapa coasts and in inland Southland and Otago. Conditions on the South Otago coastline exceed the CSI threshold on around 15 days, and on 10 days in adjacent inland areas. The 75% percentile extends these areas, and in particular suggests that the Southland coast is affected on ≥ 20 days. The 90th percentile indicates that South Taranaki, Manawatu Hawkes Bay and Wairarapa currently exceed the CSI threshold on around 10 days in the shoulder months.

CCC model

The CSI predictions using this model data (Appendix A4, Figure A4-11) suggest that the threshold would not be exceeded in any dairying area, except a narrow coastal strip in Southland and South Otago where it may be exceeded on 5 days in the winter shoulder months. The 75% percentile suggests that the South Otago coastline areas would be affected more often, on 15 days in the shoulder months, and the area that would be affected on 5 days extends further inland. The 90th percentile extends the areas affected in Taranaki, Wairarapa and Hawkes Bay, but the overall effects in dairying areas would be minimal.

Planck model

The predictions using this model data (Appendix A4, Figure A4-12) are very similar to those of the CCC model, except that the exceedances are slightly larger, in the proportion of days and in the area affected, than for the CCC model. This would not be unexpected, as the CCC data predict a larger temperature increase.

Windier conditions exacerbate the physiological impacts of cold temperature when using the CSI model. This effect is not taken into account in the scenarios of this study, since no change was made to the daily wind speeds (i.e., winds speeds for the 15-year baseline period 1997-2011 were repeated in the future 2097-2111 period). However, relative humidity did change, and could have had some influence on the CSI model results. In the winter season, relative humidity increased in the CCC scenario and decreased in the Planck scenario (opposite to summer) in almost all regions (Appendix Figures A1-11 and A1-12).

9.5 Discussion of Results

The overall impression from this modelling is that dairy cattle will be greatly impacted by heat stress in most of the key dairying areas, and particularly in the North Island, while there will be virtually no occurrence of conditions exceeding cold stress thresholds under the future scenarios.

There are some limitations to the interpretation of the model:

- 1) While it does include a consideration for the opportunity for animals to dissipate their heat during the cooler conditions of night-time, it does not allow for adaptation by the animals over time through acclimatisation. In dairy cows, longer-term adaptation to heat load will generally affect feed intakes in the first instance (as cows become heat-stressed, an early behavioural adaptation is to reduce feed intake, and so reduce metabolic heat generation). This is likely to have a cumulative effect with resulting reduction of milk production.
- 2) Overall milk production levels have a direct influence on the internal generation of metabolic heat by the cow. As genetic improvement leads to increased individual cow production, the threshold at which thermal stress could occur will lower: i.e., it can be expected that higher-producing cows will be affected to a greater extent than the model predicts.
- 3) The effects of heat stress are likely to be underestimated by the model. This is because the model focuses on the direct impact of heat as experienced by cows as they stand out in their fields. It does not account for the additional heat generated as cows walk to the dairy shed. The average walking distance of cows currently is around 6-8 km/day, but on larger farms, these distances can be as high as 12-15 km/day. Larger herd sizes are becoming increasingly common as farmers endeavour to capture production efficiencies.
- 4) The HLI results are specific for a Friesian cow, as the thresholds adopted were based on latest knowledge of Friesian cow responses in New Zealand Jersey and crossbred dairy cattle, which make up a large proportion of the national herd, are known to have a higher tolerance to heat stress (Bryant *et al.* 2007).
- 5) Wind speed changes were not considered in the scenarios as developed by NIWA for this study.

One benefit, particularly for the South Island dairy industry, is that the reduction in cold stress will mean that feed currently partitioned to ensure that the animal maintains its internal body temperature will be reduced. This will mean that South Island dairy farmers may be able to reduce the amount of stored feed they need to have on hand for winter months, or that this extra feed might be utilised by feeding it to improve body condition and production.

These results suggest that improved methods will be needed to manage heat stress, and that these methods will need to be implemented for a longer period of time each year. There are a number of ways that this could be achieved. For example:

- 1) Use genetic diversity and introduce a greater proportion of genetics from breeds that are more heat tolerant: e.g., Jersey cattle and *Bos indicus* breeds have enhanced heat tolerance.
- 2) Modify seasonal schedules, so that cows are milked during winter months and are dry during summer months
- 3) Provide more shaded, well-ventilated areas where cows can rest.
- 4) More frequent use of sprinklers, and modifying pasture consumption so cows graze a lower proportion of their daily allocation in the heat of the day.

The models that were utilised provide an estimate of the direct impacts of the predicted changes on the animals. Examining thermal stress in isolation may not account for the full impacts of climate change, nor the full suite of potential adaptations in dairy systems. Indirect effects through changes in forage supply and quantity could have an overriding effect on dairy cow productivity and health. Other farm level impacts, such as risks to farm infrastructure and flow on to practical management implications, also need to be considered (for a more comprehensive discussion of these points, refer to Lee *et al*, 2012).

A further consideration is that dairying systems 100 years into the future will almost certainly differ from current practice, for a variety of reasons other than climate change. An expanded global human population may mean that pressures on land use for food production will radically alter dairying systems in New Zealand. Genetic improvement for dairy production will also have an impact on this. It is likely that future cows will require more supplementary feeding, while supplements that can be produced more efficiently in terms of dry matter production/area of land utilised will reduce the areas of pasture used for grazing.

Cows may therefore be managed in systems that are more confined than currently, and heat stress management may be more feasible. Our current pasture-based dairying systems may in fact become part of a niche industry, operating within the more limited geographical areas where heat load could be managed by current methods, while the majority of the industry operates systems more akin to what is currently seen in hotter countries such as Israel and southern United States.

Predicted climate change might be expected to impact upon other activities on dairy farms:

- 1) It is likely that conditions predicted to emerge in future years will favour the growth of *Pithomyces chartarum* (the fungus that results in facial eczema) in a much greater areas than the present time. It is also likely that the period of risk for facial eczema will be extended, and that the severity of outbreaks will be greater, as conditions are more favourable for fungal growth (night temperatures above 12°C with drizzly rain). Given that current methods to manage facial eczema largely rely on dosing cows with zinc salts at a rate that is close to toxic levels, improved controls for this disease may be required.
- 2) Emerging conditions are also likely to favour the growth of other fungal species in pasture, exposing cows to increased levels of mycotoxins such as zearelenone, which have an impact on animal health and production.
- 3) Hotter summer temperatures are likely to favour the multiplication of nuisance flies. It could be that fly control chemicals will need to be used more often, and across a wider period of the year to manage the impact of nuisance flies.
- 4) There has been no consideration for whether ultra-violet light levels could increase in association with other aspects of the potential climate change investigated. If this were to happen, the risk of sunburn – especially to the udder and teats – and risk of development of conditions such as cancer eye, could increase to a level that requires management intervention.

10 Further information

Queries about the technical details of this report should be directed to:

Dr Brett Mullan

National Institute of Water and Atmospheric Research

ph + 64 4 3860508

brett.mullan@niwa.co.nz

<http://www.niwa.co.nz/>

11 References

- Ainsworth, E.A.; Long, S.P. (2005). What have we learned from 15 years of free-air CO₂ enrichment (FACE)? A meta-analytic review of the responses of photosynthesis, canopy properties and plant production to rising CO₂. *New Phytologist* 165: 351–371.
- Ainsworth, E.A.; Rogers, A.; Nelson, R.; Long, S.P. (2004). Testing the “source-sink” hypothesis of down-regulation of photosynthesis in elevated [CO₂] in the field with single gene substitutions in *Glycine max*. *Agricultural and Forest Meteorology* 122: 85–94.
- Almeida, A.C.; Sands, P.J.; Bruce, J.; Siggins, A.W.; Leriche, A.; Battaglia, M.; Batista, T.R. (2009). Use of a spatial process-based model to quantify forest plantation productivity and water use efficiency under climate change scenarios. Presentation 18th World IMACS/MODSIM Congress, Cairns, Australia 13-17 July 2009.
- Anderson, K.; Bows, A. (2011). Beyond ‘dangerous’ climate change: emission scenarios for a new world. *Philosophical Transactions of the Royal Society A*, 369, 20-44. doi: 10.1098/rsta.2010.0290
- Arp, W.J. (1991). Effects of source-sink relations on photosynthetic acclimation to elevated CO₂. *Plant Cell and Environment* 14: 869–875.
- Baisden, W.T.; Keller, E.D.; Timar, L.; Smeaton, D.; Clark, A.; Ausseil, A.; Power, W.L.; Zhang, W. (2010). New Zealand's pasture production in 2020 and 2050. *GNS Science consultancy report 2010/154*. 88 p.
- Ball, J.T.; Woodrow, I.E.; Berry, J.A. (1987). A model predicting stomatal conductance and its contribution to the control of photosynthesis under different environmental conditions. In: Biggins J ed. Progress in photosynthesis research. Dordrecht, The Netherlands, Martin-Nijhoff Publishers pp. 221–224.
- Bárdossy, A; Singh, S.K. (2008). Robust estimation of hydrological model parameters. *Hydrology and Earth System Sciences* 12: 1273-1283.
- Battaglia, M.; Sands, P.J. (1997). Modelling site productivity of *Eucalyptus globulus* in response to climatic and site factors. *Australian Journal of Plant Physiology* 24: 831-850.
- Battaglia, M.; Sands, P.J. (1998). Process-based forest productivity models and their application on forest management. *Forest Ecology and Management* 119: 51-62.
- Battaglia, M.; Sands, P.J.; White, D.A.; Mummery, D. (2004). CABALA: a linked carbon, water and nitrogen model of forest growth for silvicultural decision support. *Forest Ecology and Management* 193: 251-282.
- Bryant, J.R.; López-Villalobos, N.; Pryce, J.E.; Holmes, C.W.; Johnson, D.L. (2007). Quantifying the effect of thermal environment on three breeds of dairy cattle in New Zealand. *New Zealand Journal of Agricultural Research* 50: 327-338.

- Campion, J.M.; Esprey, L.J.; Scholes, M.C. (2005). Application of the 3-PG model to a *Eucalyptus grandis* stand subjected to varying levels of water and nutrient constraints in KwaZulu-Natal, South Africa. *Southern African Forestry Journal* 203: 3-13.
- Chapin, F.S.; McGuire, A.D.; Ruess, R.W.; Hollingsworth, T.N.; Mack, M.C.; Johnstone, J.F.; Kasischke, E.S.; Jones, J.B.; Jorgenson, M.T.; Kielland, K.; Kofinas, G.P.; Turstsky, M.R.; Yarie, J.; Lloyd, A.H.; Taylor, D.L. (2010). Resilience of Alaska's boreal forest to climate change. *Canadian Journal of Forest Research* 40: 1360-1370.
- Cichota, R.; Snow, V.O.; Tait, A.B. (2008). A functional evaluation of virtual climate station rainfall data. *New Zealand Journal of Agricultural Research*, 51: 317-329.
- Clark, M. P.; Hreinsson, E. Ö; Martinez, G.; Tait, A.; Slater, A.; Hendrikx, J.; Owens, I.; Gupta, H.; Schmidt, J.; Woods, R. (2009). Simulations of seasonal snow for the South Island, New Zealand. *Journal of Hydrology (NZ)*, 48: 41-58.
- Clark, M. P.; Rupp, D.E.; Woods, R.A.; Zheng, X.; Ibbitt, R.P.; Slater, A.G.; Schmidt, J.; Uddstrom, M.J. (2008). Hydrological data assimilation with the ensemble Kalman filter: Use of streamflow observations to update states in a distributed hydrological model. *Advances in Water Resources*, 31: 1309-1324.
- Clark, A.; Mullan, B.; Porteous, A. (2011). Scenarios of regional drought under climate change. NIWA report number WLG2010-32, for Ministry for Agriculture and Forestry, 135pp.
- Clark, A.J.; Nottage, R.A.C.; Wilcocks, L.; Lee, J.M.; Burke, C.; Kalaugher, E.; Roche, J.; Beukes, P.; Lieffering, M.; Newton, P.C.D.; Li, F.Y.; Vibart, R.; Teixeira, E.I.; Brown, H.E.; Fletcher, A.L.; Hernandez-Ramirez, G.; Soltani, A.; Viljanen-Rollinson, S.; Horrocks, A.; Johnstone, P.; Clothier, B.; Hall, A.; Green, S.; Dunningham, A.; Kirschbaum, M.U.F.; Meason, D.; Payn, T.; Collins, D.B.G.; Woods, R.A.; Rouse, H.; Duncan, M.; Snelder, T.; Cowie, B. (2012). *Impacts of Climate Change on Land-based Sectors and Adaptation Options*. Clark, A.J.; Nottage, R.A.C. (eds). Technical Report to the Sustainable Land Management and Climate Change Adaptation Technical Working Group, Ministry for Primary Industries, 408 p.
- Clutter, J.L.; Fortson, J.C.; Pienaar, L.V.; Brister, G.H.; Bailey, R.L. (1992). *Timber Management: a Quantitative Approach*. Reprint edition. Krieger Publishing, Malabar.
- Comins, H.N.; McMurtrie, R.E. (1993). Long-term biotic response of nutrient-limited forest ecosystems to CO₂-enrichment; equilibrium behaviour of integrated plant-soil models. *Ecological Application* 3: 666-681.
- Coops, N.C.; Waring, R.H.; Schroeder, T.A. (2009). Combining a generic process-based productivity model and a statistical classification method to predict the presence and absence of tree species in the Pacific Northwest, U.S.A. *Ecological Modelling* 220: 1787-1796.

- Coops, N.C.; Waring, R.H. (2010). A process-based approach to estimate lodgepole pine (*Pinus contorta* Dougl.) distribution in the Pacific Northwest under climate change. *Climatic Change* 105: 313-328.
- Coops, N.C.; Waring, R. (2011). Estimating the vulnerability of fifteen tree species under changing climate in Northwest North America. *Ecological Modelling* 222: 2119-2129.
- CSIRO. (2007). Climate Change in Australia, Technical Report by CSIRO and Bureau of Meteorology, Australia, http://climatechangeinaustralia.com.au/technical_report.php.
- Curtis, P.S.; Wang, X. (1998). A meta analysis of elevated CO₂ effects on woody plant mass, form, and physiology. *Oecologia* 113: 299-313.
- Davis, M.R.; Coker, G.; Parfitt, R.L.; Simcock, R.; Clinton, P.W.; Garrett, L.G.; Watt, M.S. (2007). Relationships between soil and foliar nutrients in young densely planted mini-plots of *Pinus radiata* and *Cupressus lusitanica*. *Forest Ecology and Management* 240: 122-130.
- Farquhar, G.D.; von Caemmerer, S. (1982). Modelling of photosynthetic response to environmental conditions. In: Lange OL, Nobel PS, Osmond CB, Ziegler H, eds., *Physiological Plant Ecology II. Water Relations and Carbon Assimilation*. Encyclopaedia of Plant Physiology, New Series Vol. 12B. Berlin, Heidelberg, New York, Springer-Verlag, pp. 549-588.
- Fox, D.G.; Tylutki, T.P. (1998). Accounting for the effects of environment on the nutrient requirements of dairy cattle. *Journal of Dairy Science* 81, 3085-3095.
- Gradwell, M.W.; Birrell, K.S. (1979). Soil Bureau laboratory methods. Part C. Methods for physical analysis of soils. New Zealand Bureau scientific report 10C, Wellington, Department of Scientific and Industrial Research.
- Griffiths, E. (1985). Interpretation of soil morphology for assessing moisture movement and storage. New Zealand Soil Bureau scientific report no. 74. Wellington, Department of Scientific and Industrial Research.
- Gunderson, C.A.; Wullschleger, S.D. (1994). Photosynthetic acclimation in trees to rising atmospheric CO₂: a broader perspective. *Photosynthesis Research* 39: 369-388.
- Hunt, E.R.Jr.; Piper, S.C.; Nemani, R.; Keeling, C.D.; Otto, R.D.; Running, S.W. (1996). Global net carbon exchange and intra-annual atmospheric CO₂ concentrations predicted by an ecosystem process model and three-dimensional atmospheric transport model. *Global Biogeochemical Cycles* 10: 431-456.
- Hunter, I.R.; Gibson, A.R. (1984). Predicting *Pinus radiata* site index from environmental variables. *New Zealand Journal of Forest Science* 14: 53-64.
- IPCC. (2000). Special report on emission scenarios: a special report of working group III of the International Panel on Climate Change. Eds., Nakicenovic, N., & Swart, R. Cambridge University Press.

- IPCC. (2007). Climate change 2007: Impacts Adaptation and Vulnerability. Contribution of working group II to the fourth assessment report of the Intergovernmental Panel on Climate Change. Eds., Parry, M.L., Canziani, O.F., Palutikof, J.P, van de Linden, P.J.& Hanson, C.E. Cambridge University Press.
- Jackson, D.S.; Gifford, H.H. (1974). Environmental variables influencing the increment of radiata pine. (1) Periodic volume increment. *New Zealand Journal of Forest Science* 4: 3–26.
- Joshi, M.; Hawkins, E.; Sutton, R.; Lowe, J.; Frame, D. (2011). Projections of when temperature change will exceed 2°C above pre-industrial levels. *Nature Climate Change*, 1: 407-412.
- Karnosky, D.F. (2003). Impacts of elevated atmospheric CO₂ on forest trees and forest ecosystems: knowledge gaps. *Environment International* 29: 161-169.
- Keller, E.D.; Baisden, W.T.; Timar, L. (2011). Adapting the Biome-BGC model to New Zealand pastoral agriculture: climate change and land-use change. Abstract GC23C-0955 IN: *AGU Fall Meeting 2011, 5-9 December, San Francisco, California, USA: abstracts*. Washington, DC: American Geophysical Union.
- Kimball, J.S.; Thornton, P.E.; White, M.A.; Running, S.W. (1997). Simulating forest productivity and surface-atmosphere carbon exchange in the BOREAS study region. *Tree Physiology* 17: 589–599.
- Kimball, J.S.; White, M.A.; Running, S.W. (1997). BIOME–BGC simulations of stand hydrologic processes for BOREAS. *J. Geophysical Res.* 102: 29,043–29,051.
- Kirschbaum, M.U.F. (1999a). CenW, a forest growth model with linked carbon, energy, nutrient and water cycles. *Ecological Modelling* 118: 17–59.
- Kirschbaum, M.U.F. (1999b). Modelling forest growth and carbon storage with increasing CO₂ and temperature. *Tellus* 51B: 871–888.
- Kirschbaum, M.U.F. (2000). Forest growth and species distributions in a changing climate. *Tree Physiology* 20: 309–322.
- Kirschbaum, M.U.F. (2011). Does enhanced photosynthesis enhance growth? Lessons learnt from CO₂ enrichments studies. *Plant Physiology* 155: 117-124.
- Kirschbaum, M.U.F.; Paul, K.I. (2002). Modelling carbon and nitrogen dynamics in forest soils with a modified version of the CENTURY model. *Soil Biology & Biochemistry* 34: 341–354.
- Kirschbaum, M.U.F.; Mason, N.W.H.; Watt, M.S.; Tait, A.; Ausseil, A-G.E.; Palmer, D.J.; Carswell, F.E. (2010). Productivity surfaces for *Pinus radiata* and a range of indigenous forest species under current climatic conditions, and exploration of the effect of future climatic changes on *Pinus radiata* productivity. Landcare Research contract report LC0910/176, prepared for the Ministry of Agriculture and Forestry, 119 pp.

- Kirschbaum, M.U.F.; Watt, M.S. (2011). Use of a process-based model to describe spatial variation in *Pinus radiata* productivity in New Zealand. *Forest Ecology and Management* 262: 1008-1019.
- Kirschbaum, M.U.F., Watt, M.S., Tait, A., Ausseil, A-G.E. (2012). Future wood productivity of *Pinus radiata* in New Zealand under expected climatic changes. *Global Change Biology* 18: 1342-1356.
- Körner, C. (2006). Plant CO₂ responses: an issue of definition, time and resource supply. *New Phytologist* 172: 393-411.
- Körner, C.; Morgan, J.; Norby, R. (2007). CO₂ fertilization: when, where, how much? In: Canadell JG, Pataki DE, Pitelka LF eds Terrestrial ecosystems in a changing world. Berlin/Heidelberg, Springer Verlag, pp. 9–21.
- Landsberg, J.J.; Waring, R.H. (1997). A generalised model of forest productivity using simplified concepts of radiation-use efficiency, carbon balance and partitioning. *Forest Ecology and Management* 95: 209-228.
- Landsberg, J.J.; Waring, R.H.; Coops, N.C. (2003). Performance of the forest productivity model 3-PG applied to a wide range of forest types. *Forest Ecology and Management* 172: 199-214.
- Ledgard, N.J.; Knowles, R.L.; de la Mare, P. (2005). Douglas-fir – the current New Zealand scene. *New Zealand Journal of Forestry* 50: 14-16.
- Lee, J.M.; Burke, C.; Kalaugher, E.; Roche, J.; Beukes, P.; Clark, A.J. (2012). Adapting dairy farming systems in a changing climatic environment. Chapter 3 in: *Impacts of Climate Change on Land-based Sectors and Adaptation Options*. Clark, A.J.; Nottage, R.A.C. (eds). Technical Report to the Sustainable Land Management and Climate Change Adaptation Technical Working Group, Ministry for Primary Industries, 408 p.
- Lewis, J.D.; Wang, X.Z.; Griffin, K.L.; Tissue, D.T. (2002). Effects of age and ontogeny on photosynthetic responses of a determinate annual plant to elevated CO₂ concentration. *Plant Cell and Environment* 25: 359-368.
- Long, S.P.; Osborne, C.P.; Humphries, S.W. (1996). Photosynthesis, rising atmospheric carbon dioxide concentration and climate change. In: Breymer AI, Hall DO, Melillo JM, Ågren GI eds SCOPE 56 – Global change: effects on coniferous forests and grasslands. Chichester, John Wiley & Sons Ltd, pp. 121–159.
- Long, S.P.; Zhu, X.-G.; Naidu, S.L.; Ort, D.R. (2006). Can improvements in photosynthesis increase crop yields? *Plant, Cell and Environment* 29: 315–330.
- Luxmoore, R.J.; Wullschlegel, S.D.; Hanson, P.J. (1993). Forest responses to CO₂ enrichment and climate warming. *Water, Air, and Soil Pollution* 70: 309–323.
- Manning, M.R.; Edmonds, J.; Emori, S.; Grubler, A.; Hibbard, K.; Joos, F.; van Vuuren, D.P. (2010). Misrepresentation of the IPCC CO₂ emission scenarios. *Nature Geoscience* 3: 376-377.

- Matthews, L.R.; Arnold, M.A (in press). Trading off rest for shading by dairy cattle reveals thermal comfort threshold from the animal's point of view. *Physiology and Behavior*.
- McCarthy, H.R.; Oren, R.; Johnsen, K.H.; Gallet-Budynek, A.; Pritchard, S.G.; Cook, C.W.; LaDeau, S.L.; Jackson, R.B.; Finzi, A.C. (2010). Re-assessment of plant carbon dynamics at the Duke free-air CO₂ enrichment site: interactions of atmospheric [CO₂] with nitrogen and water availability over stand development. *New Phytologist* 185: 514-528.
- McKerchar, A.I.; Pearson, C.P. (1997). Quality of long flow records for New Zealand rivers. *Journal of Hydrology (NZ)*. 36(1): 15-41
- McMillan, H.K.; Clark, M.P. (2009). Rainfall-runoff model calibration using informal likelihood measures within a Markov chain Monte Carlo sampling scheme. *Water Resources Research* 45(W04418). <http://dx.doi.org/doi:10.1029/2008WR007288>
- McMillan, H.K.; Jackson, B.; Poyck, S. (2010a). Flood risk under climate change: A framework for assessing the impacts of climate change on river flow and floods, using dynamically-downscaled climate scenarios. NIWA Client Report CHC2010-033 for Ministry of Agriculture and Forestry.
- McMillan, H.; Freer, J.; Pappenberger, F.; Krueger, T.; Clark, M. (2010b). Impacts of Uncertain River Flow Data on Rainfall-Runoff Model Calibration and Discharge Predictions. *Hydrological Processes* 24(10): 1270-1284 DOI: 10.1002/hyp.7587
- McMillan, H.; Jackson, B.; Clark, M.; Kavetski, D.; Woods, R. (2011). Rainfall Uncertainty in Hydrological Modelling: An Evaluation of Multiplicative Error Models. *Journal of Hydrology* 400(1-2): 83-94
- McMurtrie, R.E.; Rook, D.A.; Kelliher, F.M. (1990). Modelling the yield of *Pinus radiata* on a site limited by water and nitrogen. *Forest Ecology and Management* 30: 381-413.
- Meason, D.F.; Beets, P.; Dungey, H. (2010). *Development of a carbon sequestration web tool for Eucalyptus fastigata*. Unpublished report No. 17610. Rotorua: New Zealand Forest Research Institute Limited.
- Meason, D.F.; Almeida, A.; Manning, L.; Nicholas, I. (2011). Preliminary parameterisation of the hybrid model 3-PG for Eucalyptus fastigata in New Zealand. Unpublished report No. 18500. Rotorua: New Zealand Forest Research Institute Limited.
- Medlyn, B.E.; Barton, C.V.M.; Broadmeadow, M.S.J.; Ceulemans, R.; De Angelis, P.; Forstreuter, M.; Freeman, M.; Jackson, S.B.; Kellomäki, S.; Laitat, E.; Rey, A.; Roberntz, P.; Sigurdsson, B.D.; Strassemeier, J.; Wang, K.; Curtis, P.S.; Jarvis, P.G. (2001). Stomatal conductance of forest species after long-term exposure to elevated CO₂ concentration: a synthesis. *New Phytologist* 149: 247-264.

- Medlyn, B.E.; Duursma, R.A.; Zeppel, M.J.B. (2011). Forest productivity under climate change: a checklist for evaluating model studies. *Wiley Interdisciplinary Reviews-Climate Change* 2: 332-355.
- Meehl, G.A.; and co-authors. (2007). Global Climate Projections. In S. Solomon & M. M. D. Qin, Z. Chen, M. Marquis, K.B. Averyt, M. Tignor and H.L. Miller (Eds.), *Climate Change 2007: The Physical Science Basis. Contribution of Working Group I to the Fourth Assessment Report of the Intergovernmental Panel on Climate Change* (pp. 747-845). Cambridge, United Kingdom and New York, NY, USA: Cambridge University Press.
- Meinshausen, M.; Meinshausen, N.; Hare, W.; Raper, S.C.B.; Frieler, K.; Knutti, R.; Allen, M.R. (2009). Greenhouse-gas emission targets for limiting global warming to 2°C. *Nature*, 458. doi: 10.1038/nature08017
- Ministry for the Environment. (2008). *Climate Change Effects and Impacts Assessment. A Guidance Manual for Local Government in New Zealand*. 2nd Edition. Prepared by Mullan, B; Wratt, D; Dean, S; Hollis, M. (NIWA); Allan, S; Williams, T. (MWH NZ Ltd), and Kenny, G. (Earthwise Consulting Ltd), in consultation with Ministry for the Environment. NIWA Client Report WLG2007/62, February 2008, 156p.
- Ministry for the Environment. (2010). *Tools for estimating the effects of climate change on flood flow: A guidance manual for local government in New Zealand*. Woods R, Mullan AB, Smart G, Rouse H, Hollis M, McKerchar A, Ibbitt R, Dean S, and Collins D (NIWA). Prepared for Ministry for the Environment.
- Mullan, A.B.; Carey-Smith, T.; Griffiths, G.; Sood, A. (2011). *Scenarios of Storminess and Regional Wind Extremes under Climate Change*. NIWA Client Report for the Ministry of Agriculture and Forestry, Report no. WLG2010-31, 80p.
- Nakicenovic, N; Swart, R (Eds). (2000). *Special Report on Emissions Scenarios*. A Special Report of Working Group III of the Intergovernmental Panel on Climate Change. Cambridge University Press, Cambridge, United Kingdom and New York, NY, USA, 599 p. Available at: <http://www.ipcc.ch/ipccreports/sres/emission/index.php?idp=0>
- Nash, J.E.; Sutcliffe, J.V. (1970). River flow forecasting through conceptual models part I - A discussion of principles. *Journal of Hydrology* 10: 282–290.
- Newsome, P.F.J.; Wilde, R.H.; Willoughby, E.J. (2008). Land resource information system spatial data layers. Data dictionary. Palmerston North; Landcare Research New Zealand.
- Norby, R.J.; DeLucia, E.H.; Gielen, B.; Calfapietra, C.; Giardina, C.P.; King, J.S.; Ledford, J.; McCarthy, H.R.; Moore, D.J.P.; Ceulemans, R.; De Angelis, P.; Finzi, A.C.; Karnosky, D.F.; Kubiske, M.E.; Lukac, M.; Pregitzer, K.S.; Scarascia-Mugnozza, G.E.; Schlesinger, W.H.; Oren, R. (2005). Forest response to elevated CO₂ is conserved across a broad range of productivity. *Proceedings of the National Academy of Science* 102: 18052–18056.

- Norby, R.J.; Wullschleger, S.D.; Gunderson, C.A.; Johnson, D.W.; Ceulemans, R. (1999). Tree responses to rising CO₂ in field experiments: implications for the future forest. *Plant, Cell and Environment* 22: 683-714.
- Norby, R.J.; Warren, J.M.; Iversen, C.M.; Medlyn, B.E.; McMurtrie, R.E. (2010). CO₂ enhancement of forest productivity constrained by limited nitrogen availability. *Proceedings of the National Academy of Science* 107: 19368–19373.
- Norton, D.A. (1985). A multivariate technique for estimating New Zealand temperature normals. *Weather and Climate* 5: 64-74.
- Nowak, R.S.; Ellsworth, D.S.; Smith, S.D. (2004). Functional responses of plants to elevated atmospheric CO₂ – do photosynthetic and productivity data from FACE experiments support early predictions? *New Phytologist* 162: 253–280.
- NZCCC. (2011). Climate Brief No. 1, New Zealand Climate Change Centre, November 2011, 6p.
- Parton, W.J.; Schimel, D.S.; Cole, C.V.; Ojima, D.S. (1987). Analysis of factors controlling soil organic matter levels in Great Plains grasslands. *Soil Science Society of America Journal* 51: 1173-1179.
- Payn, T.W.; Skinner, M.F.; Hill, R.B.; Thorn, A.J.; Scott, J.; Downs, S.; Chapman, H. (2000). Scaling up or scaling down: the use of foliage and soil information for optimising the phosphate nutrition of radiata pine. *Forest Ecology and Management* 138: 79-89.
- Poorter, H.; Navas, M.-L. (2003). Plant growth and competition at elevated CO₂: on winners, losers and functional groups. *New Phytologist* 157: 175–198.
- Randall, D.A.; Wood, R.A.; Bony, S.; Colman, R.; Fichelet, T.; Fyfe, J.; Kattsov, V.; Pitman, A.; Shukla, J.; Srinivasan, J.; Stouffer, R.J.; Sumi, A.; Taylor, K.E. (2007). Climate Models and their Evaluation. In: *Climate Change 2007: The Physical Science Basis. Contribution of Working Group I to the Fourth Assessment Report of the Intergovernmental Panel on Climate Change* [Solomon S, Qin SD, Manning M, Chen Z, Marquis M, Averyt KB, Tignmor M, Miller HL (eds.)]. Cambridge University Press, Cambridge, United Kingdom and New York, NY, USA.
- Rastetter, E.B.; McKane, R.B.; Shaver, G.R.; Melillo, J.M. (1992). Changes in C storage by terrestrial ecosystems: how C-N interactions restrict responses to CO₂ and temperature. *Water, Air, and Soil Pollution* 64: 327–344.
- Reisinger, A.; Mullan, A.B.; Manning, M.; Wratt, D.W.; Nottage, R.A.C. (2010). Global and local climate change scenarios to support adaptation in New Zealand. In: *Climate change adaptation in New Zealand: Future scenarios and some sectoral perspectives*. Nottage, R.A.C., Wratt, D.S., Bornman, J.F., Jones, K. (eds). New Zealand Climate Change Centre, Wellington, pp 26-43.

- Richardson, B.; Whitehead, D.; McCracken, I.J. (2002). Root-zone water storage and growth of *Pinus radiata* in the presence of a broom understorey. *New Zealand Journal of Forestry Science* 32: 208–220.
- Running, S.W.; Hunt, E.R.Jr. (1993). Generalization of a forest ecosystem process model for other biomes, BIOME–BGC, and an application for global-scale models. *Scaling Physiological Processes: Leaf to Globe*, edited by J. R. Ehleringer and C. B. Field, Academic Press, San Diego, 141–157.
- Sands, P.J. (1995). Modelling canopy production. II. From single-leaf photosynthesis parameters to daily canopy photosynthesis. *Australian Journal of Plant Physiology* 22: 603–614.
- Sands, P. (2004). Adaptation of 3-PG to novel species: guidelines for data collection and parameter assignment. Technical Report 141. Cooperative Research Centre for Sustainable Production Forestry. CSIRO.
- Simioni, G.; Ritson, P.; Kirschbaum, M.U.F.; McGrath, J.; Dumbrell, I.; Copeland, B. (2009). The carbon budget of *Pinus radiata* plantations in south-western Australia under four climate change scenarios. *Tree Physiology* 29: 1081–1093.
- Smith, C.T.; Lowe, A.T.; Skinner, M.F.; Beets, P.N.; Schoenholtz, S.H.; Fang, S.Z. (2000). Response of radiata pine forests to residue management and fertilisation across a fertility gradient in New Zealand. *Forest Ecology and Management* 138: 203–223.
- Snelder, T.H.; Biggs, B.J.F. (2002). Multiscale river environment classification for water resources management. *JAWRA Journal of the American Water Resources Association* 38: 1225–1239
- Srinivisan, M.S.; Schmidt, J.; Poyck, S.; Hreinsson, E. (2011). Irrigation reliability under climate change scenarios: A modelling investigation in a river based irrigation scheme in New Zealand. Submitted to *Journal of the American Water Resources Association*.
- Sutherst, R.W.; Baker, R.H.A.; Coakley, S.M.; Harrington, R.; Kriticos, D.J.; Scherm, H. (2007). Pests under global change - meeting your future landlords? In: *Terrestrial ecosystems in a changing world*. Springer, Berlin Heidelberg New York, pp. 211–223.
- Tait, A.; Turner, R. (2005). Generating Multiyear Gridded Daily Rainfall over New Zealand. *Journal of Applied Meteorology* 44: 1315–1323.
- Tait, A.; Henderson, R.; Turner, R.; Zheng, X. (2006). Thin-plate smoothing spline interpolation of daily rainfall for New Zealand using a climatological rainfall surface. *International Journal of Climatology* 26: 2097–2115, DOI:2010.1002/joc.1350.
- Tait, A.B. (2008). Future projections of growing degree days and frost in New Zealand and some implications for grape growing. *Weather and Climate* 28: 17–36.

- Tait A.; Liley, B. (2009). Interpolation of daily solar radiation for New Zealand using a satellite-derived cloud cover surface. *Weather and Climate* 29: 70–88.
- Thornton, P.E. (1998). Description of a numerical simulation model for predicting the dynamics of energy, water, carbon, and nitrogen in a terrestrial ecosystem. Ph.D. dissertation, University of Montana, Missoula, MT, 280 pp. [Available from Mansfield Library, University of Montana, Missoula, MT 59812.]
- Thornton, P.E.; Running, S.W. (1999). An improved algorithm for estimating incident daily solar radiation from measurements of temperature, humidity, and precipitation. *Agricultural and Forest Meteorology* 93: 211–228.
- Thornton, P.E.; Law, B.E.; Gholz, H.L.; Clark, K.L.; Falge, E.; Ellsworth, D.S.; Goldstein, A.H.; Monson, R.K.; Hollinger, D.; Falk, M.; Chen, J.; Sparks, J.P. (2002). Modeling and measuring the effects of disturbance history and climate on carbon and water budgets in evergreen needleleaf forests. *Agricultural and Forest Meteorology* 113:185-222.
- Waring, R.; Milner, K.S.; Jolly, W.M.; Phillips, L.; McWethy, D. (2005). A basis for predicting site index and maximum growth potential across the Pacific and Inland Northwest U.S.A. with a MODIS satellite-derived vegetation index. *Forest Ecology and Management* 228: 285-291.
- Watt, M.S.; Kirschbaum, M.U.F. (2011). Moving beyond simple linear allometric relationships between tree height and diameter. *Ecological Modelling* 222: 3910-3916.
- Watt, M.S.; Palmer, D.J.; Bulman, L.S. (2011). Predicting the severity of Dothistroma needle blight on *Pinus radiata* under climate change. *New Zealand Journal of Forestry Science* 41: 207-215
- Watt, M.S.; Palmer, D.J.; Kimberley, M.O.; Höck, B.K.; Payn, T.W.; Lowe, D.J. (2010). Development of models to predict *Pinus radiata* productivity throughout New Zealand. *Canadian Journal of Forest Research* 40: 488–499.
- Watt, M.S.; Whitehead, D.; Richardson, B.; Mason, E.G.; Leckie, A.C. (2003). Modelling the influence of weed competition on the growth of young *Pinus radiata* at a dryland site. *Forest Ecology and Management* 178: 271–286.
- Webb, T.H.; Wilson, A.D. (1995). A manual of land characteristics for evaluation of rural land. Landcare research science series No. 10. Lincoln; Landcare Research New Zealand.
- White, M.A.; Thornton, P.E.; Running, S.W. (1997). A continental phenology model for monitoring vegetation responses to interannual climatic variability. *Global Biogeochemical Cycles* 11: 217–234.
- White, M.A.; Running, S.W.; Thornton, P.E. (1999). The impact of growing-season length variability on carbon assimilation and evapotranspiration over 88 years in the eastern U.S. deciduous forest. *International J. Biometeorology* 42: 139–145.

- White, M.A.; Thornton, P.E.; Running, S.W.; Nemani, R.R. (2000). Parameterization and Sensitivity Analysis of the BIOME-BGC Terrestrial Ecosystem Model: Net Primary Production Controls. *Earth Interactions 4*: Paper 4-003.
- Will, G. (1985). Nutrient deficiencies and fertiliser use in New Zealand exotic forests. *Forest Research Institute Bulletin No. 97*, 54 pp.
- Wilson, A.D.; Giltrap, D.J. (1982). Prediction and mapping of soil water retention properties. New Zealand Soil Bureau district office report WN7. Wellington, Department of Scientific and Industrial Research.
- Woods, R.; Hendrikx, J.; Henderson, R.; Tait, A. (2006). Estimating mean flow of New Zealand rivers. *Journal of Hydrology (New Zealand) 45*: 95-110.
- Woods, R.A.; Tait, A.B.; Mullan, A.B.; Hendrikx, J.; Diettrich, J. (2008). Projected climate and river flow for the Rangitata catchment for 2040. NIWA Client Report No. CHC2008-097. 36 p.
- Zammit, C.; Woods, R.A. (2011a). Projected climate and river flow for the Waimakariri catchment for 2040 and 2090. NIWA Client Report No 25.
- Zammit, C.; Woods, R.A. (2011b). Projected climate and river flow for the Ashley catchment for 2040 and 2090. NIWA Client Report No 26.

12 Appendices

12.1 Appendix A1: Seasonal climate change scenarios

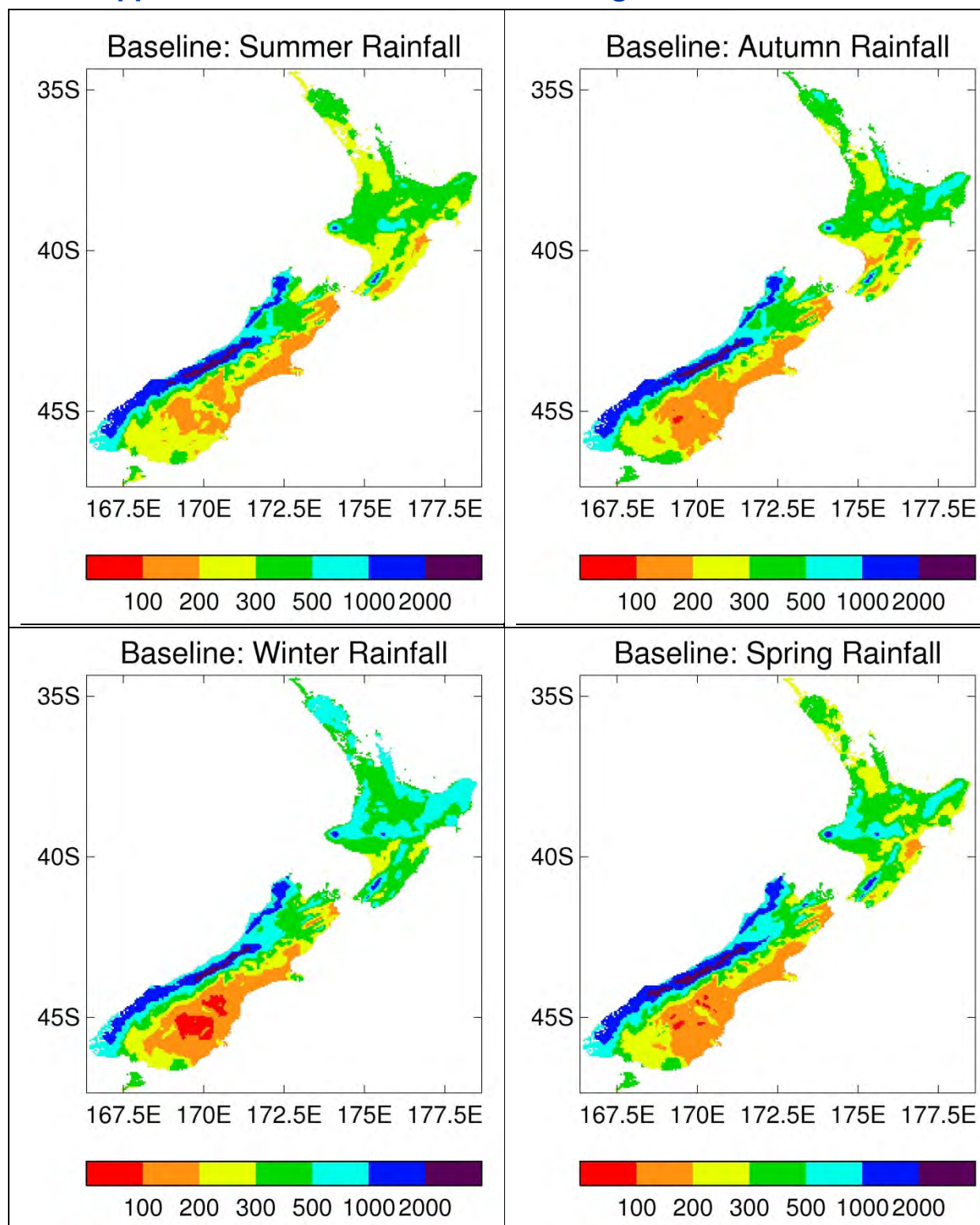


Figure A1-1: Seasonal rainfall totals (in mm) for 1997-2011 baseline period.

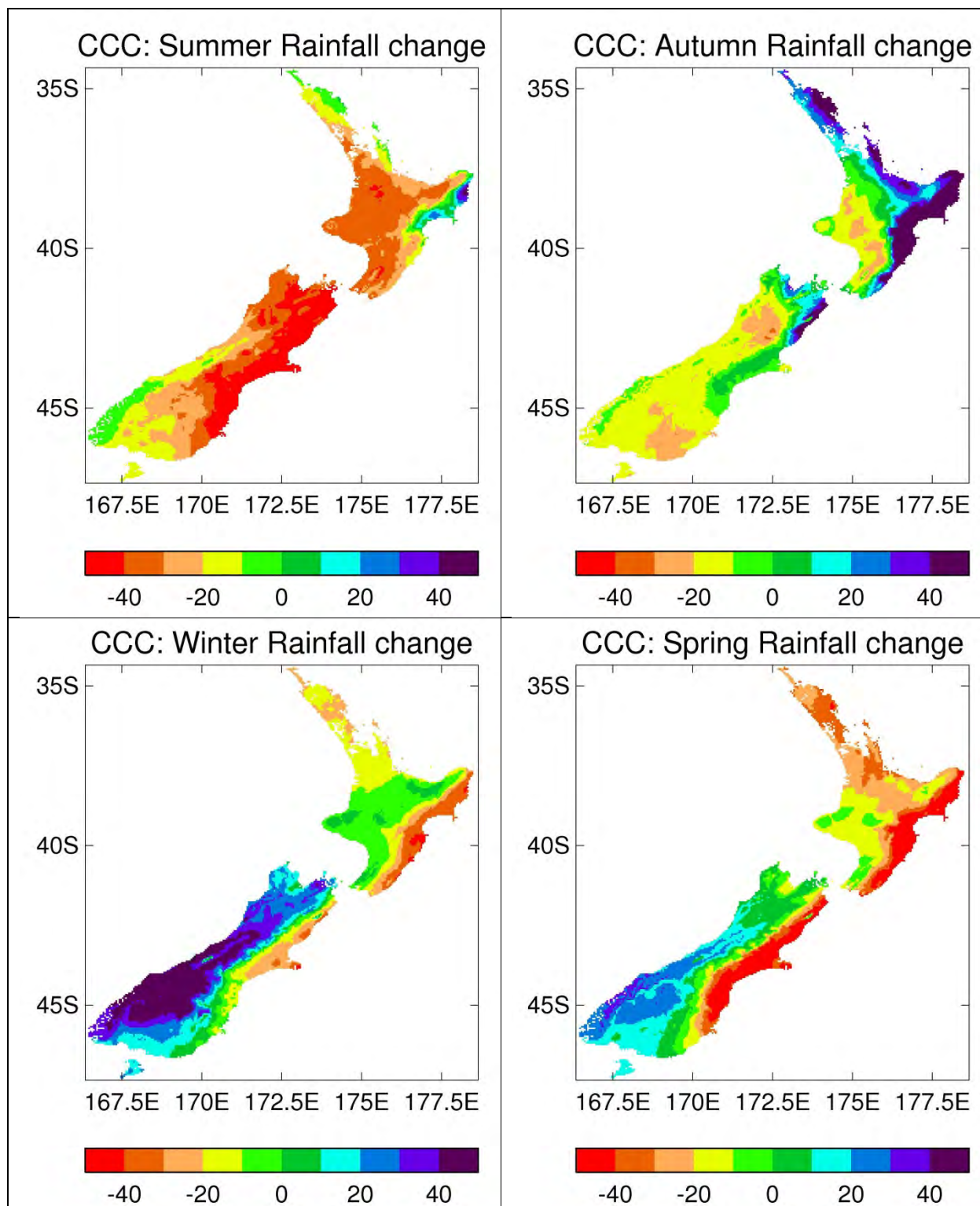


Figure A1-2: Downscaled projections of seasonal rainfall changes (as a %) between 1990 and date of 4°C global warming, from CCC model.

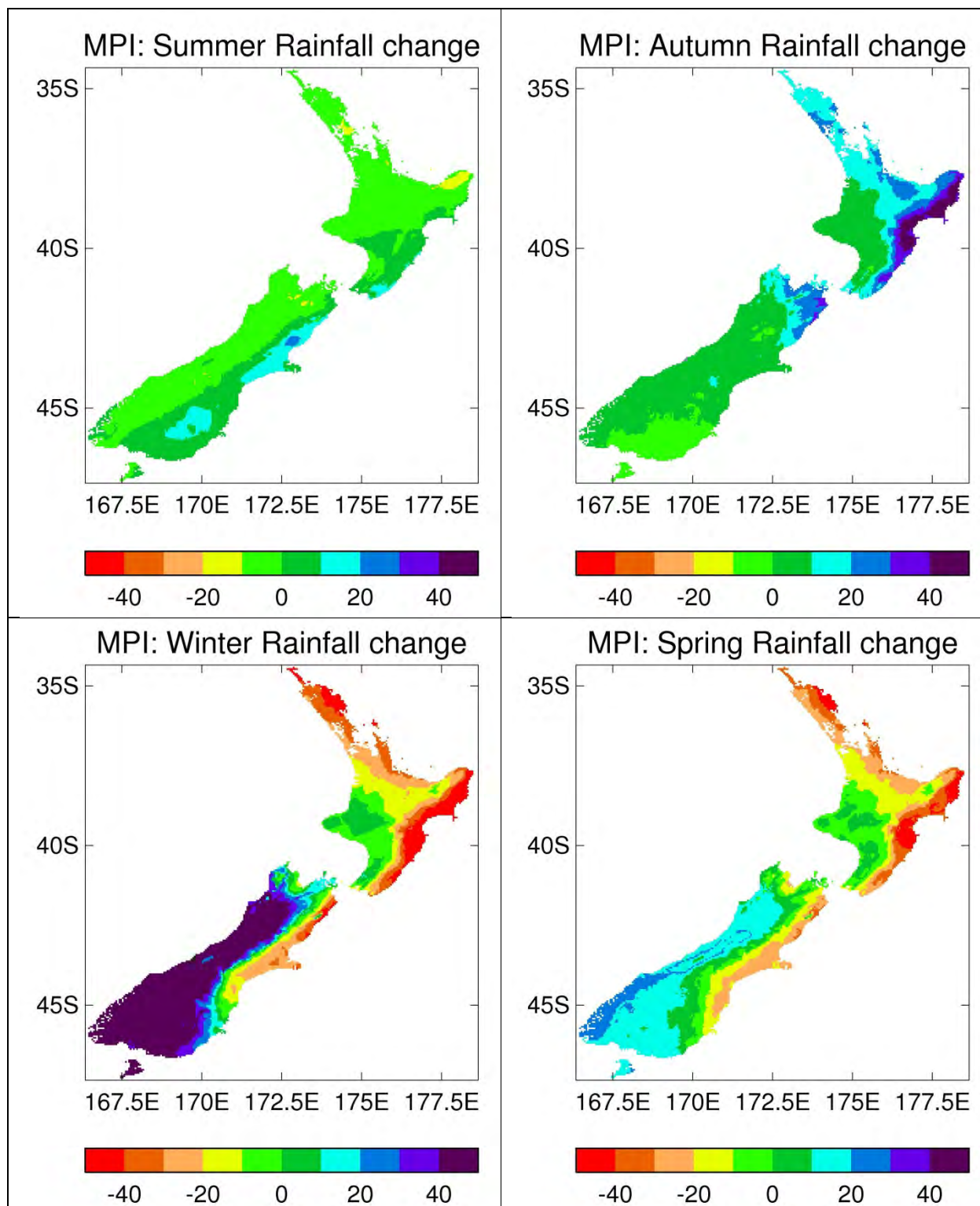


Figure A1-3: Downscaled projections of seasonal rainfall changes (as a %) between 1990 and date of 4°C global warming, from Planck model.

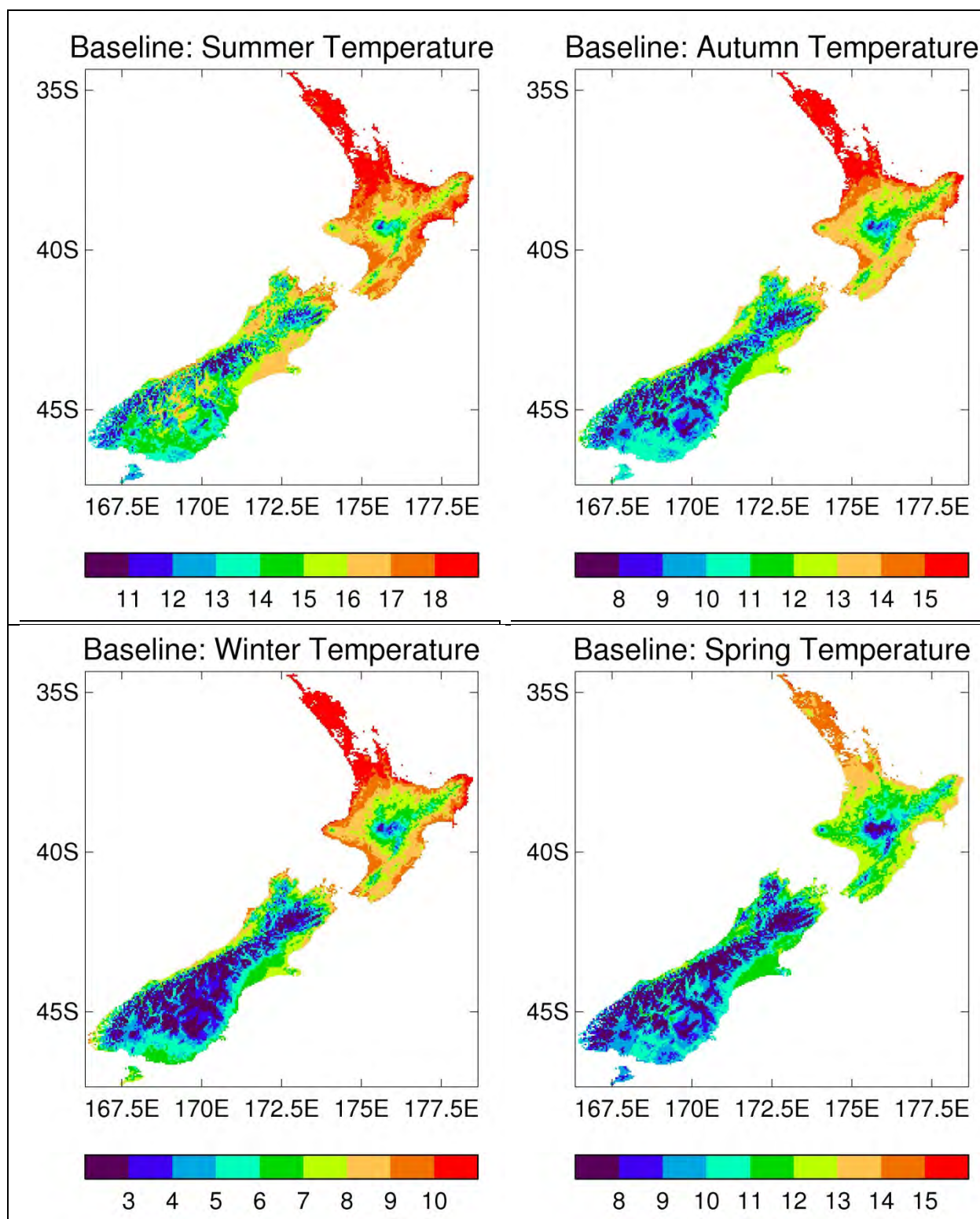


Figure A1-4: Seasonal mean temperature (in °C) for 1997-2011 baseline period.

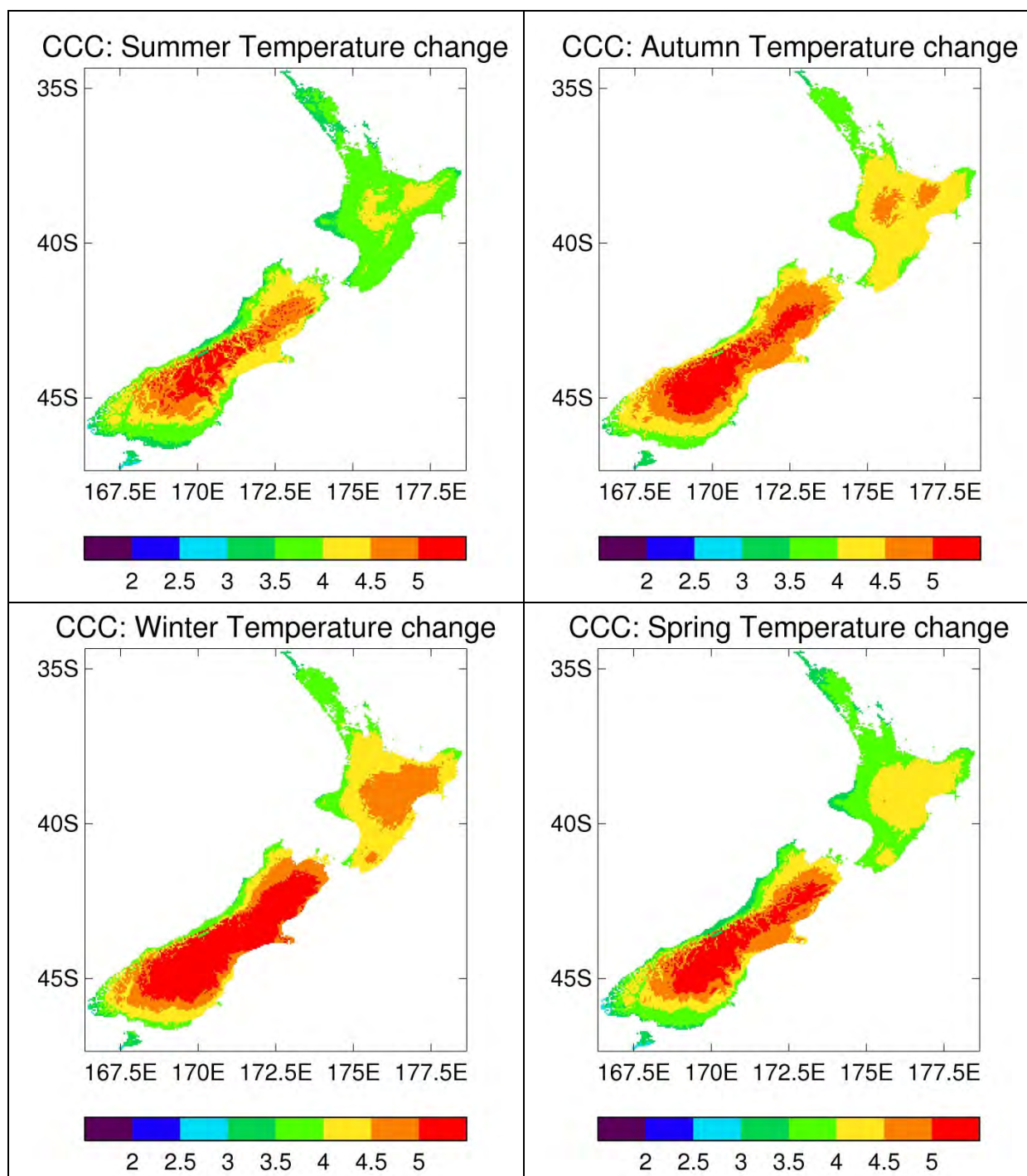


Figure A1-5: Downscaled projections of seasonal mean temperature changes (in °C) between 1990 and date of 4°C global warming, from CCC model.

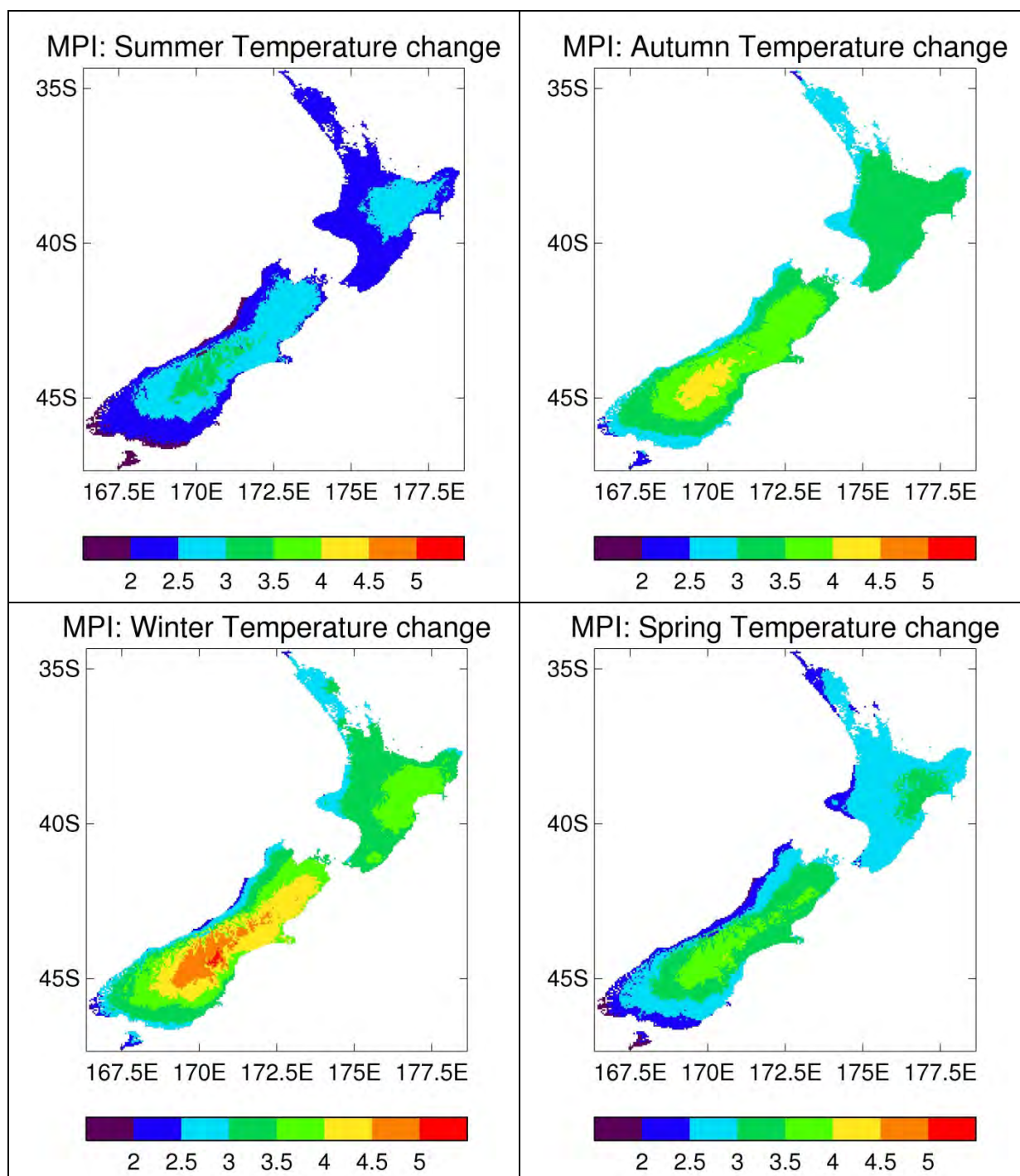


Figure A1-6: Downscaled projections of seasonal mean temperature changes (in °C) between 1990 and date of 4°C global warming, from Planck model.

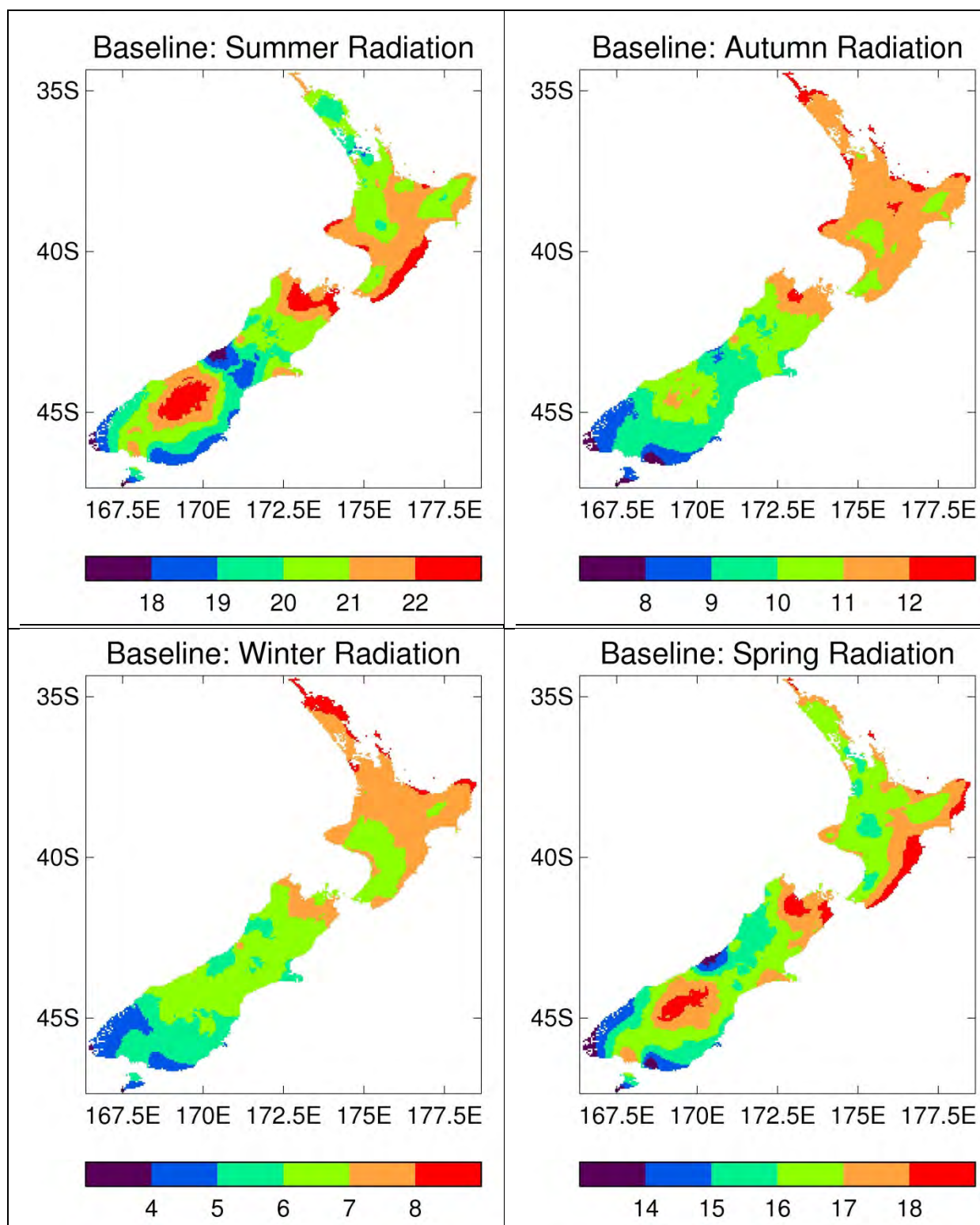


Figure A1-7: Seasonal mean-daily solar radiation (in MJ.m⁻².day⁻¹) for 1997-2011 baseline period.

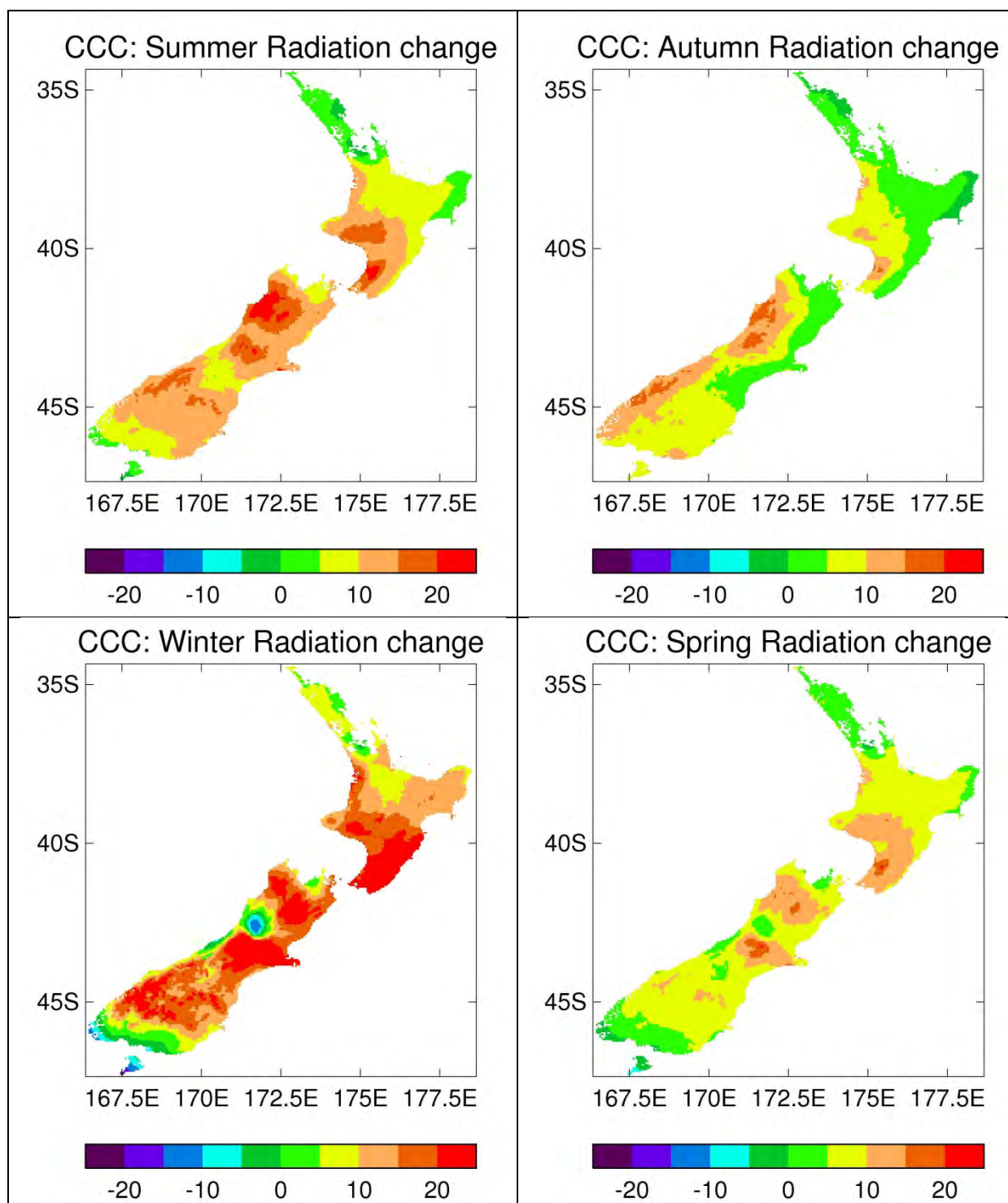


Figure A1-8: Downscaled projections of seasonal solar radiation changes (as a %) between 1990 and date of 4°C global warming, from CCC model.

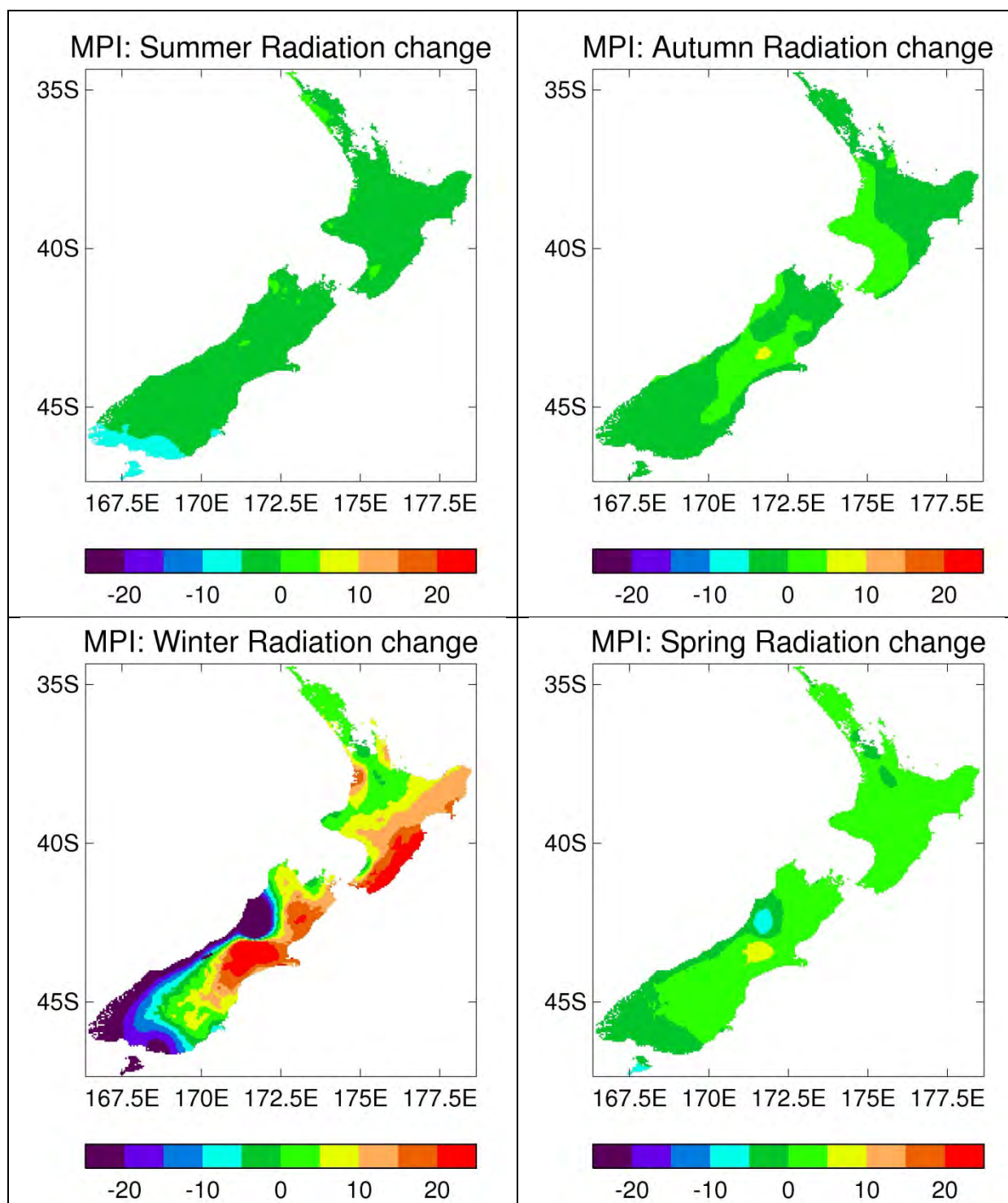


Figure A1-9: Downscaled projections of seasonal solar radiation changes (as a %) between 1990 and date of 4°C global warming, from Planck model.

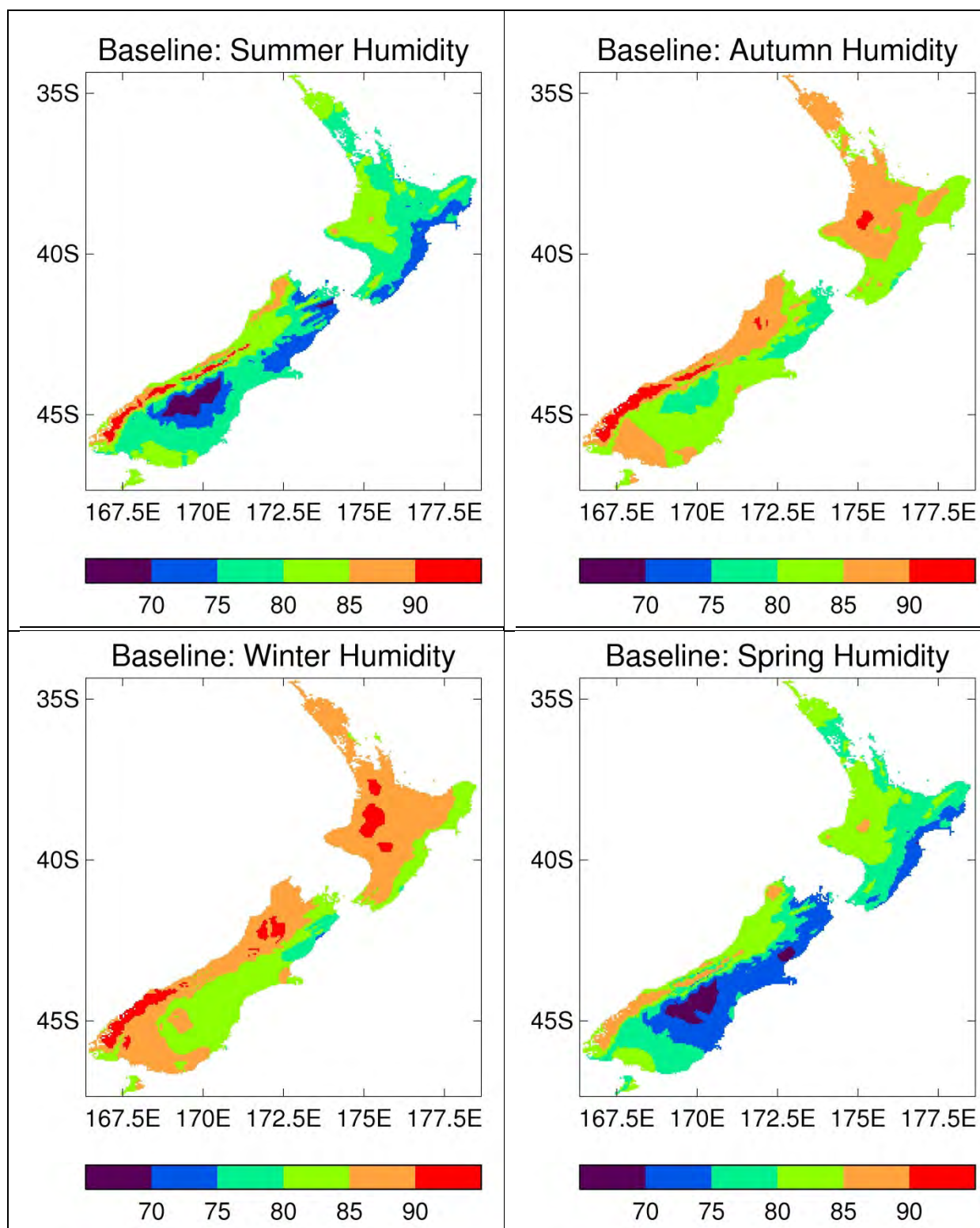


Figure A1-10: Seasonal relative humidity (in %) for 1997-2011 baseline period.

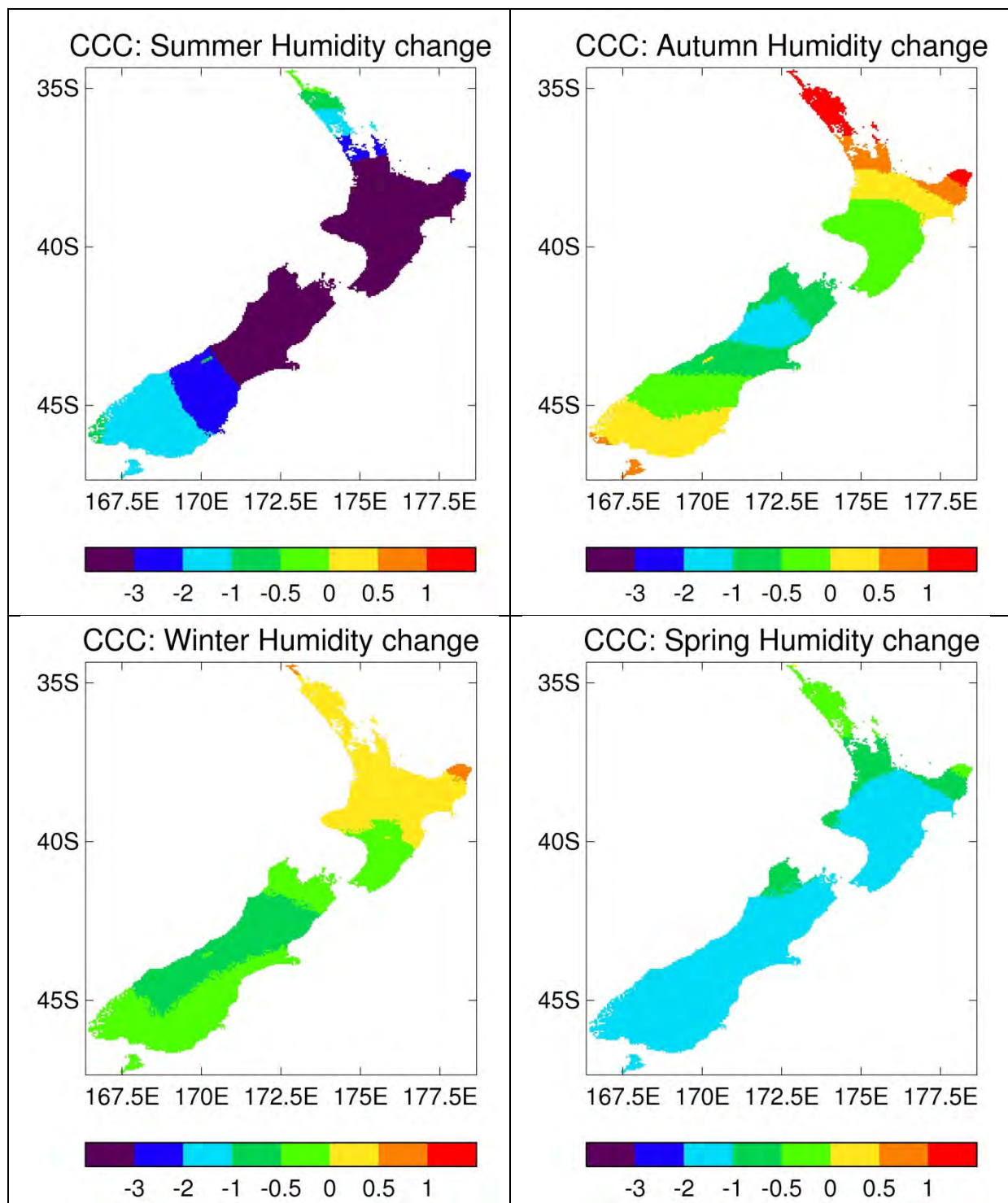


Figure A1-11: Downscaled projections of seasonal relative humidity changes (in %) between 1990 and date of 4°C global warming, from CCC model.

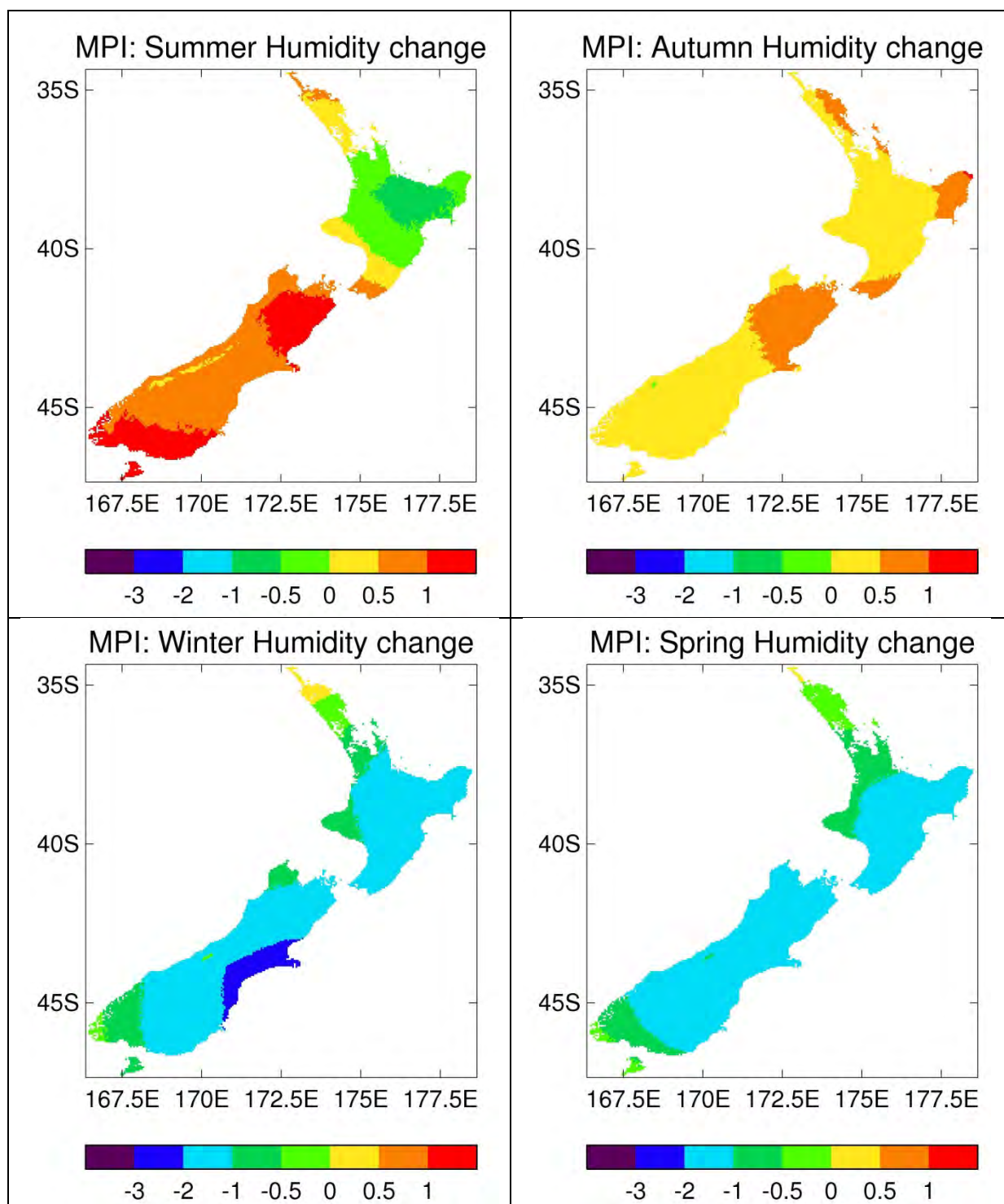


Figure A1-12: Downscaled projections of seasonal relative humidity changes (in %) between 1990 and date of 4°C global warming, from Planck model.

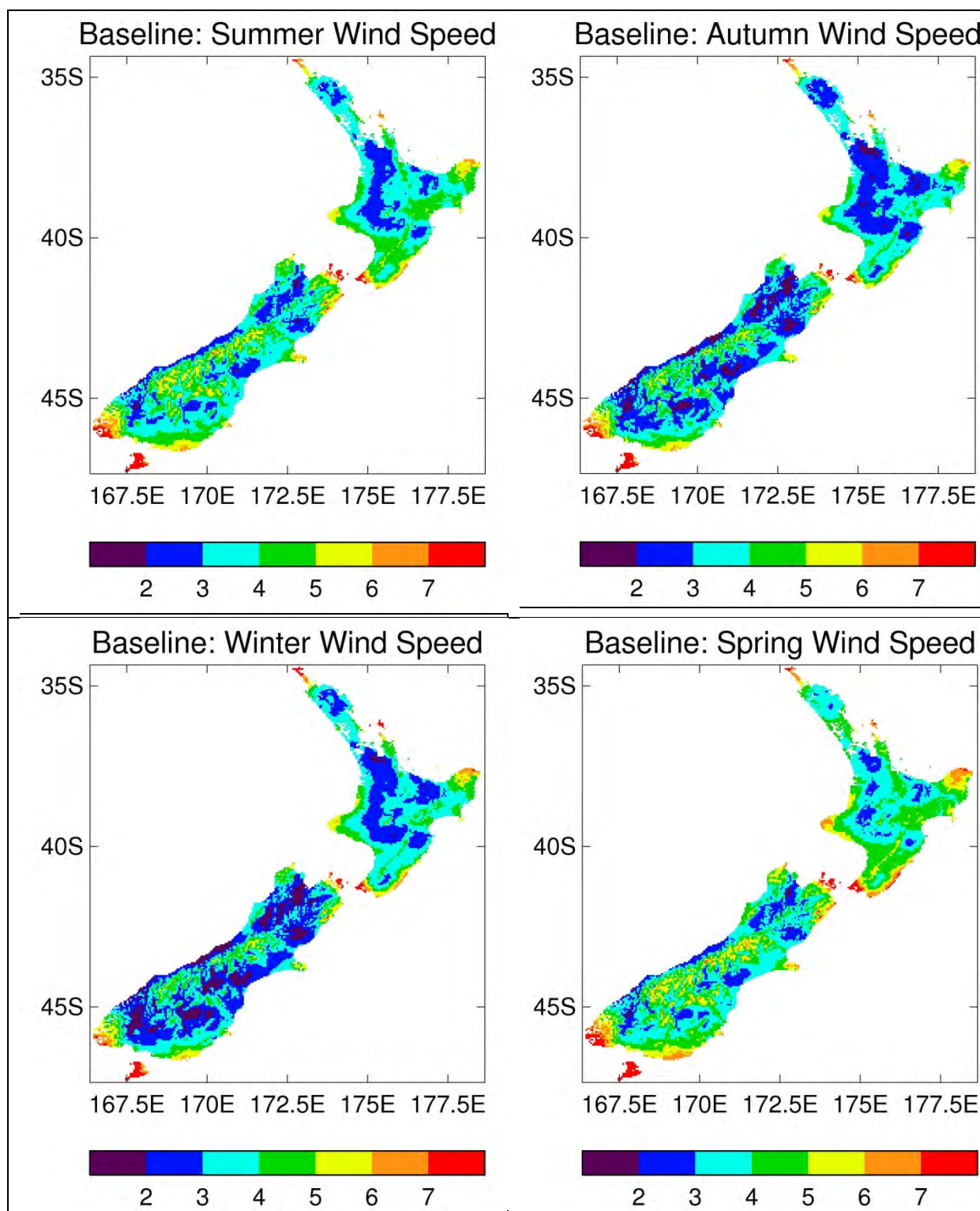


Figure A1-13: Seasonal mean-daily wind speed (in m.sec⁻¹) for 1997-2011 baseline period.

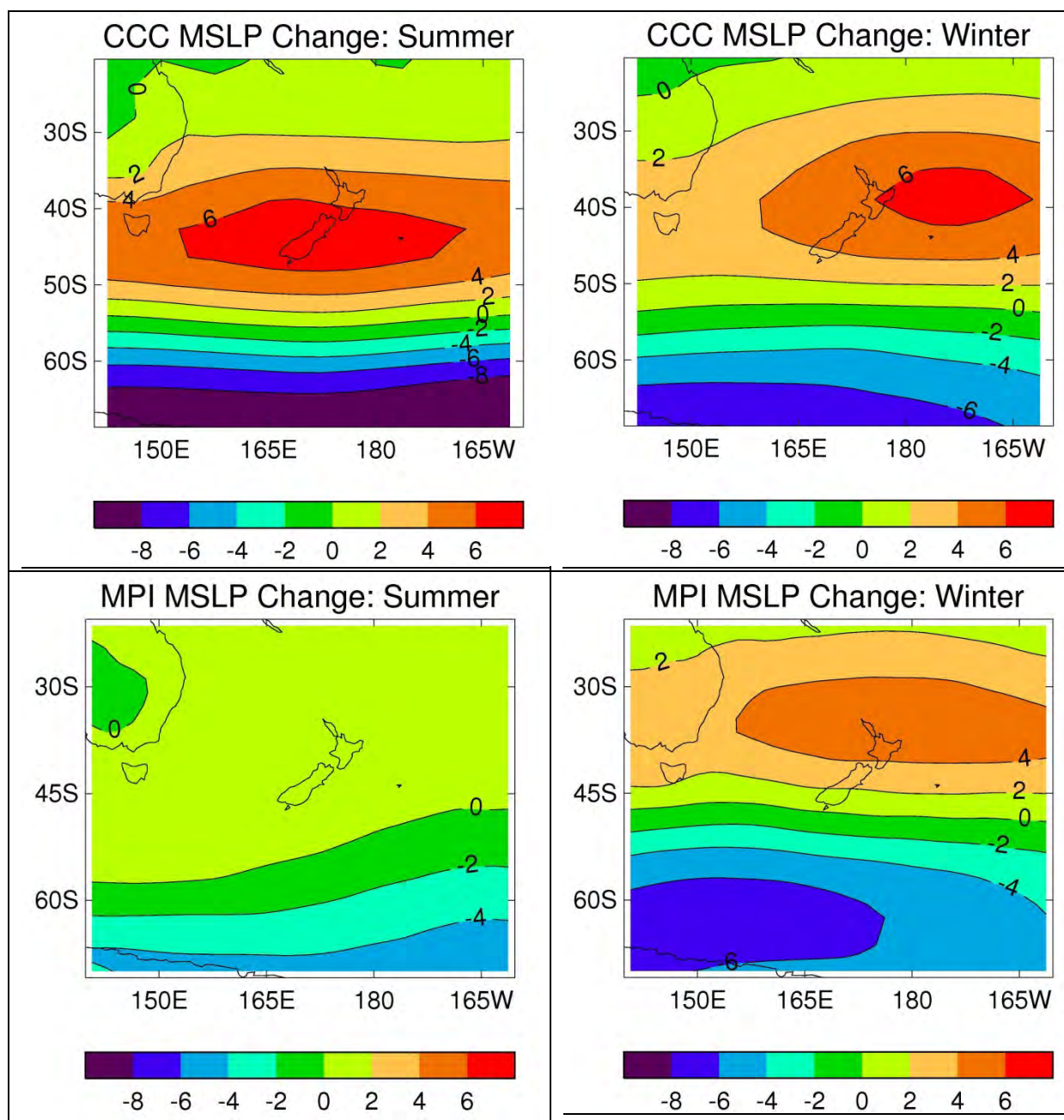


Figure A1-14: Global model projections of mean sea-level pressure changes (in hPa) between 1990 and date of 4°C global warming: CCC model, for the summer and winter seasons (top panels); Planck model, for the summer and winter seasons (bottom panels).

12.2 Appendix A2: Details of daily scenarios for APSIM files

The impacts models require daily weather data, which are provided in what is known as APSIM Met file format. Section 3.3.6 shows an example of APSIM file data. The climate scenario changes are specified at the monthly time scale, but the APSIM file requires daily values. The approach taken in this study is to apply the scenario changes as offsets to the current climate. This Appendix provides details of the methodology.

12.2.1 Baseline APSIM files

Table A2-1 describes the 12 weather elements (or 11 elements plus CO₂ concentration) given in each row of the APSIM file. Not all these weather elements are independent of each other. The primary variables available through the VCSN interpolated data set are:

- Column 3: Rainfall
- Columns 4, 5: Maximum and minimum temperature
- Column 7: Solar radiation
- Column 8: Wind Speed
- Column 10: 9am water vapour pressure (VP, or e_a)
- Column 11: 9am relative humidity (RH)

The other meteorological variables are calculated from these primary weather elements:

- Column 6: Mean temperature: the average of columns 4 and 5
- Column 9: Daily-average vapour pressure deficit (VPD), defined as
$$VPD = [e_s(T_{max}) + e_s(T_{min})]/2 - e_a(9 \text{ am}),$$
where T_{max} and T_{min} are taken from Columns 4 and 5 respectively, and e_a from column 10.
The formula used for saturation vapour pressure (e_s) is given by:
$$e_s = a * \exp[(b * T) / (T+c)], \text{ where } T = \text{temperature, } a = 6.108, \\ b=17.27, c = 237.3, \text{ for } e_s \text{ in units of hPa}$$
- Column 12: 9am saturation vapour pressure (svp_9am, or $e_s(9am)$), where svp is calculated from the 9am vapour pressure e_a (column10), and 9am RH (column 11), as:
$$e_a = 0.01 * RH * e_s$$
- Column 13: 9am vapour pressure deficit, calculated from 9am saturation vapour pressure (column 12) and actual 9am vapour pressure (column10):
$$VPD(9am) = e_s(9 \text{ am}) - e_a(9 \text{ am}).$$

In addition, the CO₂ concentration is specified independently, as given in Table 3-5. Every day of the calendar year is assigned the same CO₂ concentration, which is updated to the new year's value on each 1st January.

The following sub-section describes how the adjustments are applied for the future daily weather scenarios. In all cases the starting point is the 15 years of daily VCSN values for the baseline climate period of 1997-2011. From this 15 years of daily current climate data, a

monthly climatology is determined for the primary weather variables (Figures A1-1, A1-4, A1-7, A1-10, A1-13 show the seasonal maps). The monthly change fields for these primary variables, scaled to represent a local climate consistent with a 4° warming world as described in Section 3, are then applied (Figures A1-2, 3, 5, 6, 8, 9, 11, 12 show the seasonal change fields).

Table A2-1: Information on daily elements in the APSIM Met files

Column	Description
1	Year
2	Julian day of the year. Local day.
3	24 hour accumulated rainfall for the period from 9 am local day to 9 am the following day. Units = mm/24 hours
4	Daily maximum temperature for the period from 9 am local day to 9 am the following day. Units = degrees Celsius
5	Daily minimum temperature for the period from 9 am on the previous day to 9 am local day. Units = degrees Celsius
6	Daily mean temperature for the 24 hour period (midnight to midnight local day), taken as the average of columns 4 and 5. Units = degrees Celsius
7	Daily global (direct + diffuse) downward shortwave solar radiation received at the surface for the 24 hour period midnight to midnight local day. Units = MJ per square metre per day.
8	Mean wind speed at 10 m above the ground for the 24 hour period from midnight local day. Units = m/s
9	Daily vapour pressure deficit for use with crop evapotranspiration models that use a daily value of vapour pressure deficit. Defined as $vpd = [es(T_{max}) + es(T_{min})]/2 - ea(9 \text{ am})$ where $es(T)$ is the saturated vapour pressure in mbar of water at temperature T and ea is the actual water vapour pressure in mbar at 9 am local day. Follows convention used in FAO 56 (Crop evapotranspiration - Guidelines for computing crop water requirements - FAO Irrigation and Drainage Paper 56, http://www.fao.org/docrep/X0490E/X0490E00.htm). Units = mbar = hPa.
10	Actual water vapour pressure in mbar at 9 am local day. For use with crop models that model the diurnal cycle of water vapour pressure and use a 9 am value to calibrate the model. Units = mbar = hPa.
11	Relative humidity as a percentage at 9 am local day. Units = %
12	Saturated water vapour pressure at 9 am local day. Calculated from 9 am actual water vapour pressure and 9 am RH for each VCSN point. Units = mbar = hPa.
13	Vapour pressure deficit at 9 am local day. Calculated as $es(9 \text{ am}) - ea(9 \text{ am})$. Units = mbar = hPa.
14	Global atmospheric Carbon Dioxide concentration in ppm. Units = ppm.

12.2.2 4° warming APSIM files

- **Rainfall:** There are two steps involved in adjusting the daily rainfall. The first step is to apply the rainfall scenario (e.g., Figure A1-2) as a percentage offset. However, we do not multiply each daily rainfall by this factor, since this would impose a change in inter-annual variability which might not be justified. Thus, the monthly rainfall climatology is used to calculate the change in mm of total rainfall for that calendar

month (e.g., all Januaries), and this change is pro-rated according to the daily rainfall totals across all days in the selected month (e.g., all rain-days in all January months).

An *ad hoc* constraint is applied, such that future rainfall monthly climatology cannot be less than 25% of the current monthly rainfall. This constraint was activated for 148 gridpoint-months with the CCC scenario, and 342 gridpoint-months for the Planck scenario. All gridpoints involved were in the lower South Island, and mainly in the low rainfall central Otago region.

The second step involves redistributing the daily rainfall totals, as described in Woods et al. (2009), such that there is an increase in daily extremes which scale as the temperature increase, and a compensating increase in dry days and decrease in rainfall for average or low rainfall days.

- **Temperature:** The temperature offset (e.g., Figure A1-5) is applied additively to every day of the selected month, equally for maximum, minimum and mean temperature.
- **Solar radiation:** The solar radiation offset (e.g., Figure A1-8) is applied as a percentage change of the climatology of the month in question (as with the first step in the rainfall adjustment). Two *ad hoc* constraints are applied: the future radiation monthly climatology cannot be less than 25% of the current monthly radiation climatology; and no future daily radiation level is allowed to go above the maximum value ever currently observed for that calendar month (this is to ensure the new radiation level can never be higher than the maximum allowed by astronomical considerations). The low daily radiation constraint was not needed for the CCC scenario, but was activated at 22 gridpoint-months for the Planck scenario: all months were either June or July, and the gridpoints were all southern South Island, where the winter radiation was very low anyway.
- **Wind Speed:** This is left unchanged from the current climate daily values.
- **Relative humidity:** The relative humidity offset (e.g., Figure A1-11) is applied additively to every day of the selected month. A test is applied to ensure the daily RH is capped at 100% (which otherwise would sometimes occur). Similarly, the RH is never allowed to fall below 0%.
- **9am vapour pressure & 9am saturation vapour pressure:** The calculated 9am saturation vapour pressure for each day of the current climate is 'inverted', using the formula for e_s given above in A2.1, to determine $T(9am)$, the current-climate 9am temperature. The 9am temperature in the future 4° scenario is then calculated by adding the appropriate temperature offset as above. The formula for e_s is then applied to obtain the future 9am saturation vapour pressure. The future actual 9am vapour pressure is calculated from:

$$e_a = 0.01 * RH * e_s$$
 using the future relative humidity and future e_s
- **9am vapour pressure deficit:** This is calculated as the difference of the future saturation and actual vapour pressures, as described above for the current climate VPD (column 13).

- **Mean-daily vapour deficit:** This is calculated using the formula given above in A2.1 for the current climate (column 9), but using the future climate values of maximum and minimum temperature, and 9am vapour pressure.
- **CO₂ concentration:** This is taken from Table 3-5, and updated annually, as described in Appendix section 1.2.1.

12.3 Appendix A3: Detailed catchment-based TopNet results

See separate document detailing catchment results.

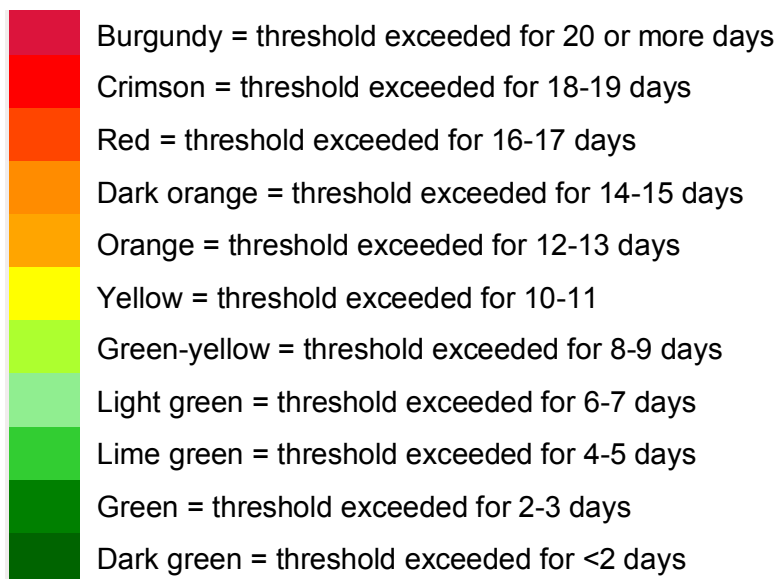
12.4 Appendix A4: Heat Stress Predictive risk maps

Maps are presented for the average conditions of each respective dataset, and for the 75th and 90th percentile conditions of each respective dataset.

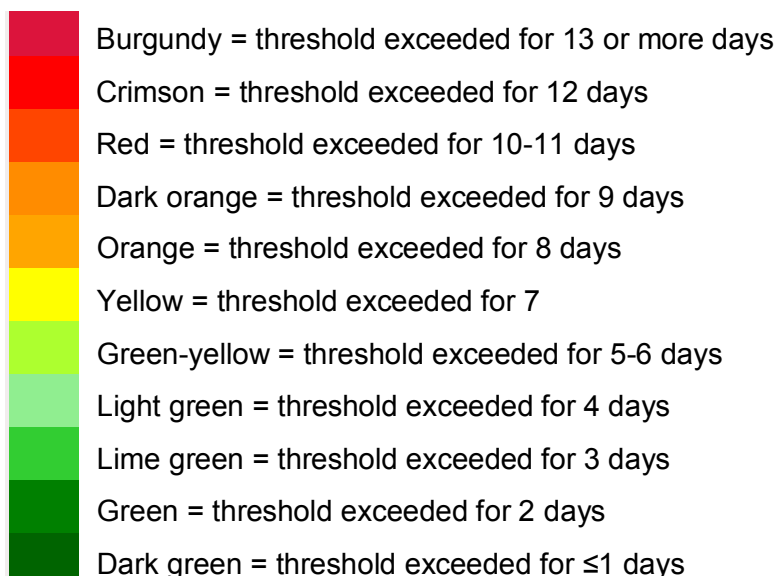
Key to interpretation:

Maps were rendered using colour bands to represent exposure gradients as follows:

For seasonal periods (summer: December-February; winter; June-August):



For shoulder periods (summer: November/ March; winter: May/September):



12.4.1 Summer months (December, January, February)

Current actual data

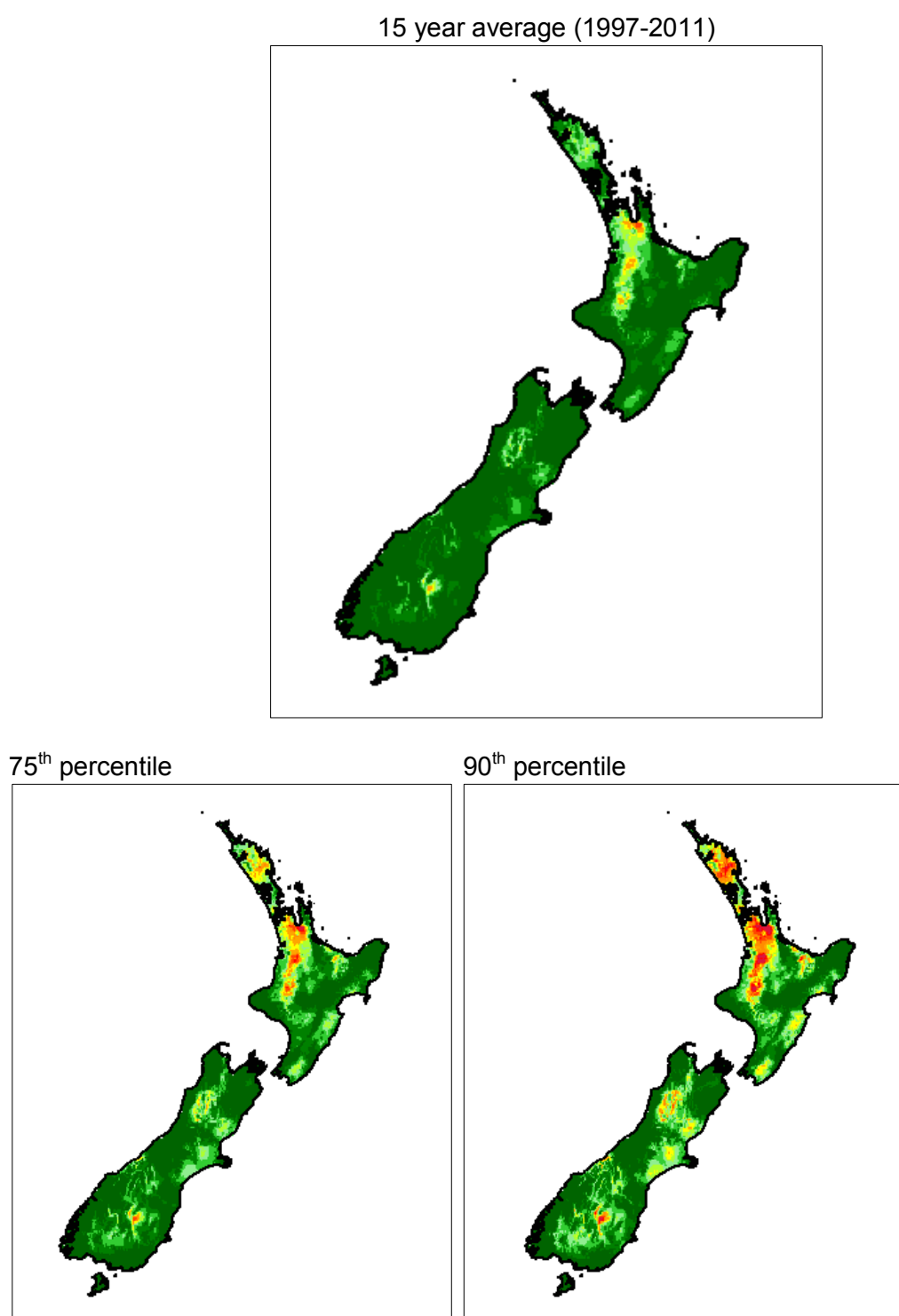
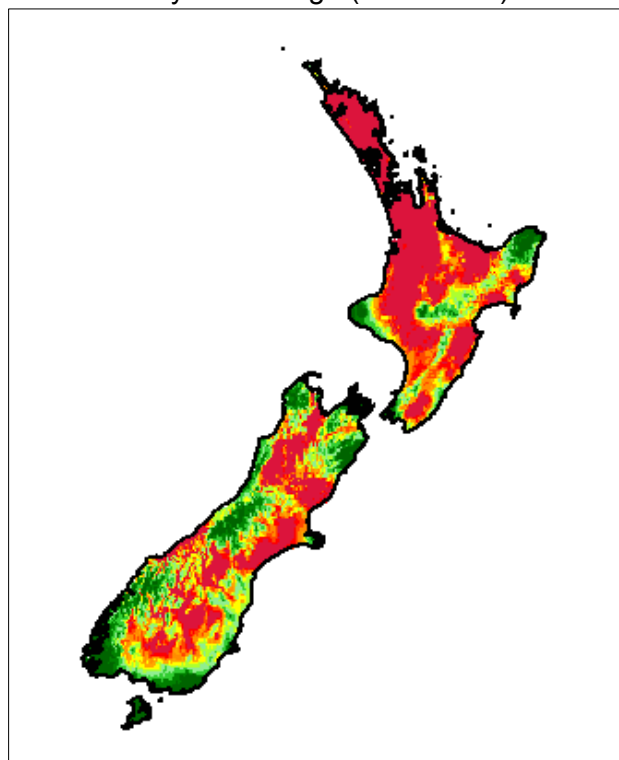


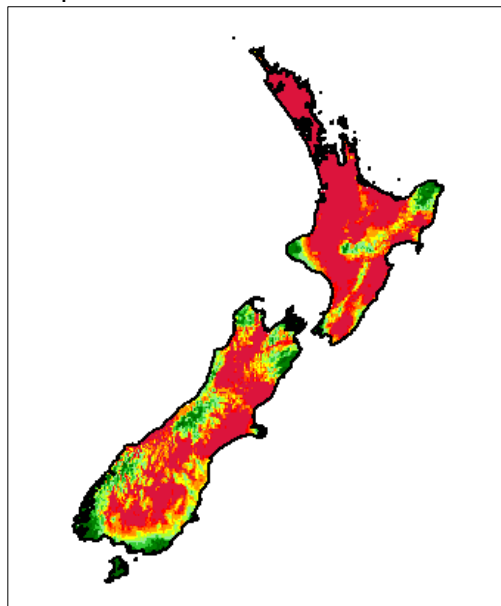
Figure A4-1: Days of HLI threshold exceedance, summer, for present-day conditions. Scale is as described at the beginning of Appendix A4. Top panel is the average, lower panels are 75th (left) and 90th (right) percentiles.

CCC model scenario

15 year average (2097-2111)



75th percentile



90th percentile

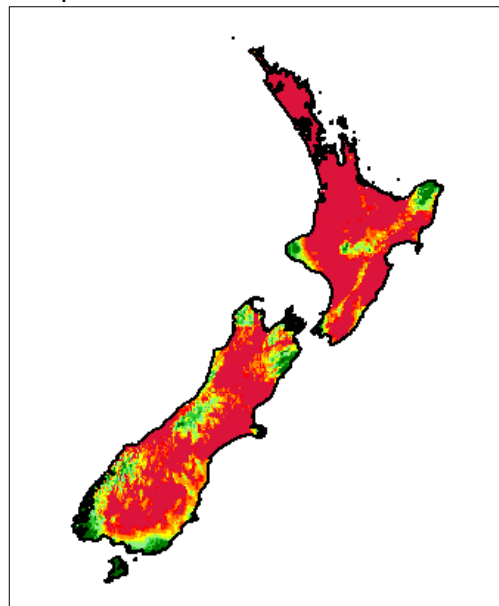


Figure A4-2: Days of HLI threshold exceedance, summer, for CCC future scenario. Scale is as described at the beginning of Appendix A4. Top panel is the average, lower panels are 75th (left) and 90th (right) percentiles.

Planck model scenario

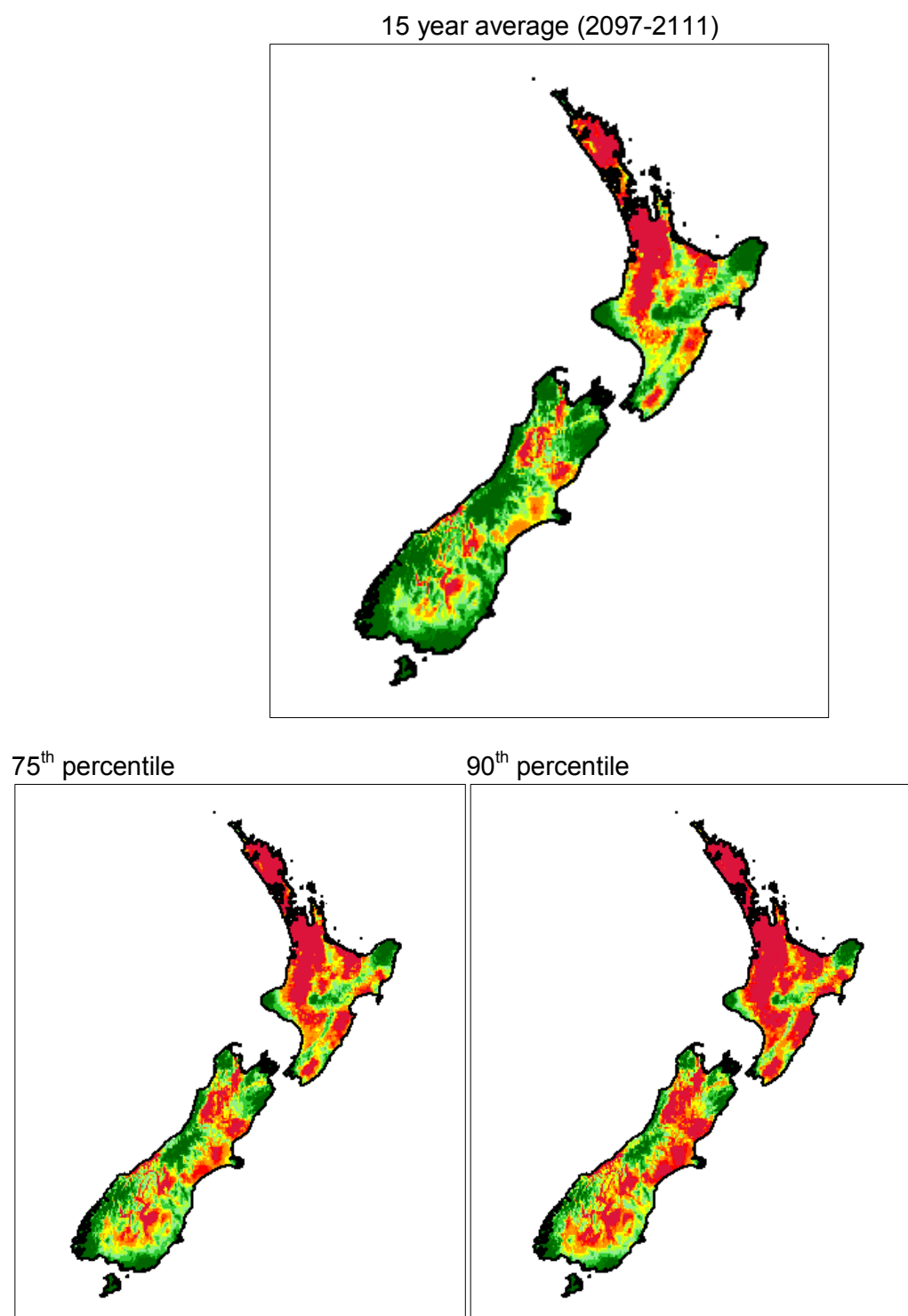


Figure A4-3: Days of HLI threshold exceedance, summer, for Planck future scenario. Scale is as described at the beginning of Appendix A4. Top panel is the average, lower panels are 75th (left) and 90th (right) percentiles.

12.4.2 Summer shoulder months (November, March)

Current actual data

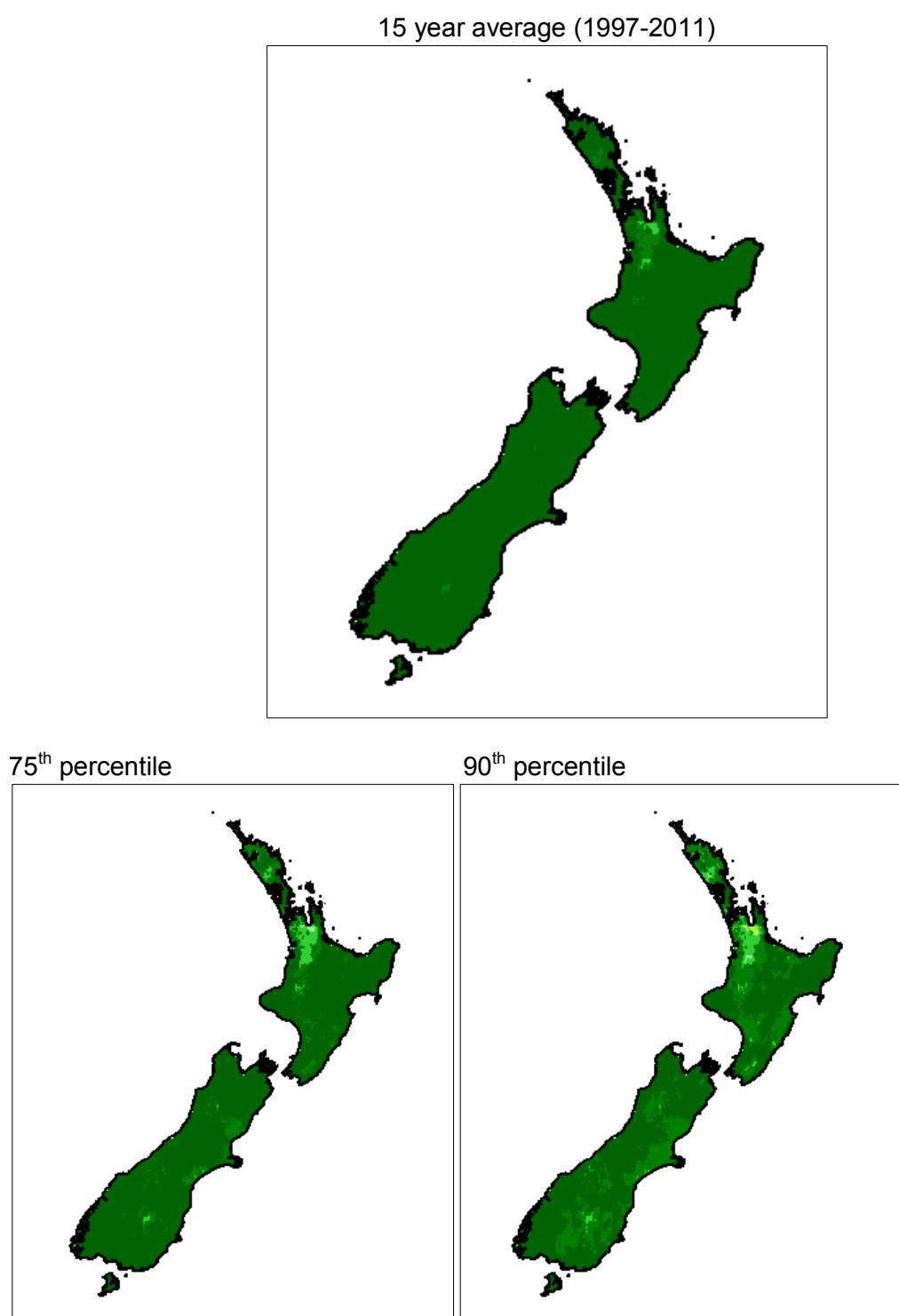


Figure A4-4: Days of HLI threshold exceedance, summer shoulder months, for present-day conditions. Scale is as described at the beginning of Appendix A4. Top panel is the average, lower panels are 75th (left) and 90th (right) percentiles.

CCC model scenario

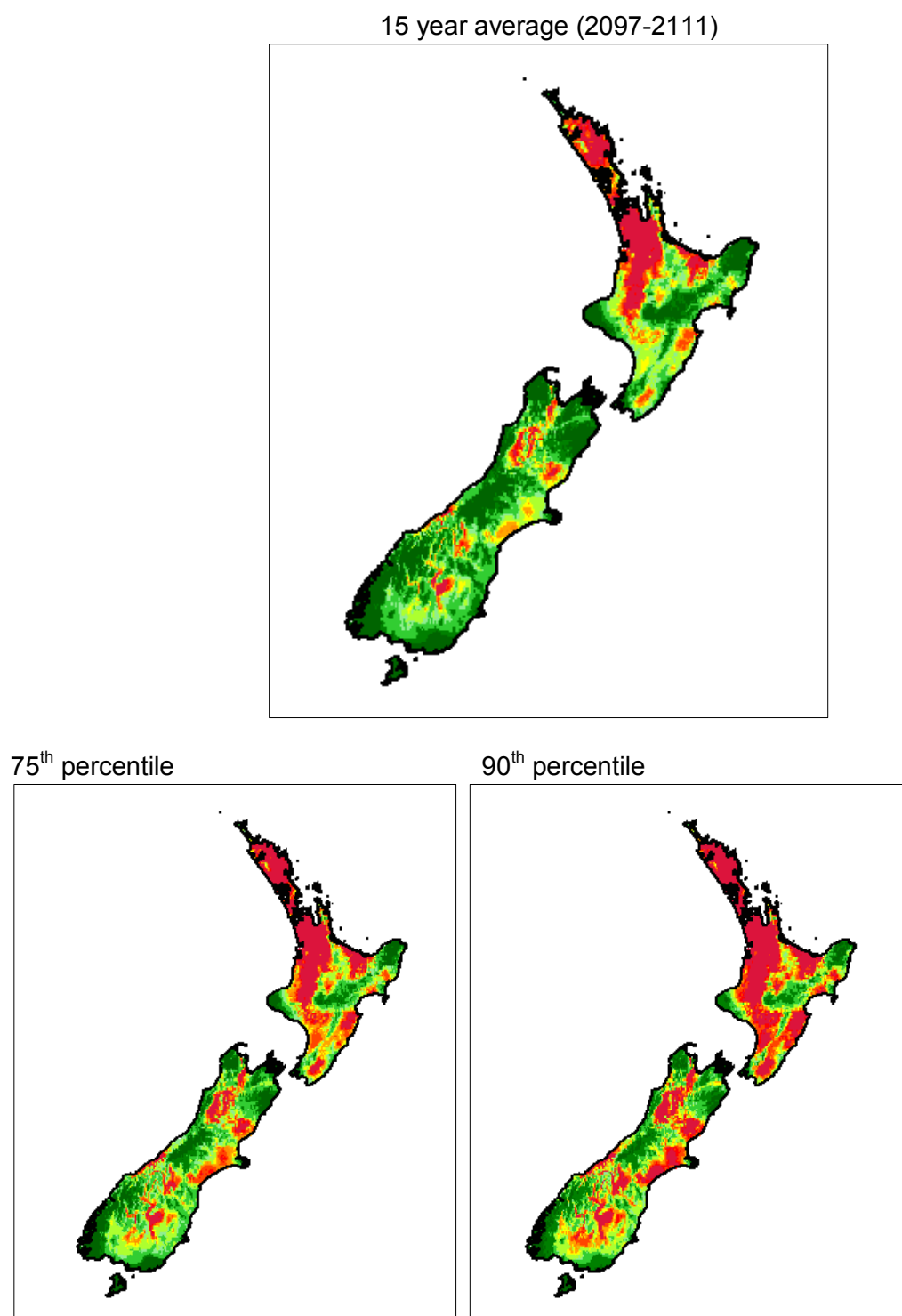


Figure A4-5: Days of HLI threshold exceedance, summer shoulder months, for CCC future scenario. Scale is as described at the beginning of Appendix A4. Top panel is the average, lower panels are 75th (left) and 90th (right) percentiles.

Planck model scenario

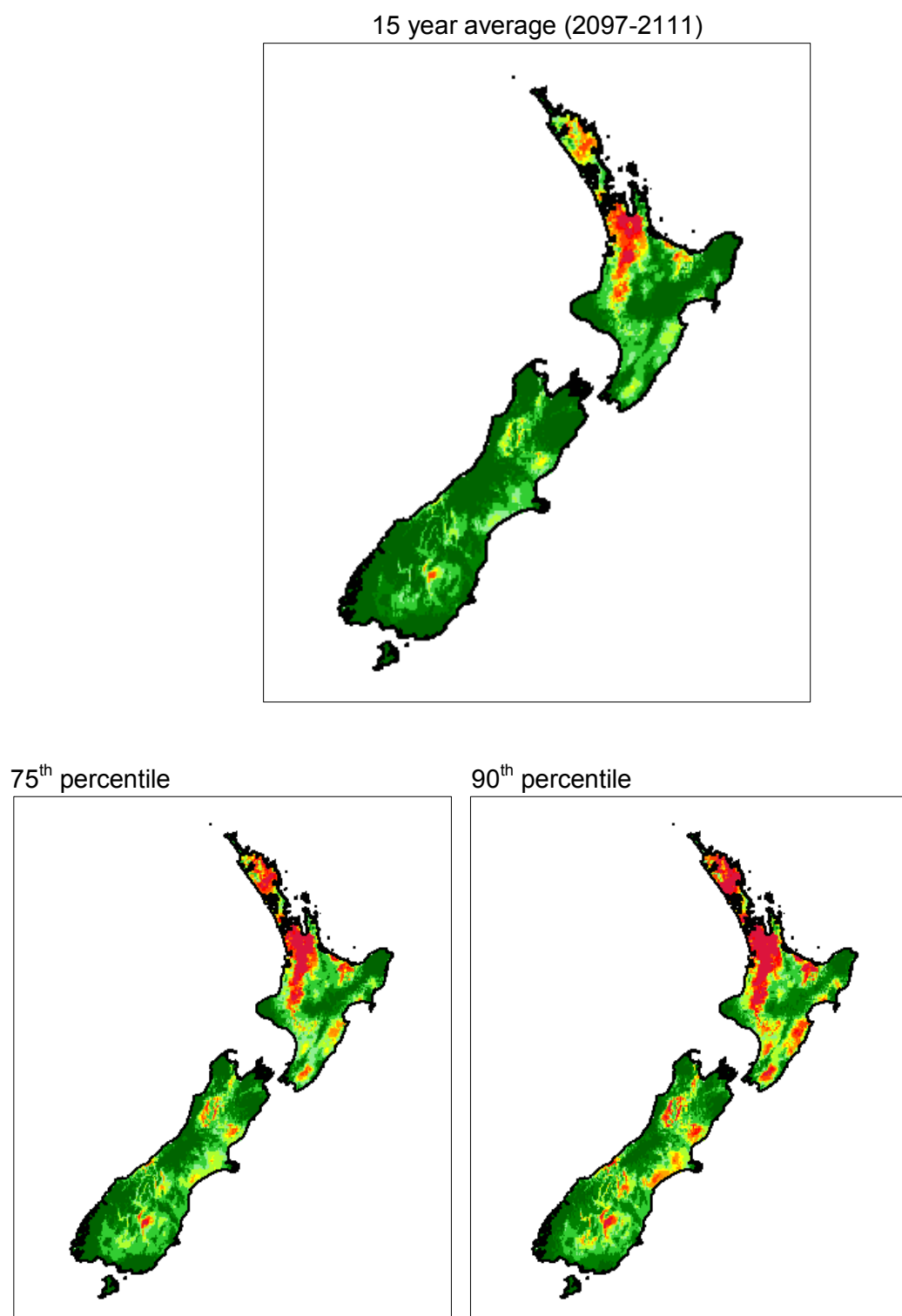


Figure A4-6: Days of HLI threshold exceedance, summer shoulder months, for Planck future scenario. Scale is as described at the beginning of Appendix A4. Top panel is the average, lower panels are 75th (left) and 90th (right) percentiles.

12.4.3 Winter months (June, July, August)

Current actual data

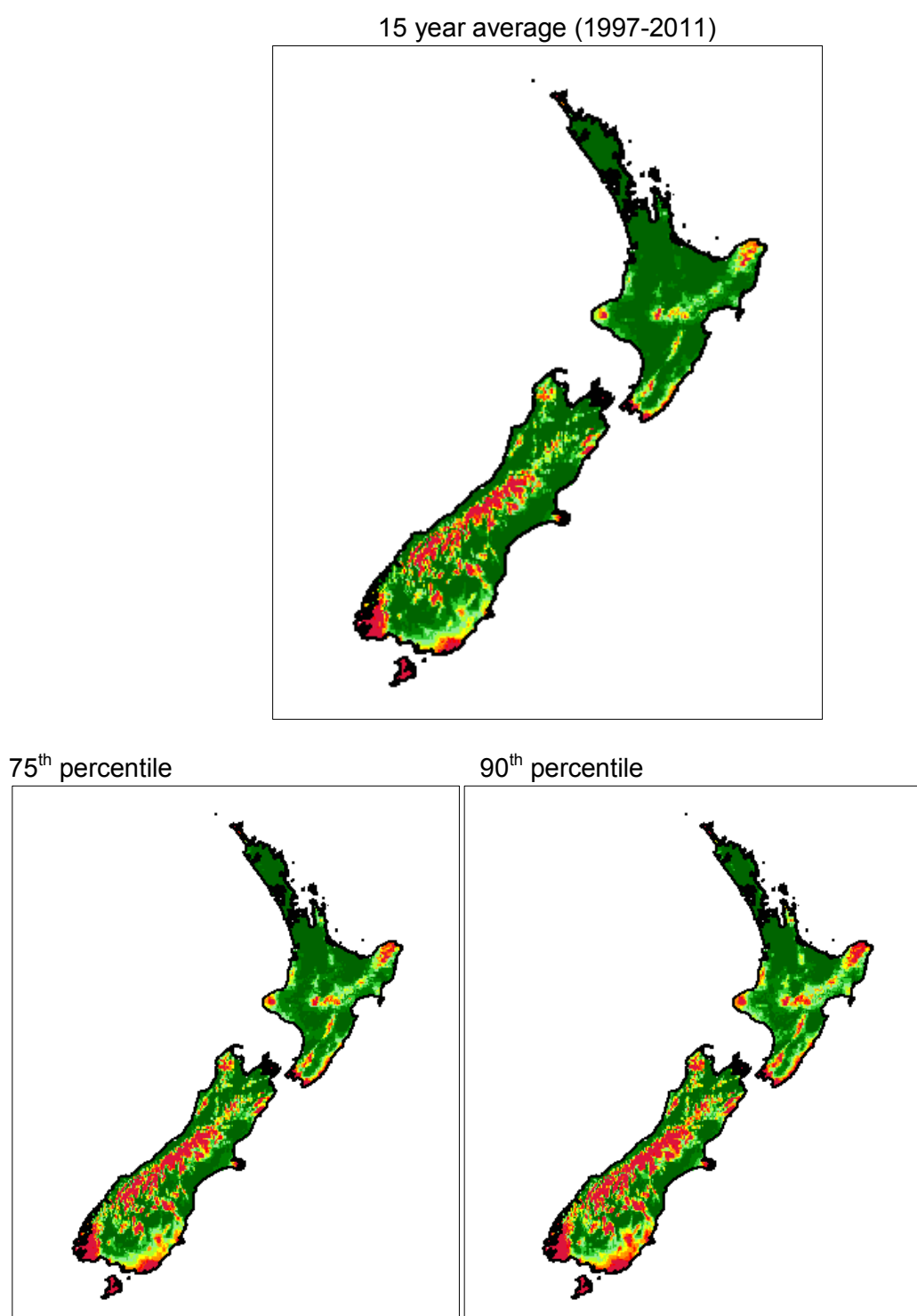


Figure A4-7: Days of CSI threshold exceedance, winter, for present-day conditions. Scale is as described at the beginning of Appendix A4. Top panel is the average, lower panels are 75th (left) and 90th (right) percentiles.

CCC model scenario

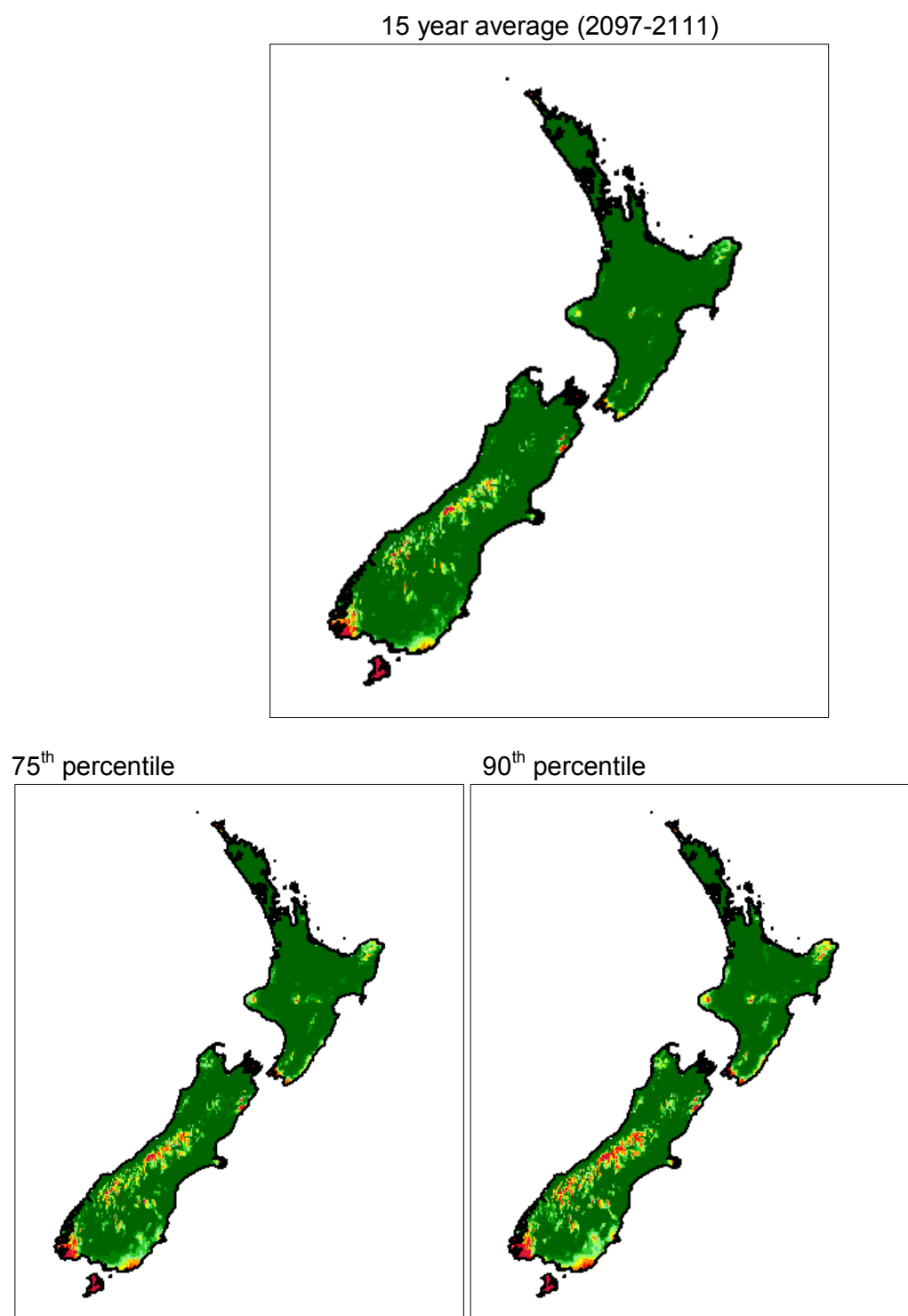


Figure A4-8: Days of CSI threshold exceedance, winter, for CCC future scenario. Scale is as described at the beginning of Appendix A4. Top panel is the average, lower panels are 75th (left) and 90th (right) percentiles.

Planck model scenario

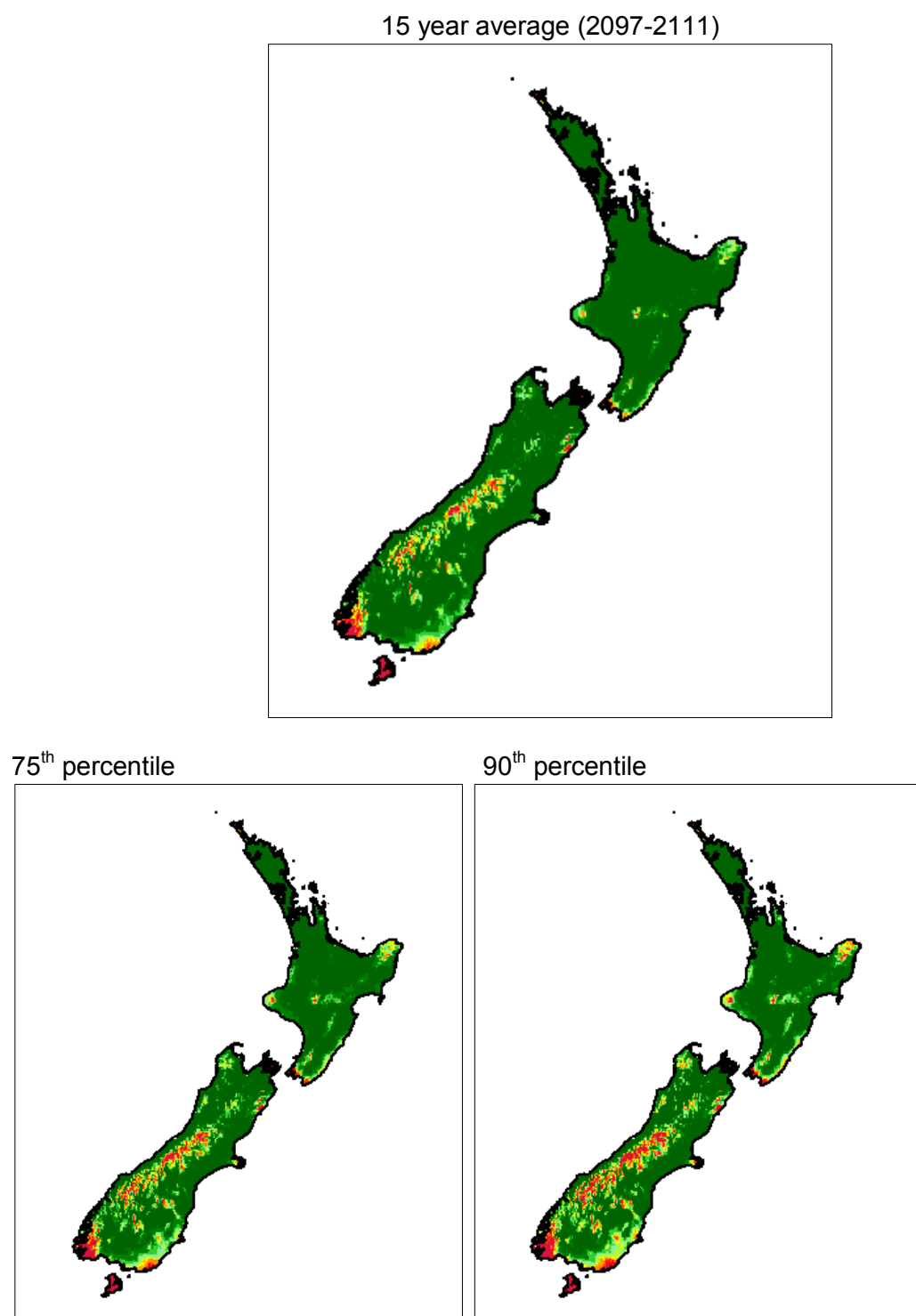


Figure A4-9: Days of CSI threshold exceedance, winter, for Planck future scenario. Scale is as described at the beginning of Appendix A4. Top panel is the average, lower panels are 75th (left) and 90th (right) percentiles.

12.4.4 Winter shoulder months (May, September)

Current actual data

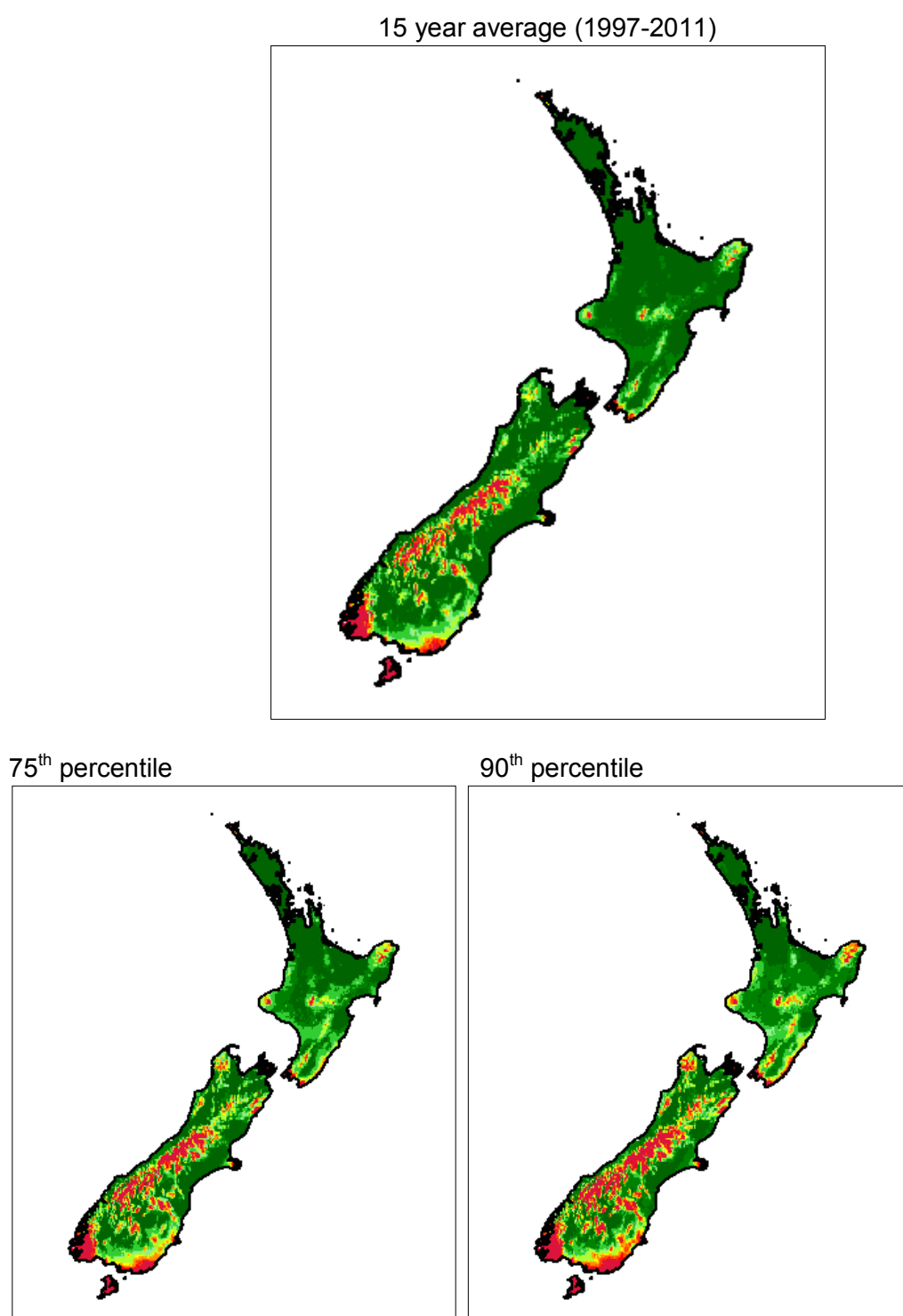


Figure A4-10: Days of CSI threshold exceedance, winter shoulder months, for present-day conditions. Scale is as described at the beginning of Appendix A4. Top panel is the average, lower panels are 75th (left) and 90th (right) percentiles.

CCC model scenario

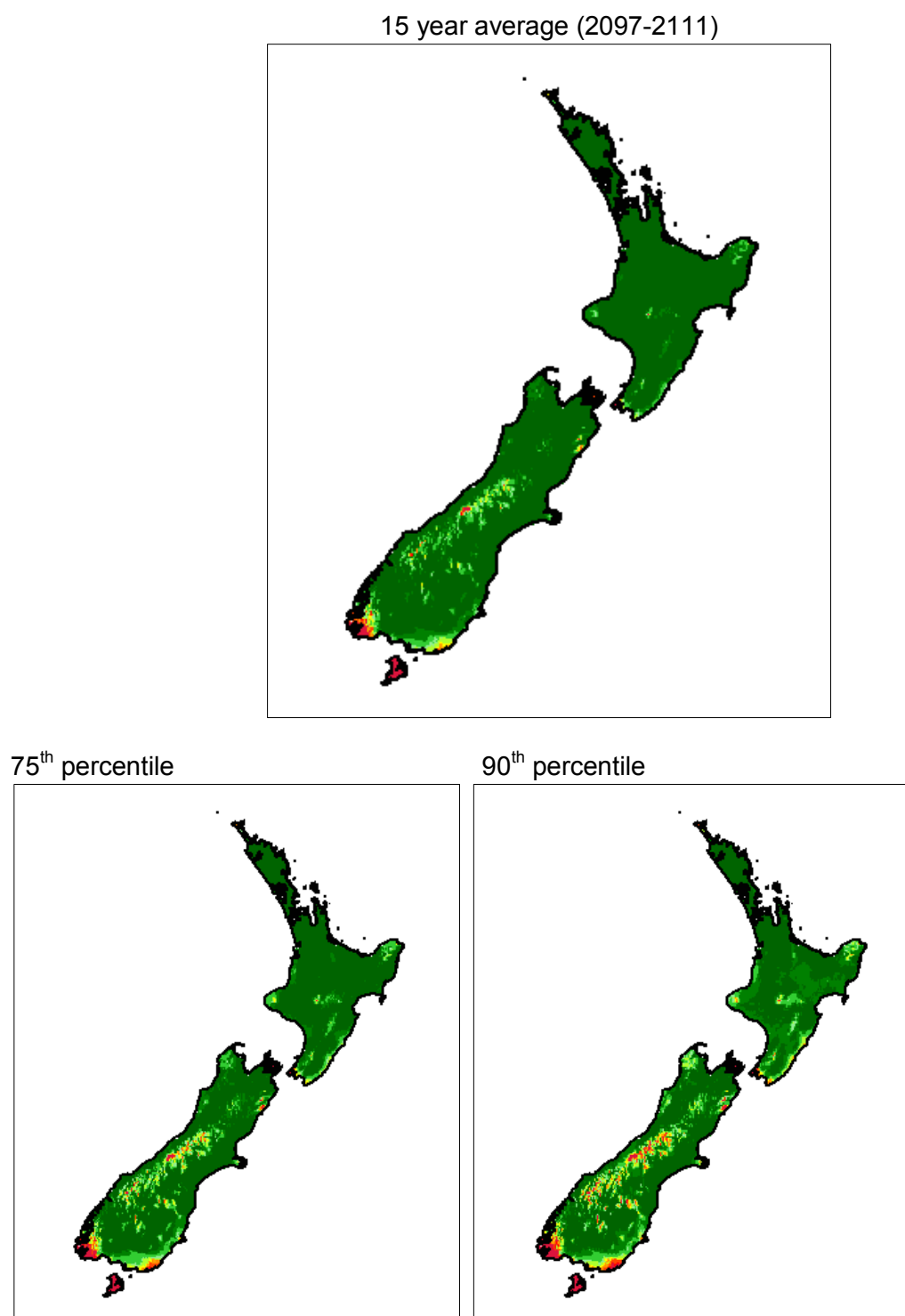


Figure A4-11: Days of CSI threshold exceedance, winter shoulder months, for CCC future scenario. Scale is as described at the beginning of Appendix A4. Top panel is the average, lower panels are 75th (left) and 90th (right) percentiles.

Planck model scenario

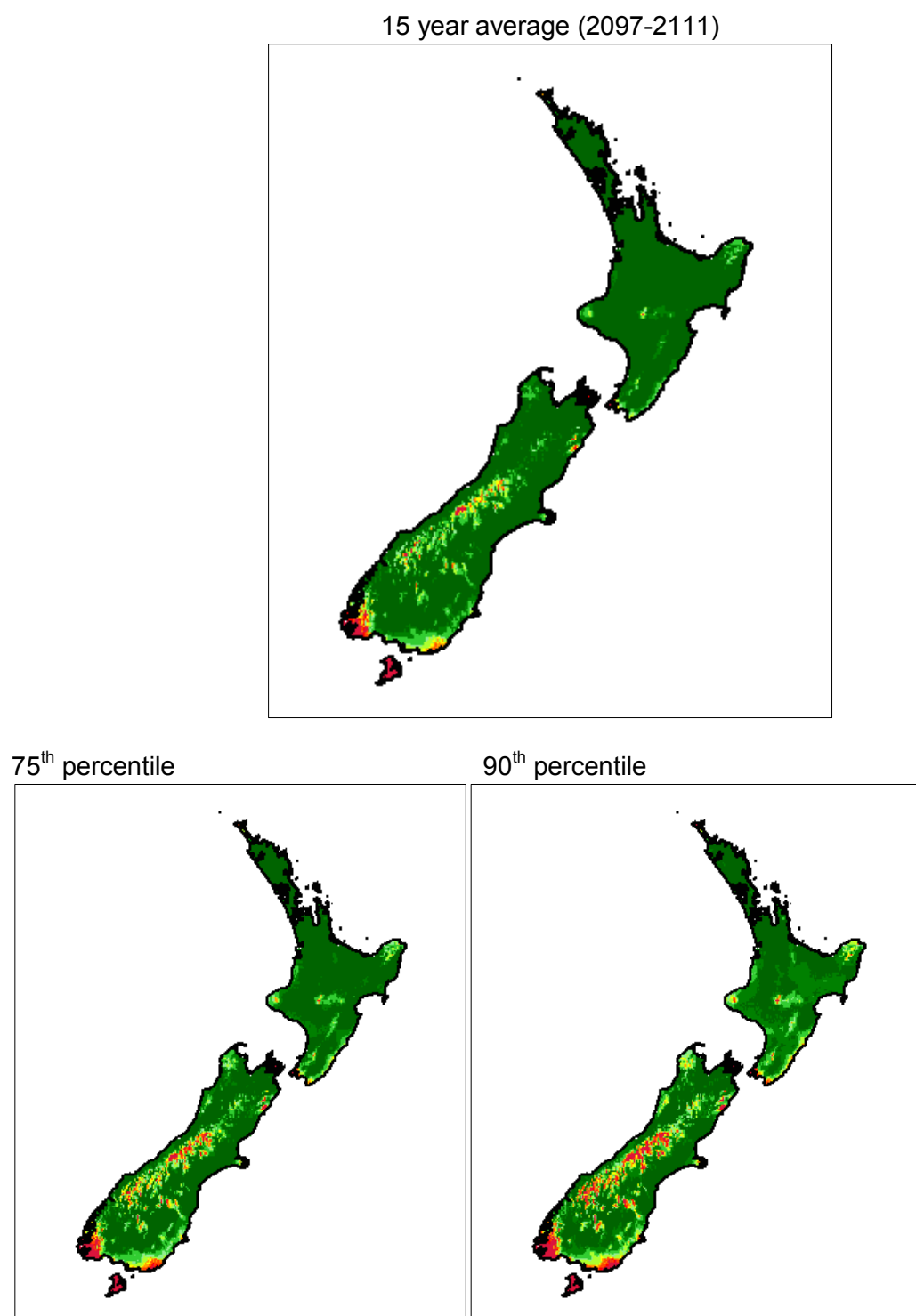


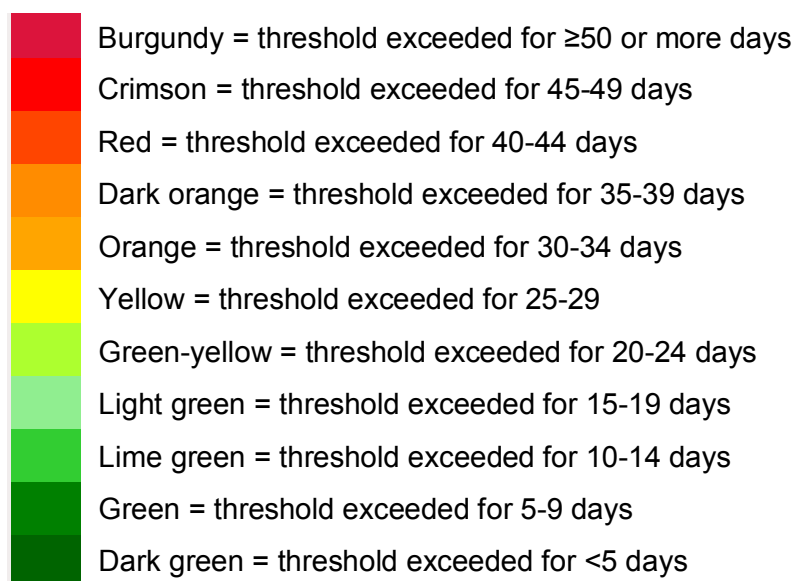
Figure A4-12: Days of CSI threshold exceedance, winter shoulder months, for CCC future scenario. Scale is as described at the beginning of Appendix A4. Top panel is the average, lower panels are 75th (left) and 90th (right) percentiles.

12.5 Appendix A5: Predictive risk maps with extended differentiation for summer and summer shoulder months

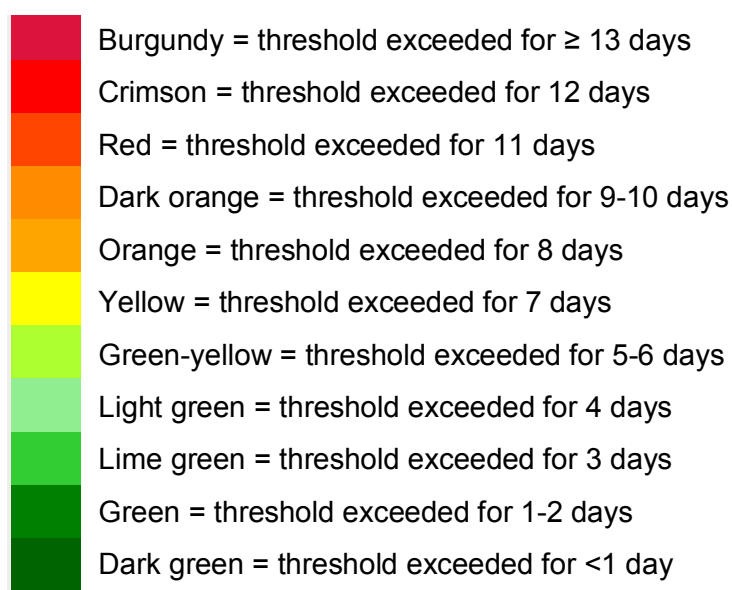
Key to interpretation:

These maps are based on mapping with a colour gradient to represent extended periods, in order to refine interpretation of the HLI risk maps as follows:

For summer (December-February):



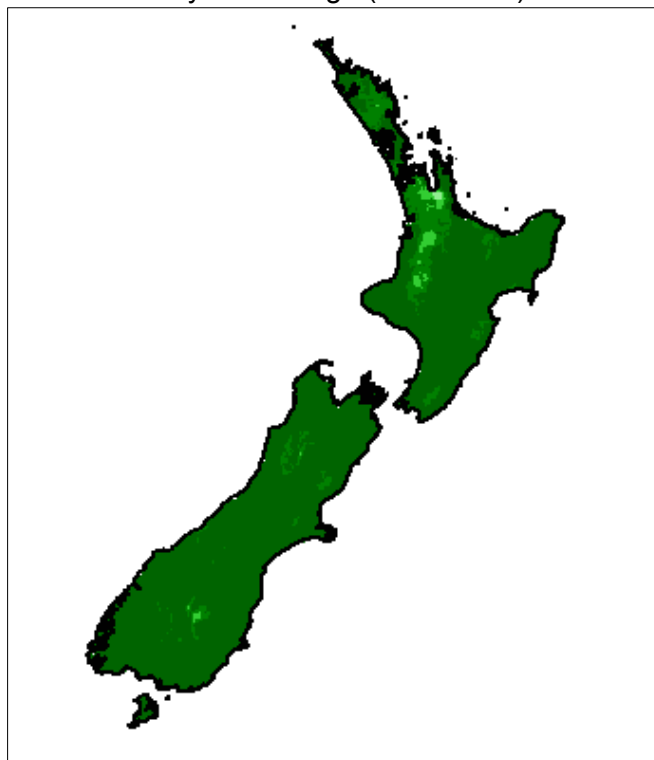
For summer shoulder (November/ March):



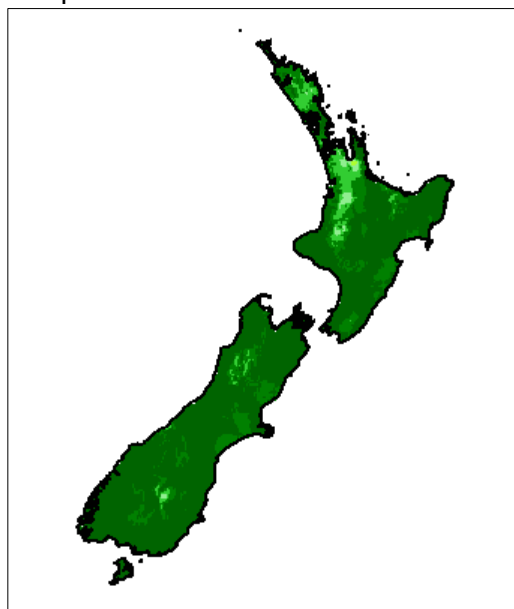
12.5.1 Summer months (December, January, February)

Current actual data

15 year average (1997-2011)



75th percentile



90th percentile

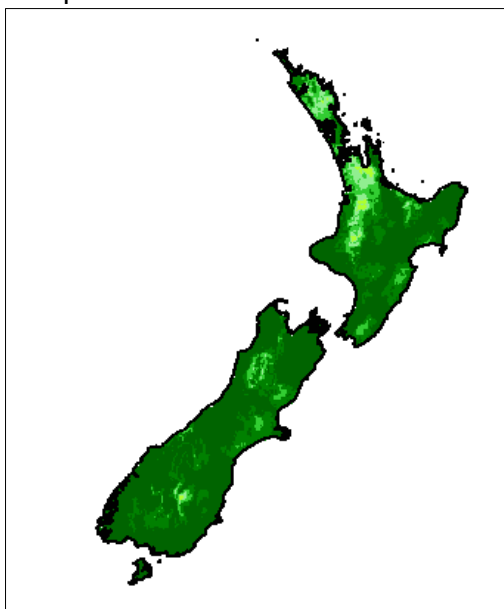


Figure A5-1: Days of HLI threshold exceedance, summer, for present-day conditions. Scale is as described at the beginning of Appendix A5. Top panel is the average, lower panels are 75th (left) and 90th (right) percentiles.

CCC model scenario

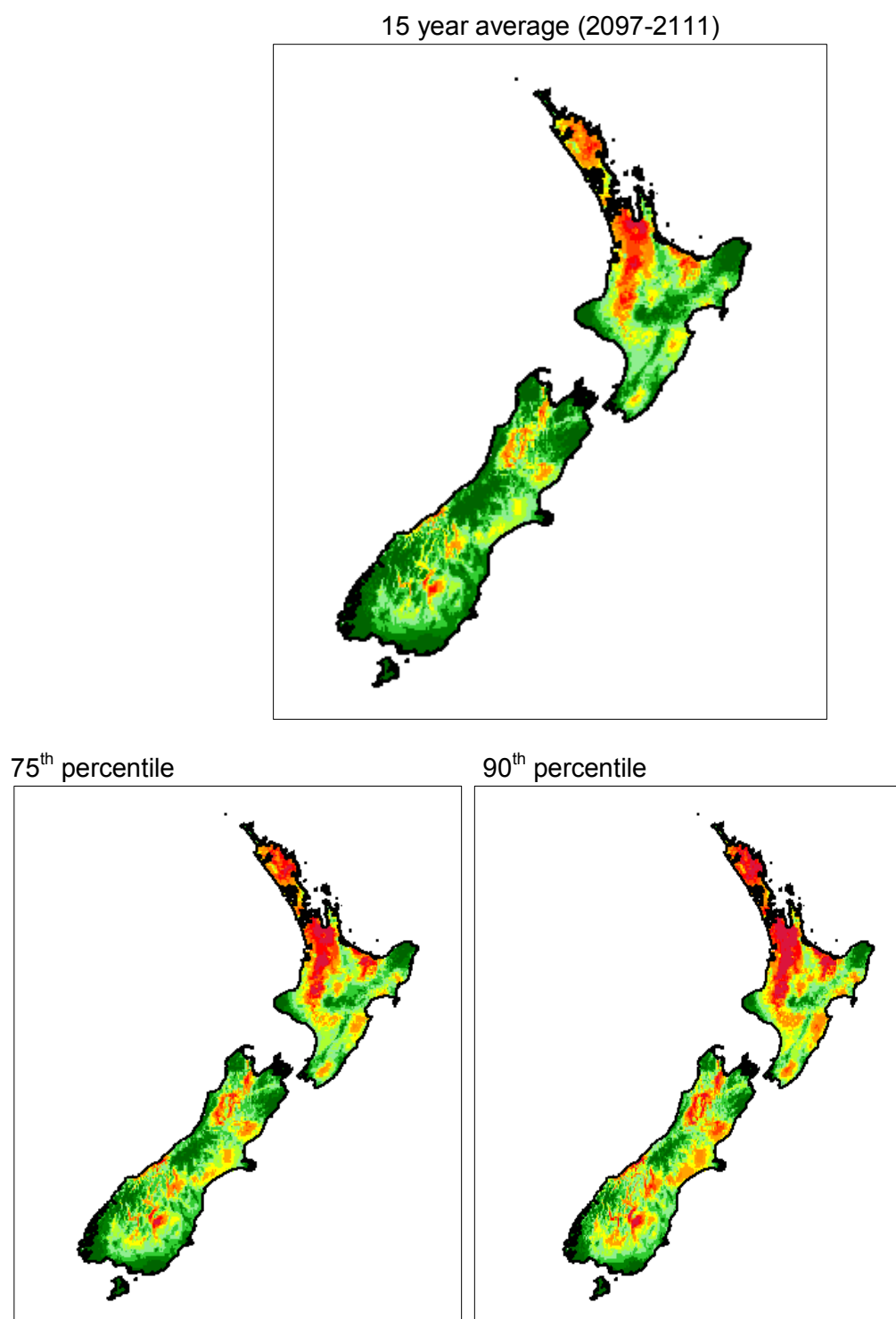
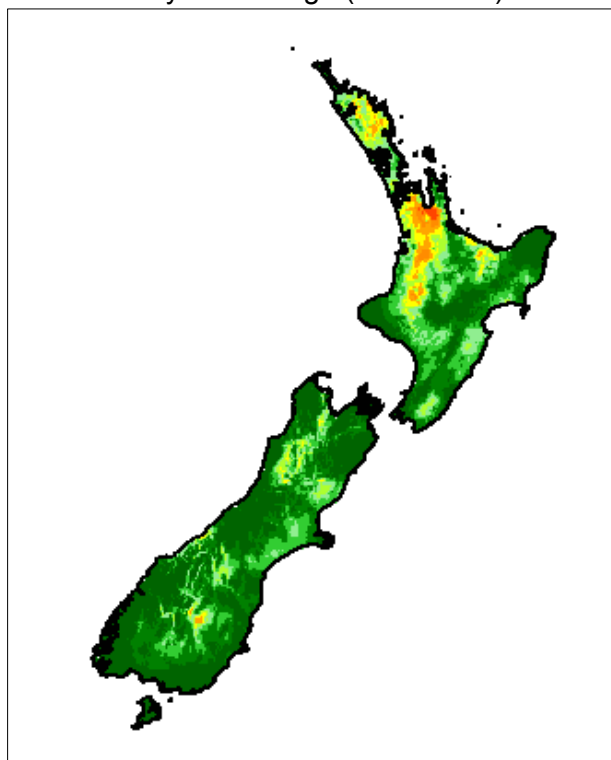


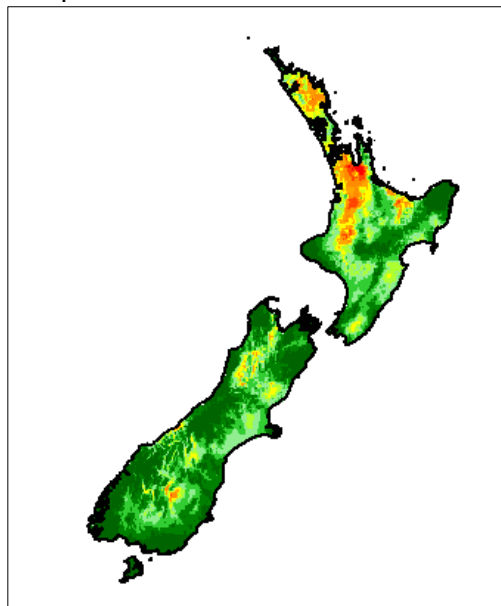
Figure A5-2: Days of HLI threshold exceedance, summer, for CCC future scenario. Scale is as described at the beginning of Appendix A5. Top panel is the average, lower panels are 75th (left) and 90th (right) percentiles.

Planck model scenario

15 year average (2097-2111)



75th percentile



90th percentile

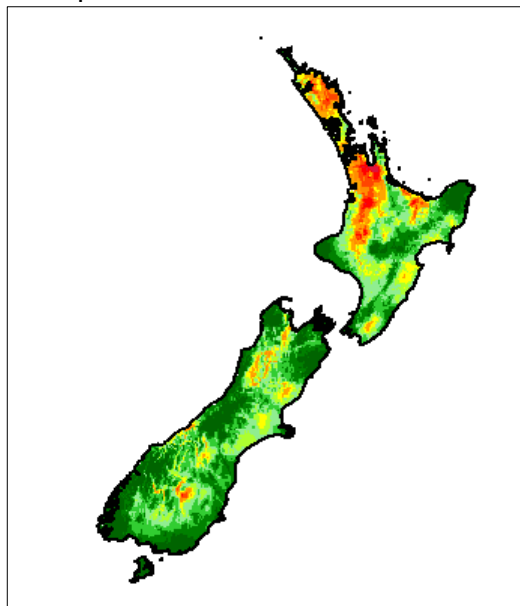


Figure A5-3: Days of HLI threshold exceedance, summer, for Planck future scenario. Scale is as described at the beginning of Appendix A5. Top panel is the average, lower panels are 75th (left) and 90th (right) percentiles.

12.5.2 Summer shoulder months (November, March)

Current actual data

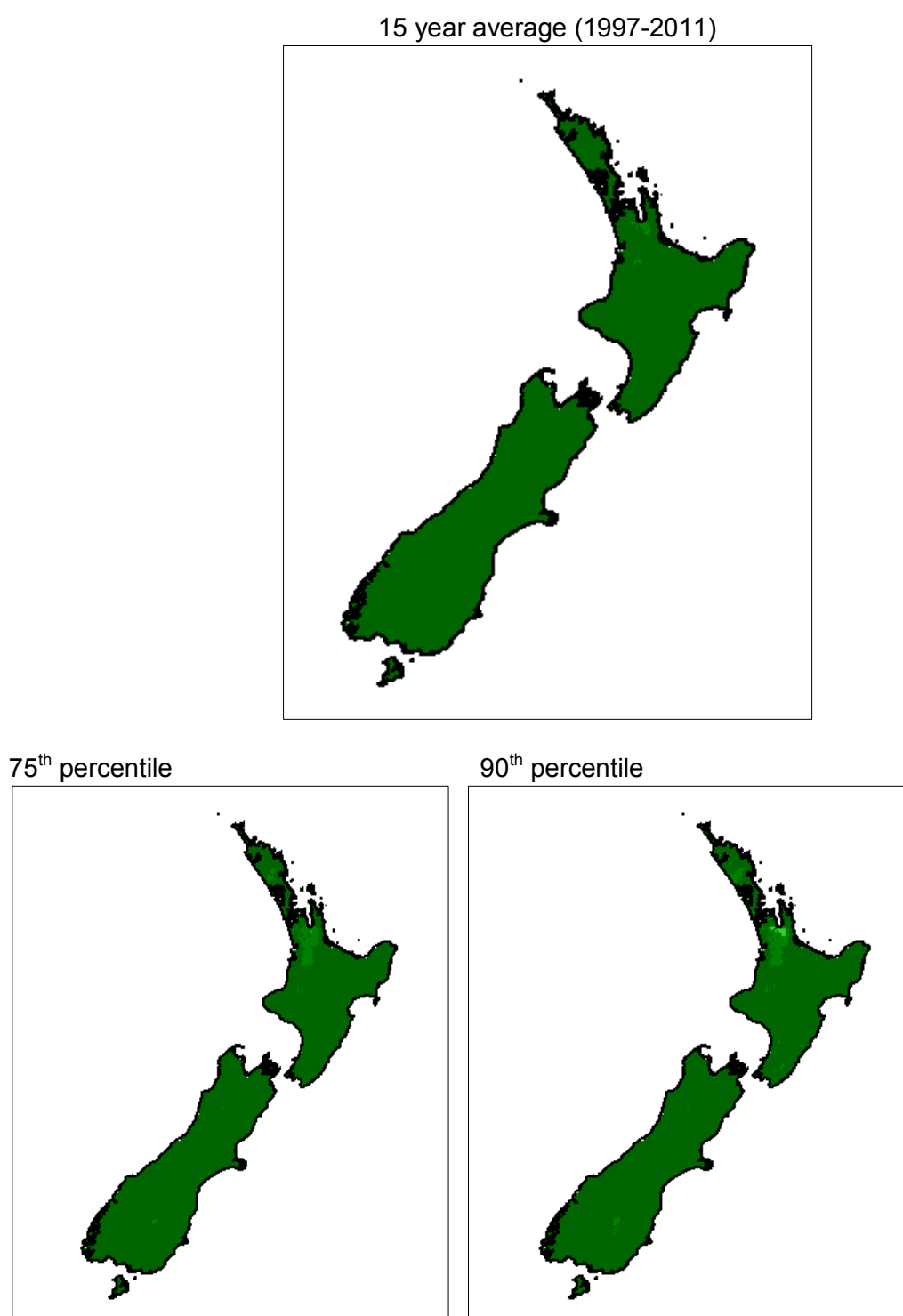


Figure A5-4: Days of HLI threshold exceedance, summer shoulder months, for present-day conditions. Scale is as described at the beginning of Appendix A5. Top panel is the average, lower panels are 75th (left) and 90th (right) percentiles.

CCC model scenario

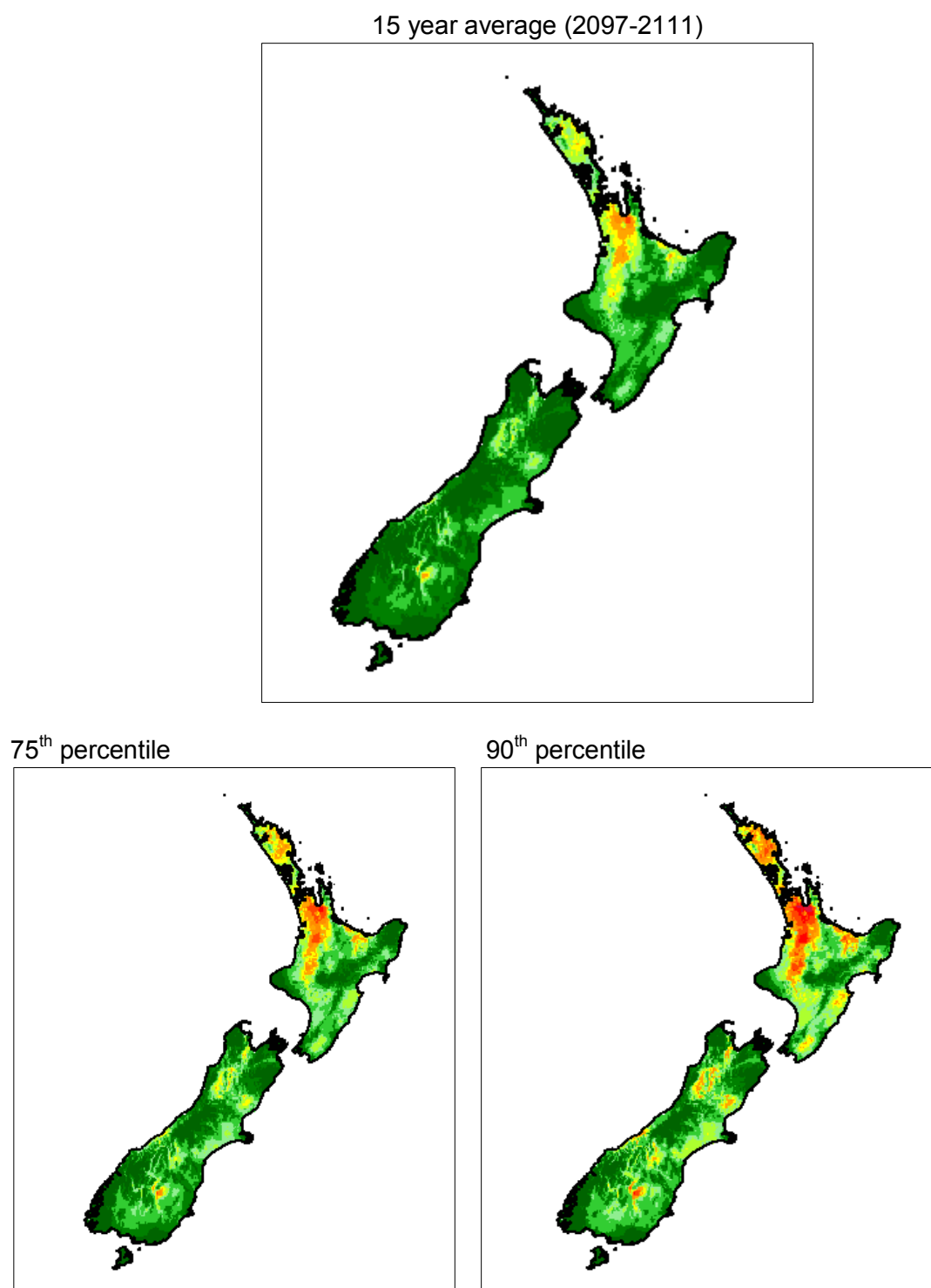


Figure A5-5: Days of HLI threshold exceedance, summer shoulder months, for CCC future scenario. Scale is as described at the beginning of Appendix A5. Top panel is the average, lower panels are 75th (left) and 90th (right) percentiles.

Planck model scenario

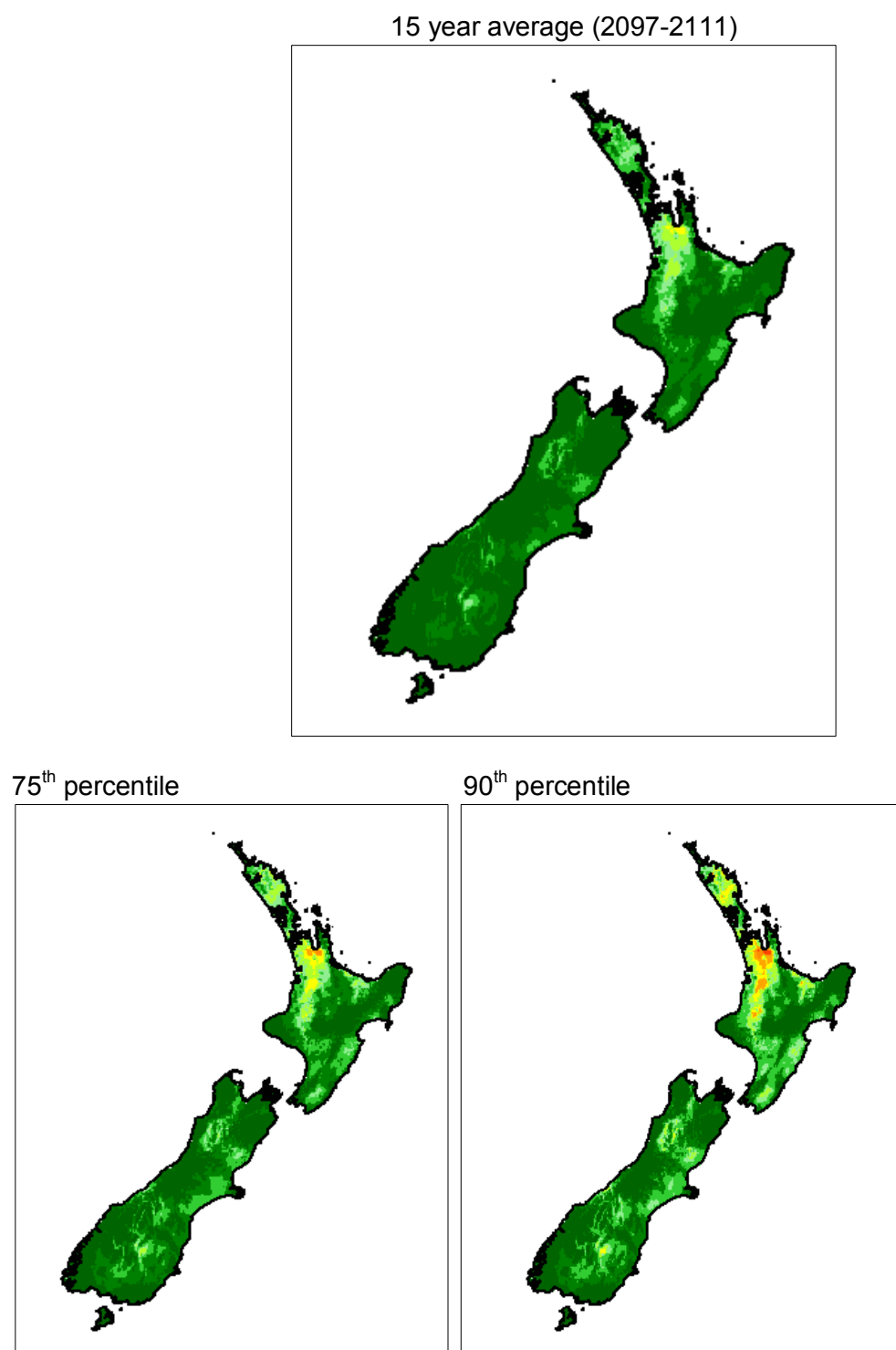


Figure A5-6: Days of HLI threshold exceedance, summer shoulder months, for Planck future scenario. Scale is as described at the beginning of Appendix A5. Top panel is the average, lower panels are 75th (left) and 90th (right) percentiles.